Electronic Supplementary Material (ESI) for Chemical Science.

Supporting Information

Manipulating Electron-Transfer – The Influence of Substituents on Novel Copper Guanidine Quinolinyl Complexes

Joshua Heck,[a] Fabian Metz,[a] Sören Buchenau,[b] Melissa Teubner,[a,b] Benjamin Grimm-Lebsanft,[b] Thomas P. Spaniol,[a] Alexander Hoffmann,[a] Michael A. Rübhausen[b] and Sonja Herres-Pawlis*[a]

Table of contents

1. Experimental Part

1.1 General

All manipulations required inert conditions were carried out under nitrogen atmosphere. Nitrogen was dried by passage through P_2O_5. If necessary, the solvents were dried by standard literature procedures.[1] All chemicals were purchased from commercial suppliers and used without further purification. The Cu(I) salts $[Cu(MeCN)_4]X$ (X = PF_6, OTf, BF_4) and the Cu(II) salts $[Cu(MeCN)_4](X)_2$ (X = OTf, BF_4) were synthesized according to the literature.[2] The Vilsmeier salt chloro-*N,N,N′,N′*-tetramethylformamidinium chloride (TMG-VS) was synthesized according to the literature.[3,4] Column chromatography was performed with Geduran Si 60 (40-63 µm, Merck) or with alumina B (activity Super I, MP Biomedicals).

1.2 Compound characterization

NMR spectra were recorded on a Bruker Avance III HD 400 and a Bruker Avance II 400 nuclear resonance spectrometer at 25°C. Resonances were referenced to the residual solvent signal, relative to TMS. Chemical shifts were assigned with the use of two-dimensional NMR experiments (COSY, HSQC, HMBC). For the Bruker Avance III HD 400 the software Topspin (Version 3.5 pl 7) from Bruker and for the Bruker Avance II 400 the software TopSpin (Version 2.1) from Bruker were used for data acquisition. For visualization and examination of the NMR spectra the software MestReNova (Version 12.0.1-20560) from Mestrelab Research was used. All NMR data were deposited as original data in the Chemotion Repository and are published under an Open Access model. The link to the original data is given in the analytical description. NMR spectra of the compounds are also shown (see Fig S49 − S154).

FT-IR spectra were recorded on a Shimadzu IRTracer 100 using a CsI beam splitter in combination with an ATR unit (Quest model from Specac utilising a robust monolithic crystalline diamond) in a resolution of 2 cm^{-1}. For data acquisition, the software LabSolution IR (Version 2.15) from Shimadzu was used.

Electron spray ionization (ESI) high-resolution mass spectra were recorded on an UHR-TOF Bruker Daltonik maXis II or a ThermoFisher Scientific LTQ Orbitrap XL. The measurements were performed on an UHR-TOF Bruker Daltonik maXis II, an ESI-quadrupole time-of-flight (qToF) mass spectrometer capable of a resolution of at least 80.000 FWHM. Detection was either in positive or in the negative ion mode. The mass spectrometer was calibrated subsequently to every experiment via direct infusion of a L-proline sodium salt solution, which provided a m/z range of singly charged peaks up to 3000 Da in both ion modes. For the ThermoFisher Scientific LTQ Orbitrap XL the source voltage was 4.49 kV and the capillary temperature was 299.54 °C. The tube lens voltage was set between 110 and 130 V.

Powder X-ray diffraction (PXRD) experiments were performed at ambient conditions on flat samples using a STOE STADI P diffractometer with Guinier geometry (Cu-$K_{\alpha1}$, λ = 1.54059 Å, STOE image plate detector IP-PSD). For data acquisition, the software WinXPOW (Version 3.7.0.7) from Stoe was used. For visualization of the PXRD spectra the software OriginPro 2021b (Version 9.8.5.212) from OriginLab was used.

Thin layer chromatography sheets were received from MACHEREY-NAGEL with a layer thickness of 0.20 mm and a pre-coating of a fluorescent indicator. Column chromatography was performed with silica gel 60 (40-63 µm) from Merck.

1.3 Ligand synthesis

1.3.1 Resynthesis of TMG2Mequ (L2) and corresponding precursor

1.3.1.1 Resynthesis of 2-methyl-8-aminoquinoline (2-Me-8-NH_2-qu)

This molecule has been synthesized before.[5] The synthesis was performed following a modified procedure of the literature.[6]

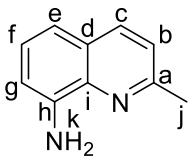

$C_{10}H_{10}N_2$
158.20 g mol^{-1}

2-Methyl-8-nitroquinoline (7.60 g, 40.4 mmol, 1 eq.) and palladium on active charcoal (10 w% Pd, 215 mg Pd/C, 0.202 mmol Pd, 0.005 eq. Pd) were suspended in methanol (350 mL) under nitrogen. Then the gas phase was exchanged by hydrogen. The reaction mixture was stirred for 5 hours at rt. The solvent was removed under reduced pressure. The resulting solid was solved in DCM and the solution was filtered through Geduran. The solvent was removed under reduced pressure. 2-methyl-8-aminoquinoline was obtained as a yellow solid (6.26 g, 39.6 mmol, 98.0 %).

^{1}H NMR (400 MHz, $CDCl_3$, 25 °C): δ = 7.95 (d, J = 8.4 Hz, 1H, c), 7.26 (t, J = 7.8 Hz, 1H, f), 7.24 (d, J = 8.4 Hz, 1H, b), 7.11 (dd, J = 8.1, 1.3 Hz, 1H, e), 6.90 (dd, J = 7.5, 1.3 Hz, 1H, g), 5.01 (s, 2H, k), 2.72 (s, 3H, j) ppm.

^{13}C NMR (101 MHz, $CDCl_3$, 25 °C) δ = 156.3 (a), 143.5 (h), 137.9 (i), 136.3 (c), 127.04 (d), 126.5 (f), 122.2 (b), 116.0 (e), 110.3 (g), 25.30 (j) ppm.

IR (ATR, neat): $\tilde{\nu}$ = 3469 (w, ν(N-H)), 3386 (w, ν(N-H)), 3342 (w, ν(N-H)), 3051 (vw, ν(C-H_{arom})), 2917 (vw, ν(C-H_{aliph})), 1616 (m), 1595 (s), 1564 (m), 1507 (s), 1476 (m), 1431 (m), 1373 (m), 1344 (m), 1324 (m), 1285 (w), 1274 (w), 1243 (m), 1180 (w), 1138 (m), 1083 (w), 1033 (w), 973 (vw), 953 (vw), 910 (vw), 866 (vw), 829 (vs), 795 (m), 745 (s), 719 (m), 693 (m), 556 (w), 514 (m), 434 (w), 420 (w) cm^{-1}.

HRMS (ESI+, MeOH): m/z (found) = 159.09148 (100 %), 160.09480 (9 %); m/z (calc.) = 159.09167 (100 %, $^{12}C_{10}{}^{1}H_{11}{}^{14}N_2{}^{+}$), 160.09503 (11 %, $^{12}C_9{}^{13}C^{1}H_{11}{}^{14}N_2{}^{+}$).

Additional information on the synthesis of the target compound and original analysis data files are available via Chemotion Repository: https://dx.doi.org/10.14272/reaction/SA-FUHFF-UHFFFADPSC-JHIAOWGCGN-UHFFFADPSC-NUHFF-NUHFF-NUHFF-ZZZ

1.3.1.2 Resynthesis of TMG2Mequ (L2)

This molecule has been synthesized before.[5] The synthesis was performed following a modified procedure of the literature.[4]

2-Methyl-8-aminoquinoline (6.36 g, 40.2 mmol, 1 eq.) and TMG-VS (8.25 g, 48.2 mmol, 1.2 eq.) were dissolved in MeCN (100 mL) and triethylamine (11.2 mL, 80.4 mmol, 2 eq.) was added. The reaction mixture was heated to reflux for 30 min under stirring. After cooling to rt a solution of NaOH (1.61 g, 40.2 mmol, 1 eq.) in water (20 ml) was added and the solvent was removed under reduced pressure. An aqueous KOH solution (25 mL, 50 w%) was added and the aqueous layer was extracted with MeCN (3x 100 mL). The combined organic layers were dried over Na_2SO_4 and filtered. The solvent was removed under reduced pressure and the crude product was distillated in vacuum (<10^{-1} mbar) starting at 150 °C and increasing the temperature stepwise up to 350 °C. Remained urea derivative was removed in vacuum (<10^{-1} mbar) at 100 °C. TMG2Mequ was obtained as a yellow oil that turns into a pale yellow solid after a few months (7.51 g, 29.3 mmol, 72.8 %).

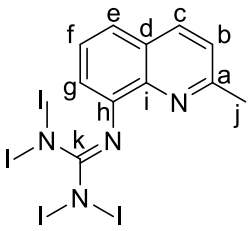

$C_{15}H_{20}N_4$
256.35 g mol^{-1}

^{1}H NMR (400 MHz, $CDCl_3$, 25 °C): δ = 7.91 (d, J = 8.3 Hz, 1H, c), 7.31 (t, J = 7.7 Hz, 1H, f), 7.19 (dd, J = 8.0, 1.4 Hz, 1H, e), 7.13 (d, J = 8.3 Hz, 1H, b), 7.04 (dd, J = 7.4, 1.5 Hz, 1H, g), 2.66 (s, 12H, l), 2.61 (s, 3H, j) ppm.

^{13}C NMR (101 MHz, $CDCl_3$, 25 °C) δ = 162.6 (k), 156.1 (a), 149.8 (h), 142.0 (i), 136.1 (c), 127.4 (d), 126.5 (f), 121.2 (b), 119.8 (g), 118.2 (e), 39.5 (l), 25.6 (j) ppm.

IR (ATR, neat): $\tilde{\nu}$ = 3043 (vw, ν(C-H_{arom})), 3003 (vw, ν(C-H_{arom})), 2921 (w, ν(C-H_{aliph})), 2876 (w, ν(C-H_{aliph})), 2790 (vw, ν(C-H_{aliph})), 1609 (m), 1578 (s, ν(C-N_{gua})), 1551 (vs, ν(C-N_{gua})), 1498 (s), 1474 (m), 1452 (m), 1428 (m), 1373 (s), 1360 (m), 1313 (w), 1297 (w), 1274 (w), 1222 (m), 1137 (vs), 1105 (w), 1085 (w), 1060 (m), 1013 (s), 925 (w), 904 (w), 865 (w), 834 (s), 801 (m), 749 (s), 702 (w), 687 (m), 666 (m), 619 (w), 566 (w), 538 (w), 516 (w), 491 (w), 439 (w), 422 (w) cm^{-1}.

HRMS (ESI+, MeOH): m/z (found) = 257.17642 (100 %), 258.17960 (17 %), 259.18283 (1 %); m/z (calc.) = 257.17607 (100 %, $^{12}C_{15}{}^{1}H_{21}{}^{14}N_4{}^{+}$), 258.17943 (18 %, $^{12}C_{14}{}^{13}C^{1}H_{21}{}^{14}N_4{}^{+}$), 259.18278 (1 %, $^{12}C_{13}{}^{13}C_2{}^{1}H_{21}{}^{14}N_4{}^{+}$).

Additional information on the synthesis of the target compound and original analysis data files are available via Chemotion Repository: https://dx.doi.org/10.14272/reaction/SA-FUHFF-UHFFFADPSC-XNDIRRNFWB-UHFFFADPSC-NUHFF-NUHFF-NUHFF-ZZZ

1.3.2 Resynthesis of TMG2^{t}Buqu (L3) and corresponding precursors

1.3.2.1 Resynthesis of 2-*tert*-butyl-8-nitroquinoline (2-^{t}Bu-8-NO_2-qu)

This molecule has been synthesized before.[7] The synthesis was performed following a modified procedure of the literature.[8]

8-Nitroquinoline (10.00 g, 57.4 mmol, 1 eq.), pivalic acid (20.52 g, 201.0 mmol, 3.5 eq.), ammonium peroxydisulfate (32.78 g, 143.5 mmol, 2.5 eq.) and silver nitrate (0.98 g, 5.7 mmol, 0.1 eq.) were combined in a mixture of water (480 mL) and sulfuric acid (11.26 g, 6.14 mL, 114.8 mmol, 2 eq.). The reaction mixture was heated to reflux under stirring for 4.5 h. After cooling to rt the reaction mixture was made basic with an

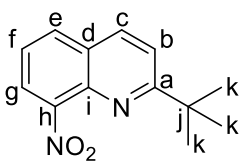

$C_{13}H_{14}N_2O_2$
230.27 g mol^{-1}

aqueous NaOH solution (15 M). The aqueous layer was extracted with DCM (4x 200 mL). The organic phase was dried over Na_2SO_4 and filtered. The solvent was removed under reduced pressure and the resulting black oil was purified by column chromatography (isohexane:ethyl acetate = 5:1, Geduran, R_f = 0.41). 2-*tert*-Butyl-8-nitroquinoline was obtained as a pale brown solid (2.69 g, 11.7 mmol, 20.3 %).

^{1}H NMR (400 MHz, $CDCl_3$, 25 °C): δ = 8.15 (d, J = 8.7 Hz, 1H, c), 7.95 (m, 2H, e, g), 7.65 (d, J = 8.7 Hz, 1H, b), 7.52 (t, J = 7.9 Hz, 1H, f), 1.44 (s, 9H, k) ppm.

^{13}C NMR (101 MHz, $CDCl_3$, 25 °C) δ = 172.1 (a), 148.6 (h), 138.7 (i), 135.9 (c), 131.2 (e), 127.5 (d), 124.4 (f), 123.1 (g), 120.1 (b), 38.9 (j), 30.0 (k) ppm.

IR (ATR, neat): $\tilde{\nu}$ = 2965 (w, ν(C-H_{aliph})), 2866 (vw, ν(C-H_{aliph})), 1624 (w), 1601 (m), 1560 (w), 1526 (vs, ν(C-NO_2)), 1499 (m), 1479 (w), 1460 (w), 1429 (w), 1393 (w), 1362 (m), 1312 (w), 1277 (vw), 1219 (w), 1152 (w), 1126 (s), 1026 (vw), 980 (vw), 924 (vw), 897 (w), 872 (m), 839 (vs), 816 (w), 797 (m), 766 (m), 758 (m), 735 (m), 658 (m), 610 (w), 513 (vw), 498 (vw), 455 (w), 405 (w) cm^{-1}.

HRMS (ESI+, MeOH): m/z (found) = 231.11237 (100 %), 232.11563 (14 %), 233.11935 (1 %); m/z (calc.) = 231.11280 (100 %, $^{12}C_{13}{}^{1}H_{15}{}^{14}N_2{}^{16}O_2{}^{+}$), 232.11616 (14 %, $^{12}C_{12}{}^{13}C^{1}H_{15}{}^{14}N_2{}^{16}O_2{}^{+}$), 233.11951 (1 %, $^{12}C_{11}{}^{13}C_2{}^{1}H_{15}{}^{14}N_2{}^{16}O_2{}^{+}$).

Additional information on the synthesis of the target compound and original analysis data files are available via Chemotion Repository: https://dx.doi.org/10.14272/reaction/SA-FUHFF-UHFFFADPSC-YLBKXSDEWV-UHFFFADPSC-NUHFF-NUHFF-NUHFF-ZZZ

1.3.2.2 Resynthesis of 2-*tert*-butyl-8-aminoquinoline (2-^{t}Bu-8-NH_2-qu)

This molecule has been synthesized before.[5,7] The synthesis was performed following a modified procedure of the literature.[6]

2-*tert*-Butyl-8-aminoquinoline was synthesized analogous to 2-methyl-8-aminoquinoline starting from 2-*tert*-butyl-8-nitroquinoline (1.00 g, 4.34 mmol, 1eq.) and was obtained as a brown oil (0.85 g, 4.24 mmol, 97.7 %).

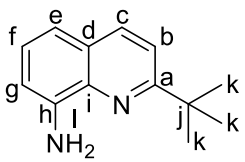

$C_{13}H_{16}N_2$
200.29 g mol^{-1}

^{1}H NMR (400 MHz, $CDCl_3$, 25 °C): δ = 8.00 (d, *J* = 8.7 Hz, 1H, c), 7.50 (d, *J* = 8.6 Hz, 1H, b), 7.27 (t, *J* = 7.8 Hz, 1H, f), 7.12 (dd, *J* = 8.2, 1.2 Hz, 1H, e), 6.92 (dd, *J* = 7.4, 1.3 Hz, 1H, g), 4.93 (s, 2H, l), 1.47 (s, 9H, k) ppm.

^{13}C NMR (101 MHz, $CDCl_3$, 25 °C) δ = 166.5 (a), 143.9 (h), 137.1 (i), 136.2 (c), 127.0 (d), 126.6 (f), 118.6 (b), 115.8 (e), 110.1 (g), 38.2 (j), 30.3 (k) ppm.

IR (ATR, neat): $\tilde{\nu}$ = 3478 (vw, ν(N-H)), 3374 (vw, ν(N-H)), 3047 (vw, ν(C-H_{arom})), 2960 (m, ν(C-H_{aliph})), 2901 (w, ν(C-H_{aliph})), 2865 (w, ν(C-H_{aliph})), 1617 (m), 1589 (s), 1560 (w), 1503 (m), 1481 (m), 1466 (m), 1432 (m), 1382 (m), 1363 (m), 1343 (w), 1323 (w), 1278 (w), 1227 (vw), 1214 (vw), 1203 (vw), 1183 (vw), 1148 (w), 1124 (m), 1079 (w), 1021 (vw), 972 (vw), 928 (vw), 906 (w), 831 (vs), 809 (w), 745 (s), 717 (w), 647 (vw), 553 (w), 478 (w), 420 (w) cm^{-1}.

HRMS (ESI+, MeOH): m/z (found) = 201.13809 (100 %), 202.14145 (14 %), 203.14493 (1 %); m/z (calc.) = 201.13863 (100 %, $^{12}C_{13}{}^{1}H_{17}{}^{14}N_2{}^{+}$), 202.14198 (15 %, $^{12}C_{12}{}^{13}C^{1}H_{17}{}^{14}N_2{}^{+}$), 203.14533 (1 %, $^{12}C_{11}{}^{13}C_2{}^{1}H_{17}{}^{14}N_2{}^{+}$).

Additional information on the synthesis of the target compound and original analysis data files are available via Chemotion Repository: https://dx.doi.org/10.14272/reaction/SA-FUHFF-UHFFFADPSC-MTPUXEIATO-UHFFFADPSC-NUHFF-NUHFF-NUHFF-ZZZ

1.3.2.3 Resynthesis of TMG2^{t}Buqu (L3)

This molecule has been synthesized before.[5] The synthesis was performed following a modified procedure of the literature.[4]

TMG2^{t}Buqu was synthesized and purified analogous to TMG2Mequ starting from 2-*tert*-butyl-8-aminoquinoline (3.90 g, 19.47 mmol, 1eq.) and was obtained as a pale yellow solid (4.40 g, 14.74 mmol, 75.7 %).

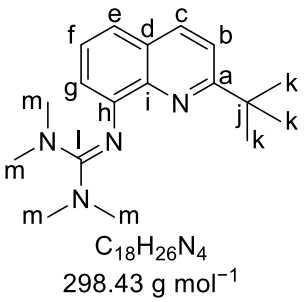

^{1}H NMR (400 MHz, $CDCl_3$, 25 °C): δ = 7.97 (d, *J* = 8.7 Hz, 1H, c), 7.40 (d, *J* = 8.6 Hz, 1H, b), 7.35 (t, *J* = 7.9 Hz, 1H, f), 7.22 (m, 2H, e, g), 2.67 (s, 12H, m), 1.38 (s, 9H, k) ppm.

^{13}C NMR (101 MHz, $CDCl_3$, 25 °C) δ = 166.5 (a), 162.2 (l), 150.4 (h), 141.1 (i), 136.2 (c), 127.4 (d), 126.6 (f), 120.7 (g), 118.3 (e), 117.9 (b), 39.7 (m), 38.4 (j), 30.2 (k) ppm.

IR (ATR, neat): $\tilde{\nu}$ = 2989 (vw, ν(C-H$_{aliph}$)), 2946 (w, ν(C-H$_{aliph}$)), 2920 (m, ν(C-H$_{aliph}$)), 2864 (w, ν(C-H$_{aliph}$)), 2793 (vw, ν(C-H$_{aliph}$)), 1608 (s, ν(C-N$_{gua}$)), 1597 (s, ν(C-N$_{gua}$)), 1556 (m), 1495 (s), 1444 (m), 1430 (m), 1420 (w), 1370 (s), 1363 (s), 1342 (w), 1307 (w), 1271 (w), 1230 (m), 1214 (w), 1178 (vw), 1134 (s), 1125 (s), 1081 (w), 1056 (m), 1008 (s), 924 (w), 900 (w), 872 (vw), 843 (vs), 822 (w), 811 (w), 778 (m), 752 (w), 719 (w), 679 (m), 645 (vw), 628 (w), 564 (m), 540 (w), 502 (w), 457 (w), 427 (vw) cm^{-1}.

HRMS (ESI+, MeOH): m/z (found) = 299.22232 (100 %), 300.22559 (20 %), 301.22864 (2 %); m/z (calc.) = 299.22302 (100 %, $^{12}C_{18}{}^{1}H_{27}{}^{14}N_4{}^{+}$), 300.22638 (20 %, $^{12}C_{17}{}^{13}C^{1}H_{27}{}^{14}N_4{}^{+}$), 301.22973 (2 %, $^{12}C_{16}{}^{13}C_2{}^{1}H_{27}{}^{14}N_4{}^{+}$).

Additional information on the synthesis of the target compound and original analysis data files are available via Chemotion Repository: https://dx.doi.org/10.14272/reaction/SA-FUHFF-UHFFFADPSC-DYIBODSCVM-UHFFFADPSC-NUHFF-NUHFF-NUHFF-ZZZ

1.3.3 Synthesis of TMG2^{c}Hexqu (L4) and corresponding precursors

1.3.3.1 Resynthesis of 2-cyclohexyl-8-nitroquinoline (2-^{c}Hex-8-NO$_2$-qu)

This molecule has been synthesized before.[7] The synthesis was performed following a modified procedure of the literature.[8]

8-Nitroquinoline (10.00 g, 57.42 mmol, 1 eq.), cyclohexanecarboxylic acid (20.59 g, 160.77 mmol, 2.8 eq.), ammonium peroxydisulfate (29.48 g, 129.20 mmol, 2.25 eq.) and silver nitrate (0.98 g, 5.74 mmol, 0.1 eq.) were combined in a mixture of water (500 mL) and sulfuric acid (11.26 g, 6.12 mL, 114.84 mmol, 2 eq.). The reaction mixture was heated to reflux under stirring for 4.5 h. After cooling to rt the reaction mixture was made basic with an aqueous NaOH solution (15 M). The aqueous layer was extracted with DCM (3x 200 mL). The organic phase was dried over Na_2SO_4 and filtered. The solvent was removed under reduced pressure and the resulting black oil was purified two times by column chromatography (1. isohexane:ethyl acetate = 5:1, Geduran, R_f = 0.40; 2. isohexane:DCM = 1:1, Geduran, R_f = 0.56). 2-Cyclohexyl-8-nitroquinoline was obtained as a colorless crystalline solid (2.20 g, 8.58 mmol, 14.9 %).

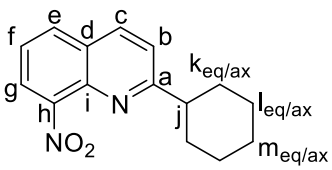

$C_{15}H_{16}N_2O_2$
256.31 g mol^{-1}

^{1}H NMR (400 MHz, $CDCl_3$, 25 °C): δ = 8.13 (d, J = 8.6 Hz, 1H, c), 7.99 – 7.91 (m, 2H, e, g), 7.51 (dd, J = 8.2, 7.5 Hz, 1H, f), 7.44 (d, J = 8.6 Hz, 1H, b), 2.92 (tt, J = 11.8, 3.5 Hz, 1H, j), 2.06 – 1.96 (m, 2H, k_{eq}), 1.88 (dt, J = 12.8, 3.3 Hz, 2H, l_{eq}), 1.76 (dtt, J = 12.6, 3.2, 1.5 Hz, 1H, m_{eq}), 1.63 (qd, J = 12.5, 3.0 Hz, 2H, k_{ax}), 1.44 (qt, J = 12.5, 3.2 Hz, 2H, l_{ax}), 1.31 (qt, J = 12.6, 3.2 Hz, 1H, m_{ax}) ppm.

^{13}C NMR (101 MHz, $CDCl_3$, 25 °C) δ = 169.5 (a), 148.5 (h), 139.2 (i), 136.0 (c), 131.4 (e), 127.9 (d), 124.2 (f), 123.1 (g), 122.1 (b), 47.2 (j), 32.5 (k), 26.5 (l), 26.1 (m) ppm.

IR (ATR, neat): $\tilde{\nu}$ = 2915 (m, ν(C-H_{aliph})), 2847 (m, ν(C-H_{aliph})), 2161 (w), 1625 (w), 1599 (m), 1563 (w), 1521 (s, ν(C-NO_2)), 1498 (m), 1453 (m), 1430 (w), 1372 (m), 1313 (m), 1299 (m), 1268 (w), 1248 (w), 1209 (w), 1177 (m), 1138 (m), 1126 (w), 1059 (w), 1035 (w), 1008 (w), 927 (w), 888 (w), 877 (m), 839 (s), 812 (w), 797 (s), 752 (s), 719 (m), 712 (m), 657 (vs), 610 (w), 565 (w) cm^{-1}.

HRMS (ESI+, MeOH): m/z (found) = 257.12821 (100 %), 258.13146 (16 %), 259.13470 (1 %); m/z (calc.) = 257.12845 (100 %, $^{12}C_{15}{}^{1}H_{17}{}^{14}N_2{}^{16}O_2{}^{+}$), 258.13181 (16 %, $^{12}C_{14}{}^{13}C^{1}H_{17}{}^{14}N_2{}^{16}O_2{}^{+}$), 259.13516 (1 %, $^{12}C_{13}{}^{13}C_2{}^{1}H_{17}{}^{14}N_2{}^{16}O_2{}^{+}$).

Additional information on the synthesis of the target compound and original analysis data files are available via Chemotion Repository: https://dx.doi.org/10.14272/reaction/SA-FUHFF-UHFFFADPSC-YSUUDYJLPD-UHFFFADPSC-NUHFF-NUHFF-NUHFF-ZZZ

1.3.3.2 Resynthesis of 2-cyclohexyl-8-aminoquinoline (2-^{c}Hex-8-NH_2-qu)

This molecule has been synthesized before.[7] The synthesis was performed following a modified procedure of the literature.[6]

2-Cyclohexyl-8-aminoquinoline was synthesized analogous to 2-methyl-8-aminoquinoline starting from 2-cyclohexyl-8-nitroquinoline (0.50 g, 1.95 mmol, 1 eq.) and was obtained as a yellow solid (0.44 g, 1.94 mmol, 99.5 %).

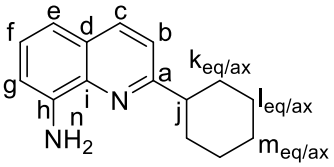

$C_{15}H_{18}N_2$
226.32 g mol^{-1}

^{1}H NMR (400 MHz, $CDCl_3$, 25 °C): δ = 7.98 (d, J = 8.5 Hz, 1H, c), 7.28 (d, J = 8.6 Hz, 1H, b), 7.26 (t, J = 7.8 Hz, 1H, f), 7.11 (dd, J =

8.1, 1.3 Hz, 1H, e), 6.90 (dd, *J* = 7.5, 1.3 Hz, 1H, g), 5.10 (s, 2H, n), 2.90 (t, *J* = 12.1 Hz, 1H, j), 2.04 (ddq, *J* = 12.4, 3.8, 2.2 Hz, 2H, k_{eq}), 1.90 (dt, *J* = 12.7, 3.3 Hz, 2H, l_{eq}), 1.79 (dtt, *J* = 12.7, 3.3, 1.5 Hz, 1H, m_{eq}), 1.66 (qd, *J* = 12.5, 3.3 Hz, 2H, k_{ax}), 1.47 (qt, *J* = 12.7, 3.3 Hz, 2H, l_{ax}), 1.32 (qt, *J* = 12.6, 3.4 Hz, 1H, m_{ax}) ppm.

^{13}C NMR (101 MHz, $CDCl_3$, 25 °C) δ = 163.9 (a), 143.7 (h), 137.6 (i), 136.4 (c), 127.4 (d), 126.5 (f), 120.4 (b), 115.9 (e), 110.1 (g), 47.0 (j), 33.0 (k), 26.7 (l), 26.4 (m) ppm.

IR (ATR, neat): $\tilde{\nu}$ = 3441 (w, ν(N-H)), 3317 (w, ν(N-H)), 3042 (vw, ν(C-H_{arom})), 2923 (s, ν(C-H_{aliph})), 2850 (m, ν(C-H_{aliph})), 1618 (m), 1591 (m), 1560 (m), 1503 (m), 1474 (m), 1446 (m), 1433 (m), 1381 (m), 1344 (w), 1334 (w), 1301 (vw), 1277 (w), 1261 (vw), 1242 (w), 1195 (w), 1173 (w), 1136 (w), 1125 (w), 1079 (w), 1035 (vw), 1008 (vw), 968 (vw), 927 (w), 890 (w), 862 (vw), 846 (w), 829 (vs), 805 (w), 739 (vs), 710 (w), 578 (w), 541 (w), 529 (w), 498 (w), 479 (w), 442 (w), 421 (w) cm^{-1}.

HRMS (ESI+, MeOH): m/z (found) = 227.15411 (100 %), 228.15739 (16 %), 229.16069 (1 %); m/z (calc.) = 227.15428 (100 %, $^{12}C_{15}{}^{1}H_{19}{}^{14}N_2{}^{+}$), 228.15763 (16 %, $^{12}C_{14}{}^{13}C^{1}H_{19}{}^{14}N_2{}^{+}$), 229.16098 (1 %, $^{12}C_{13}{}^{13}C_2{}^{1}H_{19}{}^{14}N_2{}^{+}$).

Additional information on the synthesis of the target compound and original analysis data files are available via Chemotion Repository: https://dx.doi.org/10.14272/reaction/SA-FUHFF-UHFFFADPSC-BRNGTXITIQ-UHFFFADPSC-NUHFF-NUHFF-NUHFF-ZZZ

1.3.3.3 Synthesis of TMG2^{c}Hexqu (L4)

TMG2^{c}Hexqu was synthesized and purified analogous to TMG2Mequ starting from 2-cyclohexyl-8-aminoquinoline (2.60 g, 11.49 mmol, 1 eq.) and was obtained as a yellow oil that turns into a pale yellow solid after a few weeks (2.56 g, 7.89 mmol, 68.7 %).

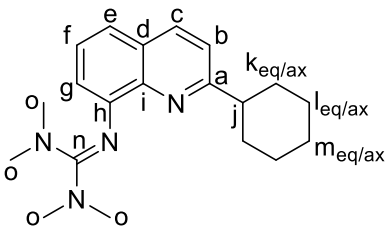

$C_{20}H_{28}N_4$
324.47 g mol^{-1}

^{1}H NMR (400 MHz, $CDCl_3$, 25 °C): δ = 7.95 (d, *J* = 8.5 Hz, 1H, c), 7.33 (t, *J* = 7.6 Hz, 1H, f), 7.20 (dd, *J* = 8.1, 1.5 Hz, 1H, e), 7.17 (d, *J* = 8.5 Hz, 1H, b), 7.15 (dd, *J* = 7.4, 1.5 Hz, 1H, g), 2.78 (tt, *J* = 11.8, 3.5 Hz, 1H, j), 2.69 (s, 12H, o), 2.02 – 1.93 (m, 2H, k_{eq}), 1.85 (dt, *J* = 12.8, 3.4 Hz, 2H, l_{eq}), 1.77 (dtt, *J* = 12.7, 3.2, 1.5 Hz, 1H, m_{eq}), 1.58 (qd, *J* = 12.6, 3.2 Hz, 2H, k_{ax}), 1.42 (qt, *J* = 12.7, 3.3 Hz, 2H, l_{ax}), 1.26 (qt, *J* = 12.7, 3.4 Hz, 1H, m_{ax}) ppm.

^{13}C NMR (101 MHz, $CDCl_3$, 25 °C) δ = 163.9 (a), 162.5 (n), 149.8 (h), 141.8 (i), 136.2 (c), 127.8 (d), 126.5 (f), 120.3 (g), 119.5 (b), 118.5 (e), 47.3 (j), 39.6 (o), 32.7 (k), 26.8 (l), 26.5 (m) ppm.

IR (ATR, neat): $\tilde{\nu}$ = 3046 (vw, ν(C-H_{arom})), 2998 (vw, ν(C-H_{aliph})), 2920 (m, ν(C-H_{aliph})), 2882 (w, ν(C-H_{aliph})), 2848 (m, ν(C-H_{aliph})), 2810 (vw, ν(C-H_{aliph})), 2786 (vw, ν(C-H_{aliph})), 1610 (m), 1582 (s, ν(C-N_{gua})), 1552 (s, ν(C-N_{gua})), 1495 (m), 1461 (w), 1446 (m), 1426 (m), 1421 (m), 1408 (w), 1373 (s), 1305 (w), 1263 (vw), 1236 (w), 1221 (m), 1193 (vw), 1164 (vw), 1138 (s), 1105 (w), 1083 (w), 1058 (m), 1010 (s), 964 (w), 952 (vw), 929 (w), 919 (w), 891 (w), 881 (w), 847 (vw), 830 (vs), 812 (m), 787 (vw), 773 (vw), 755 (m), 743 (s), 712 (m), 675 (m), 629 (vw), 564 (w), 533 (w), 510 (vw), 456 (w), 447 (m), 420 (w) cm^{-1}.

HRMS (ESI+, MeOH): m/z (found) = 325.23816 (100 %), 326.24142 (22 %), 327.24466 (2 %); m/z (calc.) = 325.23867 (100 %, $^{12}C_{20}{}^{1}H_{29}{}^{14}N_4{}^{+}$), 326.24203 (22 %, $^{12}C_{19}{}^{13}C^{1}H_{29}{}^{14}N_4{}^{+}$), 327.24538 (2 %, $^{12}C_{18}{}^{13}C_2{}^{1}H_{29}{}^{14}N_4{}^{+}$).

Additional information on the synthesis of the target compound and original analysis data files are available via Chemotion Repository: https://dx.doi.org/10.14272/reaction/SA-FUHFF-UHFFFADPSC-ACOFZHHYLN-UHFFFADPSC-NUHFF-NUHFF-NUHFF-ZZZ

1.3.4 Synthesis of TMG2Meequ (L5) and corresponding precursors

1.3.4.1 Resynthesis of 2-tribromomethyl-8-nitroquinoline (2-CBr_3-8-NO_2-qu)

The synthesis was performed following a modified procedure of the literature.[9]

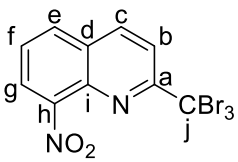

$C_{10}H_5Br_3N_2O_2$
424.87 g mol^{-1}

2-Methyl-8-nitroquinoline (18.82 g, 100 mmol, 1 eq.) was suspended in a saturated solution of anhydrous sodium acetate in glacial acetic acid (500 mL). A solution of bromine (53.27 g, 17.07 mL, 333 mmol, 3.33 eq.) in glacial acetic acid (100 mL) was added under stirring over 1 h at rt. Then, the reaction mixture was heated to 80 °C for 40 min. After cooling to rt the mixture was poured into water (1 L) under stirring and the resulting yellow precipitate was filtered off and then solved in DCM. The organic layer was washed with an aqueous solution of NaS_2O_3. The organic layer was separated, dried over Na_2SO_4 and filtered. The solvent was reduced under reduced pressure. By the addition of pentane to the solution, a colorless precipitate was formed. The precipitate was filtered off, washed with pentane and dried under reduced pressure. 2-Tribromomethyl-8-nitroquinoline was obtained as a colorless crystalline solid (39.27 g, 92.64 mmol, 92.6 %).

^{1}H NMR (400 MHz, $CDCl_3$, 25 °C): δ = 8.39-8.34 (m, 2H, b+c), 8.13 (dd, J = 7.5, 1.4 Hz, 1H, g), 8.09 (dd, J = 8.3, 1.4 Hz, 1H, e), 7.72 (dd, J = 8.3, 7.5 Hz, 1H, f) ppm.

^{13}C NMR (101 MHz, $CDCl_3$, 25 °C) δ = 160.5 (a), 148.4 (h), 137.9 (c), 136.4 (i), 131.4 (e), 128.3 (d), 127.3 (f), 125.0 (g), 120.0 (b), 39.7 (j) ppm.

IR (ATR, neat): $\tilde{\nu}$ = 3076 (vw, ν(C-H_{arom})), 1623 (vw) 1597 (w), 1562 (w), 1528 (s, ν(C-NO_2)), 1496 (m), 1427 (w), 1384 (w), 1358 (m), 1304 (m), 1217 (vw), 1191 (vw), 1161 (w), 1147 (w), 1024 (w), 927 (m), 875 (m), 845 (m), 798 (m), 771 (m), 763 (s), 737 (vs), 652 (vs), 638 (s), 594 (w), 544 (w), 526 (m), 459 (w), 439 (w) cm^{-1}.

HRMS (ESI+, MeOH): m/z (found) = 444.77887 (35 %), 445.78206 (4 %), 446.77686 (100 %), 447.78000 (12 %), 448.77483 (99 %), 449.77797 (11 %), 450.77290 (33 %), 451.77591 (3 %); m/z (calc.) = 444.77934 (34 %, $^{23}Na^{12}C_{10}{}^{1}H_5{}^{79}Br_3{}^{14}N_2{}^{16}O_2{}^{+}$), 445.78269 (4 %, $^{23}Na^{12}C_9{}^{13}C^{1}H_5{}^{79}Br_3{}^{14}N_2{}^{16}O_2{}^{+}$), 446.77729 (100 %, $^{23}Na^{12}C_{10}{}^{1}H_5{}^{79}Br_2{}^{81}Br^{14}N_2{}^{16}O_2{}^{+}$), 447.78065 (11 %, $^{23}Na^{12}C_9{}^{13}C^{1}H_5{}^{79}Br_2{}^{81}Br^{14}N_2{}^{16}O_2{}^{+}$), 448.77524 (97 %, $^{23}Na^{12}C_{10}{}^{1}H_5{}^{79}Br^{81}Br_2{}^{14}N_2{}^{16}O_2{}^{+}$), 449.77860 (11 %, $^{23}Na^{12}C_9{}^{13}C^{1}H_5{}^{79}Br^{81}Br_2{}^{14}N_2{}^{16}O_2{}^{+}$), 450.77320 (32 %, $^{23}Na^{12}C_{10}{}^{1}H_5{}^{81}Br_3{}^{14}N_2{}^{16}O_2{}^{+}$), 451.77655 (3 %, $^{23}Na^{12}C_9{}^{13}C^{1}H_5{}^{81}Br_3{}^{14}N_2{}^{16}O_2{}^{+}$).

Additional information on the synthesis of the target compound and original analysis data files are available via Chemotion Repository: https://dx.doi.org/10.14272/reaction/SA-FUHFF-UHFFFADPSC-QLLLYNCAUW-UHFFFADPSC-NUHFF-NUHFF-NUHFF-ZZZ

1.3.4.2 Resynthesis of 8-nitroquinoline-2-carboxylic acid (2-COOH-8-NO_2-qu)

The synthesis was performed following a modified procedure of the literature.[9]

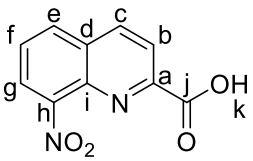

$C_{10}H_6N_2O_4$
218.17 g mol^{-1}

2-Tribromomethyl-8-nitroquinoline (20.00 g, 47.18 mmol, 1 eq.) was suspended in 30 w% aqueous H_2SO_4 (400 mL, 333.6 mL H_2O + 84.4 mL conc. H_2SO_4). The reaction mixture was heated to 120 °C for 72 h. After cooling the mixture was warm filtrated through a porous glass frit with glass wool. After cooling to rt the reaction mixture was poured into water (750 ml) under stirring. The resulting precipitate was filtrated and washed with water. A beige solid that contains water was obtained. The solid can be used in the next step without any further purification. To remove the water the solid was dissolved in DCM or MeOH but because of the poor dissolubility big amounts are necessary to dissolve the solid completely. The organic layer was dried over Na_2SO_4 and filtrated. The solvent was removed under reduced pressure. 8-Nitroquinoline-2-carboxylic acid was obtained as a beige solid (9.28 g, 42.56 mmol, 90.2 %).

^{1}H NMR (400 MHz, $CDCl_3$, 25 °C): δ = 10.91 (s, 1H, k), 8.58 (d, J = 8.5 Hz, 1H, c), 8.46 (d, J = 8.5 Hz, 1H, b), 8.32 (dd, J = 7.6, 1.3 Hz, 1H, g), 8.22 (dd, J = 8.3, 1.3 Hz, 1H, e), 7.84 (dd, J = 8.4, 7.5 Hz, 1H, f) ppm.

^{13}C NMR (101 MHz, $CDCl_3$, 25 °C) δ = 163.1 (j), 148.1 (a), 139.6 (c), 137.5 (i), 132.7 (e), 130.6 (d), 128.1 (f), 126.4 (g), 121.2 (b) ppm.

IR (ATR, neat): $\tilde{\nu}$ = 3180 (w), 3071 (vw, ν(C-H_{arom})), 1716 (w), 1664 (w), 1631 (m), 1585 (m), 1557 (w), 1522 (m, ν(C-NO_2)), 1493 (m), 1459 (m), 1429 (w), 1387 (vw), 1350 (m), 1338 (s), 1314 (m), 1298 (m), 1253 (m), 1219 (m), 1171 (w), 1130 (w), 1110 (m), 1029 (w), 921 (w), 904 (w), 895 (w), 868 (m), 860 (m), 826 (m), 803 (w), 796 (w), 780 (m), 771 (m), 753 (m), 746 (vs), 657 (m), 641 (w), 607 (m), 599 (w), 589 (w), 534 (m), 511 (m), 482 (w), 473 (m), 400 (m) cm^{-1}.

HRMS (ESI+, MeOH): m/z (found) = 219.04001 (100 %), 220.04327 (11 %), 221.04506 (1 %); m/z (calc.) = 219.04003 (100 %, $^{12}C_{10}{}^{1}H_7{}^{14}N_2{}^{16}O_4{}^{+}$), 220.04339 (11 %, $^{12}C_9{}^{13}C^{1}H_7{}^{14}N_2{}^{16}O_4{}^{+}$), 221.04428 (<1 %, $^{12}C_{10}{}^{1}H_7{}^{14}N_2{}^{16}O_3{}^{18}O^{+}$), 221.04674 (<1%, $^{12}C_8{}^{13}C_2{}^{1}H_7{}^{14}N_2{}^{16}O_4{}^{+}$).

Additional information on the synthesis of the target compound and original analysis data files are available via Chemotion Repository: https://dx.doi.org/10.14272/reaction/SA-FUHFF-UHFFFADPSC-YKNRUBPOGQ-UHFFFADPSC-NUHFF-NUHFF-NUHFF-ZZZ

1.3.4.3 Synthesis of methyl 8-nitroquinoline-2-carboxylate (2-Mee-8-NO_2-qu)

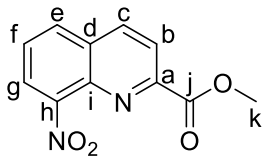

$C_{11}H_8N_2O_4$
232.20 g mol^{-1}

8-Nitroquinoline-2-carboxylic acid (9.28 g, 42.56 mmol, 1 eq.) was dissolved in methanol (150 mL) and conc. H_2SO_4 (14 ml) was added under stirring at 0 °C. The reaction mixture was heated to reflux for 18 h. After cooling to rt water (120 mL) was added to the mixture under stirring. A precipitate formed which was dissolved by adding DCM (130 mL). The organic layer was separated and the aqueous layer was extracted with DCM (3x 100 mL). The organic layer was dried over Na_2SO_4 and filtered through Geduran. The solution was concentrated under reduced pressure. Pentane was added to the solution and a beige precipitate formed. The solid was

filtered off, washed with pentane and dried under reduced pressure. Methyl 8-nitroquinoline-2-carboxylate was obtained as a beige crystalline solid (9.49 g, 40.90 mmol, 96.1 %).

^{1}H NMR (400 MHz, $CDCl_3$, 25 °C): δ = 8.42 (d, *J* = 8.6 Hz, 1H, c), 8.32 (d, *J* = 8.6 Hz, 1H, b), 8.14 (dd, *J* = 7.5, 1.3 Hz, 1H, g), 8.11 (dd, *J* = 8.3, 1.4 Hz, 1H, e), 7.73 (dd, *J* = 8.3, 7.5 Hz, 1H, f), 4.05 (s, 3H, k) ppm.

^{13}C NMR (101 MHz, $CDCl_3$, 25 °C) δ = 165.4 (j), 150.2 (a), 148.7 (h), 139.1 (i), 137.6 (c), 132.0 (e), 129.9 (d), 127.4 (f), 124.9 (g), 122.8 (b), 53.4 (k) ppm.

IR (ATR, neat): $\tilde{\nu}$ = 3067 (vw, ν(C-H_{arom})), 2965 (vw, ν(C-H_{aliph})) 1742 (m), 1623 (vw), 1595 (vw), 1564 (w), 1520 (m, ν(C-NO_2)), 1499 (w), 1464 (w), 1423 (w), 1367 (m), 1315 (m), 1281 (s), 1223 (m), 1192 (m), 1160 (m), 1127 (s), 1063 (w), 1025 (vw), 998 (vw), 977 (m), 888 (w), 862 (s), 827 (w), 799 (m), 793 (m), 767 (vs), 727 (w), 658 (s), 518 (m), 498 (w), 400 (w) cm^{-1}.

HRMS (ESI+, MeOH): m/z (found) = 233.05572 (100 %), 234.05894 (12 %), 235.06093 (1 %); m/z (calc.) = 233.05568 (100 %, $^{12}C_{11}{}^{1}H_9{}^{14}N_2{}^{16}O_4{}^{+}$), 234.05904 (12 %, $^{12}C_{10}{}^{13}C^{1}H_9{}^{14}N_2{}^{16}O_4{}^{+}$), 235.05993 (1 %, $^{12}C_{11}{}^{1}H_9{}^{14}N_2{}^{16}O_3{}^{18}O^{+}$).

Additional information on the synthesis of the target compound and original analysis data files are available via Chemotion Repository: https://dx.doi.org/10.14272/reaction/SA-FUHFF-UHFFFADPSC-ZJSFNHZUYT-UHFFFADPSC-NUHFF-NUHFF-NUHFF-ZZZ

1.3.4.4 Synthesis of methyl 8-aminoquinoline-2-carboxylate (2-Mee-8-NH_2-qu)

Methyl 8-aminoquinoline-2-carboxylate was synthesized analogous to 2-methyl-8-aminoquinoline starting from methyl 8-nitroquinoline-2-carboxylate (15 g, 64.64 mmol, 1 eq.). The reaction mixture was purified by column chromatography (isoexane:ethyl acetate = 3:2, Geduran, R_f = 0.49). Methyl 8-aminoquinoline-2-carboxylate was obtained as an orange solid (11.02 g, 54.50 mmol, 84.3 %).

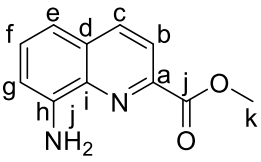

$C_{11}H_{10}N_2O_2$

202.21 g mol^{-1}

^{1}H NMR (400 MHz, $CDCl_3$, 25 °C): δ = 8.18 (d, *J* = 8.6 Hz, 1H, c), 8.11 (d, *J* = 8.5 Hz, 1H, b), 7.42 (dd, *J* = 8.2, 7.6 Hz, 1H, f), 7.16 (dd, *J* = 8.2, 1.2 Hz, 1H, e), 6.95 (dd, *J* = 7.6, 1.2 Hz, 1H, g), 5.17 (s, 2H, l), 4.04 (s, 3H, k) ppm.

^{13}C NMR (101 MHz, $CDCl_3$, 25 °C) δ = 166.2 (j), 145.3 (h), 144.9 (a), 137.7 (i), 137.1 (c), 130.2 (d), 130.0 (f), 121.3 (b), 115.4 (e), 110.3 (g), 52.9 (k) ppm.

IR (ATR, neat): $\tilde{\nu}$ = 3431 (w, ν(N-H)), 3343 (m, ν(N-H)), 3077 (vw, ν(C-H_{arom})), 3041 (vw, ν(C-H_{arom})), 2998 (vw, ν(C-H_{aliph})), 2948 (w, ν(C-H_{aliph})) 1731 (vs, ν(C=O)), 1613 (s), 1586 (m), 1504 (m), 1473 (m), 1433 (m), 1375 (m), 1343 (m), 1289 (s), 1263 (vs), 1226 (w), 1190 (m), 1149 (m), 1129 (s), 1090 (w), 989 (m), 959 (vw), 903 (vw), 869 (m), 854 (m), 842 (m), 816 (m), 790 (m), 771 (s), 758 (vs), 652 (w), 613 (w), 583 (w), 526 (w), 508 (m), 445 (m), 425 (m) cm^{-1}.

HRMS (ESI+, MeOH): m/z (found) = 203.08118 (100 %) 204.08446 (12 %), 205.08678 (1 %); m/z (calc.) = 203.08150 (100 %, $^{12}C_{11}{}^{1}H_{11}{}^{14}N_2{}^{16}O_2{}^{+}$), 204.08486 (12 %, $^{12}C_{10}{}^{13}C^{1}H_{11}{}^{14}N_2{}^{16}O_2{}^{+}$), 205.08728 (1 %, $^{12}C_9{}^{13}C_2{}^{1}H_{11}{}^{14}N_2{}^{16}O_2{}^{+}$, $^{12}C_{11}{}^{1}H_{11}{}^{14}N_2{}^{16}O^{18}O^{+}$).

Additional information on the synthesis of the target compound and original analysis data files are available via Chemotion Repository: https://dx.doi.org/10.14272/reaction/SA-FUHFF-UHFFFADPSC-HXVOLPKNEJ-UHFFFADPSC-NUHFF-NUHFF-NUHFF-ZZZ

1.3.4.5 Synthesis of TMG2Meequ (L5)

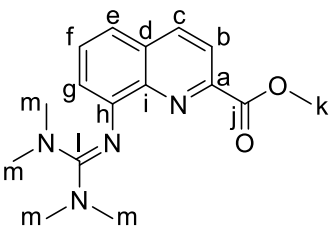

$C_{16}H_{20}N_4O_2$
300.36 g mol^{-1}

Due to the sensitivity of the ester group against bases the synthesis was modified compared to the synthesis of TMG2Mequ.

Methyl 8-aminoquinoline-2-carboxylate (5.00 g, 24.7 mmol, 1 eq.) and TMG-VS (5.06 g, 29.6 mmol, 1.2 eq.) were dissolved in MeCN (80 mL) and triethylamine (6.9 mL, 49.4 mmol, 2 eq.) was added. The reaction mixture was heated to reflux for 30 min under stirring. After cooling to rt the solvent was removed under reduced pressure. To the resulting solid a less concentrated aqueous KOH solution (20 mL, 33 w%) was added and the mixture was mixed for several seconds. The aqueous layer was extracted with MeCN (100 mL). The organic layer was dried over Na_2SO_4 and the solvent was removed under reduced pressure. The resulting red oil was dissolved in DCM (4 mL) and the solution was filtered through aluminia with DCM as eluent. The solvent was removed under reduced pressure. TMG2Meequ was obtained as a red oil (5.38 g, 17.9 mmol, 72.4 %). The ligand cannot be distilled due to decomposition of the ester group.

^{1}H NMR (400 MHz, $CDCl_3$, 25 °C): δ = 8.13 (d, J = 8.5 Hz, 1H, c), 8.00 (d, J = 8.5 Hz, 1H, b), 7.50 (dd, J = 8.1, 7.5 Hz, 1H, f), 7.23 (dd, J = 8.2, 1.4 Hz, 1H, e), 7.20 (dd, J = 7.6, 1.4 Hz, 1H, g), 3.95 (s, 3H, k), 2.68 (s, 12H, m) ppm.

^{13}C NMR (101 MHz, $CDCl_3$, 25 °C) δ = 166.3 (j), 163.9 (l), 152.1 (h), 145.2 (a), 141.4 (i), 136.9 (c), 130.5 (d), 130.2 (f), 120.4 (b), 120.3 (g), 117.3 (e), 52.4 (k), 39.4 (m) ppm.

IR (ATR, neat): $\tilde{\nu}$ = 2997 (vw, ν(C-H_{arom})), 2924 (w, ν(C-H_{aliph})), 2878 (w, ν(C-H_{aliph})), 2791 (vw, ν(C-H_{aliph})), 1742 (m), 1717 (s, ν(C=O)), 1569 (s, ν(C-N_{gua})), 1542 (s, ν(C-N_{gua})), 1506 (m), 1496 (m), 1472 (m), 1447 (m), 1423 (m), 1382 (m), 1357 (m), 1315 (m), 1289 (m), 1262 (m), 1224 (m), 1191 (w), 1136 (vs), 1122 (vs), 1085 (w), 1060 (w), 1012 (s), 969 (w), 923 (w), 895 (w), 872 (w), 848 (s), 822 (w), 789 (m), 779 (m), 768 (s), 752 (s), 680 (m), 660 (m), 621 (vw), 601 (w), 563 (w), 539 (vw), 452 (m), 425 (w) cm^{-1}.

HRMS (ESI+, MeOH): m/z (found) = 301.16497 (100 %), 302.16795 (20 %), 303.17062 (2 %); m/z (calc.) = 301.16590 (100 %, $^{12}C_{16}{}^{1}H_{21}{}^{14}N_4{}^{16}O_2{}^{+}$), 302.16926 (17 %, $^{12}C_{15}{}^{13}C^{1}H_{21}{}^{14}N_4{}^{16}O_2{}^{+}$), 303.17261 (1 %, $^{12}C_{14}{}^{13}C_2{}^{1}H_{21}{}^{14}N_4{}^{16}O_2{}^{+}$).

Additional information on the synthesis of the target compound and original analysis data files are available via Chemotion Repository: https://dx.doi.org/10.14272/reaction/SA-FUHFF-UHFFFADPSC-FYZDDQVKLM-UHFFFADPSC-NUHFF-NUHFF-NUHFF-ZZZ

1.3.5 Synthesis of TMG4NMe$_2$qu (L6) and corresponding precursors

1.3.5.1 Synthesis of 4-chloro-8-nitroquinoline (4-Cl-8-NO$_2$-qu)

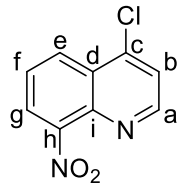

$C_9H_5ClN_2O_2$
208.60 g mol^{-1}

4-Chloroquinoline (19.50 g, 119.19 mmol, 1 eq.) was dissolved in conc. H_2SO_4 (92 mL). Fuming HNO_3 (26.29 g, 17.41 mL, 417.24 mmol, 3.5 eq.) was added under stirring at 0 °C. The reaction mixture was stirred for 4 h at rt and then poured on ice water. The mixture was neutralized with a saturated aqueous $NaHCO_3$ solution. The formed yellow solid was filtered off and then dissolved in DCM. The organic layer was dried over Na_2SO_4 and the solvent was removed under reduced pressure. The resulting solid was purified by column chromatography (isohexane:DCM; = 1:1, Geduran, R_f = 0.37). 4-Chloro-8-nitroquinoline was obtained as a pale yellow solid (11.27 g, 54.03 mmol, 45.3 %).

^{1}H NMR (400 MHz, $CDCl_3$, 25 °C): δ = 8.93 (d, J = 4.7 Hz, 1H, a), 8.48 (dd, J = 8.6, 1.3 Hz, 1H, e), 8.08 (dd, J = 7.5, 1.4 Hz, 1H, g), 7.74 (dd, J = 8.5, 7.5 Hz, 1H, f), 7.66 (d, J = 4.7 Hz, 1H, b) ppm.

^{13}C NMR (101 MHz, $CDCl_3$, 25 °C) δ = 152.1 (a), 148.8 (h), 143.2 (c), 140.6 (i), 128.3 (e), 127.5 (d), 126.5 (f), 124.4 (g), 123.1 (b) ppm.

IR (ATR, neat): $\tilde{\nu}$ = 3077 (w, ν(C-H$_{arom}$)), 3059 (vw, ν(C-H$_{arom}$)), 3048 (w, ν(C-H$_{arom}$)), 1960 (w), 1621 (w), 1588 (w), 1559 (w), 1523 (m, ν(C-NO$_2$)), 1486 (m), 1463 (m), 1406 (w), 1355 (s), 1297 (m), 1216 (m), 1206 (m), 1090 (m), 1047 (m), 929 (w), 880 (m), 865 (s), 827 (m), 820 (m), 807 (m), 767 (m), 748 (vs), 717 (s), 652 (w), 593 (w), 554 (vw), 509 (m), 465 (m), 404 (m) cm^{-1}.

HRMS (ESI+, MeOH): m/z (found) = 209.01115 (100 %), 210.01437 (10 %), 211.00812 (32 %), 212.01141 (3 %); m/z (calc.) = 209.01123 (100 %, $^{12}C_9{}^1H_6{}^{35}Cl^{14}N_2{}^{16}O_2{}^+$), 210.01459 (10 %, $^{12}C_8{}^{13}C^1H_6{}^{35}Cl^{14}N_2{}^{16}O_2{}^+$), 211.00828 (32 %, $^{12}C_9{}^1H_6{}^{37}Cl^{14}N_2{}^{16}O_2{}^+$), 212.01164 (3 %, $^{12}C_8{}^{13}C^1H_6{}^{37}Cl^{14}N_2{}^{16}O_2{}^+$).

Additional information on the synthesis of the target compound and original analysis data files are available via Chemotion Repository: https://dx.doi.org/10.14272/reaction/SA-FUHFF-UHFFFADPSC-AOATVJLAFL-UHFFFADPSC-NUHFF-NUHFF-NUHFF-ZZZ

1.3.5.2 Synthesis of 4-dimethylamine-8-nitroquinoline (4-NMe$_2$-8-NO$_2$-qu)

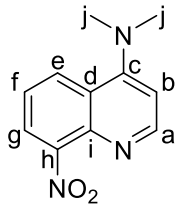

$C_{11}H_{11}N_3O_2$
217.23 g mol^{-1}

4-Chloro-8-nitroquinoline (11.00 g, 52.73 mmol, 1 eq.), dimethylamine hydrochloride (25.80 g, 316.41 mmol, 6 eq.), water (50 mL) and ethanol (10 mL) were combined in high pressure flask. NaOH (12.66 g, 316.41 mmol, 6 eq.) was added and the flask was sealed quickly. Instantly a gas formation was observable. The mixture was stirred for 4 h at 130 °C. After cooling to rt the flask was opened and the reaction mixture was extracted with DCM (6x 50 mL). The organic layer was dried over Na_2SO_4 and concentrated under reduced pressure. The solution was filtered through alumina with DCM as eluent and the solvent was removed under reduced pressure resulting 4-dimethylamine-8-nitroquinoline as an intensive yellow solid (8.80 g, 40.51 mmol, 76.8 %).

^{1}H NMR (400 MHz, $CDCl_3$, 25 °C): δ = 8.75 (d, *J* = 5.3 Hz, 1H, a), 8.24 (dd, *J* = 8.6, 1.4 Hz, 1H, e), 7.92 (dd, *J* = 7.5, 1.4 Hz, 1H, g), 7.48 (dd, *J* = 8.6, 7.5 Hz, 1H, f), 6.84 (d, *J* = 5.3 Hz, 1H, b), 3.09 (s, 6H, j) ppm.

^{13}C NMR (101 MHz, $CDCl_3$, 25 °C) δ = 157.6 (c), 152.4 (a), 149.0 (h), 141.4 (i), 128.9 (e), 124.1 (d), 123.2 (g), 122.8 (f), 108.3 (b), 44.1 (j) ppm.

IR (ATR, neat): $\tilde{\nu}$ = 2924 (w, ν(C-H_{aliph})), 2857 (w, ν(C-H_{aliph})), 1573 (m), 1517 (s, ν(C-NO_2)), 1485 (w), 1448 (m), 1420 (m), 1396 (w), 1374 (m), 1364 (m), 1331 (m), 1288 (m), 1242 (w), 1197 (m), 1166 (w), 1135 (m), 1125 (w), 1108 (vw), 1088 (w), 1064 (m), 965 (m), 917 (w), 878 (s), 830 (m), 816 (s), 763 (vs), 710 (m), 699 (m), 606 (w), 589 (vw), 545 (m), 509 (vw), 489 (w), 468 (w), 415 (vw) cm^{-1}.

HRMS (ESI+, MeOH): m/z (found) = 218.09232 (100 %), 219.09554 (11 %), 220.09959 (1 %); m/z (calc.) = 218.09240 (100 %, $^{12}C_{11}{}^{1}H_{12}{}^{14}N_3{}^{16}O_2{}^{+}$), 219.09576 (12 %, $^{12}C_{10}{}^{13}C^{1}H_{12}{}^{14}N_3{}^{16}O_2{}^{+}$), 220.09911 (1 %, $^{12}C_9{}^{13}C_2{}^{1}H_{12}{}^{14}N_3{}^{16}O_2{}^{+}$).

Additional information on the synthesis of the target compound and original analysis data files are available via Chemotion Repository: https://dx.doi.org/10.14272/reaction/SA-FUHFF-UHFFFADPSC-XTTRESRELV-UHFFFADPSC-NUHFF-NUHFF-NUHFF-ZZZ

1.3.5.3 Synthesis of 4-dimethylamine-8-aminoquinoline (4-NMe_2-8-NH_2-qu)

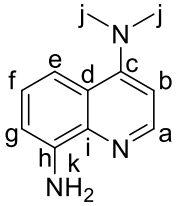

$C_{11}H_{13}N_3$
187.25 g mol^{-1}

4-Dimethylamine-8-aminoquinoline was synthesized analogous to 2-methyl-8-aminoquinoline starting from 4-dimethylamine-8-nitroquinoline (10.00 g, 46.03 mmol, 1 eq.) and was obtained as a pale brown oil (5.07 g, 27.08 mmol, 58.8 %).

^{1}H NMR (400 MHz, $CDCl_3$, 25 °C): δ = 8.54 (d, *J* = 5.0 Hz, 1H, a), 7.37 (dd, *J* = 8.5, 1.3 Hz, 1H, e), 7.24 (dd, *J* = 8.5, 7.4 Hz, 1H, f), 6.87 (dd, *J* = 7.4, 1.3 Hz, 1H, g), 6.75 (d, *J* = 5.1 Hz, 1H, b), 4.97 (s, 2H, k), 3.00 (s, 6H, j) ppm.

^{13}C NMR (101 MHz, $CDCl_3$, 25 °C) δ = 157.7 (c), 147.6 (a), 144.5 (h), 139.8 (i), 125.5 (f), 123.6 (d), 113.0 (e), 109.9 (g), 107.8 (b), 44.0 (j) ppm.

IR (ATR, neat): $\tilde{\nu}$ = 3433 (m, ν(N-H)), 3278 (m, ν(N-H)), 3002 (vw, ν(C-H_{arom})), 2986 (vw, ν(C-H_{aliph})), 2952 (w, ν(C-H_{aliph})), 2874 (w, ν(C-H_{aliph})), 2839 (w, ν(C-H_{aliph})), 2789 (w, ν(C-H_{aliph})), 2171 (vw), 1613 (m), 1574 (m), 1513 (vs), 1471 (m), 1455 (m), 1444 (m), 1418 (m), 1402 (s), 1368 (m), 1331 (m), 1312 (m), 1283 (w), 1217 (w), 1196 (w), 1185 (m), 1144 (m), 1098 (w), 1058 (m), 1050 (m), 970 (s), 895 (m), 880 (w), 852 (m), 829 (m), 818 (m), 797 (w), 765 (s), 731 (w), 690 (m), 638 (w), 614 (m), 559 (m), 532 (m), 448 (m) cm^{-1}.

HRMS (ESI+, MeOH): m/z (found) = 188.11815 (100 %), 189.12148 (11 %), 190.12523 (1 %); m/z (calc.) = 188.11822 (100 %, $^{12}C_{11}{}^{1}H_{14}{}^{14}N_3{}^{+}$), 189.12158 (12 %, $^{12}C_{10}{}^{13}C^{1}H_{14}{}^{14}N_3{}^{+}$), 190.12493 (1 %, $^{12}C_9{}^{13}C_2{}^{1}H_{14}{}^{14}N_3{}^{+}$).

Additional information on the synthesis of the target compound and original analysis data files are available via Chemotion Repository: https://dx.doi.org/10.14272/reaction/SA-FUHFF-UHFFFADPSC-MCYXBNUZMI-UHFFFADPSC-NUHFF-NUHFF-NUHFF-ZZZ

1.3.5.4 Synthesis of TMG4NMe$_2$qu (L6)

TMG4NMe$_2$qu was synthesized analogous to TMG2Mequ starting from 4-dimethylamine-8-aminoquinoline (5.00 g, 26.70 mmol, 1 eq.) and was obtained as a yellow oil that turns into a pale yellow solid after a few weeks (5.58 g, 19.54 mmol, 73.2 %).

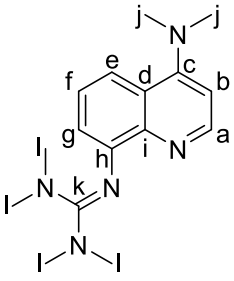

$C_{16}H_{23}N_5$
285.40 g mol^{-1}

^{1}H NMR (400 MHz, $CDCl_3$, 25 °C): δ = 8.63 (d, J = 4.9 Hz, 1H, a), 7.51 (dd, J = 8.4, 1.4 Hz, 1H, e), 7.28 (dd, J = 8.4, 7.4 Hz, 1H, f), 6.76 (dd, J = 7.4, 1.3 Hz, 1H, g), 6.71 (d, J = 5.0 Hz, 1H, b), 2.96 (s, 6H, j), 2.70 (s, 12H, l) ppm.

^{13}C NMR (101 MHz, $CDCl_3$, 25 °C) δ = 161.2 (k), 157.6 (c), 150.6 (h), 148.8 (a), 144.5 (i), 125.3 (f), 124.3 (d), 118.7 (g), 115.5 (e), 107.6 (b), 44.1 (j), 39.7 (l) ppm.

IR (ATR, neat): $\tilde{\nu}$ = 2998 (vw, ν(C-H$_{aliph}$)), 2925 (w, ν(C-H$_{aliph}$)), 2871 (w, ν(C-H$_{aliph}$)), 2788 (w, ν(C-H$_{aliph}$)), 1595 (m), 1579 (s, ν(C-N$_{gua}$)), 1558 (s, ν(C-N$_{gua}$)), 1500 (vs, ν(C-N$_{gua}$)), 1454 (s), 1422 (m), 1406 (m), 1376 (s), 1352 (m), 1328 (w), 1284 (m), 1226 (w), 1200 (w), 1185 (vw), 1136 (s), 1100 (w), 1056 (w), 1020 (m), 970 (s), 924 (w), 890 (w), 815 (m), 802 (m), 758 (m), 723 (w), 710 (w), 615 (vw), 600 (vw), 570 (w), 538 (vw), 520 (vw), 473 (w) cm^{-1}.

HRMS (ESI+, MeOH): m/z (found) = 286.20273 (100 %), 287.20581 (17 %), 288.20898 (1 %); m/z (calc.) = 286.20262 (100 %, $^{12}C_{16}{}^{1}H_{24}{}^{14}N_5{}^{+}$), 287.20598 (17 %, $^{12}C_{15}{}^{13}C^{1}H_{24}{}^{14}N_5{}^{+}$), 288.20933 (1 %, $^{12}C_{14}{}^{13}C_2{}^{1}H_{24}{}^{14}N_5{}^{+}$).

Additional information on the synthesis of the target compound and original analysis data files are available via Chemotion Repository: https://dx.doi.org/10.14272/reaction/SA-FUHFF-UHFFFADPSC-NNDILYOKJA-UHFFFADPSC-NUHFF-NUHFF-NUHFF-ZZZ

1.4 Complex synthesis

1.4.1 Synthesis of [Cu(TMG2Mequ)$_2$]$^{+/2+}$ (R2) complexes

1.4.1.1 Synthesis of [Cu(TMG2Mequ)$_2$]PF$_6$ (C3–PF$_6$)

To a solution of TMG2Mequ (25.6 mg, 0.1 mmol, 2 eq.) in DCM (1 ml) a solution of [Cu(MeCN)$_4$]PF$_6$ (18.6 mg, 0.05 mmol, 1 eq.) in DCM (1 mL) was added. The resulting solution became instantly dark red. By slow diffusion of pentane the complex [Cu(TMG2Mequ)$_2$]PF$_6$ crystallized as dark red crystals.

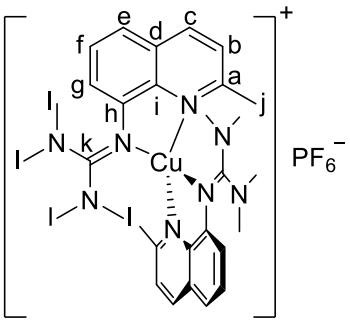

$C_{30}H_{40}CuF_6N_8P$
721.22 g mol^{-1}

^{1}H NMR (400 MHz, MeCN-d$_3$, 25 °C): δ = 8.26 (dd, J = 8.4 Hz, 2H, c), 7.48 (dd, J = 8.1, 7.1 Hz, 2H, f), 7.45 (d, J = 8.5 Hz, 2H, b), 7.44 (dd, J = 8.1, 1.8 Hz, 2H, e), 6.84 (dd, J = 7.0, 1.8 Hz, 2H, g), 2.81 (s, 8H, l), 2.58 (s, 6H, j), 2.39 (s, 16H, l) ppm.

^{13}C NMR (101 MHz, MeCN-d$_3$, 25 °C) δ = 163.5 (k), 156.4 (a), 147.7 (h), 141.9 (i), 137.7 (c), 128.8 (d), 128.0 (f), 124.0 (b), 119.7 (e), 118.8 (g), 39.4 (l), 26.9 (j) ppm.

IR (ATR, neat): $\tilde{\nu}$ = 2930 (w, ν(C-H_{aliph})), 2876 (w, ν(C-H_{aliph})), 1598 (vw), 1563 (w), 1527 (s, ν(C-N_{gua})), 1503 (m), 1472 (m), 1434 (w), 1423 (m), 1412 (m), 1391 (m), 1346 (w), 1318 (vw), 1273 (w), 1228 (m), 1153 (m), 1141 (m), 1097 (m), 1066 (m), 1053 (m), 1022 (m), 1004 (m), 929 (vw), 911 (w), 877 (m), 836 (s, ν(PF_6)), 829 (s), 812 (w), 783 (m), 775 (m), 757 (m), 748 (m), 697 (w), 640 (w), 585 (w), 556 (vs), 537 (vw), 515 (w), 495 (w), 480 (m), 471 (vw), 446 (m) cm^{-1}.

HRMS (ESI+, MeOH): m/z (found) = 575.26605 (100 %), 576.26898 (33 %), 577.26453 (45 %), 578.26746 (14 %), 579.27087 (2 %), 580.27362 (<1 %); m/z (calc.) = 575.26664 (100 %, $^{12}C_{30}{}^{1}H_{40}{}^{63}Cu^{14}N_8^+$), 576.27000 (32 %, $^{12}C_{29}{}^{13}C^{1}H_{40}{}^{63}Cu^{14}N_8^+$), 577.26483 (45 %, $^{12}C_{30}{}^{1}H_{40}{}^{65}Cu^{14}N_8^+$), 578.26819 (14 %, $^{12}C_{29}{}^{13}C^{1}H_{40}{}^{65}Cu^{14}N_8^+$), 579.27154 (2 %, $^{12}C_{28}{}^{13}C_2{}^{1}H_{40}{}^{65}Cu^{14}N_8^+$), 580.27490 (<1 %, $^{12}C_{27}{}^{13}C_3{}^{1}H_{40}{}^{65}Cu^{14}N_8^+$).

Additional information on the synthesis of the target compound and original analysis data files are available via Chemotion Repository: https://dx.doi.org/10.14272/reaction/SA-FUHFF-UHFFFADPSC-DMWOEMCLSH-UHFFFADPSC-NUHFF-NUHFF-NUHFF-ZZZ

1.4.1.2 Synthesis of [Cu(TMG2Mequ)$_2$]OTf (C3–OTf)

To a solution of TMG2Mequ (25.6 mg, 0.1 mmol, 2 eq.) in DCM (1 ml) a solution of [Cu(MeCN)$_4$]OTf (18.8 mg, 0.05 mmol, 1 eq.) in DCM (1 mL) was added. The resulting solution became instantly dark red. By slow diffusion of pentane the complex [Cu(TMG2Mequ)$_2$]OTf crystallized as dark red crystals.

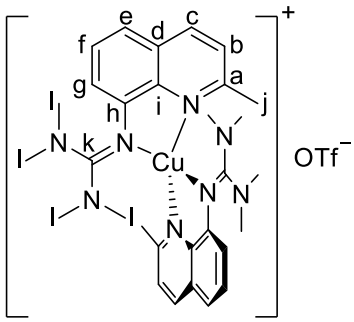

$C_{31}H_{40}CuF_3N_8O_3S$
725.32 g mol^{-1}

^{1}H NMR (400 MHz, MeCN-d_3, 25 °C): δ = 8.26 (d, J = 8.4 Hz, 2H, c), 7.48 (dd, J = 8.2, 7.1 Hz, 2H, f), 7.45 (d, J = 8.4 Hz, 2H, b), 7.44 (dd, J = 8.1, 1.8 Hz, 2H, e), 6.84 (dd, J = 7.0, 1.8 Hz, 2H, g), 2.78 (s, 8H, l), 2.58 (s, 6H, j), 2.39 (s, 16H, l) ppm.

^{13}C NMR (101 MHz, MeCN-d_3, 25 °C) δ = 163.5 (k), 156.4 (a), 147.7 (h), 141.9 (i), 137.7 (c), 128.9 (d), 128.0 (f), 124.0 (b), 122.2 (q, J = 321.2 Hz, OTf), 119.7 (e), 118.8 (g), 39.4 (l), 26.9 (j) ppm.

IR (ATR, neat): $\tilde{\nu}$ = 3062 (vw, ν(C-H_{arom})), 3010 (vw, ν(C-H_{arom})), 2924 (w, ν(C-H_{aliph})), 2873 (w, ν(C-H_{aliph})), 1598 (w), 1562 (m), 1525 (s, ν(C-N_{gua})), 1503 (m), 1471 (m), 1423 (m), 1413 (m), 1391 (m), 1346 (w), 1261 (vs, ν(OTf)), 1223 (m), 1138 (s), 1097 (w), 1066 (w), 1029 (s, ν(OTf)), 1004 (m), 930 (vw), 912 (w), 877 (w), 840 (m), 808 (w), 784 (w), 750 (m), 701 (w), 635 (vs, ν(OTf)), 585 (w), 571 (m), 538 (vw), 516 (m), 497 (w), 483 (vw), 445 (w) cm^{-1}.

HRMS (ESI+, MeCN): m/z(found) = 575.26979 (100 %), 576.27193 (52 %), 577.26797 (71 %), 578.27028 (23 %), 579.27307 (4 %), 580.27602 (<1 %); m/z(calc.) = 575.26664 (100 %, $^{12}C_{30}{}^{1}H_{40}{}^{63}Cu^{14}N_8$), 576.27000 (32 %, $^{12}C_{29}{}^{13}C^{1}H_{40}{}^{63}Cu^{14}N_8$), 577.26483 (45 %, $^{12}C_{30}{}^{1}H_{40}{}^{65}Cu^{14}N_8$), 578.26819 (14 %, $^{12}C_{29}{}^{13}C^{1}H_{40}{}^{65}Cu^{14}N_8$), 579.27154 (2 %, $^{12}C_{28}{}^{13}C_2{}^{1}H_{40}{}^{65}Cu^{14}N_8$), 580.27490 (<1 %, $^{12}C_{27}{}^{13}C_3{}^{1}H_{40}{}^{65}Cu^{14}N_8$).

Additional information on the synthesis of the target compound and original analysis data files are available via Chemotion Repository: https://dx.doi.org/10.14272/reaction/SA-FUHFF-UHFFFADPSC-JZHZQROLCJ-UHFFFADPSC-NUHFF-MUHFF-NUHFF-ZZZ

1.4.1.3 Synthesis of $[Cu(TMG2Mequ)_2](BF_4)_2$ (C4−BF_4)

To a solution of TMG2Mequ (25.6 mg, 0.1 mmol, 2 eq.) in MeCN (1 ml) a solution of $[Cu(MeCN)_4](BF_4)_2$ (20.1 mg, 0.05 mmol, 1 eq.) in MeCN (1 mL) was added. The resulting solution became instantly dark green. Then DCM (1 mL) was added. By slow diffusion of pentane the complex $[Cu(TMG2Mequ)_2](BF_4)_2$ crystallized as dark green crystals.

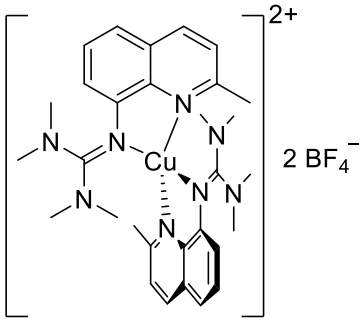

$C_{30}H_{40}B_2CuF_8N_8$
749.86 g mol^{-1}

IR (ATR, neat): $\tilde{\nu}$ = 2936 (vw, ν(C-H_{aliph})), 2167 (vw), 1629 (w), 1603 (w), 1573 (m), 1520 (m, ν(C-N_{gua})), 1507 (m), 1469 (m), 1423 (m), 1401 (m), 1335 (m), 1316 (w), 1273 (w), 1226 (w), 1165 (w), 1148 (w), 1046 (vs, ν(BF_4)), 1028 (vs, ν(BF_4)), 933 (w), 909 (w), 881 (vw), 841 (m), 768 (m), 704 (w), 646 (vw), 581 (vw), 542 (w), 520 (m), 483 (vw), 444 (w), 403 (vw) cm^{-1}.

HRMS (ESI+, MeCN): m/z (found) = 287.63554 (100 %), 288.13638 (68 %), 288.63450 (90 %), 289.13563 (30 %), 289.63704 (5 %); m/z (calc.) = 287.63305 (100 %, $^{12}C_{30}{}^{1}H_{40}{}^{63}Cu^{14}N_8{}^{2+}$), 288.13472 (32 %, $^{12}C_{29}{}^{13}C^{1}H_{40}{}^{63}Cu^{14}N_8{}^{2+}$), 288.63214 (45 %, $^{12}C_{30}{}^{1}H_{40}{}^{65}Cu^{14}N_8{}^{2+}$), 289.13382 (14 %, $^{12}C_{29}{}^{13}C^{1}H_{40}{}^{65}Cu^{14}N_8{}^{2+}$), 289.63550 (2 %, $^{12}C_{28}{}^{13}C_2{}^{1}H_{40}{}^{65}Cu^{14}N_8{}^{2+}$).

EA: calc. (%) for $C_{30}H_{40}B_2CuF_8N_8$: C: 48.05, H: 5.38, N: 14.94; found: C: 48.14, H: 5.30, N: 14.72.

The bulk material was analyzed with powder X-ray diffraction and was confirmed to be the desired compound (Fig. S141).

Additional information on the synthesis of the target compound and original analysis data files are available via Chemotion Repository: https://dx.doi.org/10.14272/reaction/SA-FUHFF-UHFFFADPSC-FNFSJYCLRP-UHFFFADPSC-NUHFF-NUHFF-NUHFF-ZZZ

1.4.1.4 Synthesis of $[Cu(TMG2Mequ)_2](OTf)_2$ (C4−OTf)

To a solution of TMG2Mequ (25.6 mg, 0.1 mmol, 2 eq.) in MeOH (1 ml) a solution of $[Cu(MeCN)_4](OTf)_2$ (26.3 mg, 0.05 mmol, 1 eq.) in MeOH (1 mL) was added. The resulting solution became instantly dark green. By slow diffusion of Et_2O the complex $[Cu(TMG2Mequ)_2](OTf)_2$ crystallized as dark green crystals.

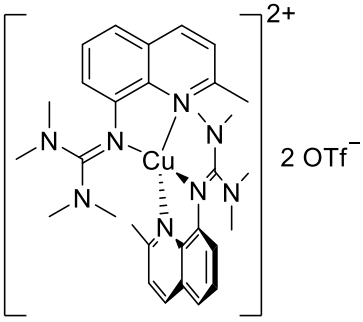

$C_{32}H_{40}CuF_6N_8O_6S_2$
874.38 g mol^{-1}

IR (ATR, neat): $\tilde{\nu}$ = 2931 (vw, ν(C-H_{aliph})), 2887 (vw), 1573 (m), 1519 (m, ν(C-N_{gua})), 1469 (m), 1399 (m), 1385 (w), 1337 (m), 1260 (vs, ν(OTf)), 1223 (m), 1142 (s), 1105 (w), 1060 (vw), 1030 (vs, ν(OTf)), 936 (vw), 911 (vw), 881 (w), 841 (m), 827 (m), 772 (m), 754 (w), 709 (w), 651 (w), 637 (vs, ν(OTf)), 572 (m), 542 (w), 516 (m), 496 (w), 480 (vw), 453 (w), 446 (w) cm^{-1}.

HRMS (ESI+, MeCN): m/z (found) = 287.63281 (100 %), 288.13425 (34 %), 288.63230 (48 %), 289.13351 (16 %), 289.63492 (3 %), 724.21853 (100 %), 725.22145 (36 %), 726.21738 (53 %), 727.21985 (18 %), 728.21930 (4 %); m/z (calc.) = 287.63305 (100 %, $^{12}C_{30}{}^{1}H_{40}{}^{63}Cu^{14}N_8{}^{2+}$), 288.13472 (32 %, $^{12}C_{29}{}^{13}C^{1}H_{40}{}^{63}Cu^{14}N_8{}^{2+}$), 288.63214 (45 %, $^{12}C_{30}{}^{1}H_{40}{}^{65}Cu^{14}N_8{}^{2+}$), 289.13382

(14 %, $^{12}C_{29}{}^{13}C^{1}H_{40}{}^{65}Cu^{14}N_8{}^{2+}$), 289.63550 (2 %, $^{12}C_{28}{}^{13}C_2{}^{1}H_{40}{}^{65}Cu^{14}N_8{}^{2+}$), 724.21867 (100 %, $^{19}F_3{}^{12}C_{31}{}^{1}H_{40}{}^{63}Cu^{14}N_8{}^{16}O_3{}^{32}S^{+}$), 725.22202 (34 %, $^{19}F_3{}^{12}C_{30}{}^{13}C^{1}H_{40}{}^{63}Cu^{14}N_8{}^{16}O_3{}^{32}S^{+}$), 726.21686 (45 %, $^{19}F_3{}^{12}C_{31}{}^{1}H_{40}{}^{65}Cu^{14}N_8{}^{16}O_3{}^{32}S^{+}$), 727.22021 (15 %, $^{19}F_3{}^{12}C_{30}{}^{13}C^{1}H_{40}{}^{65}Cu^{14}N_8{}^{16}O_3{}^{32}S^{+}$), 728.22357 (2 %, $^{19}F_3{}^{12}C_{29}{}^{13}C_2{}^{1}H_{40}{}^{65}Cu^{14}N_8{}^{16}O_3{}^{32}S^{+}$).

EA: calc. (%) for $C_{32}H_{40}CuF_6N_8O_6S_2$: C: 43.96, H: 4.61, N: 12.82; found: C: 43.86, H: 4.29, N: 12.70.

Additional information on the synthesis of the target compound and original analysis data files are available via Chemotion Repository: https://dx.doi.org/10.14272/reaction/SA-FUHFF-UHFFFADPSC-UMMQIWZYOP-UHFFFADPSC-NUHFF-LUHFF-NUHFF-ZZZ

1.4.2 Synthesis of $[Cu(TMG2^cHexqu)_2]^{+/2+}$ (R3) complexes

1.4.2.1 Synthesis of $[Cu(TMG2^cHexqu)_2]PF_6$·DCM (C5–PF_6)

To a solution of TMG2^{c}Hexqu (32.4 mg, 0.1 mmol, 2 eq.) in DCM (1 ml) a solution of $[Cu(MeCN)_4]PF_6$ (18.6 mg, 0.05 mmol, 1 eq.) in DCM (1 mL) was added. The resulting solution became instantly dark red. By slow diffusion of pentane the complex $[Cu(TMG2^cHexqu)_2]PF_6$·DCM crystallized as dark red crystals.

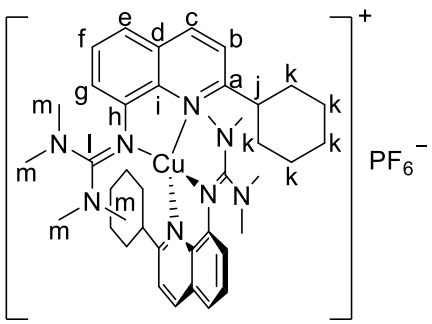

$C_{40}H_{56}CuF_6N_8P$
857.45 g mol^{-1}

^{1}H NMR (400 MHz, MeCN-d_3, 25 °C): δ = 8.20 (d, J = 8.6 Hz, 2H, c), 7.48 (t, J = 7.6 Hz, 2H, f), 7.41 (dd, J = 8.2, 1.4 Hz, 2H, e), 7.32 (d, J = 8.6 Hz, 2H, b), 6.90 (d, J = 7.4 Hz, 2H, g), 2.90 (s, 20H, j+m), 2.44 (s, 6H, m), 1.68 – 0.71 (m, 20H, k) ppm.

^{13}C NMR (101 MHz, MeCN-d_3, 25 °C) δ = 164.4 (k), 164.2 (a), 148.6 (h), 141.4 (i), 137.9 (c), 129.4 (d), 128.0 (f), 121.0 (b), 119.8 (e), 118.6 (g), 49.5 (j), 40.5 (m), 33.0 (k), 32.7 (k), 26.8 (k), 26.3 (k), 26.1 (k) ppm.

IR (ATR, neat): $\tilde{\nu}$ = 2926 (m, ν(C-H_{aliph})), 2850 (w, ν(C-H_{aliph})), 1596 (w), 1527 (s, ν(C-N_{gua})), 1501 (m), 1471 (m), 1453 (m), 1423 (m), 1410 (m), 1394 (m), 1342 (w), 1274 (w), 1228 (w), 1153 (m), 1091 (w), 1054 (m), 1036 (w), 1017 (m), 998 (w), 918 (w), 899 (vw), 837 (vs, ν(PF_6)), 798 (w), 763 (m), 731 (m), 713 (m), 691 (m), 641 (w), 590 (w), 577 (w), 557 (m), 536 (w), 513 (vw), 472 (w), 449 (w), 441 (w) cm^{-1}.

HRMS (ESI+, MeOH): m/z (found) = 711.39191 (100 %), 712.39465 (46 %), 713.39099 (56 %), 714.39294 (20 %), 715.39655 (4 %), 716.40027 (<1 %); m/z (calc.) = 711.39184 (100 %, $^{12}C_{40}{}^{1}H_{56}{}^{63}Cu^{14}N_8{}^{+}$), 712.39520 (43 %, $^{12}C_{39}{}^{13}C^{1}H_{56}{}^{63}Cu^{14}N_8{}^{+}$), 713.39003 (45 %, $^{12}C_{40}{}^{1}H_{56}{}^{65}Cu^{14}N_8{}^{+}$), 714.39339 (19 %, $^{12}C_{39}{}^{13}C^{1}H_{56}{}^{65}Cu^{14}N_8{}^{+}$), 715.39674 (4 %, $^{12}C_{38}{}^{13}C_2{}^{1}H_{56}{}^{65}Cu^{14}N_8{}^{+}$), 716.40010 (<1 %, $^{12}C_{37}{}^{13}C_3{}^{1}H_{56}{}^{65}Cu_1{}^{14}N_8{}^{+}$).

Additional information on the synthesis of the target compound and original analysis data files are available via Chemotion Repository: https://dx.doi.org/10.14272/reaction/SA-FUHFF-UHFFFADPSC-GCLZBRQZKM-UHFFFADPSC-NUHFF-NUHFF-NUHFF-ZZZ

1.4.2.2 Synthesis of [Cu(TMG2^{c}Hexqu)$_2$](OTf)$_2$ (C6–OTf)

To a solution of TMG2^{c}Hexqu (32.4 mg, 0.05 mmol, 2 eq.) in MeOH (1 ml) a solution of [Cu(MeCN)$_4$](OTf)$_2$ (26.3 mg, 0.1 mmol, 1 eq.) in MeOH (1 mL) was added. The resulting solution became instantly dark green. By slow diffusion of Et_2O the complex [Cu(TMG2^{c}Hexqu)$_2$](OTf)$_2$ crystallized as dark green crystals.

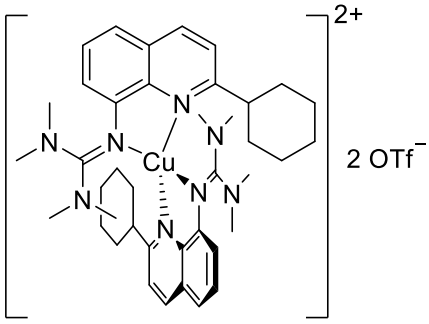

$C_{42}H_{56}CuF_6N_8O_6S_2$
1010.62 g mol^{-1}

IR (ATR, neat): $\tilde{\nu}$ = 3057 (vw, ν(C-H$_{arom}$)), 2945 (w, ν(C-H$_{aliph}$)), 2857 (vw, ν(C-H$_{aliph}$)), 1580 (m), 1567 (w), 1521 (m, ν(C-N$_{gua}$)), 1504 (m), 1456 (m), 1426 (w), 1417 (w), 1405 (m), 1384 (w), 1367 (vw), 1332 (w), 1320 (w), 1263 (s, ν(OTf)), 1225 (m), 1179 (w), 1156 (m), 1132 (m), 1096 (w), 1064 (w), 1030 (vs, ν(OTf)), 999 (w), 917 (vw), 866 (m), 848 (w), 831 (m), 803 (w), 765 (m), 754 (w), 714 (w), 696 (w), 652 (w), 636 (vs, ν(OTf)), 592 (vw), 572 (w), 541 (w), 516 (m), 468 (vw), 448 (vw) cm^{-1}.

HRMS (ESI+, MeCN): m/z (found) = 355.69534 (100 %), 356.19683 (46 %), 356.69511 (51 %), 357.19616 (21 %), 357.69761 (4 %), 358.19905 (<1 %); m/z (calc.) = 355.69565 (100 %, $^{12}C_{40}{}^{1}H_{56}{}^{63}Cu^{14}N_8{}^{2+}$), 356.19732 (43 %, $^{12}C_{39}{}^{13}C^{1}H_{56}{}^{63}Cu^{14}N_8{}^{2+}$), 356.69474 (45 %, $^{12}C_{40}{}^{1}H_{56}{}^{65}Cu^{14}N_8{}^{2+}$), 357.19642 (19 %, $^{12}C_{39}{}^{13}C^{1}H_{56}{}^{65}Cu^{14}N_8{}^{2+}$), 357.69810 (4 %, $^{12}C_{38}{}^{13}C_2{}^{1}H_{56}{}^{65}Cu^{14}N_8{}^{2+}$), 358.19978 (<1 %, $^{12}C_{37}{}^{13}C_3{}^{1}H_{56}{}^{65}Cu^{14}N_8{}^{2+}$).

The bulk material was analyzed with powder X-ray diffraction and was confirmed to be the desired compound (Fig. S142).

Additional information on the synthesis of the target compound and original analysis data files are available via Chemotion Repository: https://dx.doi.org/10.14272/reaction/SA-FUHFF-UHFFFADPSC-XYXSWFSTLI-UHFFFADPSC-NUHFF-LUHFF-NUHFF-ZZZ

1.4.3 Syntheses of [Cu(TMG2Meequ)$_2$]$^{+/2+}$ (R4) complexes

1.4.3.1 Synthesis of [Cu(TMG2Meequ)$_2$]PF$_6$ (C7–PF$_6$)

To a solution of TMG2Meequ (30.0 mg, 0.1 mmol, 2 eq.) in DCM (1 ml) a solution of [Cu(MeCN)$_4$]PF$_6$ (18.6 mg, 0.05 mmol, 1 eq.) in DCM was added. The resulting solution became instantly dark violet. By slow diffusion of pentane the complex [Cu(TMG2Meequ)$_2$]PF$_6$ crystallized as dark violet crystals.

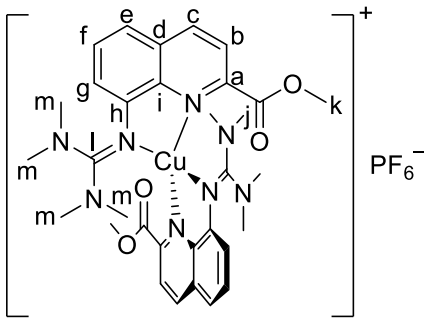

$C_{32}H_{40}CuF_6N_8O_4P$
809.23 g mol^{-1}

^{1}H NMR (400 MHz, MeCN-d$_3$, 25 °C): δ = 8.48 (d, J = 8.6 Hz, 2H, c), 8.09 (d, J = 8.6 Hz, 2H, b), 7.61 (dd, J = 8.1, 7.6 Hz, 2H, f), 7.49 (dd, J = 8.1, 1.2 Hz, 2H, e), 6.86 (d, J = 7.6 Hz, 2H, g), 3.51 (s, 6H, k), 2.80 (s, 3H, m), 2.38 (s, 9H, m) ppm.

^{13}C NMR (101 MHz, MeCN-d$_3$, 25 °C) δ = 165.9 (j), 163.9 (l), 150.0 (h), 143.0 (a), 142.3 (i), 138.2 (c), 132.4 (d), 130.8 (f), 123.0 (b), 119.1 (g), 118.9 (e), 53.2 (k), 39.6 (m) ppm.

IR (ATR, neat): $\tilde{\nu}$ = 2946 (vw, ν(C-H_{aliph})), 2869 (vw, ν(C-H_{aliph})), 1726 (m), 1592 (vw), 1523 (m, ν(C-N_{gua})), 1497 (w), 1469 (w), 1451 (w), 1418 (w), 1392 (m), 1368 (m), 1348 (w), 1312 (vw), 1280 (m), 1228 (w), 1192 (w), 1171 (w), 1149 (m), 1128 (m), 1096 (vw), 1062 (vw), 1017 (m), 985 (w), 924 (vw), 904 (w), 875 (w), 831 (vs, ν(PF_6)), 796 (m), 788 (m), 763 (m), 699 (w), 661 (w), 636 (w), 604 (vw), 579 (w), 556 (m), 519 (w), 465 (vw), 447 (w) cm^{-1}.

HRMS (ESI+, MeOH): m/z (found) = 663.24609 (100 %), 664.24890 (38 %), 665.24500 (51 %), 666.24707 (16 %), 667.25055 (2 %); m/z (calc.) = 663.24630 (100 %, $^{12}C_{32}{}^{1}H_{40}{}^{63}Cu^{14}N_8{}^{16}O_4{}^{+}$), 664.24966 (35 %, $^{12}C_{31}{}^{13}C^{1}H_{40}{}^{63}Cu^{14}N_8{}^{16}O_4{}^{+}$), 665.24449 (45 %, $^{12}C_{32}{}^{1}H_{40}{}^{65}Cu^{14}N_8{}^{16}O_4{}^{+}$), 666.24785 (15 %, $^{12}C_{31}{}^{13}C^{1}H_{40}{}^{65}Cu^{14}N_8{}^{16}O_4{}^{+}$), 667.25120 (3 %, $^{12}C_{30}{}^{13}C_2{}^{1}H_{40}{}^{65}Cu^{14}N_8{}^{16}O_4{}^{+}$).

Additional information on the synthesis of the target compound and original analysis data files are available via Chemotion Repository: https://dx.doi.org/10.14272/reaction/SA-FUHFF-UHFFFADPSC-JBXRXORXEO-UHFFFADPSC-NUHFF-NUHFF-NUHFF-ZZZ

1.4.3.2 Synthesis of $[Cu(TMG2Meequ)_2](BF_4)_2 \cdot 2$ MeCN (C8–BF_4)

To a solution of TMG2Meequ (30.0 mg, 0.1, 2 eq.) in MeCN (1 ml) a solution of $[Cu(MeCN)_4](BF_4)_2$ (20.1 mg, 0.05 mmol, 1 eq.) in MeCN (1 mL) was added. The resulting solution became instantly dark red. By slow diffusion of diethyl ether the complex $[Cu(TMG2Meequ)_2](BF_4)_2 \cdot 2$ MeCN crystallized as dark red crystals.

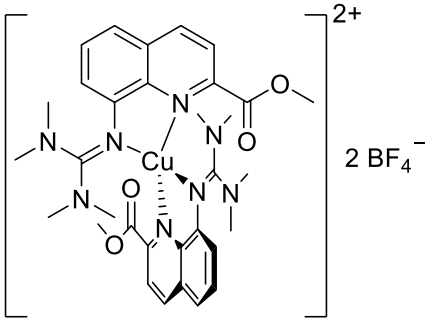

$C_{32}H_{40}B_2CuF_8N_8O_4$
837.88 g mol^{-1}

IR (ATR, neat): $\tilde{\nu}$ = 2947 (vw, ν(C-H_{aliph})), 1690 (m), 1567 (m), 1521 (m, ν(C-N_{gua})), 1503 (m), 1461 (m), 1423 (w), 1401 (m), 1384 (m), 1346 (m), 1323 (s), 1308 (m), 1273 (m), 1230 (w), 1205 (w), 1164 (w), 1023 (vs, ν(BF_4)), 963 (m), 907 (w), 865 (m), 854 (m), 825 (m), 812 (w), 793 (w), 764 (s), 701 (m), 657 (w), 639 (w), 579 (w), 519 (m), 474 (w), 440 (w) cm^{-1}.

HRMS (ESI+, MeCN): m/z (found) = 331.61806 (100 %), 332.11873 (66 %). 332.61696 (84 %), 333.11792 (31 %), 333.61917 (6 %); m/z (calc.) = 331.62288 (100 %, $^{12}C_{32}{}^{1}H_{40}{}^{63}Cu^{14}N_8{}^{16}O_4{}^{2+}$), 332.12455 (35 %, $^{12}C_{31}{}^{13}C^{1}H_{40}{}^{63}Cu^{14}N_8{}^{16}O_4{}^{2+}$), 332.62197 (45 %, $^{12}C_{32}{}^{1}H_{40}{}^{65}Cu^{14}N_8{}^{16}O_4{}^{2+}$), 333.12365 (15 %, $^{12}C_{31}{}^{13}C^{1}H_{40}{}^{65}Cu^{14}N_8{}^{16}O_4{}^{2+}$), 333.62533 (3 %, $^{12}C_{30}{}^{13}C_2{}^{1}H_{40}{}^{65}Cu^{14}N_8{}^{16}O_4{}^{2+}$).

EA: calc. (%) for $C_{36}H_{46}B_2CuF_8N_{10}O_4$ (+2/3 Et_2O): C: 47.91, H: 5.48, N: 14.45; found: C: 47.88, H: 5.26, N: 14.06.

Additional information on the synthesis of the target compound and original analysis data files are available via Chemotion Repository: https://dx.doi.org/10.14272/reaction/SA-FUHFF-UHFFFADPSC-GQFHEVHUGU-UHFFFADPSC-NUHFF-NUHFF-NUHFF-ZZZ

1.4.3.3 Synthesis of [Cu(TMG2Meequ)$_2$](OTf)$_2$·2 MeCN (C8–OTf)

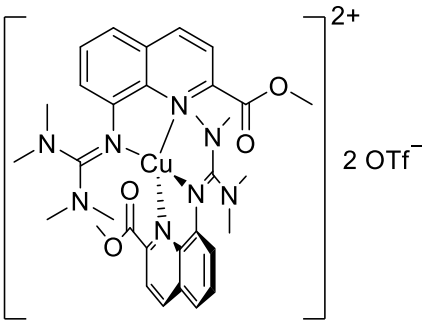

$C_{34}H_{40}CuF_6N_8O_{10}S_2$
962.40 g mol^{-1}

To a solution of TMG2Meequ (30.0 mg, 0.1, 2 eq.) in MeCN (1 ml) a solution of [Cu(MeCN)$_4$](OTf)$_2$ (26.3 mg, 0.05 mmol, 1 eq.) in MeCN (1 mL) was added. The resulting solution became instantly dark red. By slow diffusion of diethyl ether the complex [Cu(TMG2Meequ)$_2$](OTf)$_2$·2 MeCN crystallized as dark red crystals.

IR (ATR, neat): $\tilde{\nu}$ = 3535 (vw), 2954 (vw, ν(C-H$_{aliph}$)), 1696 (m), 1567 (m), 1520 (m, ν(C-N$_{gua}$)), 1505 (m), 1461 (m), 1401 (m), 1383 (w), 1345 (m), 1325 (m), 1257 (vs, ν(OTf)), 1224 (m), 1151 (s), 1104 (m), 1067 (vw), 1028 (vs, ν(OTf)), 968 (w), 910 (vw), 867 (m), 854 (m), 824 (w), 811 (w), 794 (w), 766 (m), 701 (w), 636 (vs, ν(OTf)), 573 (m), 517 (m), 475 (vw), 445 (vw) cm^{-1}.

HRMS (ESI+, MeCN): m/z (found) = 331.62241 (100 %), 332.12391 (38 %), 332.62201 (50 %), 333.12320 (18 %), 333.62447 (3 %); m/z (calc.) = 331.62288 (100 %, $^{12}C_{32}{}^{1}H_{40}{}^{63}Cu^{14}N_8{}^{16}O_4{}^{2+}$), 332.12455 (35 %, $^{12}C_{31}{}^{13}C^{1}H_{40}{}^{63}Cu^{14}N_8{}^{16}O_4{}^{2+}$), 332.62197 (45 %, $^{12}C_{32}{}^{1}H_{40}{}^{65}Cu^{14}N_8{}^{16}O_4{}^{2+}$), 333.12365 (15 %, $^{12}C_{31}{}^{13}C^{1}H_{40}{}^{65}Cu^{14}N_8{}^{16}O_4{}^{2+}$), 333.62533 (3 %, $^{12}C_{30}{}^{13}C_2{}^{1}H_{40}{}^{65}Cu^{14}N_8{}^{16}O_4{}^{2+}$).

Additional information on the synthesis of the target compound and original analysis data files are available via Chemotion Repository: https://dx.doi.org/10.14272/reaction/SA-FUHFF-UHFFFADPSC-UMXPYYQOWK-UHFFFADPSC-NUHFF-LUHFF-NUHFF-ZZZ

1.4.4 Syntheses of [Cu(TMG4NMe$_2$qu)$_2$]$^{+/2+}$ (R5) complexes

1.4.4.1 Synthesis of [Cu(TMG4NMe$_2$qu)$_2$]BF$_4$ (C9–BF$_4$)

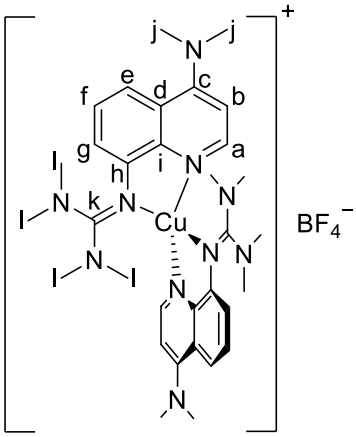

$C_{32}H_{46}BCuF_4N_{10}$
721.14 g mol^{-1}

To a solution of TMG4NMe$_2$qu (28.5 mg, 0.1 mmol, 2 eq.) in DCM (1 ml) a solution of [Cu(MeCN)$_4$]BF$_4$ (15.6 mg, 0.05 mmol, 1 eq.) in DCM (1 mL) was added. The resulting solution became instantly dark red. By slow diffusion of pentane the complex [Cu(TMG4NMe$_2$qu)$_2$]BF$_4$ crystallized as dark red crystals.

It was not possible to record acceptable ^{1}H and ^{13}C NMR spectra due to small amounts of paramagnetic Cu(II) species formed from disproportionation in solution. This is caused by the low redox potential of this complex. A similar case was observed by Matyjaszewski *et al.*[10]

IR (ATR, neat): $\tilde{\nu}$ = 2943 (w, ν(C-H$_{aliph}$)), 2875 (w, ν(C-H$_{aliph}$)), 2795 (vw, ν(C-H$_{aliph}$)), 1739 (vw), 1620 (vw), 1580 (m), 1563 (m), 1505 (vs, ν(C-N$_{gua}$)), 1464 (m), 1406 (m), 1380 (m), 1328 (m), 1293 (w), 1231 (w), 1206 (w), 1151 (w), 1091 (m), 1047 (vs, ν(BF$_4$)), 1032 (vs, ν(BF$_4$)), 974 (m), 923 (w), 894 (w), 853 (w), 837 (w), 821 (m), 801 (m), 759 (m), 722 (w), 706 (vw), 669 (vw), 615 (vw), 599 (vw), 570 (vw), 558 (w), 520 (m), 471 (w), 411 (vw) cm^{-1}.

HRMS (ESI+, MeOH): m/z (found) = 633.32037 (100 %), 634.32373 (26 %), 635.31848 (39 %), 636.32202 (9 %), 637.32513 (1 %); m/z (calc.) = 633.31974 (100 %, $^{12}C_{32}{}^{1}H_{46}{}^{63}Cu^{14}N_{10}{}^{+}$), 634.32310 (35 %, $^{12}C_{31}{}^{13}C^{1}H_{46}{}^{63}Cu^{14}N_{10}{}^{+}$), 635.31793 (45 %, $^{12}C_{32}{}^{1}H_{46}{}^{65}Cu^{14}N_{10}{}^{+}$), 636.32129 (15 %, $^{12}C_{31}{}^{13}C^{1}H_{46}{}^{65}Cu^{14}N_{10}{}^{+}$), 637.32464 (3 %, $^{12}C_{30}{}^{13}C_{2}{}^{1}H_{46}{}^{65}Cu^{14}N_{10}{}^{+}$).

Additional information on the synthesis of the target compound and original analysis data files are available via Chemotion Repository: https://dx.doi.org/10.14272/reaction/SA-FUHFF-UHFFFADPSC-JQDGMCVIMF-UHFFFADPSC-NUHFF-NUHFF-NUHFF-ZZZ

1.4.4.2 Synthesis of $[Cu(TMG4NMe_2qu)_2](OTf)_2 \cdot Et_2O$ (C10–OTf)

To a solution of $TMG4NMe_2qu$ (28.5 mg, 0.1 mmol, 2 eq.) in MeOH (1 ml) a solution of $[Cu(MeCN)_4](OTf)_2$ (26.3 mg, 0.1 mmol, 1 eq.) in MeOH (1 mL) was added. The resulting solution became instantly dark brown. By slow diffusion of Et_2O the complex $[Cu(TMG4NMe_2qu)_2](OTf)_2 \cdot Et_2O$ crystallized as dark brown crystals.

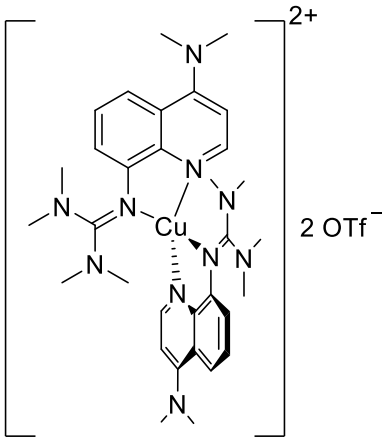

$C_{34}H_{46}CuF_6N_{10}O_6S_2$
932.46 g mol^{-1}

IR (ATR, neat): $\tilde{\nu}$ = 2909 (vw, ν(C-H_{aliph})), 1600 (vw), 1580 (m), 1559 (w), 1513 (m, ν(C-N_{gua})), 1468 (w), 1421 (m), 1402 (m), 1392 (m), 1323 (m), 1298 (w), 1259 (s, ν(OTf)), 1224 (m), 1209 (w), 1185 (vw), 1145 (m), 1095 (vw), 1064 (w), 1046 (vw), 1030 (s, ν(OTf)), 981 (m), 926 (w), 856 (w), 827 (m), 811 (w), 806 (m), 764 (w), 750 (m), 728 (w), 704 (w), 674 (vw), 637 (vs, ν(OTf)), 582 (w), 571 (m), 559 (w), 536 (w), 518 (m), 469 (w) cm^{-1}.

HRMS (ESI+, MeCN): m/z (found) = 316.65969 (100 %), 317.16104 (38 %), 317.65919 (49 %), 318.16027 (17 %), 318.66166 (3 %), 319.16302 (<1 %); m/z (calc.) = 316.65960 (100 %, $^{12}C_{32}{}^{1}H_{46}{}^{63}Cu^{14}N_{10}{}^{2+}$), 317.16127 (35 %, $^{12}C_{31}{}^{13}C^{1}H_{46}{}^{63}Cu^{14}N_{10}{}^{2+}$), 317.65869 (45 %, $^{12}C_{32}{}^{1}H_{46}{}^{65}Cu^{14}N_{10}{}^{2+}$), 318.16037 (15 %, $^{12}C_{31}{}^{13}C^{1}H_{46}{}^{65}Cu^{14}N_{10}{}^{2+}$), 318.66205 (3 %, $^{12}C_{30}{}^{13}C_{2}{}^{1}H_{46}{}^{65}Cu^{14}N_{10}{}^{2+}$), 319.16372 (<1 %, $^{12}C_{29}{}^{13}C_{3}{}^{1}H_{46}{}^{65}Cu^{14}N_{10}{}^{2+}$).

EA: calc. (%) for $C_{38}H_{56}CuF_6N_{10}O_7S_2$: C: 45.34; H: 5.61; N: 13.92; found: C: 45.33, H: 5.54, N: 13.81.

Additional information on the synthesis of the target compound and original analysis data files are available via Chemotion Repository: https://dx.doi.org/10.14272/reaction/SA-FUHFF-UHFFFADPSC-DRQHCTISPL-UHFFFADPSC-NUHFF-LUHFF-NUHFF-ZZZ

1.4.5 Resynthesis of the counter complex $[Co(bpy)_3](PF_6)_3$

The synthesis was performed following a modified procedure of the literature.[11] $NOPF_6$ has to be used instead of $NOBF_4$ because otherwise the resulting product contains a mixture of PF_6^- and BF_4^- anions.

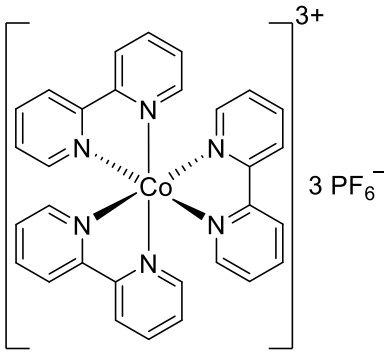

$C_{30}H_{24}CoF_{18}N_6P_3$
962.39 g mol^{-1}

$CoCl_2 \cdot 6\ H_2O$ (5.0 g, 21.0 mmol, 1 eq.) and bipyridine (10.8 g, 69.3 mmol, 3.3 eq.) were dissolved in MeOH (250 mL). The solution was refluxed for 3 h under stirring. A solution of NH_4PF_6 (34.25 g, 210.1 mmol, 10 eq.) in MeOH (50 mL) was added. The resulting precipitate was filtered, washed with MeOH and Et_2O and dried under reduced pressure. The solid was dissolved in MeCN (150 mL) and $NOPF_6$ (5.51 g, 31.5 mmol, 1.5 eq.) was added slowly under stirring at rt. The solution was stirred for additional 30 min. Then nitrogen was passed in the solution to remove the nitrogen oxide. The solvent was removed under reduced pressure. MeCN was added until the solid was dissolved completely. NH_4PF_6 (34.25 g, 210.1 mmol, 10 eq.) was added under stirring. The resulting precipitate was filtrated, washed with MeOH and Et_2O. Again, MeCN was added until the solid was dissolved completely. The solution was filtrated and MeOH was added until no further precipitation occurred. The precipitate was filtrated, washed with MeOH and Et_2O and dried under reduced pressure. $[Co(bpy)_3](PF_6)_3$ was obtained as a yellow solid (16.45 g, 17.09 mmol, 81.3%).

^{1}H NMR (400 MHz, MeCN-d_3, 25 °C): δ = 8.68 (dd, *J* = 8.1, 1.5 Hz, 6H), 8.47 (td, *J* = 7.9, 1.3 Hz, 6H), 7.73 (ddd, *J* = 7.6, 6.0, 1.5 Hz, 6H), 7.26 (dd, *J* = 6.0, 1.3 Hz, 6H).

2. XRD measurements

2.1 Experimental

The crystallographic data for 2-^{c}Hex-8-NO_2-qu, **L2**, **L3**, **L6**, **C3−PF$_6$**, **C3−OTf**, **C4−BF$_4$**, **C4−OTf**, **C5−PF$_6$, C6−OTf**, **C7−PF$_6$**, **C8−BF$_4$**, **C8−OTf**, **C9−BF$_4$** and **C10−OTf** are presented in Table S11 – S15. The data for **C4−OTf**, **C5−PF$_6$** and **C8−BF$_4$** were collected with a *Bruker D8* goniometer with *APEX CCD* using an *Incoatec* microsource with Mo-K_α radiation (λ = 0.71073 Å). Temperature control was achieved with an Oxford Cryostream 700. Crystals were mounted with grease on glass fibers and data were collected at 100 K in ω-scan mode. Data were collected with SMART, integrated with SAINT and corrected for absorption by multi-scan methods with SADABS.[12] The data for 2-^{c}Hex-8-NO_2-qu, **L2**, **L3**, **L6**, **C3−PF$_6$**, **C3−OTf**, **C4−BF$_4$**, **C6−OTf**, **C7−PF$_6$**, **C8−OTf**, **C9−BF$_4$** and **C10−OTf** and were collected with a four-circle goniometer Stoe Stadivari with Dectris Pilatus3 R 200 K hybrid pixel detector using Geni 3D high flux Mo-Kα radiation (λ = 0.71073 Å) or GeniX 3D high flux Cu radiation (λ = 1.54056 Å) at 100 K (240 K: **C3−OTf**). The temperature was controlled by an Oxford Cryostream 800. Crystals were mounted with grease on glass fibers. Data were collected with X-Area Pilatus[13] and integrated with X-Area Integrate[14] and X-Area Recipe.[15] The absorption correction was performed by Gaussian integration with Stoe X-Red32, afterwards scaling of reflections with X-Area LANA.[16]

The structure was solved by direct and conventional Fourier methods and all non-hydrogen atoms were refined anisotropically with full-matrix least-squares based on F^2 (XPREP,[17] ShelXS,[18] ShelXT,[19] ShelXL[20] or ShelXle[21]). Hydrogen atoms were derived from difference Fourier maps and placed at idealised positions, riding on their parent C atoms, with isotropic displacement parameters Uiso(H) = 1.2Ueq(C) and 1.5Ueq (C methyl). All methyl groups were allowed to rotate but not to tip.

In **L2**, the space group was checked with the ADDSYM routine as implemented in Platon and ADDSYM suggest pseudo-translations (I) or/and a smaller unit cell.[22,23] Also a C-alert of the checkcif-routine is occured. The thermal ellipsoids in the smaller unit cell are not well-shaped and the structure solutions are not suited. Because of this it is pseudo-translation.

In **C3−PF6**, we have a twin and the second domain has an amount about 5%.

In **C10−OTf** it was not possible to model the disordered solvent molecules (1 molecule diethyl ether per asymmetric unit) in an adequate manner, and the data set was treated with the SQUEEZE routine as implemented in PLATON.[22,23]

Full crystallographic data for 2-^{c}Hex-8-NO_2-qu, **L2**, **L3**, **L6**, **C3−PF$_6$**, **C3−OTf**, **C4−BF$_4$**, **C4−OTf**, **C5−PF$_6$, C6−OTf**, **C7−PF$_6$**, **C8−BF$_4$**, **C8−OTf**, **C9−BF$_4$** and **C10−OTf** have been deposited with the Cambridge Crystallographic Data Centre as supplementary no. CCDC – 2132917 for 2-^{c}Hex-8-NO_2-qu, CCDC – 2132918 for **L2**, CCDC – 2132919 for **L3**, CCDC – 2132920 for **L6**, CCDC – 2132921 for **C3−PF$_6$**, CCDC – 2132922 for **C3−OTf**, CCDC – 2132923 for **C4−BF$_4$**, CCDC – 2132924 for **C4−OTf**, CCDC – 2132925 for **C5−PF$_6$**, CCDC – 2132926 for **C6−OTf**, CCDC – 2132927 for **C7−PF$_6$**, CCDC – 2132928 for **C8−BF$_4$**, CCDC – 2132929 for **C8−OTf**, CCDC – 2132930 for **C9−BF$_4$** and CCDC – 2132931 for **C10−OTf**. Copies of the data can be obtained free of charge on application to CCDC, 12 Union Road, Cambridge CB2 1EZ, UK (fax: (+44)1223-336-033; e-mail: deposit@ccdc.cam.ac.uk).

2.2 Results

The results of the complexes **C3−OTf**, **C4−OTf** and **C8−OTf** that are not shown in the main article are shown in Table S1. The results of the complexes **C3−PF_6**, **C4−BF_4** and **C8−BF_4** are shown for comparison in Table S1. The complexes **C3−PF_6** and **C3−OTf** possess two independent molecules (**C3−PF_6−1**, **C3−PF_6−2** and **C3−OTf−1**, **C3−OTf−2**) in the unit cell. The results of all independent molecules are shown in Table S1.

Table S1: Key bond lengths, bond angles and structure parameters of the Cu(I) and Cu(II) complexes **C3−PF_6**, **C3−OTf**, **C4−BF_4**, **C4−OTf**, **C8−BF_4** and **C8−OTf**.

	C3−PF_6−1	**C3−PF_6−2**	**C3−OTf−1**	**C3−OTf−1**	**C4−BF_4**	**C4−OTf**	**C8−BF_4**	**C8−OTf**
	Bond lengths [Å]							
Cu-$N_{gua,1/2}$	2.091(3), 2.097(3)	2.101(3), 2.101(3)	2.092(3), 2.110(3)	2.108(3), 2.108(3)	1.979(4), 1.978(4)	2.014(5), 2.002(4)	2.039(2), 2.043(2)	2.051(2), 2.052(2)
Cu-$N_{qu,1/2}$	1.994(3), 1.994(3)	2.007(3), 2.007(3)	2.012(3), 1.994(3)	2.015(3), 2.015(3)	1.987(4), 1.972(4)	1.978(4), 1.965(5)	1.960(2), 1.959(2)	1.957(2), 1.957(2)
Cu-$O_{carb,1/2}$							2.616(2), 2.595(2)	2.540(2), 2.550(2)
Cu-$O_{alc,1/2}$							4.428(2), 4.441(2)	4.415(2), 4.380(2)
	Bond angles [°]							
$N_{gua,1/2}$-Cu-$N_{qu,1/2}$	81.7(2), 81.6(2)	81.3(2), 81.3(2)	81.5(2), 81.4(2)	81.0(2), 81.0(2)	83.2(2), 83.6(2)	83.2(2), 83.3(2)	82.15(7), 82.16(7)	82.05(6), 81.70(6)
$N_{gua,1}$-Cu-$N_{gua,2}$	126.0(2)	127.4(2)	125.5(2)	126.1(2)	135.9(2)	132.9(2)	120.20(7)	115.22(6)
$N_{gua,1/2}$-Cu-$N_{qu,2/1}$	111.7(2), 113.2(2)	114.0(2), 114.0(2)	117.8(2), 110.8(2)	114.1(2), 114.1(2)	105.3(2), 107.2(2)	104.5(2), 107.0(2)	105.33(7), 106.88(7)	107.43(6), 105.73(6)
$N_{qu,1}$-Cu-$N_{qu,2}$	149.9(2)	146.5(2)	146.3(2)	147.7(2)	154.6(2)	157.8(2)	163.72(7)	164.49(6)
	Structure parameters							
τ_4[a]	0.60	0.61	0.63	0.61	0.49	0.49	0.54	0.57
∢ (CuN_2, CuN'_2)	68.2	69.6	71.0	70.1	54.7	55.6	65.6	70.4
ρ[b]	0.98	0.97	0.97	0.97	1.00	1.00	1.00	1.00

3. XAS measurements

3.1 Experimental

X-ray absorption spectroscopy (XAS) data were collected in the absorption mode using two ionization chambers at the beamline P65 (DESY, PETRA III, Hamburg, Germany).[24] The complexes were prepared in a glovebox under inert conditions (oxygen and water free) with a concentration of 15 mM and transferred to a custom-made PEEK cuvette with septum and Kapton (polyimide foil, DuPont) windows, which were sealed by a Teflon O-ring. The cuvette was cooled to −30 °C to prevent sample damage and improve the data quality. The measurements were conducted in a continuous flow helium cryostat Optistat CF (Oxford Instruments, UK). The measurement time for a complete scan from 8828 eV to 9978 eV was 300 s. In total, the samples were measured up to 60 min. Copper foil was measured simultaneously and the first inflection point energy was set to 8979.0 eV and all measurements were calibrated to this shift afterwards. Data processing and analysis were done with Athena and Artemis.[25]

3.2 Data reduction and analysis

For each spectrum, a second-order polynomial was fit to the pre-edge region, extrapolated and then subtracted from the data using Athena. The pre-edge region was set to 150 eV to 30 eV below the edge. The normalization range was set to -150 eV to +900 eV relative to the edge with a normalization order of 3. E_0 was set to the inflection point of the edge. For background removal, Rbkg was set to 1.0 and the k-weight to 3. The spline range was 0 to 16.1 $Å^{-1}$ in k and 0 to 1000 eV in energy above the edge for each sample. Low and high spline clamps were set to “None” and “Strong”. For the EXAFS fitting, all dominant scattering paths up to a distance of 3.2 Å to 3.4 Å, depending on the specific sample and measurement, were used. Scattering paths were calculated using FEFF and a DFT-calculated structure of the complex for each sample. For visualization of the XANES and EXAFS spectra the software OriginPro 2021b (Version 9.8.5.212) from OriginLab was used.

3.3 Results

3.3.1 XANES results

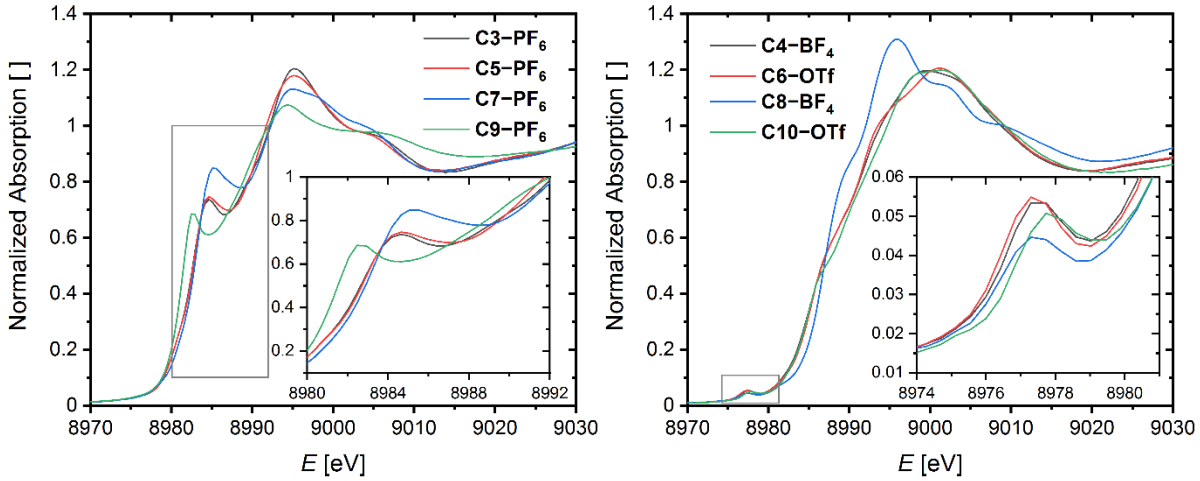

Fig. S1: Cu K-edge XANES spectra of all novel Cu(I) (left) and Cu(II) (right) complexes in solution in MeCN.

3.3.2 EXAFS results

3.3.2.1 [Cu(TMG2Mequ)$_2$]PF$_6$ (C3–PF$_6$)

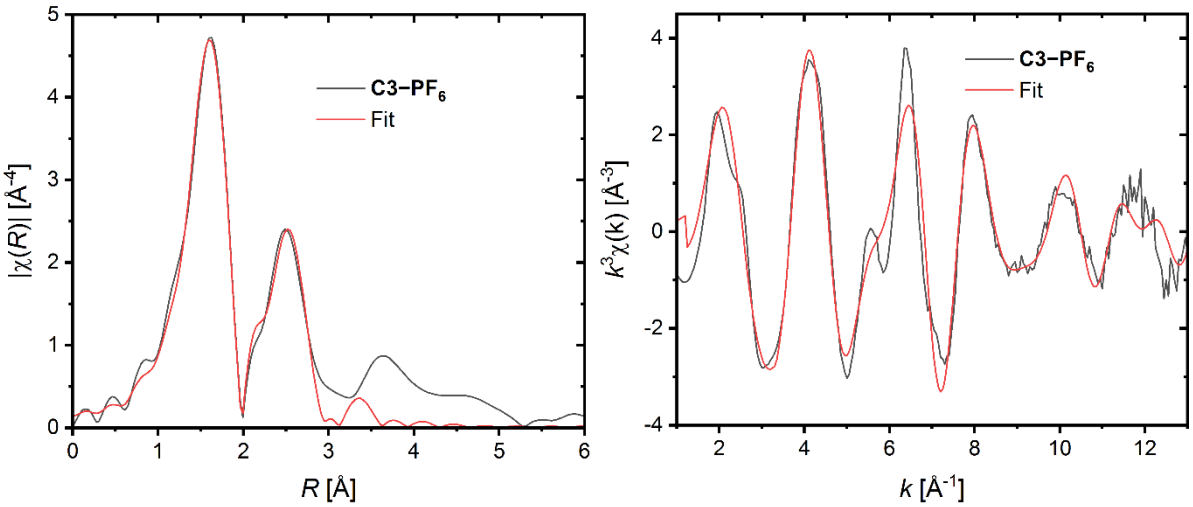

Fig. S2: Cu K-edge EXAFS spectra of [Cu(TMG2Mequ)$_2$]PF$_6$ (**C3–PF$_6$**) in solution in MeCN.

Table S2: By EXAFS determined bond lengths of the [Cu(TMG2Mequ)$_2$]PF$_6$ (**C3–PF$_6$**) in MeCN.

Bond	DFT [Å]	Fit [Å]	Δ [Å]	R-Fit Err [Å]	σ^2 [10^{-3} Å^2]	σ^2-Err [10^{-3} Å^2]
2 x Cu-N	2.001	1.998	0.003	0.009	6.2	1.3
2 x Cu-N	2.083	2.080	0.003	0.010	6.2	1.3
2 x Cu-C	2.829	2.829	<0.001	0.014	5.2	2.3
2 x Cu-C	2.874	2.875	<0.001	0.015	5.2	2.3
4 x Cu-C	3.003	3.003	<0.001	0.015	5.2	2.3
2 x Cu-C	3.253	3.253	<0.001	0.016	5.2	2.3
N-C-N/N-N (Multiple Sc.)	>3.0	>3.0	-		1.7	2.5

3.3.2.2 [Cu(TMG2Mequ)$_2$](BF$_4$)$_2$ (C4−BF$_4$)

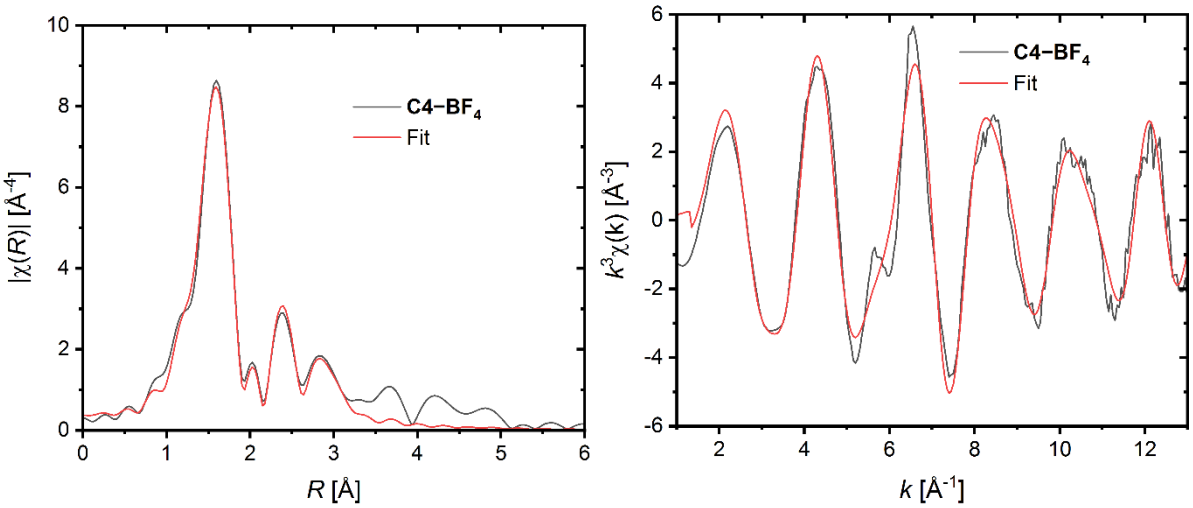

Fig. S3: Cu K-edge EXAFS spectra of [Cu(TMG2Mequ)$_2$](BF$_4$)$_2$ (**C4−BF$_4$**) in solution in MeCN.

Table S3: By EXAFS determined bond length of the [Cu(TMG2Mequ)$_2$](BF$_4$)$_2$ (**C4−BF$_4$**) in MeCN.

Bond	DFT [Å]	Fit [Å]	Δ [Å]	R-Fit Err [Å]	σ^2 [10^{-3} Å^2]	σ^2-Err [10^{-3} Å^2]
4 x Cu-N	1.987	1.979	0.009	0.006	4.3	0.8
4 x Cu-C	2.803	2.822	0.018	0.014	3.0	1.6
4 x Cu-C	2.991	3.011	0.019	0.015	3.0	1.6
8 x Cu-N-C	3.086	3.099	0.013	0.020	1.4	0.9
N-C-N/N-N (Multiple Sc.)	>3.0	>3.0	-	-	12.5	0.9

3.3.2.3 [Cu(TMG2^{c}Hexqu)$_2$]PF$_6$ (C5–PF$_6$)

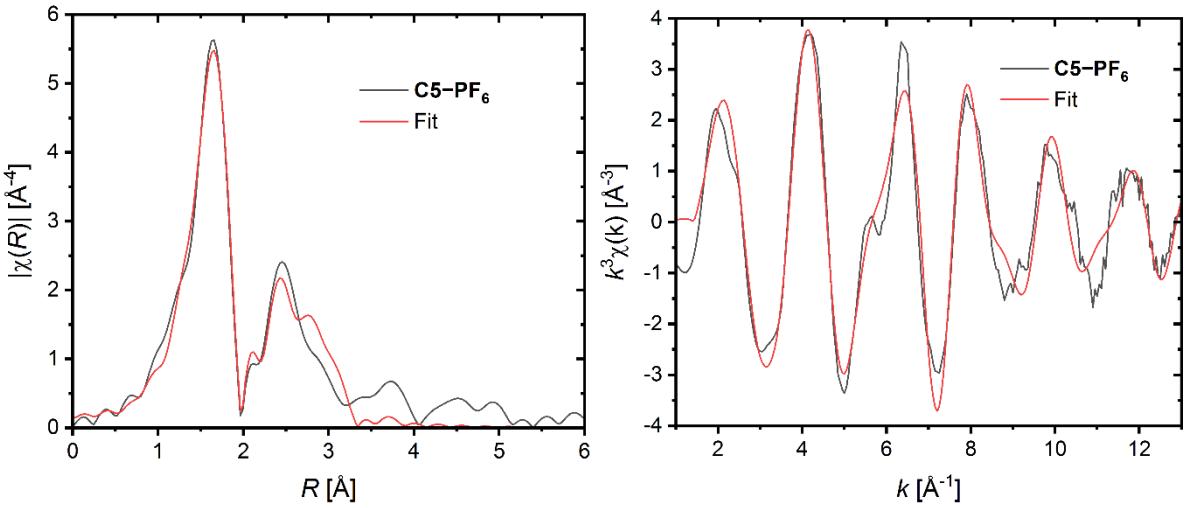

Fig. S4: Cu K-edge EXAFS spectra of [Cu(TMG2^{c}Hexqu)$_2$]PF$_6$ (**C5–PF$_6$**) in solution in MeCN.

Table S4: By EXAFS determined bond length of the [Cu(TMG2^{c}Hexqu)$_2$]PF$_6$ (**C5–PF$_6$**) in MeCN.

Bond	DFT [Å]	Fit [Å]	Δ [Å]	R-Fit Err [Å]	σ^2 [10^{-3} Å^2]	σ^2-Err [10^{-3} Å^2]
4 x Cu-N	2.043	2.048	0.005	0.006	6.5	0.8
4 x Cu-C	2.848	2.874	0.025	0.010	6.4	1.3
4 x Cu-C	3.017	3.044	0.027	0.010	6.4	1.3
4 x Cu-N-C	3.119	3.147	0.028	0.010	6.4	1.3
N-C-N/N-N (Multiple Sc.)	>3.0	>3.0	-	-	6.4	1.3

3.3.2.4 [Cu(TMG2^{c}Hexqu)$_2$](OTf)$_2$ (C6–OTf)

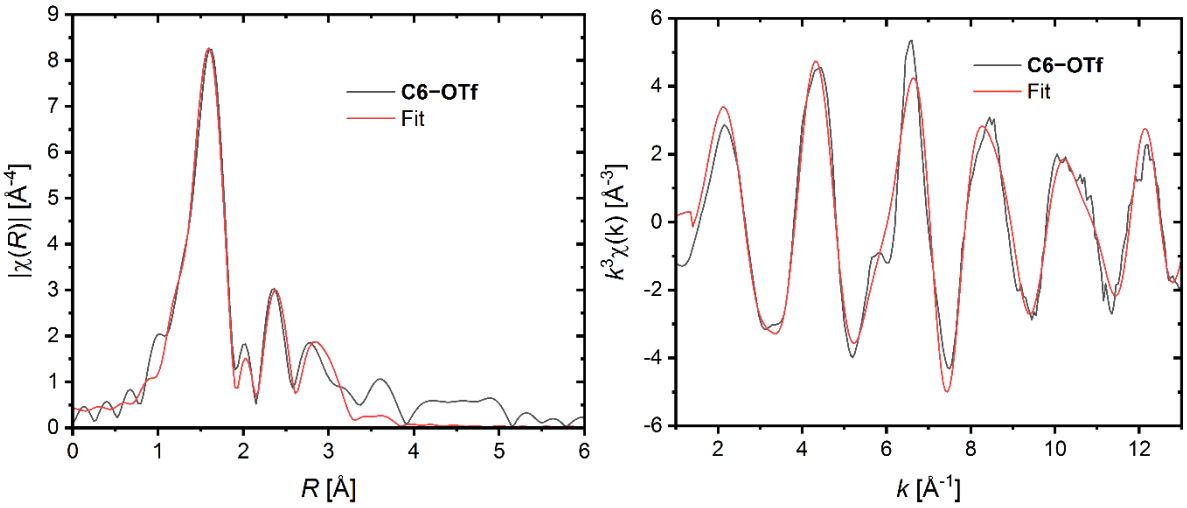

Fig. S5: Cu K-edge EXAFS spectra of [Cu(TMG2^{c}Hexqu)$_2$](OTf)$_2$ (**C6–OTf**) in solution in MeCN.

Table S5: By EXAFS determined bond length of the [Cu(TMG2^{c}Hexqu)$_2$](OTf)$_2$ (**C6–OTf**) in MeCN.

Bond	DFT [Å]	Fit [Å]	Δ [Å]	R-Fit Err [Å]	σ^2 [10^{-3} Å^2]	σ^2-Err [10^{-3} Å^2]
4 x Cu-N	1.991	1.977	0.015	0.005	4.6	0.6
4 x Cu-C	2.805	2.802	0.003	0.010	4.3	1.0
4 x Cu-C	2.997	2.994	0.003	0.010	4.3	1.0
Cu-C	>3.0	>3.0	-	-	4.3	1.0
N-C/N-N (Multiple Sc.)	>3.0	>3.0	-	-	6.5	3.2

3.3.2.5 [Cu(TMG2Meequ)$_2$]PF$_6$ (C7–PF$_6$)

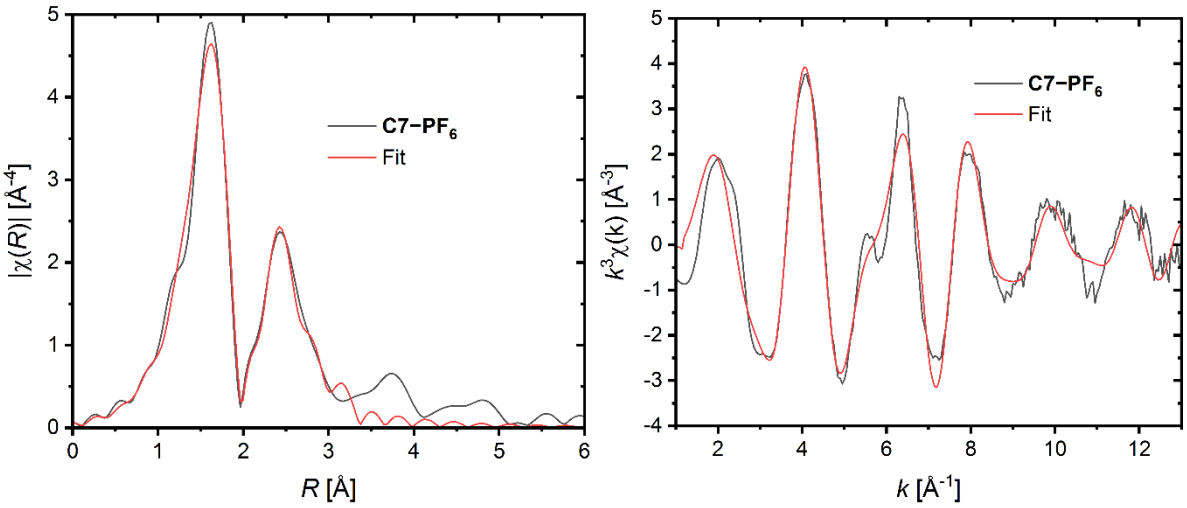

Fig. S6: Cu K-edge EXAFS spectra of [Cu(TMG2Meequ)$_2$]PF$_6$ (**C7–PF$_6$**) in solution in MeCN.

Table S6: By EXAFS determined bond length of the [Cu(TMG2Meequ)$_2$]PF$_6$ (**C7–PF$_6$**) in MeCN.

Bond	DFT [Å]	Fit [Å]	Δ [Å]	R-Fit Err [Å]	σ^2 [10^{-3} Å^2]	σ^2-Err [10^{-3} Å^2]
3 x Cu-N	2.037	2.038	0.001	0.010	9.0	1.5
Cu-N	2.064	2.065	0.001	0.001	9.0	1.5
3 x Cu-C	2.831	2.857	0.026	0.018	4.0	1.8
Cu-C	2.860	2.886	0.026	0.018	4.0	1.8
Cu-O	2.934	2.961	0.027	0.018	4.0	1.8
Cu-O	3.001	3.028	0.027	0.018	4.0	1.8
Cu-C	>3.0	>3.0	-	-	12.2	8.5
N-C/N-C-N (Multiple Sc.)	>3.0	>3.0	-	-	13.2	1.0

3.3.2.6 [Cu(TMG2Meequ)$_2$](BF$_4$)$_2$ (C8−BF$_4$)

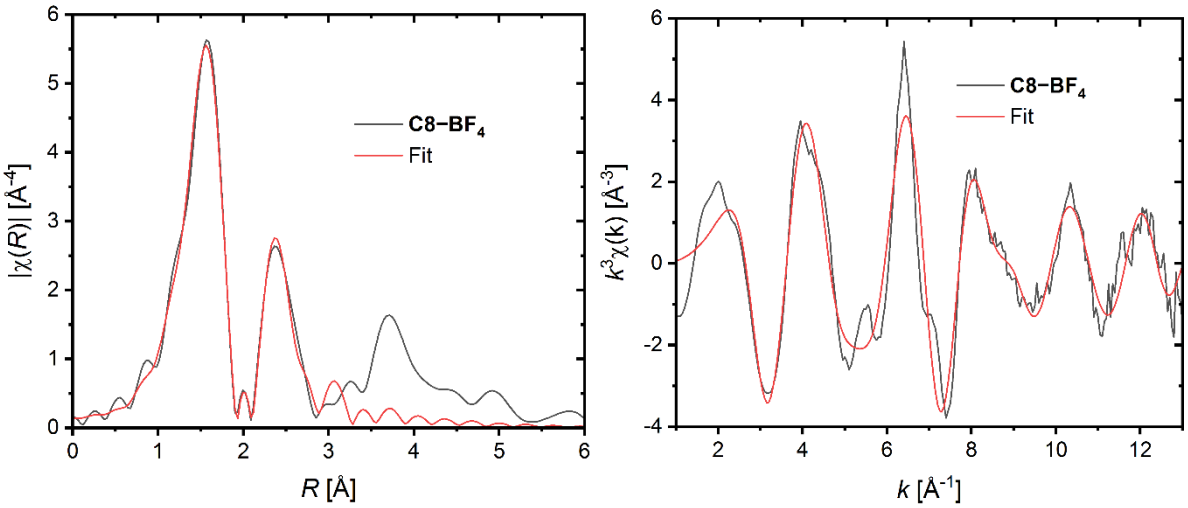

Fig. S7: Cu K-edge EXAFS spectra of [Cu(TMG2Meequ)$_2$](BF$_4$)$_2$ (**C8−BF$_4$**) in solution in MeCN.

Table S7: By EXAFS determined bond length of the [Cu(TMG2Meequ)$_2$](BF$_4$)$_2$ (**C8−BF$_4$**) in MeCN.

Bond	DFT [Å]	Fit [Å]	Δ [Å]	R-Fit Err [Å]	σ^2 [10^{-3} Å^2]	σ^2-Err [10^{-3} Å^2]
2 x Cu-N	1.957	1.935	0.022	0.013	3.5	2.1
2 x Cu-N	2.051	2.029	0.022	0.013	3.5	2.1
2 x Cu-O	2.544	2.496	0.048	0.055	12.5	1.4
2 x Cu-C	2.811	2.795	0.016	0.009	12.5	1.4
2 x Cu-C	2.864	2.848	0.016	0.010	12.5	1.4
2 x Cu-C	2.936	2.919	0.017	0.010	12.5	1.4
2 x Cu-C	3.048	3.030	0.018	0.010	12.5	1.4
Cu-C	>3.0	>3.0	-	-	2.2	7.0
N-C (Multiple Sc.)	>3.0	>3.0	-	-	1.5	1.4

3.3.2.7 [Cu(TMG4NMe$_2$qu)$_2$]PF$_6$ (C9−PF$_6$)

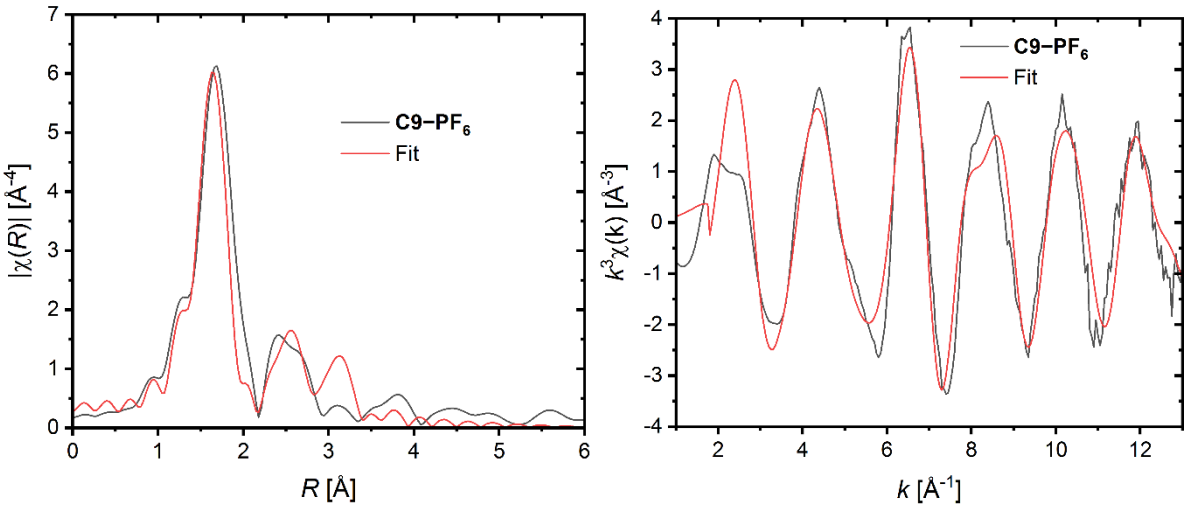

Fig. S8: Cu K-edge EXAFS spectra of [Cu(TMG4NMe$_2$qu)$_2$]PF$_6$ (**C9–PF$_6$**) in solution in MeCN.

Table S8: By EXAFS determined bond length of the [Cu(TMG4NMe$_2$qu)$_2$]PF$_6$ (**C9–PF$_6$**) in MeCN.

Bond	DFT [Å]	Fit [Å]	Δ [Å]	R-Fit Err [Å]	σ^2 [10^{-3} Å^2]	σ^2-Err [10^{-3} Å^2]
2 x Cu-N	1.991	1.958	0.033	0.016	0.03	1.6
2 x Cu-N	2.078	2.044	0.034	0.017	0.03	1.6
2 x Cu-C	2.833	2.879	0.045	0.033	2.1	4.9
2 x Cu-C	2.877	2.923	0.046	0.033	2.1	4.9
2 x Cu-C	2.961	3.008	0.048	0.345	2.1	4.6
Cu-C	>3.0	>3.0	-	-	1.6	9.8
N-C-N/N-N (Multiple Sc.)	>3.0	>3.0	-	-	2.1	8.5

3.3.2.8 [Cu(TMG4NMe$_2$qu)$_2$](OTf)$_2$ (C10−OTf)

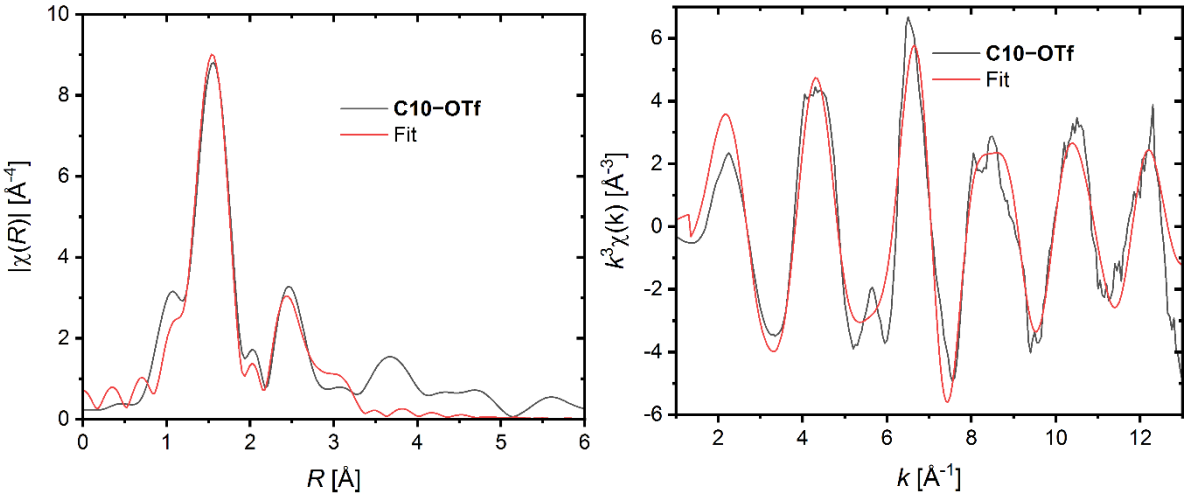

Fig. S9: Cu K-edge EXAFS spectra of [Cu(TMG4NMe$_2$qu)$_2$](OTf)$_2$ (**C10−OTf**) in solution in MeCN.

Table S9: By EXAFS determined bond length of the [Cu(TMG4NMe$_2$qu)$_2$](OTf)$_2$ (**C10−OTf**) in MeCN.

Bond	DFT [Å]	Fit [Å]	Δ [Å]	R-Fit Err [Å]	σ^2 [10^{-3} Å^2]	σ^2-Err [10^{-3} Å^2]
4 x Cu-N	1.969	1.959	0.010	0.008	3.9	1.0
4 x Cu-C	2.812	2.816	0.004	0.016	4.2	2.6
4 x Cu-C	2.963	2.966	0.003	0.017	4.2	2.6
4 x Cu-N-C	3.965	2.997	0.032	0.020	5.5	2.4
4 x Cu-N-C	3.099	3.030	0.069	0.015	5.5	2.4
4 x Cu-N-C	3.129	3.060	0.069	0.015	5.5	2.4
N-C-N/N-N (Multiple Sc.)	>3.0	>3.0	-	-	5.5	2.4

4. UV/Vis spectroscopy

4.1 Experimental

UV/Vis spectra were recorded with a Cary 60 spectrophotometer from Agilent Technologies in combination with quartz glass cuvettes (1 mm) at room temperature. The UV/Vis titration experiments were carried out on a Cary 60 spectrophotometer of Agilent Technologies connected via a Cary 50 fiber optic coupler and combined with a fiber-optic quartz glass immersion probe (Hellma, 1 mm) and a tailored Schlenk cell. For data acquisition, the software Cary WinUV (Version 5.1.3.1042) from Agilent Technologies was used. For visualization of the UV/Vis spectra and for visualization and examination of the results of the UV/Vis titration the software OriginPro 2021b (Version 9.8.5.212) from OriginLab was used.

4.2 UV/Vis spectra

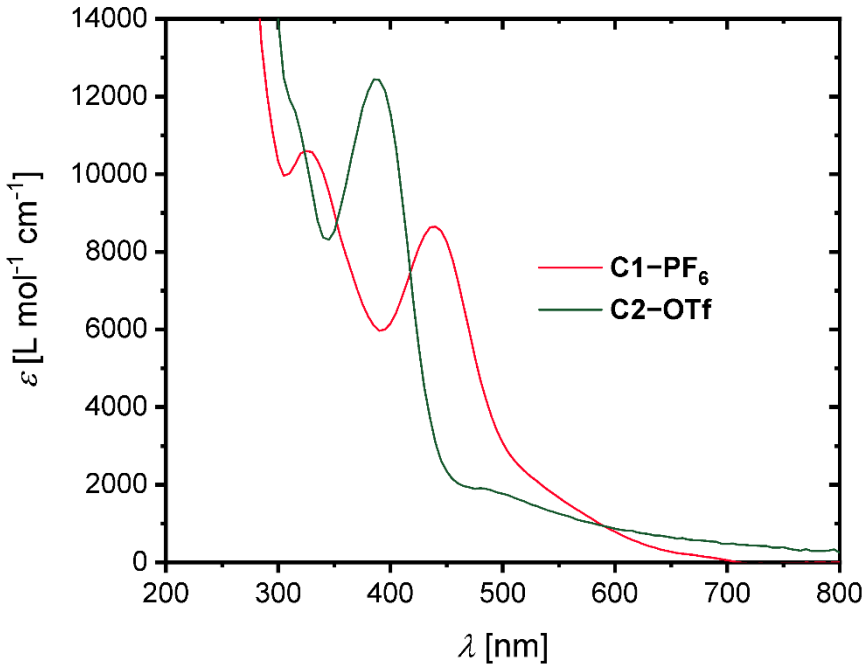

Fig. S10: UV/Vis spectra of the complexes $[Cu(TMGqu)_2]PF_6$ (**C1–PF$_6$**) and $[Cu(TMGqu)_2](OTf)_2$ (**C2–OTf**) in MeCN.

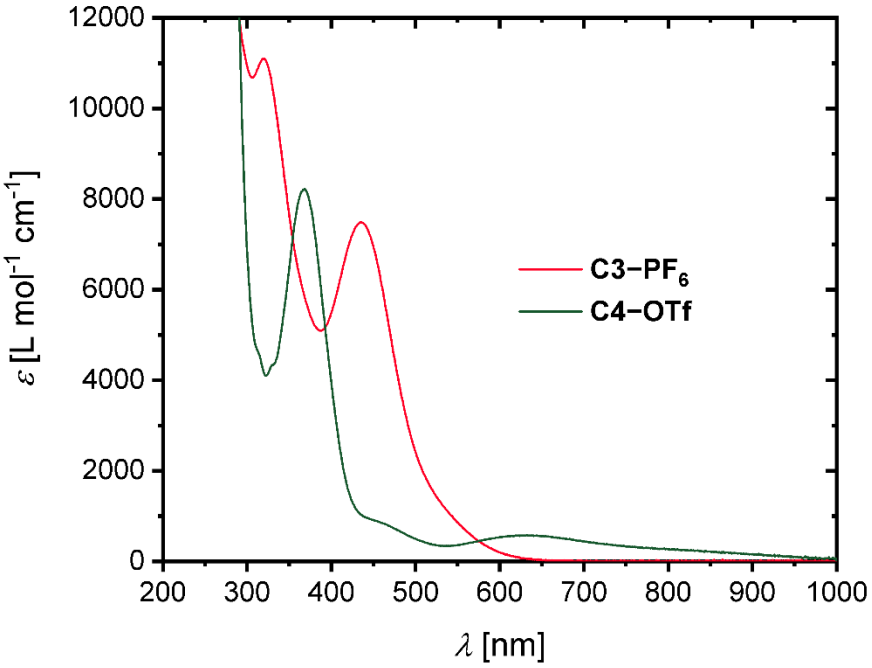

Fig. S11: UV/Vis spectra of the complexes $[Cu(TMG2Mequ)_2]PF_6$ (**C3–PF$_6$**) and $[Cu(TMG2Mequ)_2](OTf)_2$ (**C4–OTf**) in MeCN.

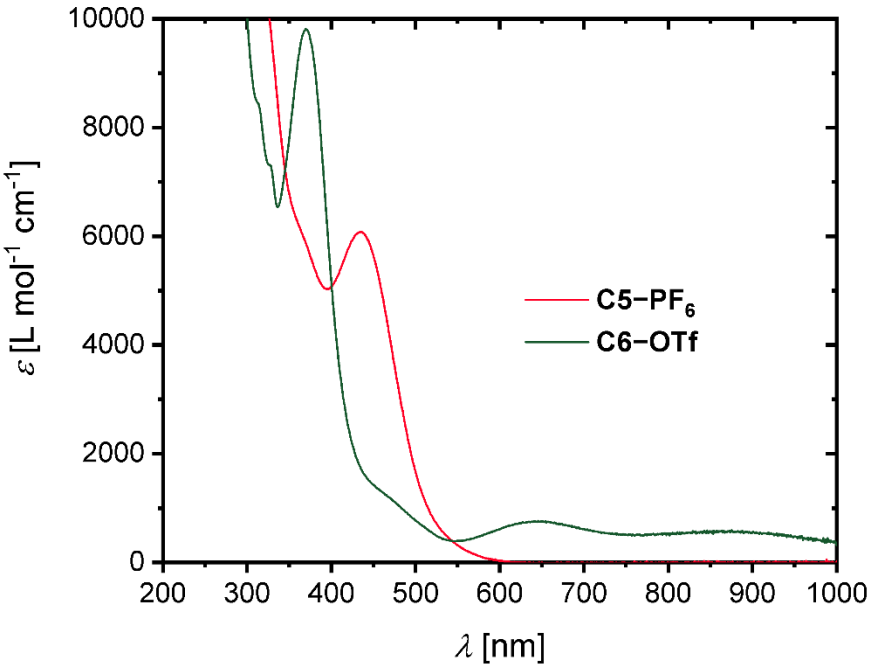

Fig. S12: UV/Vis spectra of the complexes $[Cu(TMG2^cHexqu)_2]PF_6$ (**C5–PF$_6$**) and $[Cu(TMG2^cHexqu)_2](OTf)_2$ (**C6–OTf**) in MeCN.

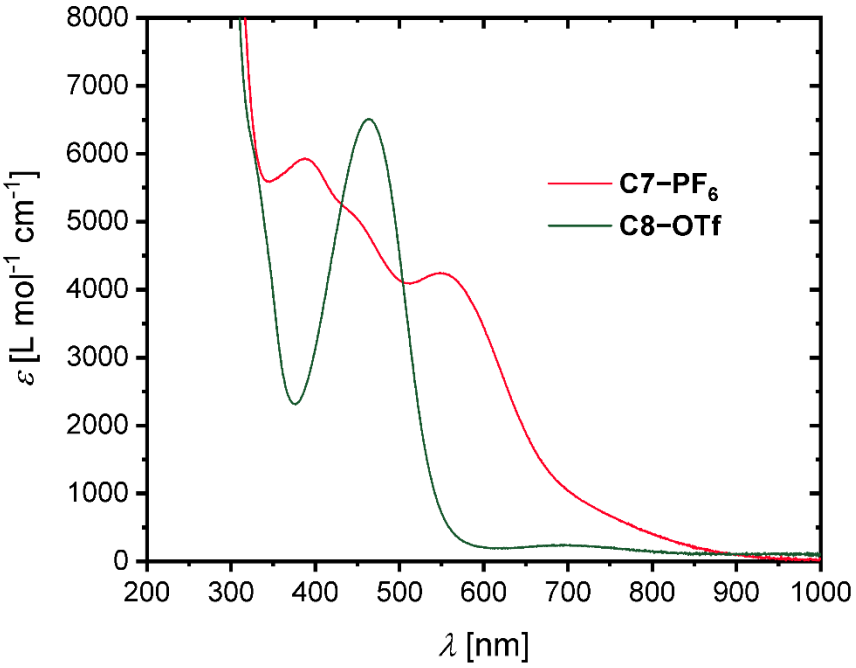

Fig. S13: UV/Vis spectra of the complexes $[Cu(TMG2Meequ)_2]PF_6$ (**C7–PF$_6$**) and $[Cu(TMG2Meequ)_2](OTf)_2$ (**C8–OTf**) in MeCN.

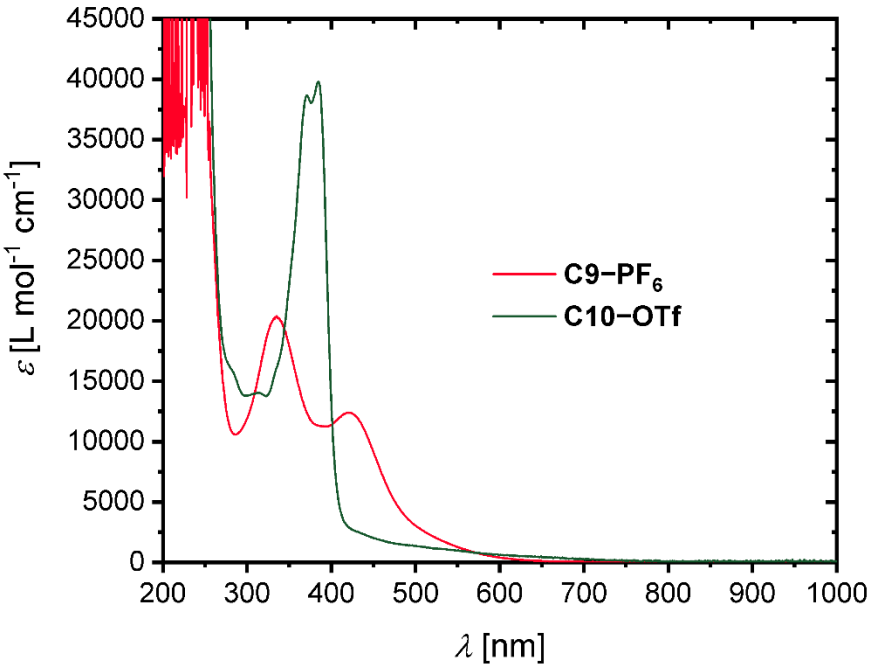

Fig. S14: UV/Vis spectra of the complexes $[Cu(TMG4NMe_2qu)_2]PF_6$ (**C9–PF$_6$**) and $[Cu(TMG4NMe_2qu)_2](OTf)_2$ (**C10–OTf**) in MeCN.

4.3 Titration experiments with TMG2^{t}Buqu (L3)

To analyze the coordination behavior of TMG2^{t}Buqu (**L3**) UV/Vis spectroscopic titration experiments were performed for the Cu(I) and the Cu(II) species. $[Cu(MeCN)_4]PF_6$ was used for the Cu(I) species and $[Cu(MeCN)_4](OTf)_2$ was used for the Cu(II) species. Solutions of $[Cu(MeCN)_4]PF_6$ (10 mL, 0.7 mM) and $[Cu(MeCN)_4](OTf)_2$ (10 mL, 1.2 mM) were prepared in MeCN and a solution of **L3** (20 mM) was successively added (40 x 50 µL) to each of these copper salt solutions under stirring. After every addition the solution was stirred for several minutes and a UV/Vis spectrum was recorded. The UV/Vis spectra of the free ligand TMG2^{t}Buqu is shown in Fig S15.

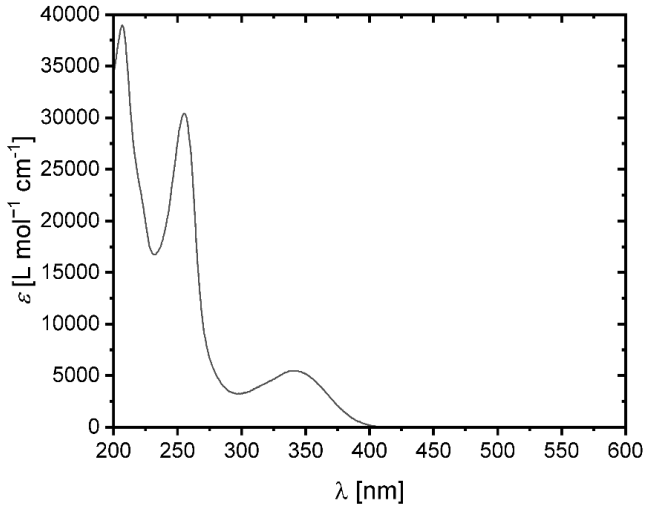

Fig. S15: UV/Vis spectra of TMG2^{t}Buqu (**L3**).

The recorded spectra during the titration of the $[Cu(MeCN)_4]PF_6$ solution are shown in Fig. S16.

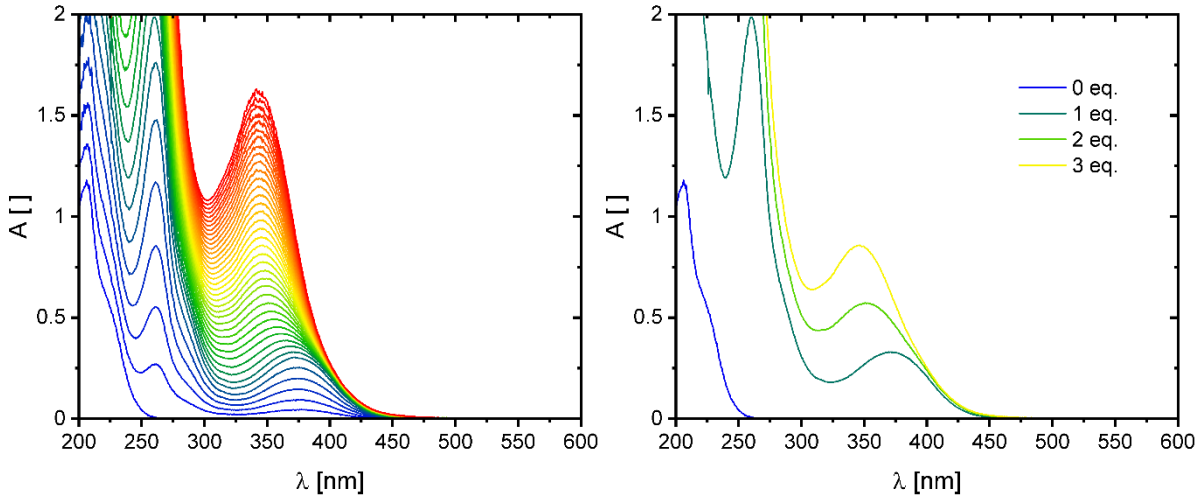

Fig. S16: All recorded UV/Vis spectra during the titration of $[Cu(MeCN)_4]PF_6$ with TMG2^{t}Buqu (**L3**) (left, titration process is visualized colorfully starting with blue and finishing with red) and selected UV/vis spectra after the addition of relevant equivalents (eq.) of TMG2^{t}Buqu (**L3**) are depicted (right).

In the beginning of the titration a formation of a transition at 375 nm is visible. By ongoing titration, the maximum shifts to 340 nm (Fig. S16). The band at 340 nm belongs to the free ligand (Fig. S15). The absorption at 400 nm was plotted against the added equivalent of **L3**

(Fig. S17). The absorption at 400 nm was chosen to minimize the influence of the free ligand on the absorption (Fig. S15). The absorption increases significantly until one equivalent of **L3** was added. Further addition of **L3** only leads to a weak increase of the absorption and is caused by the free ligand. For the transition with a maximum at 340 nm two linear correlations with the added amount of **L3** are visible (Fig. S18). After the addition of one equivalent the increase of the absorption becomes a little bit stronger. This is caused by the absorption of the free ligand at 340 nm and correlates with the extinction coefficient of the free ligand at 340 nm and the added amount of **L3** beyond the addition of one equivalent of **L3** (Fig. S15). The transition with a maximum at 255 nm is also visible for the free ligand and is not caused or affected by the coordination (Fig. S15 and S16). Therefore, the absorption increases linear with the added equivalent of **L3** (Fig. S19, results are only shown till two equivalents are added due to the noise). The discussed results and the nonexistent formation of another new transition indicate that the Cu(I) center is only coordinated by one ligand **L3** and a coordination of two ligands **L3** is not present. Due to the nonexistence of a bis(chelate) coordination motif this complex is not comparable with the other systems and therefore not further of interest for this study.

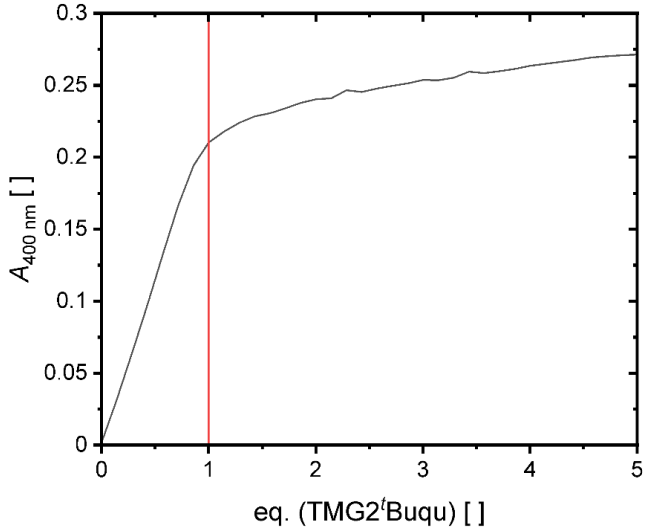

Fig. S17: Absorption at 400 nm against the added equivalent (eq.) of **L3**.

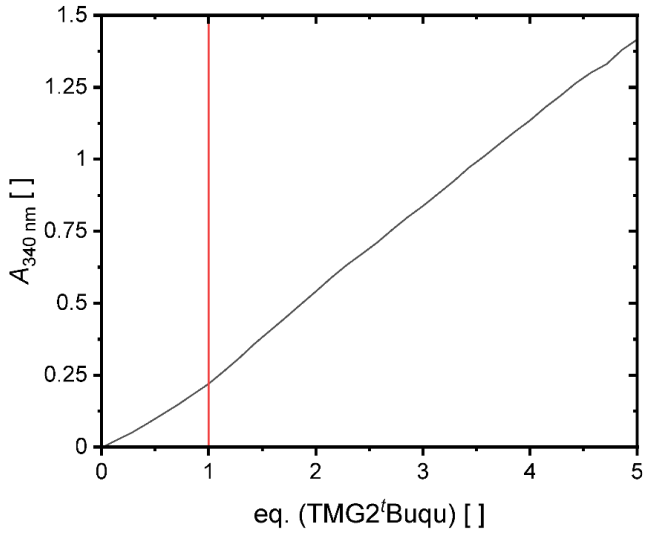

Fig. S18: Absorption at 340 nm against the added equivalent (eq.) of **L3**.

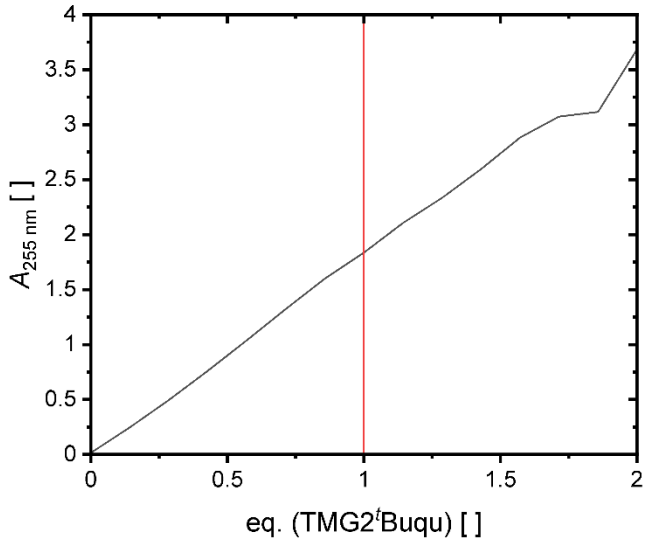

Fig. S19: Absorption at 255 nm against the added equivalent (eq.) of **L3** (after the addition of 1.5 eq. the detected absorbance is becoming noisy).

NMR spectra of the free ligand **L3** in CD_3CN and an *in situ* prepared 1:1 solution of $[Cu(MeCN)_4]PF_6$ and **L3** in CD_3CN were recorded (Fig. S82−S85). The shift of the signals in the *in situ* prepared 1:1 solution compared to the free ligand indicates the coordination of **L3** to the Cu(I) center.

The recorded spectra during the titration of the $[Cu(MeCN)_4](OTf)_2$ solution are shown in Fig. S20.

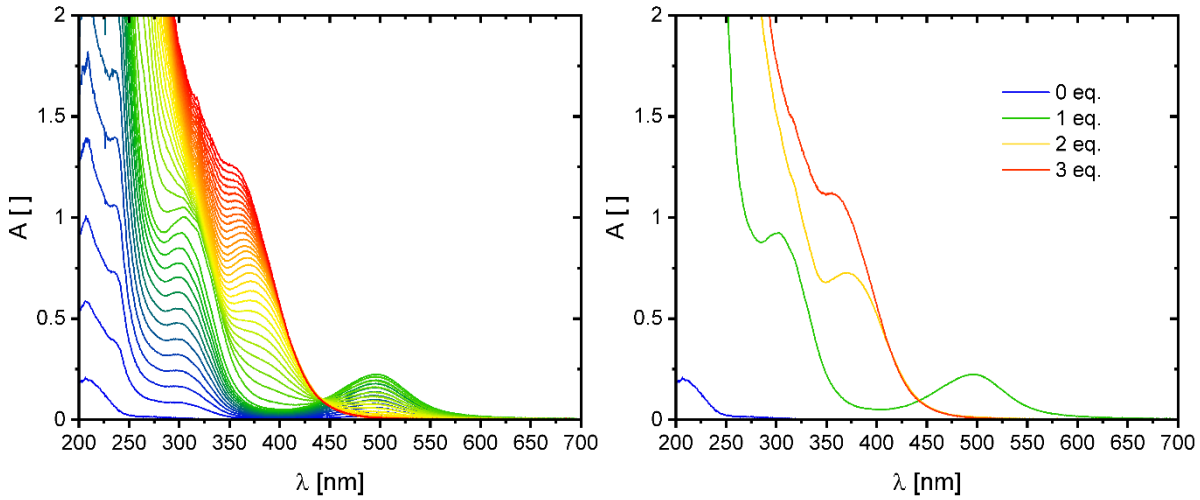

Fig. S20: All recorded UV/Vis spectra during the titration of $[Cu(MeCN)_4](OTf)_2$ with TMG2^{t}Buqu (**L3**) (left, titration process is visualized colorfully starting with blue and finishing with red) and selected UV/vis spectra after the addition of relevant equivalents (eq.) of TMG2^{t}Buqu (**L3**) are depicted (right).

In the beginning of the titration a formation of a transition at 495 nm is visible and reaches its maximum after the addition of one equivalent of **L3** (Fig. S21). With ongoing addition of **L3** this transition disappears again and is extinct after the addition of two equivalents of **L3**. A second transition with a maximum at 300 nm forms during the titration (Fig. S22). After the addition of one and two equivalent of **L3** the slope decreases. A third transition with a

maximum at 370 nm starts to form after the addition of one equivalent of **L3** (Fig. S23). The slope before the addition of one equivalent of **L3** is caused by the transitions at 300 nm and 495 nm (Fig. S20). The increase of the adsorption of the transitions at 300 nm and 370 nm beyond the addition of two equivalents of **L3** is caused by the absorption of the free ligand and correlates with the extinction coefficient of the free ligand at 300 nm and 370 nm and the added amount of **L3** beyond the addition of two equivalent of **L3** (Fig. S15). The results indicate that for Cu(II) two different coordination modes and therefore two different species are possible depending on the available equivalents of **L3**.

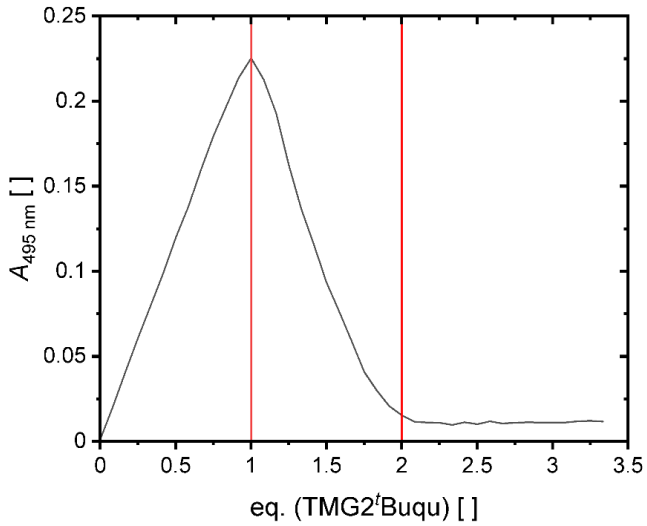

Fig. S21: Absorption at 495 nm against the added equivalent (eq.) of **L3**.

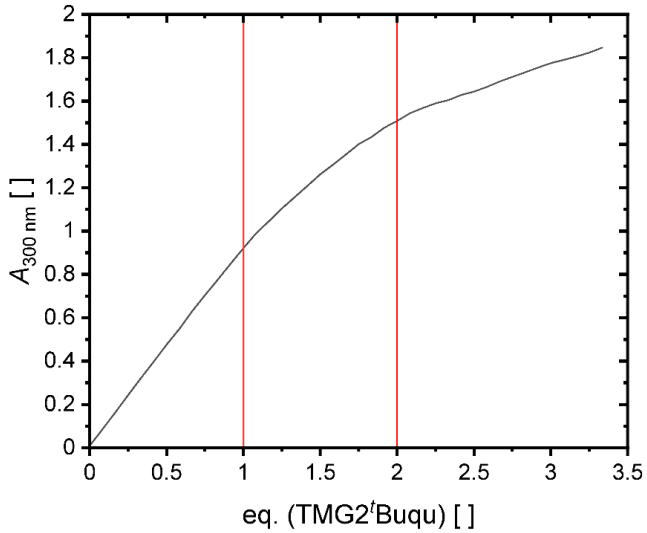

Fig. S22: Absorption at 300 nm against the added equivalent (eq.) of **L3**.

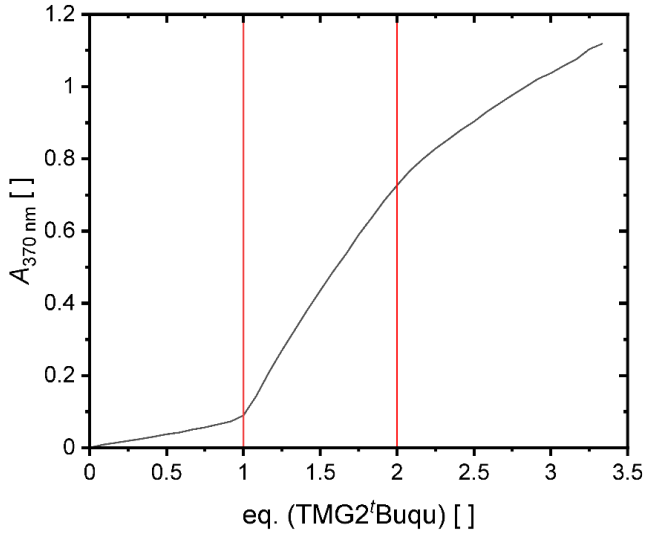

Fig. S23: Absorption at 370 nm against the added equivalent (eq.) of **L3**.

5. Cyclovoltammetry

5.1 Experimental

The measurements were performed with a METROHM AUTOLAB PGSTAT 101 potentiostat using a three-electrode arrangement with a Pt disc working electrode (1 mm diameter), a Pt wire as counter electrode and an Ag/AgCl reference electrode. The measurements were performed in MeCN and 0.1 M NBu_4PF_6 with a sample concentration of 1 mM at room temperature. Ferrocene was added as an internal standard after the measurements of the sample and all potentials are referenced relative to the Fc/Fc^+ potential. Cyclic voltammograms were measured with 200 mV·s^{-1}, 100 mV·s^{-1}, 50 mV·s^{-1}, and 20 mV·s^{-1}. For data acquisition and examination, the software NOVA 2.1.5 (Build 7691) from Metrohm Autolab was used. For visualization of the cyclic voltammograms the software OriginPro 2021b (Version 9.8.5.212) from OriginLab was used.

5.2 Results

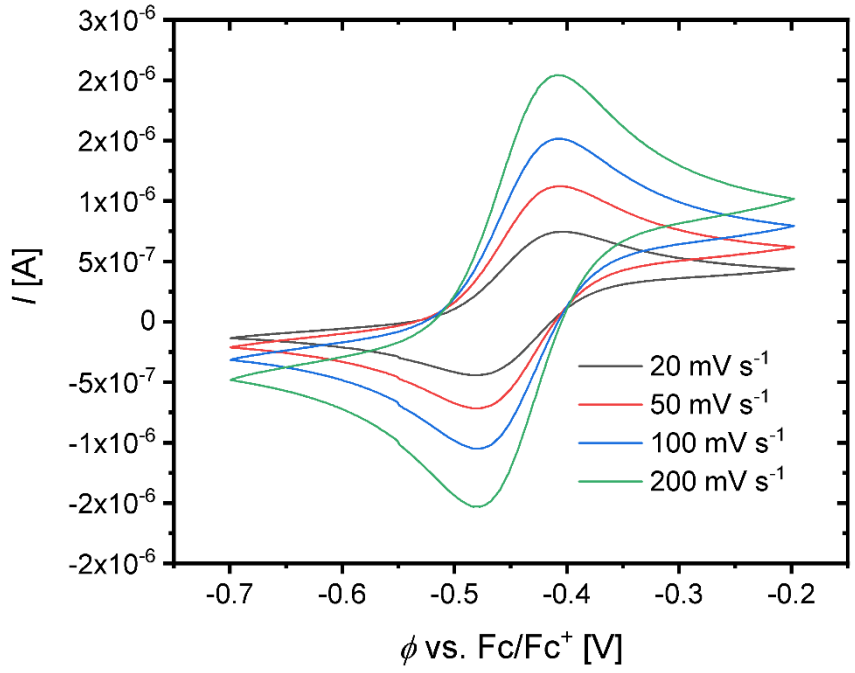

Fig. S24: Cyclic voltammogram of the complex redox couple $[Cu(TMGqu)_2]^{+/2+}$ (**R1**) starting from $[Cu(TMGqu)_2]PF_6$ (**C1–PF$_6$**) (c = 1 mM) in MeCN with $[NBu_4][PF_6]$ (c = 0.1 M).

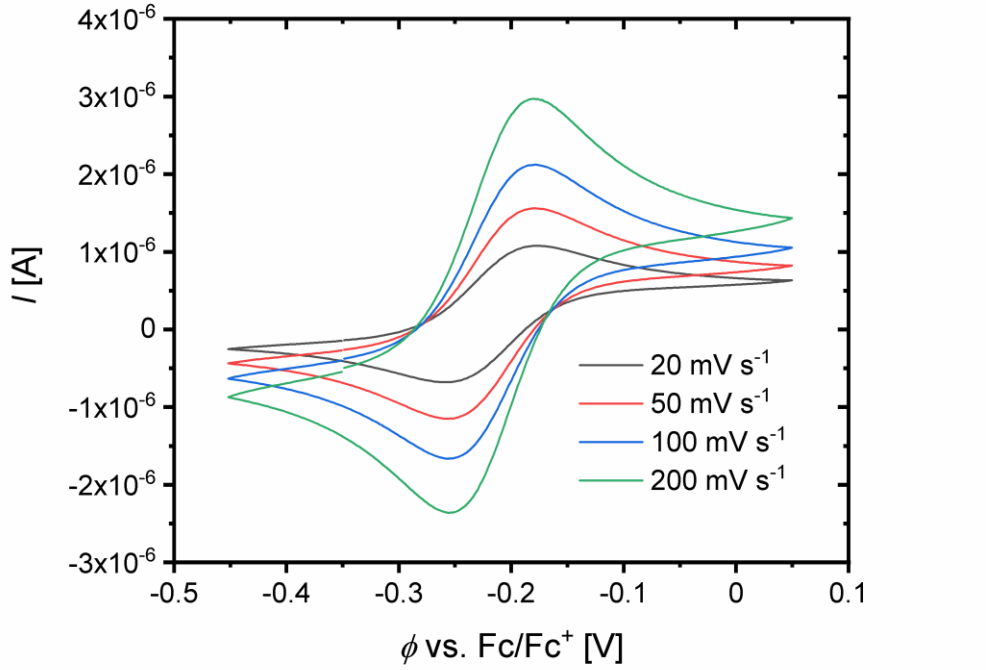

Fig. S25: Cyclic voltammogram of the complex redox couple $[Cu(TMG2Mequ)_2]^{+/2+}$ (**R2**) starting from $[Cu(TMG2Mequ)_2]PF_6$ (**C3–PF$_6$**) (c = 1 mM) in MeCN with $[NBu_4][PF_6]$ (c = 0.1 M).

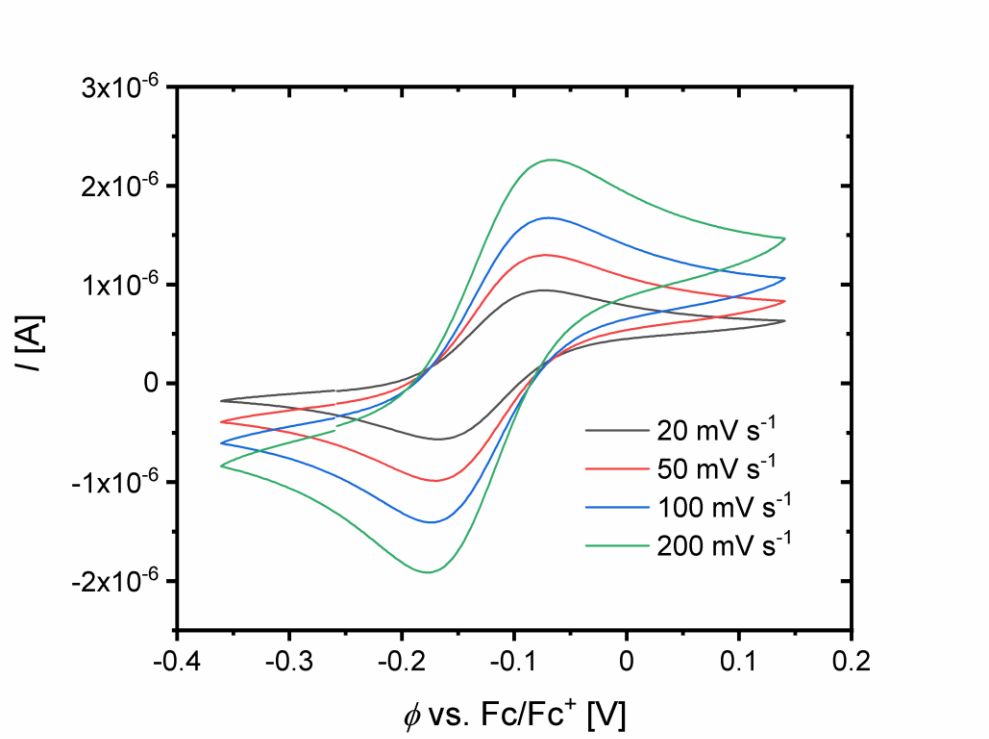

Fig. S26: Cyclic voltammogram of the complex redox couple $[Cu(TMG2^{c}Hexqu)_2]^{+/2+}$ (**R3**) starting from $[Cu(TMG^{c}Hexqu)_2]PF_6$ (**C5–PF$_6$**) (c = 1 mM) in MeCN with $[NBu_4][PF_6]$ (c = 0.1 M).

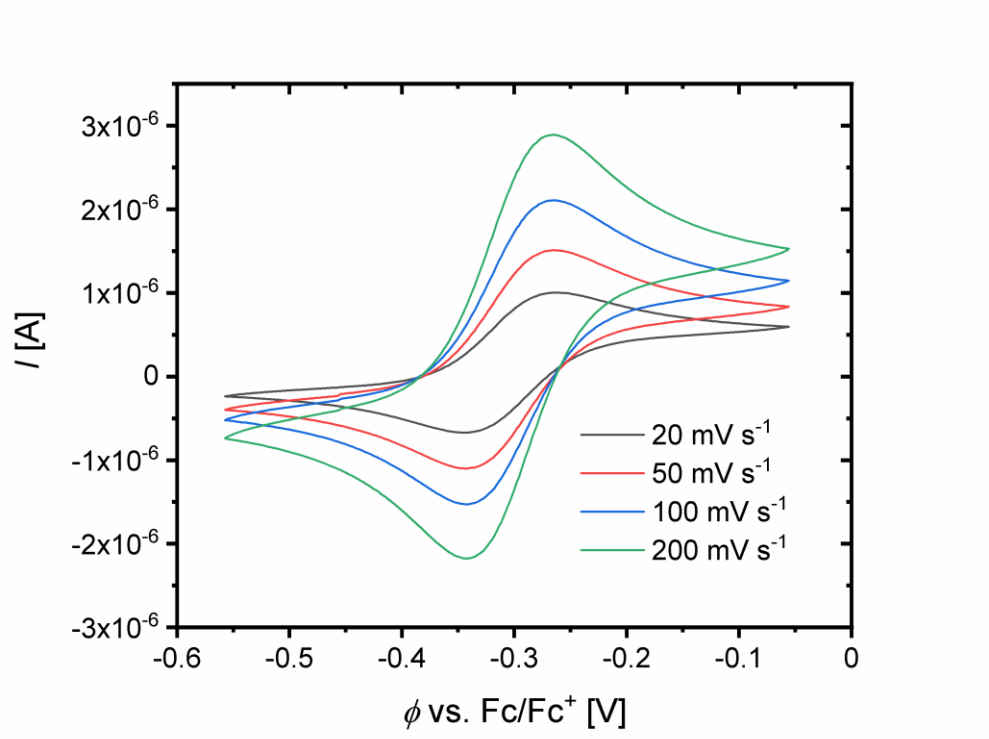

Fig. S27: Cyclic voltammogram of the complex redox couple $[Cu(TMG2Meequ)_2]^{+/2+}$ (**R4**) starting from $[Cu(TMG2Meequ)_2]PF_6$ (**C7–PF$_6$**) (c = 1 mM) in MeCN with $[NBu_4][PF_6]$ (c = 0.1 M).

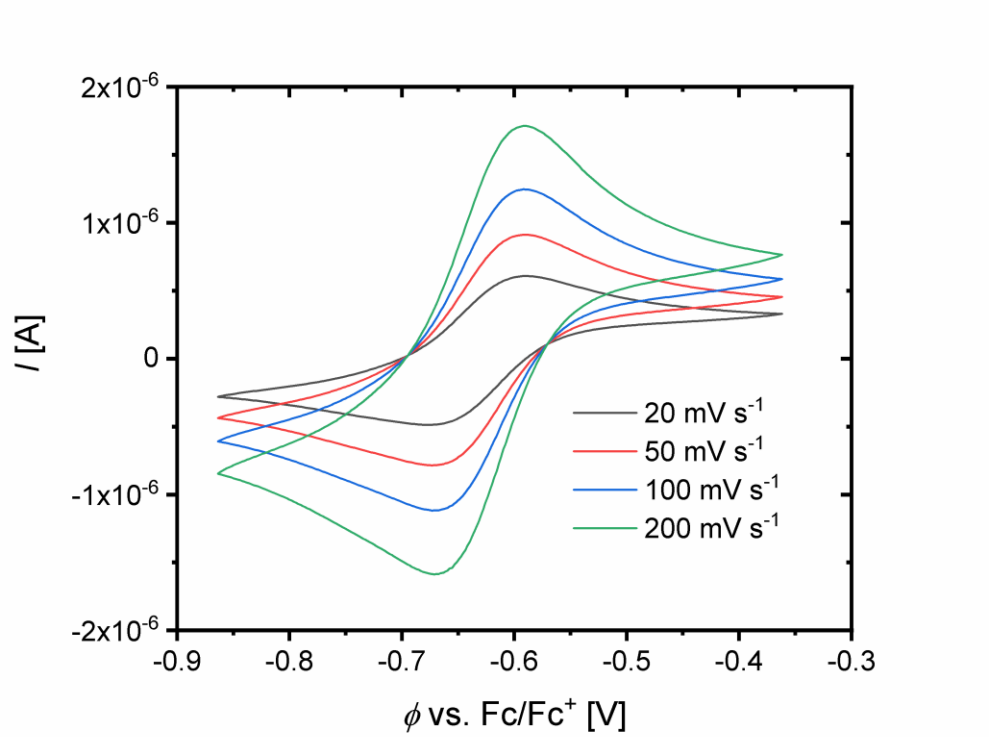

Fig. S28: Cyclic voltammogram of the complex redox couple $[Cu(TMG4NMe_2qu)_2]^{+/2+}$ (**R5**) starting from $[Cu(TMG4NMe_2qu)_2]PF_6$ (**C9–PF$_6$**) (c = 1 mM) in MeCN with $[NBu_4][PF_6]$ (c = 0.1 M).

Table S10: Redox potentials of the redox couples **R1 – R5**.

	$E_{1/2}$ [V] vs. Fc/Fc^+
$[Cu(TMGqu)_2]^{+/2+}$ (**R1**)	−0.441
$[Cu(TMG2Mequ)_2]^{+/2+}$ (**R2**)	−0.224
$[Cu(TMG2^cHexqu)_2]^{+/2+}$ (**R3**)	−0.134
$[Cu(TMG2Meequ)_2]^{+/2+}$ (**R4**)	−0.302
$[Cu(TMG4NMe_2qu)_2]^{+/2+}$ (**R5**)	−0.640

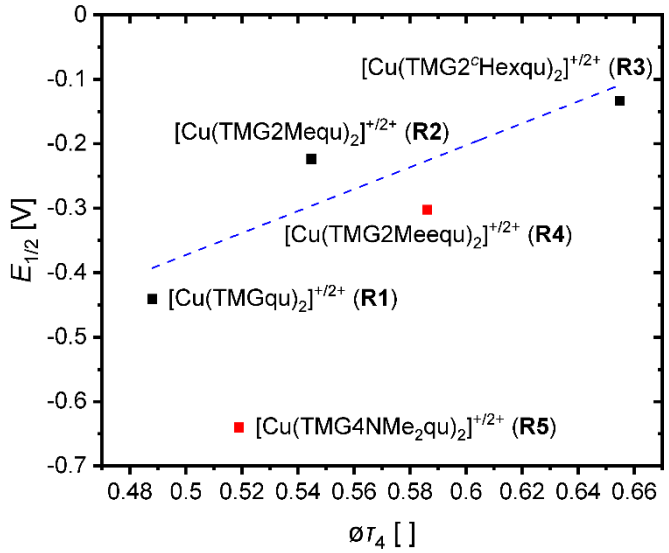

Fig. S29: Correlation between the redox potentials and the experimental $\varnothing\tau_4$ values of the redox couples (top, the redox couples **R4** and **R5** are marked red due to the misfit with the correlation caused by the electronic influence by the substituents).

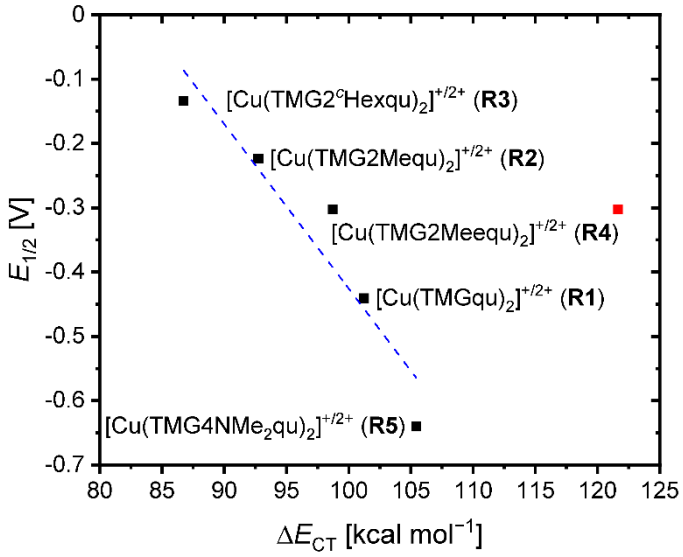

Fig. S30: Correlation between the redox potentials and the differences in the calculated charge-transfer energies ΔE_{CT} from all N donors (black) and all donors (including the O donors) for **R4** (red) to the Cu center of the corresponding Cu(II) and Cu(I) complexes.

6. Stopped-Flow-Measurements

6.1 Experimental

The stopped-flow measurements were performed with a HI-TECH Scientific SF-61SX2 device with a diode array detector. The optical light path for transmission of the quartz glass cuvette was 10 mm. The mixing time is given by HI-TECH to amount to 2 ms. UV/Vis spectra in a wavelength range of 300 nm to 800 nm were detected with a temporal resolution of 1.5 ms. The analyses were carried out with the TgK Scientific program Kinetic Studio 4.0.8.18533. UV/Vis spectra (300–800 nm) were detected. For visualization and examination of the results the software OriginPro 2021b (Version 9.8.5.212) from OriginLab was used.

The cross reactions of the Cu(I) complexes with the counter complex $[Co(bpy)_3](PF_6)_3$ were monitored. To measure the kinetic of the cross reaction a solution of each Cu(I) complex (0.2 mM) in MeCN was mixed with five differently concentrated solutions (with reactant in excess) of $[Co(bpy)_3](PF_6)_3$ complex (1 mM, 1.5 mM, 2 mM, 2.5 mM and 3 mM). The solutions of the Cu(I) complexes were prepared in situ with one equiv. of $[Cu(MeCN)_4]PF_6$ and two equiv. of the corresponding ligand. For every concentration of $[Co(bpy)_3](PF_6)_3$ 15 measurements were performed. The whole measurement for each Cu(I) complex were repeated twice.

Due to the five differently concentrated solutions of the counter complex the ionic strength was not the same for all analyzed cross reactions and varied for every solution of the counter complex with a specific concentration. The ionic strength influences the activity coefficients of the reactants. However, the influence on the activity coefficient is not significant for the determination of k_{12}. Therefore, for simplification the concentrations and not the activity coefficients were considered for the determination of k_{12}.

6.2 Results

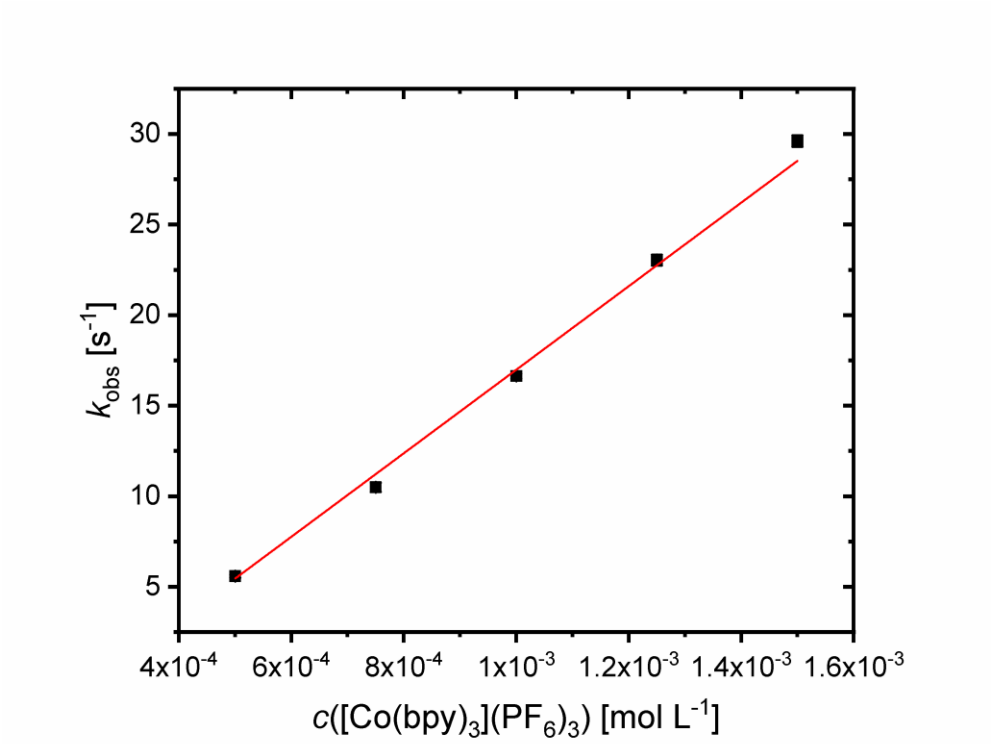

Fig. S31: Plot of the reaction rate k_{obs} of the cross reaction between $[Cu(TMGqu)_2]PF_6$ (**C1–PF$_6$**) and $[Co(bpy)_3](PF_6)_3$ against the concentration of $[Co(bpy)_3](PF_6)_3$. The error bars are too small to be visualized properly.

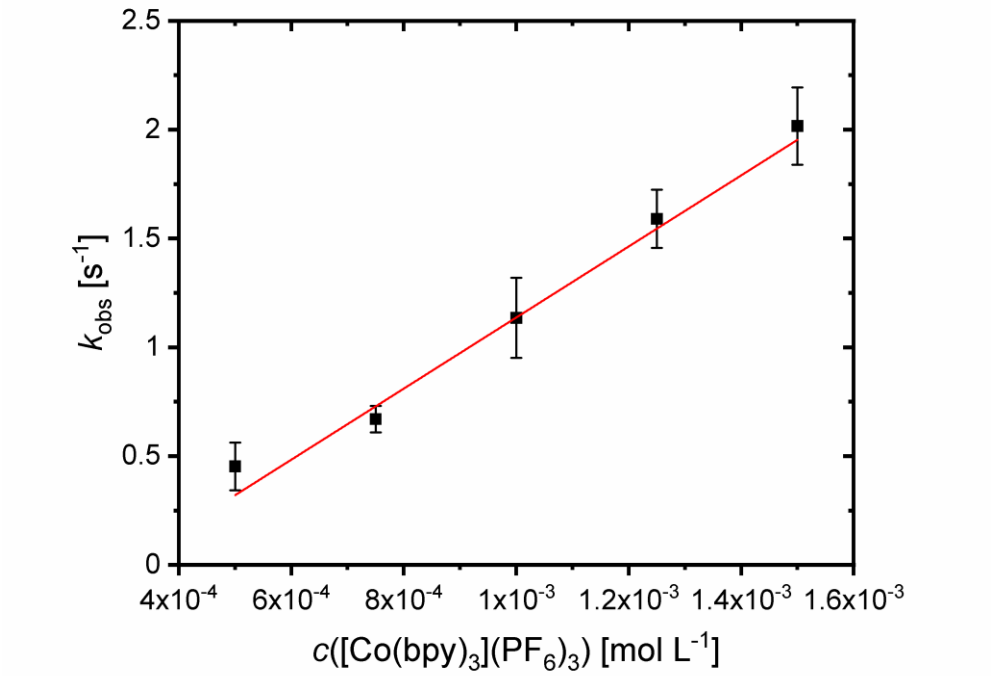

Fig. S32: Plot of the reaction rate k_{obs} of the cross reaction between $[Cu(TMG2Mequ)_2]PF_6$ (**C3–PF$_6$**) and $[Co(bpy)_3](PF_6)_3$ against the concentration of $[Co(bpy)_3](PF_6)_3$.

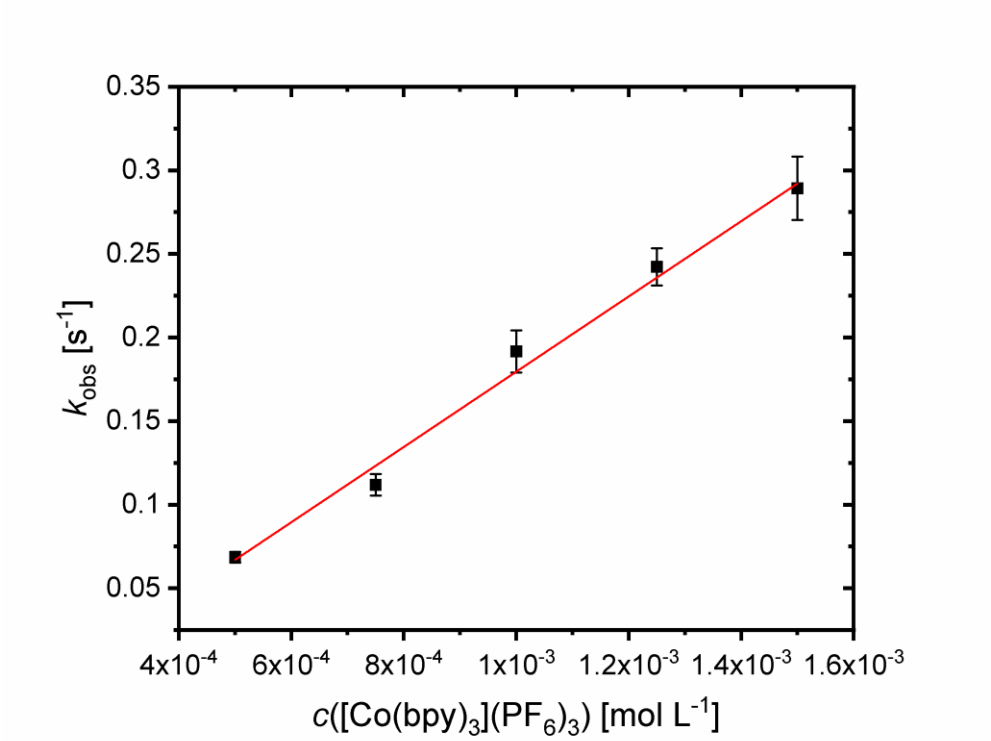

Fig. S33: Plot of the reaction rate k_{obs} of the cross reaction between $[Cu(TMG^{c}Hexqu)_2]PF_6$ (**C5–PF$_6$**) and $[Co(bpy)_3](PF_6)_3$ against the concentration of $[Co(bpy)_3](PF_6)_3$. Some error bars are too small to be visualized properly.

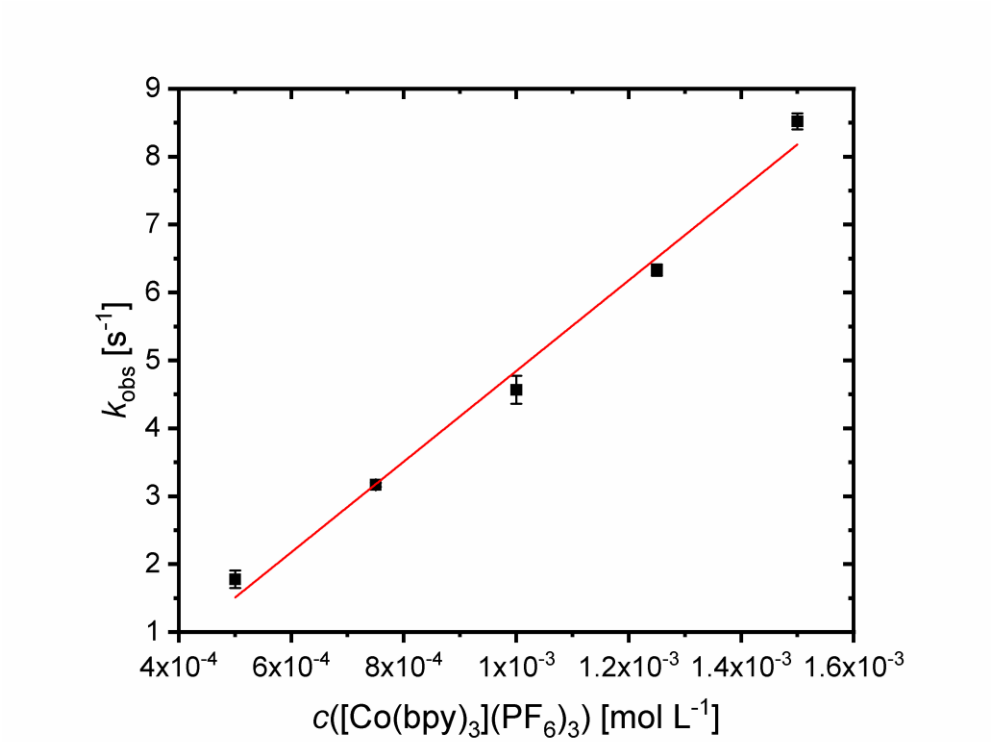

Fig. S34: Plot of the reaction rate k_{obs} of the cross reaction between $[Cu(TMG2Meequ)_2]PF_6$ (**C7–PF$_6$**) and $[Co(bpy)_3](PF_6)_3$ against the concentration of $[Co(bpy)_3](PF_6)_3$. Some error bars are too small to be visualized properly.

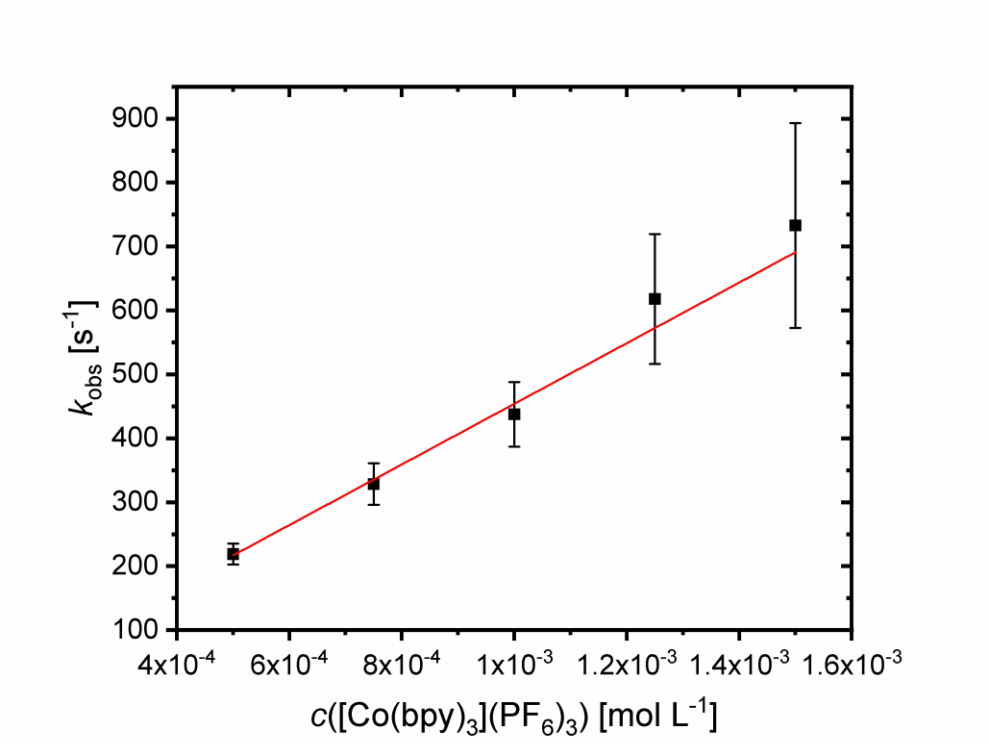

Fig. S35: Plot of the reaction rate k_{obs} of the cross reaction between $[Cu(TMG4NMe_2qu)_2]PF_6$ (**C9–PF_6**) and $[Co(bpy)_3](PF_6)_3$ against the concentration of $[Co(bpy)_3](PF_6)_3$.

7. Marcus theory

The Marcus theory describes the outer-sphere electron-transfer between two metal complexes.[26] With the Marcus cross relation which emerges from the Marcus theory the reaction rate (k_{12}) of an outer-sphere electron-transfer between two metal complexes (M_1^+ and M_2^{2+}) can be determined (Scheme S1, Equation 1). This reaction is called cross reaction. In the manuscript the complex M_1^+ corresponds to the Cu(I) complexes and the complex M_2^{2+} corresponds to the counter complex $[Co(bpy)_3]^{3+}$.

$$M_1^+ + M_2^{2+} \xrightarrow{k_{12}} M_1^{2+} + M_2^+$$

Scheme S1: Cross reaction between two complexes.

$$k_{12} = \sqrt{k_{11} \cdot k_{22} \cdot K_{12} \cdot f_{12}} \cdot W_{12} \quad (1)$$

k_{11} and k_{22} are the electron self-exchange rates of the redox couples (M_1^+/M_1^{2+} and M_2^+/M_2^{2+}) of the two involved complexes (M_1^+ and M_2^{2+}). The electron self-exchange rate is the reaction rate of the redox reaction of the reduced form with the oxidized form of the same redox couple (Scheme S2). It describes how fast an electron is transferred between the reduced form (M_1^+ or M_2^+) and the oxidized form (M_1^{2+} or M_2^{2+}) of the same redox couple (M_1^+/M_1^{2+} and M_2^+/M_2^{2+}). In the manuscript the redox couple M_1^+/M_1^{2+} corresponds to the copper complex redox couples and the redox couple M_2^+/M_2^{2+} corresponds to the counter complex redox couple $[Co(bpy)_3]^{2+/3+}$.

$$M_1^+ + M_1^{2+} \xrightarrow{k_{11}} M_1^{2+} + M_1^+$$

$$M_2^+ + M_2^{2+} \xrightarrow{k_{22}} M_2^{2+} + M_2^+$$

Scheme S2: Electron self-exchange reactions between the reduced form and the oxidized form of the same redox couple.

K_{12} is the equilibrium constant of the cross reaction. It depends on the difference between the redox potentials ΔE_{12} of the redox couples (M_1^+/M_1^{2+} and M_2^+/M_2^{2+}) of the two involved complexes (M_1^+ and M_2^{2+}).

$$K_{12} = \exp\left(\frac{\Delta E_{1/2} \cdot n \cdot F}{R \cdot T}\right) \quad (2)$$

W_{12} is the work term and describes the electrostatic work that is occurs during the cross reaction (Equation 4). It includes the electrostatic work w that has to be overcome for the approach of two charged particles, in this case complex cations.

$$W_{12} = \exp\left(\frac{w_{11} + w_{22} - w_{12} - w_{21}}{2 \cdot R \cdot T}\right) \quad (3)$$

f_{12} represents the transmission coefficient or average transition probability for the electron transfer every time the system (the two complex of the cross reaction) passes the intersection region. The intersection region is the point where the nuclear configuration of the system is suitable for the electron-transfer.

$$f_{12} = \exp\left(\frac{\left(\ln K_{12} + \frac{w_{12} - w_{21}}{\mathrm{R} \cdot T}\right)^2}{4 \cdot \left(\ln\left(\frac{k_{22} \cdot k_{22}}{Z^2}\right) + \frac{w_{11} + w_{22}}{\mathrm{R} \cdot T}\right)}\right) \tag{4}$$

Z^2 represents the formation constant of the outer-sphere complex and is usually 10^{22} M^{-2} s^{-2}.[27]

By transposition of Equation 1, Equation 5 is obtained. This equation enables the calculation of the electron self-exchange rate (k_{11}) of the redox couple (M_1^+/M_1^{2+}) after examination of the cross reaction and if the electron self-exchange rate (k_{22}) of the of the redox couple (M_2^+/M_2^{2+}) is known.

$$k_{11} = \frac{{k_{12}}^2}{k_{22} \cdot K_{12} \cdot f_{12} \cdot {W_{11}}^2} \tag{5}$$

8. Crystallographic data

8.1 Ligands

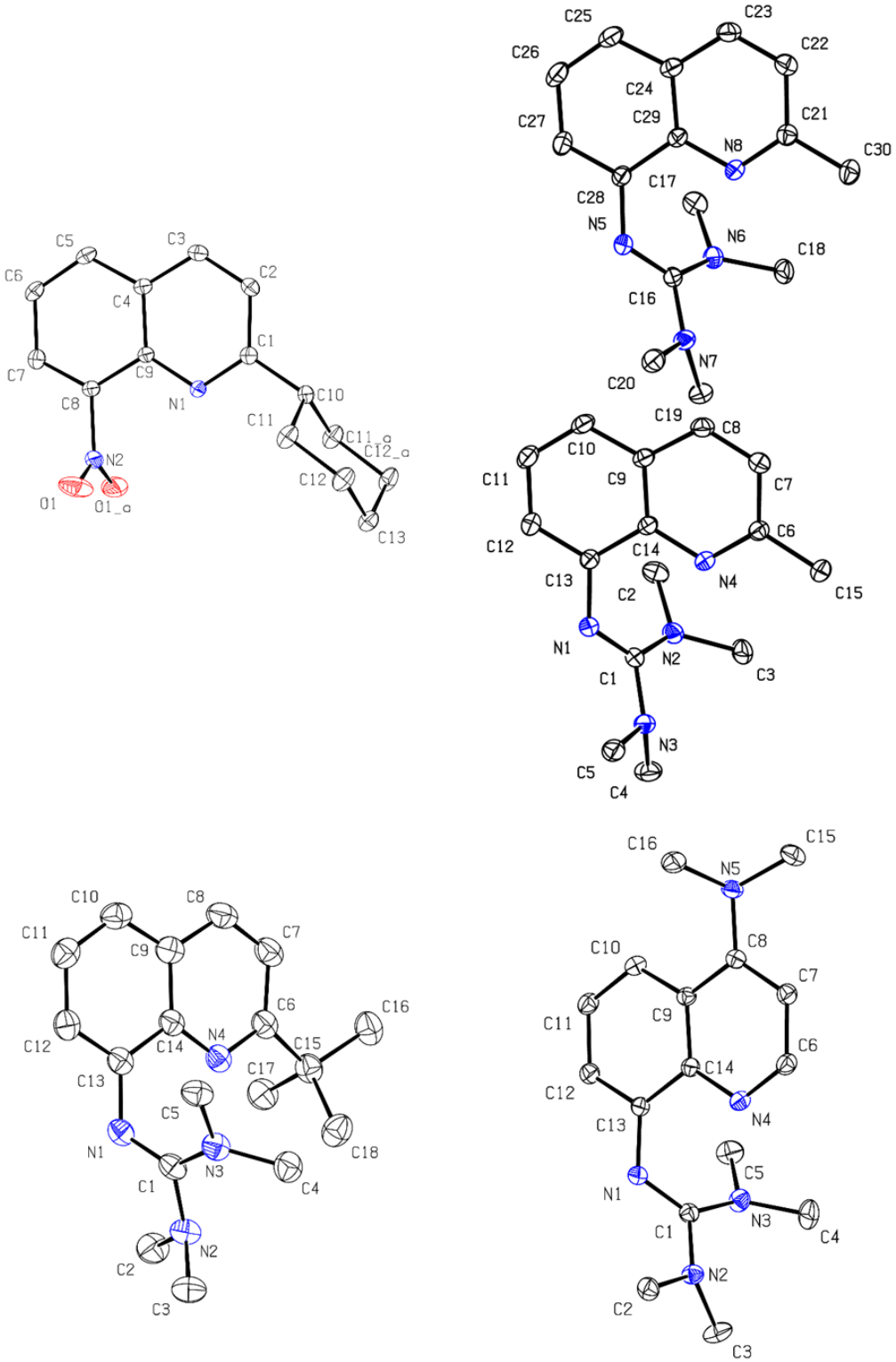

Fig. S36: Displacement ellipsoid plot of 2-^{c}Hex-8-NO_2-qu (top left), TMG2Mequ (**L2**) (top right, two independent molecules in the asymmetric unit), TMG2^{t}Buqu (**L3**) (bottom left) and TMG4NMe_2qu (**L6**) (bottom right) (50 % probability, asymmetric unit, H atoms are omitted for clarity).

Table S11: Crystallographic data 2-^{c}Hex-8-NO2-qu, **L2**, **L3** and **L6**.

	2-^{c}Hex-8-NO_2-qu	**L2**	**L3**	**L6**
Empirical formula	$C_{15}H_{16}N_2O_2$	$C_{15}H_{20}N_4$	$C_{18}H_{26}N_4$	$C_{16}H_{23}N_5$
Formula weight [g mol^{-1}]	256.30	256.35	298.43	285.39
Crystal size [mm]	0.150 x 0.147 x 0.140	0.300 x 0.280 x 0.250	0.130 x 0.070 x 0.020	0.240 x 0.190 x 0.140
T [K]	100	100	100	100
Crystal system	monoclinic	triclinic	triclinic	orthorhombic
Space group	$P2_1/m$	$P\bar{1}$	$P\bar{1}$	$Pna2_1$
a [Å]	8.4884(17)	6.8391(14)	6.8997(14)	15.194(3)
b [Å]	6.7183(13)	14.447(3)	10.446(2)	11.576(2)
c [Å]	11.755(2)	15.756(3)	12.234(2)	8.9945(18)
α [°]	90	64.51(3)	103.63(3)	90
β [°]	108.39(3)	89.05(3)	98.86(3)	90
γ [°]	90	86.95(3)	93.79(3)	90
V [Å^3]	636.1(2)	1403.2(6)	841.9(3)	1582.0(5)
Z	2	4	2	4
$\rho_{calcd.}$ [g cm^{-3}]	1.338	1.213	1.177	1.198
μ [mm^{-1}]	0.090	0.075	0.553	0.075
λ [Å]	0.71073	0.71073	1.54186	0.71073
F(000)	272	552	324	616
hkl range	±12, -5 ≤ k ≤ 10, ±18	±10, -15 ≤ k ≤ 22, -19 ≤ l ≤ 24	-7 ≤ h ≤ 8, -10 ≤ k ≤ 12, -11 ≤ l ≤ 14	±23, ±17, ±13
Reflections collected	8322	18788	4739	28900
Independent reflections	2549	10154	2782	5975
$R_{int.}$	0.0258	0.0240	0.0238	0.0288
Number of parameters	106	353	206	196
R_1 [$I \geq 2\sigma(I)$]	0.0412	0.0537	0.0507	0.0387
wR_2 (all data)	0.1213	0.1448	0.1370	0.0994
Goodness-of-fit	1.021	1.156	1.098	1.083
Abs. structure parameter				0.6(4)
Largest diff. peak, hole [e Å^{-3}]	0.444, -0.272	0.493; -0.249	0.186; -0.267	0.338; -0.186

8.2 Complexes

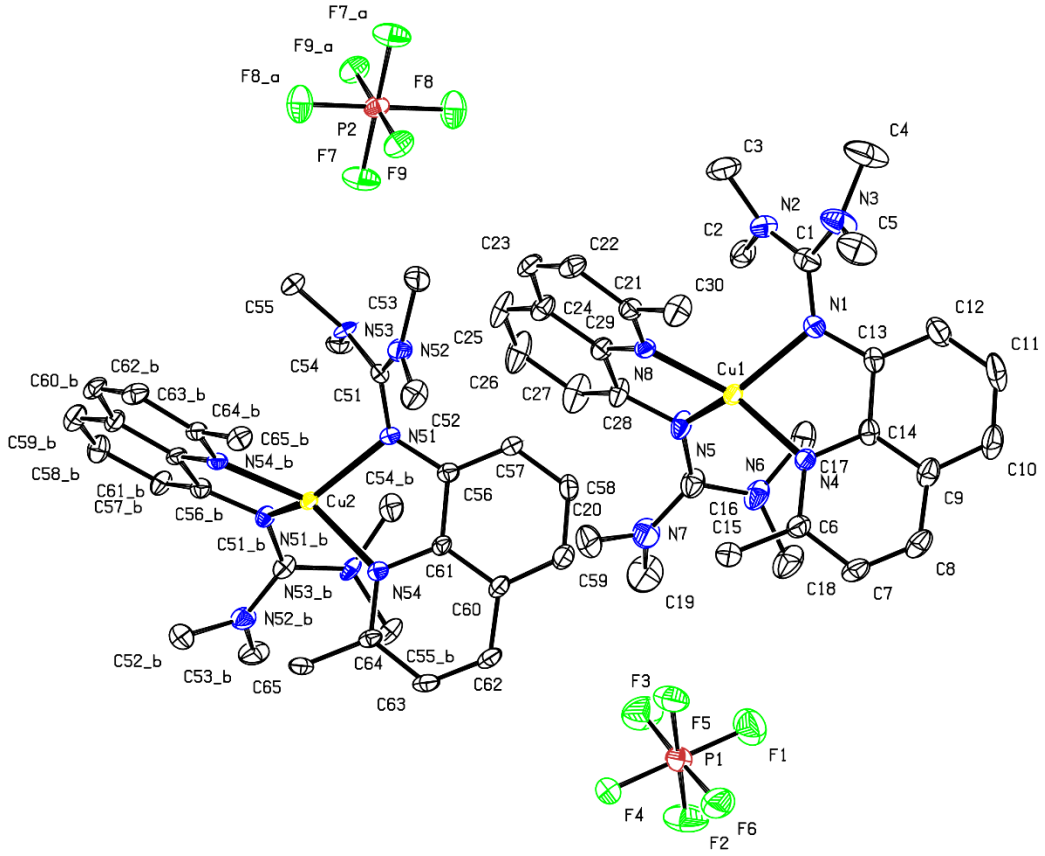

Fig. S37: Displacement ellipsoid plot of $[Cu(TMG2Mequ)_2]PF_6$ (**C3–PF$_6$**) (50 % probability, H atoms are omitted for clarity).

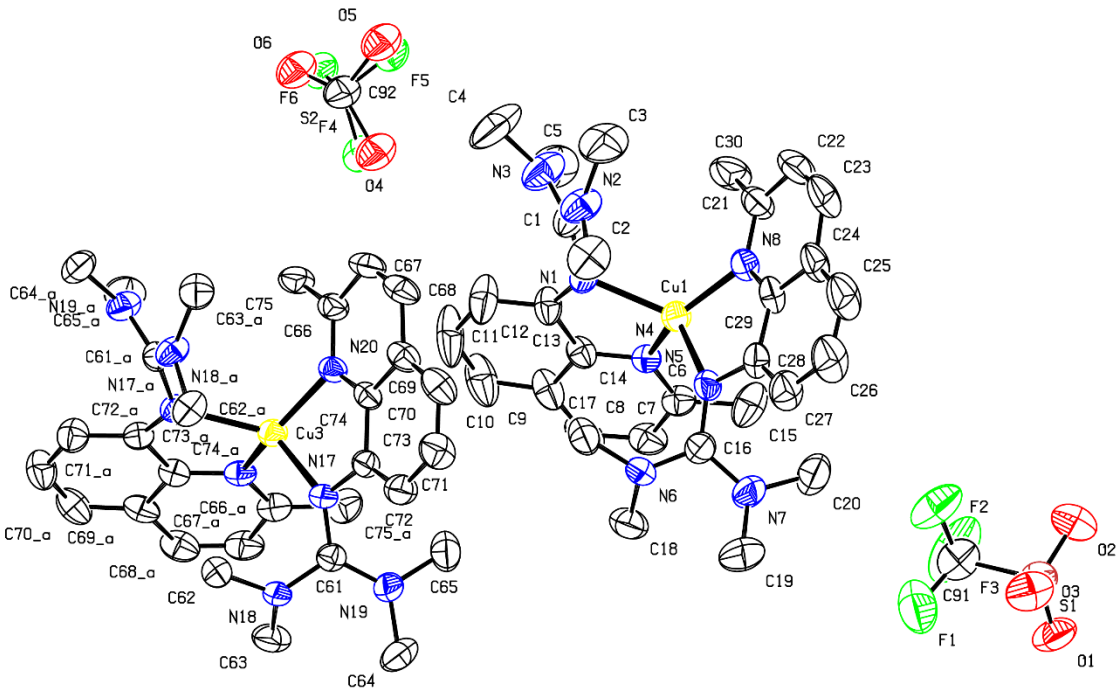

Fig. S38: Displacement ellipsoid plot of $[Cu(TMG2Mequ)_2]OTf$ (**C3–OTf**) (50 % probability, H atoms are omitted for clarity).

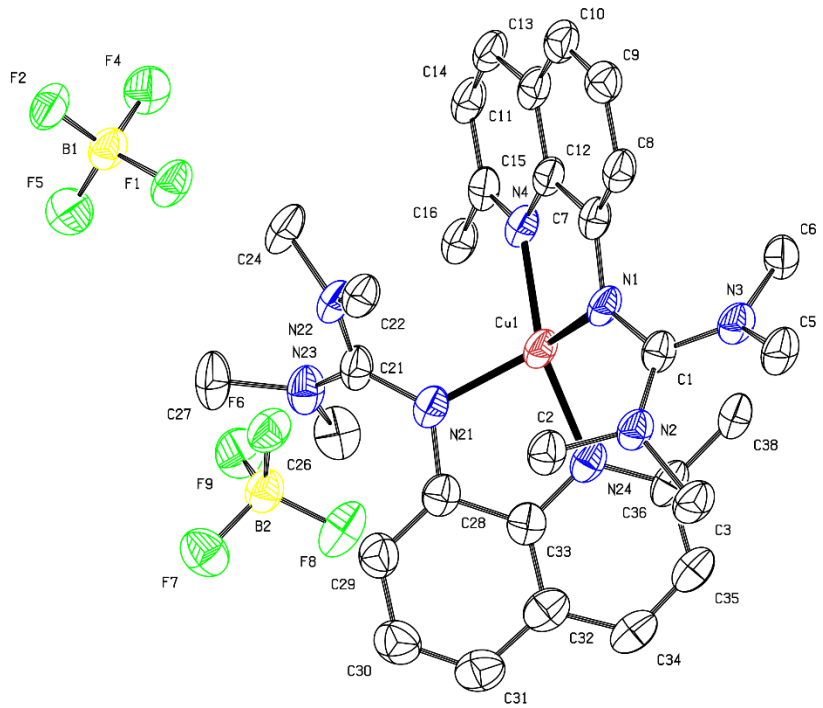

Fig. S39: Displacement ellipsoid plot of $[Cu(TMG2Mequ)_2](BF_4)_2$ (**C4–BF$_4$**) (50 % probability, asymmetric unit, H atoms are omitted for clarity).

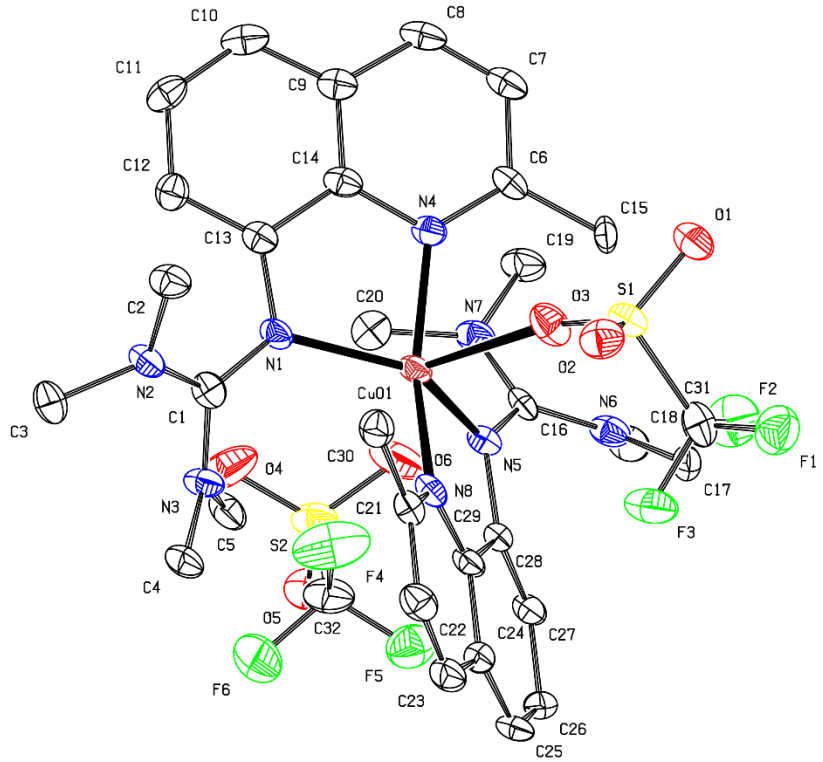

Fig. S40: Displacement ellipsoid plot of $[Cu(TMG2Mequ)_2](OTf)_2$ (**C4–OTf**) (50 % probability, asymmetric unit, H atoms are omitted for clarity).

Table S12: Crystallographic data **C3–PF_6**, **C3–OTf**, **C4–BF_4** and **C4–OTf**.

	C3–PF_6	**C3–OTf**	**C4–BF_4**	**C4–OTf**
Empirical formula	$C_{30}H_{40}CuF_6N_8P$	$C_{31}H_{40}CuF_3N_8O_3S$	$C_{30}H_{40}B_2CuF_8N_8$	$C_{32}H_{40}CuF_6N_8O_6S_2$
Formula weight [g mol^{-1}]	721.21	725.31	749.86	874.38
Crystal size [mm]	0.200 x 0.180 x 0.140	0.200 x 0.100 x 0.040	0.250 x 0.230 x 0.040	0.470 x 0.300 x 0.110
T [K]	100	240	100	100(2)
Crystal system	monoclinic	monoclinic	monoclinic	triclinic
Space group	$I2/a$	$I2/a$	$P2_1/c$	$P\bar{1}$
a [Å]	22.442(5)	22.769(5)	17.171(3)	10.318(2)
b [Å]	10.441(2)	10.613(2)	8.9412(18)	12.507(3)
c [Å]	41.640(14)	42.709(17)	22.701(5)	16.034(3)
α [°]	90	90	90	98.43(3)
β [°]	91.84(3)	90.75(3)	108.94(3)	95.28(3)
γ [°]	90	90	90	113.19(3)
V [$Å^3$]	9752(4)	10320(5)	3296.7(13)	1855.7(8)
Z	12	12	4	2
$\rho_{calcd.}$ [g cm^{-3}]	1.474	1.401	1.511	1.565
μ [mm^{-1}]	0.791	0.756	0.744	0.787
λ [Å]	0.71073	0.71073	0.71073	0.71073
F(000)	4488	4536	1548	902
hkl range	±27, ±12, ± 50	$-26 \le h \le 27$, ±12, $-41 \le l \le 51$	±20, ±10, ±27	±12, ±15, ±19
Reflections collected	52717	83812	39849	18374
Independent reflections	9051	9585	6125	6766
$R_{int.}$	0.0365	0.1011	0.1029	0.0756
Number of parameters	639	654	452	506
R_1 [$I \ge 2\sigma(I)$]	0.0682	0.0527	0.0857	0.0616
wR_2 (all data)	0.1757	0.1277	0.2265	0.2260
Goodness-of-fit	1.095	0.922	1.081	1.065
Largest diff. peak, hole [e $Å^{-3}$]	3.597; -0.502	0.924; -0.434	1.523, -0.961	2.360; -1.252

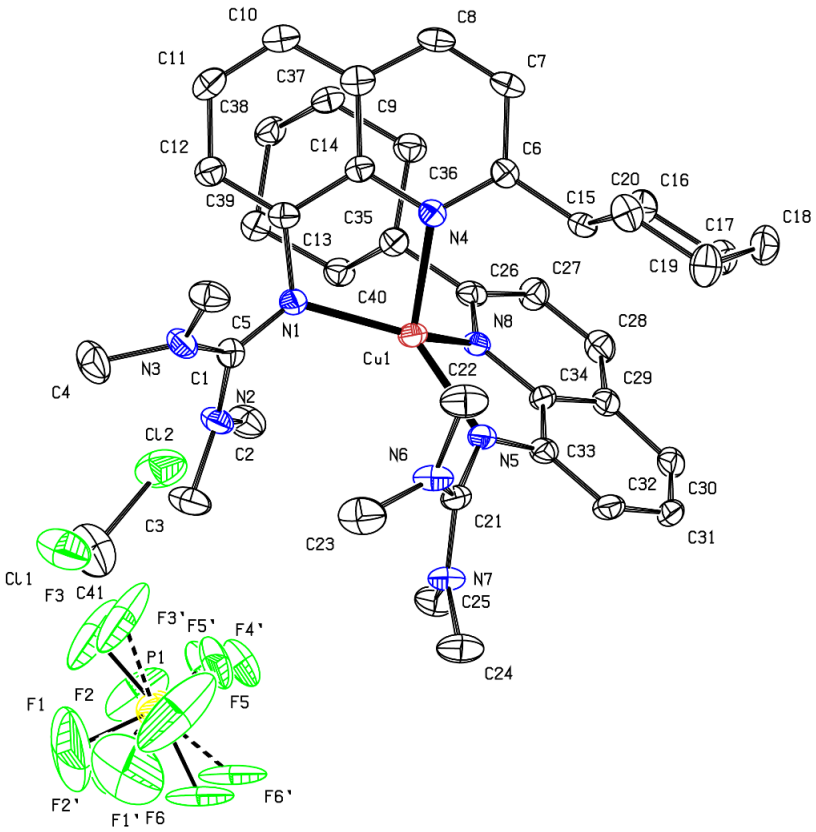

Fig. S41: Displacement ellipsoid plot of [Cu(TMG2^{c}Hexqu)$_2$]PF$_6$·DCM (**C5−PF$_6$**) (50 % probability, asymmetric unit, H atoms are omitted for clarity).

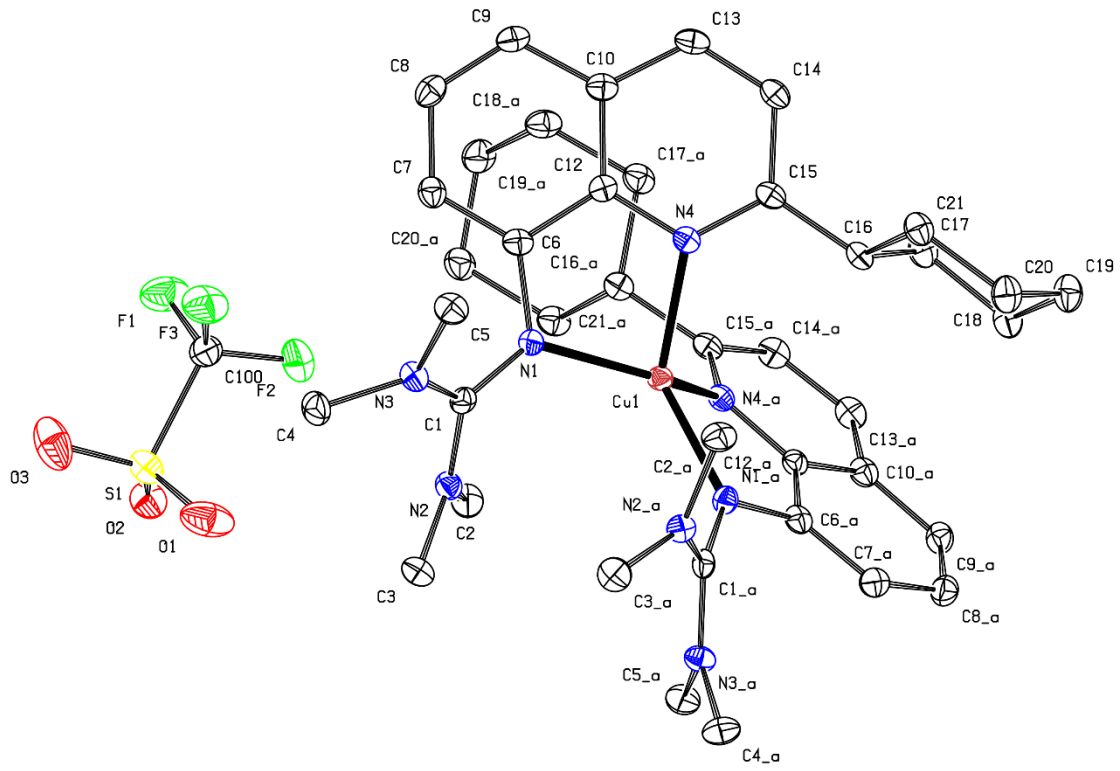

Fig. S42: Displacement ellipsoid plot of [Cu(TMG2^{c}Hexqu)$_2$](OTf)$_2$ (**C6−OTf**) (50 % probability, H atoms are omitted for clarity).

Table S13: Crystallographic data **C5–PF_6** and **C6–OTf**.

	C5–PF_6	**C6–OTf**
Empirical formula	$C_{41}H_{58}Cl_2CuF_6N_8P$	$C_{42}H_{56}CuF_6N_8O_6S_2$
Formula weight [g mol^{-1}]	942.36	1010.60
Crystal size [mm]	0.230 x 0.120 x 0.080	0.330 x 0.190 x 0.180
T [K]	100(2)	100
Crystal system	triclinic	orthorhombic
Space group	$P\bar{1}$	*Pbcn*
a [Å]	13.117(3)	12.407(3)
b [Å]	13.265(3)	21.571(4)
c [Å]	15.609(3)	16.723(3)
α [°]	73.50(3)	90
β [°]	76.04(3)	90
γ [°]	61.06(3)	90
V [Å^3]	2261.3(11)	4475.4(15)
Z	2	4
$\rho_{calcld.}$ [g cm^{-3}]	1.384	1.500
μ [mm^{-1}]	0.700	0.663
λ [Å]	0.71073	0.71073
F(000)	984	2108
hkl range	±15, ±16, ±18	±15, -27 ≤ *k* ≤ 23, -21 ≤ *l* ≤ 20
Reflections collected	26022	25415
Independent reflections	8504	4887
$R_{int.}$	0.0852	0.0335
Number of parameters	580	298
R_1 [$I \geq 2\sigma(I)$]	0.0565	0.0511
wR_2 (all data)	0.1429	0.1160
Goodness-of-fit	1.032	1.217
Largest diff. peak, hole [e Å^{-3}]	0.675; -0.821	0.574; -0.446

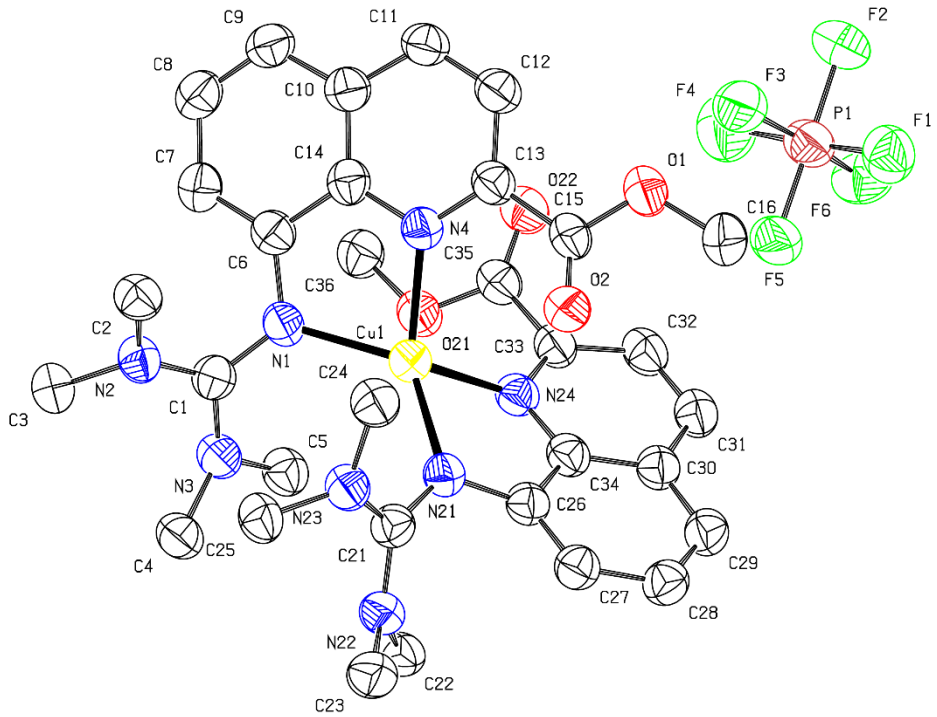

Fig. S43: Displacement ellipsoid plot of $[Cu(TMG2Meequ)_2]PF_6$ (**C7–PF$_6$**) (50 % probability, asymmetric unit, H atoms are omitted for clarity).

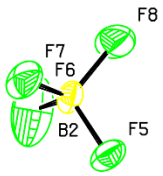

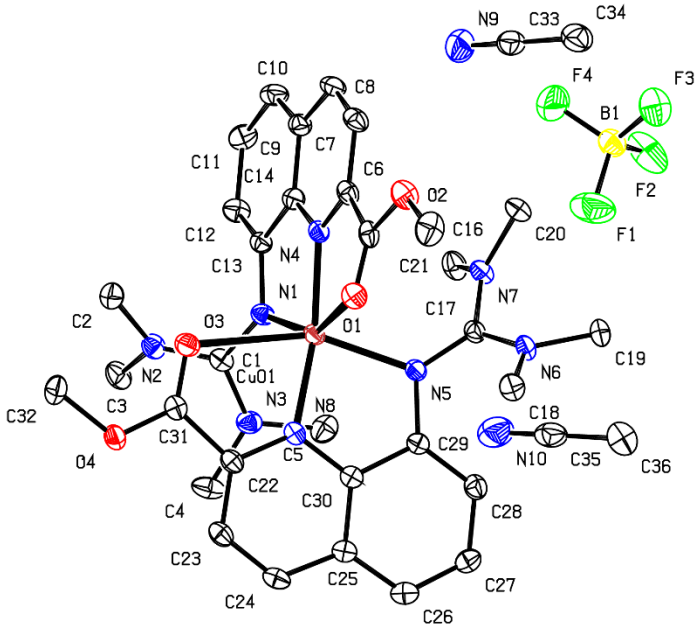

Fig. S44: Displacement ellipsoid plot of $[Cu(TMG2Meequ)_2](BF_4)_2 \cdot 2$ MeCN (**C8–BF$_4$**) (50 % probability, asymmetric unit, H atoms are omitted for clarity).

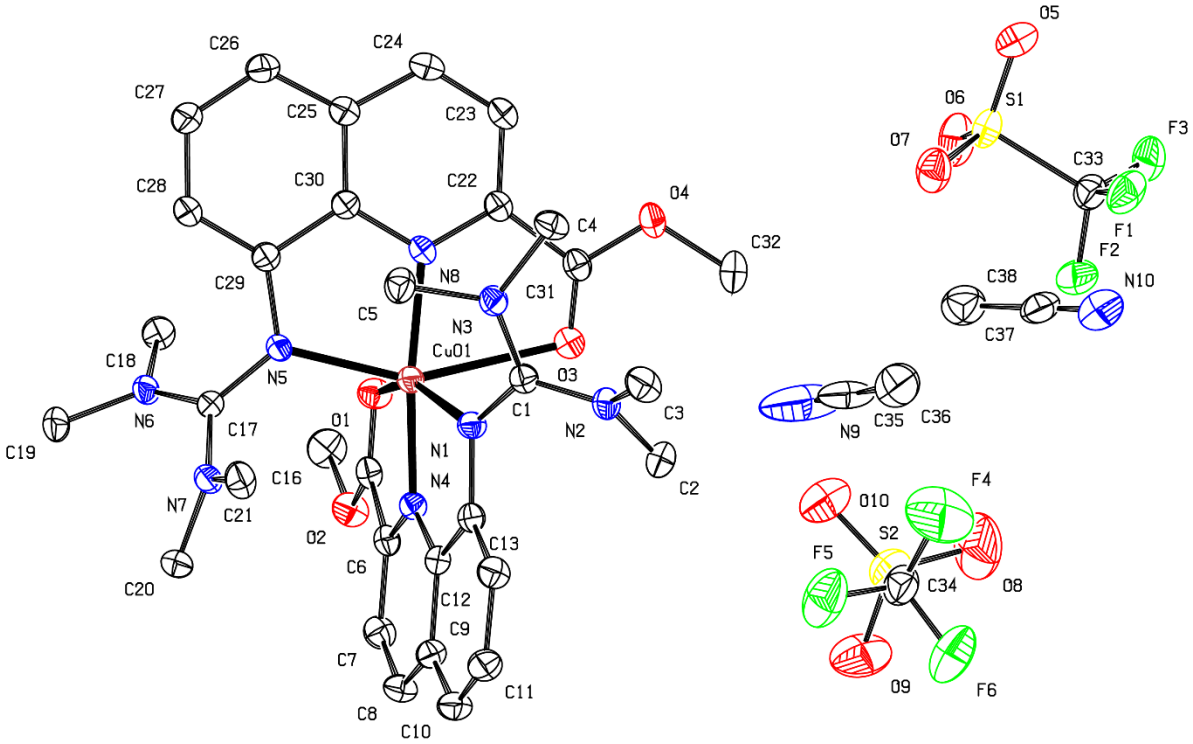

Fig. S45: Displacement ellipsoid plot of $[Cu(TMG2Meequ)_2](OTf)_2 \cdot 2$ MeCN (**C8−OTf**) (50 % probability, asymmetric unit, H atoms are omitted for clarity).

Table S14: Crystallographic data **C7–PF_6**, **C8–BF_4** and **C8–OTf**.

	C7–PF_6	**C8–BF_4**	**C8–OTf**
Empirical formula	$C_{32}H_{40}CuF_6N_8O_4P$	$C_{36}H_{46}B_2CuF_8N_{10}O_4$	$C_{38}H_{46}CuF_6N_{10}O_{10}S_2$
Formula weight [g mol^{-1}]	809.23	919.99	1044.51
Crystal size [mm]	0.210 x 0.130 x 0.040	1.000 x 0.310 x 0.230	0.270 x 0.190 x 0.120
T [K]	100	100(2)	100
Crystal system	monoclinic	monoclinic	monoclinic
Space group	$P2_1/c$	$P2_1/c$	$P2_1/c$
a [Å]	7.7600(16)	13.585(3)	13.547(3)
b [Å]	13.900(3)	25.270(5)	12.641(3)
c [Å]	32.300(7)	12.065(2)	26.447(5)
α [°]	90	90	90
β [°]	92.60(3)	91.75(3)	93.99(3)
γ [°]	90	90	90
V [Å^3]	3480.4(13)	4140.0(14)	4518.1(16)
Z	4	4	4
$\rho_{calcd.}$ [g cm^{-3}]	1.544	1.476	1.536
μ [mm^{-1}]	2.050	0.616	0.668
λ [Å]	1.54186	0.71073	0.71073
F(000)	1672	1900	2156
hkl range	$-7 \le h \le 9$, $-16 \le k \le 13$, $-37 \le l \le 38$	±18, ±34, ±16	±20, $-11 \le k \le 18$, ±39
Reflections collected	24533	61602	104293
Independent reflections	6250	11376	15723
$R_{int.}$	0.0357	0.0799	0.0654
Number of parameters	480	562	616
R_1 [$I \ge 2\sigma(I)$]	0.0756	0.0474	0.0426
wR_2 (all data)	0.2097	0.1211	0.1104
Goodness-of-fit	1.052	1.026	0.931
Largest diff. peak, hole [e Å^{-3}]	0.612; -0.642	0.561; -0.454	0.559; -0.796

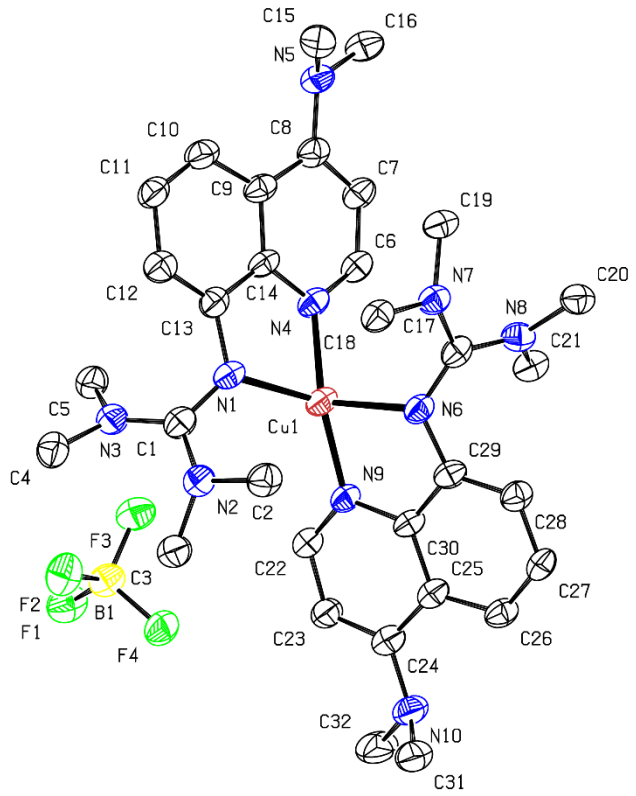

Fig. S46: Displacement ellipsoid plot of $[Cu(TMG4NMe_2qu)_2]BF_4$ (**C9–BF_4**) (50 % probability, asymmetric unit, H atoms are omitted for clarity).

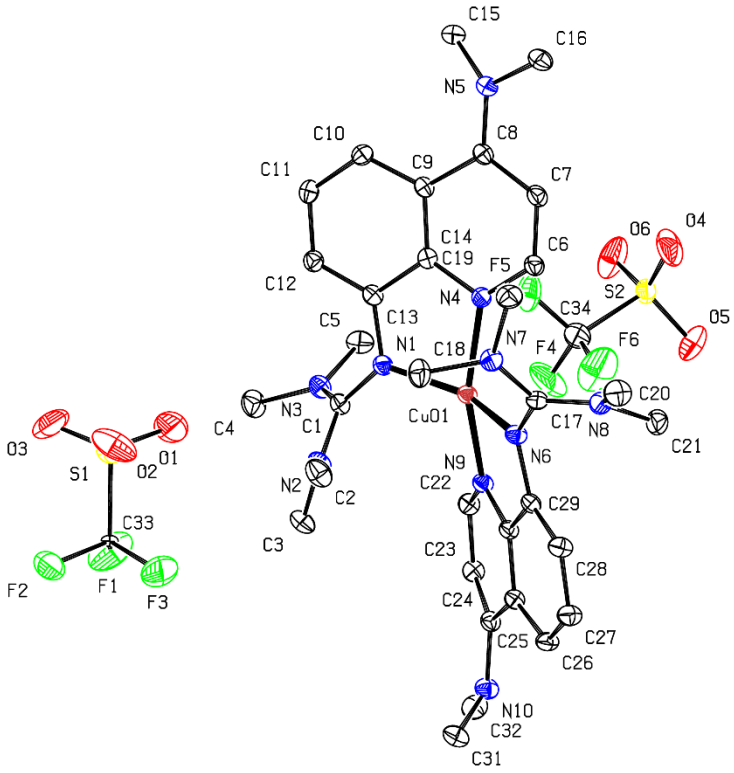

Fig. S47: Displacement ellipsoid plot of $[Cu(TMG4NMe_2qu)_2](OTf)_2{\cdot}Et_2O$ (**C10–OTf**) (50 % probability, asymmetric unit, H atoms are omitted for clarity).

Table S15: Crystallographic data **C9–BF_4** and **C10–OTf**.

	C9–BF_4	**C10–OTf**
Empirical formula	$C_{32}H_{46}BCuF_4N_{10}$	$C_{34}H_{46}CuF_6N_{10}O_6S_2$ [+ Et_2O]
Formula weight [g mol^{-1}]	721.14	932.47
Crystal size [mm]	0.270 x 0.130 x 0.060	0.280 x 0.260 x 0.230
T [K]	100	100
Crystal system	monoclinic	orthorhombic
Space group	$P2_1/c$	*Pbca*
a [Å]	11.779(2)	12.270(3)
b [Å]	19.544(4)	19.141(4)
c [Å]	15.389(3)	36.523(7)
α [°]	90	90
β [°]	94.90(3)	90
γ [°]	90	90
V [$Å^3$]	3529.8(12)	8578(3)
Z	4	8
$\rho_{calcld.}$ [g cm^{-3}]	1.357	1.444
μ [mm^{-1}]	1.376	0.687
λ [Å]	1.54186	0.71073
F(000)	1512	3864
hkl range	±13, -22 ≤ k ≤ 18, -18 ≤ l ≤ 15	±18, -28 ≤ k ≤ 27, -53 ≤ l ≤ 55
Reflections collected	21495	72546
Independent reflections	5948	15419
$R_{int.}$	0.0644	0.0398
Number of parameters	445	544
R_1 [$I \geq 2\sigma(I)$]	0.0827	0.0650
wR_2 (all data)	0.2288	0.1710
Goodness-of-fit	1.128	1.094
Largest diff. peak, hole [e $Å^{-3}$]	0.751; -0.679	1.666; -1.678

9. DFT calculations

9.1 General

Density functional theory (DFT) calculations were performed with Gaussian 16, Revision B.01 using the default UltraFine grid (a 99,590 grid).[28] The geometry optimizations were started from the geometry of the solid-state structures if available using the TPSSh functional[29] and with the Ahlrichs type basis set def2-TZVP[30] as implemented in Gaussian 16, Revision B.01.[28] As solvent model, the Polarizable Continuum Model (PCM) was used as implemented in Gaussian 16. As empirical dispersion correction, the D3 dispersion with Becke–Johnson damping was used as implemented in Gaussian 16, Revision B.01.[31] Frequency calculations did not show imaginary values. NBO calculations were accomplished using the program suite NBO 6.0 delivering the NBO charges and the charge-transfer energies by second order perturbation theory.[32] For visualization and extraction of the calculated structural information GaussView (Version 6.0.16) was used. Calculated energy values and NBO results were extracted directly from the output files using notepad++ (Version 7.8.1).

The coordination geometries of the hypersurface, all NMR spectroscopic data, all GPC data and Raman spectroscopic data were deposited as original data in the repository RADAR4Chem by FIZ Karlsruhe - Leibniz-Institut für Informationsinfrastruktur and are published under an Open Access model (CC BY-NC-SA 4.0 Attribution-NonCommercial-ShareAlike; (DOI) 10.22000/613).

9.2 Results of DFT calculations of the complexes

Table S16: DFT calculated key bond lengths, bond angles and structure parameters of the Cu(I) and Cu(II) complex cations **C1** – **C10**.

	$[Cu(TMGqu)_2]^{+/2+}$		$[Cu(TMG2Mequ)_2]^{+/2+}$		$[Cu(TMG2^cHexqu)_2]^{+/2+}$		$[Cu(TMG2Meequ)_2]^{+/2+}$		$[Cu(TMG4NMe_2qu)_2]^{+/2+}$	
	C1 (Cu(I))	**C2** (Cu(II))	**C3** (Cu(I))	**C4** (Cu(II))	**C5** (Cu(I))	**C6** (Cu(II))	**C7** (Cu(I))	**C8** (Cu(II))	**C9** (Cu(I))	**C10** (Cu(II))
	Bond length [Å]									
$Cu\text{-}N_{gua,1/2}$	2.066, 2.066	1.975, 1.975	2.083, 2.084	1.987, 1.987	2.052, 2.053	1.993, 1.993	2.064, 2.045	2.120, 2.120	2.079, 2.079	1.977, 1.982
$Cu\text{-}N_{qu,1/2}$	1.997, 1.997	1.979, 1.979	2.001, 2.001	1.987, 1.987	2.035, 2.035	1.991, 1.991	2.024, 2.044	1.951, 1.951	1.991, 1.991	1.960, 1.957
$Cu\text{-}O_{carb,1/2}$							3.001, 4.524	2.407, 2.407		
$Cu\text{-}O_{alc,1/2}$							4.448, 2.935	4.306, 4.306		
	Bond angles [°]									
$N_{gua,1/2}\text{-}Cu\text{-}N_{qu,1/2}$	82.3, 82.3	83.4, 83.4	81.9, 81.9	83.3, 83.3	81.6, 81.5	83.0, 83.0	81.7, 81.9	80.7, 80.7	81.7, 81.7	83.1, 82.9
$N_{gua,1}\text{-}Cu\text{-}N_{gua,2}$	129.3	149.4	124.6	136.2	131.1	124.7	119.6	110.0	126.7	148.1
$N_{gua,1/2}\text{-}Cu\text{-}N_{qu,2/1}$	114.3, 114.3	104.6, 104.6	115.9, 115.8	107.9, 107.9	128.1, 128.0	134.5, 134.5	137.7, 136.8	105.6, 105.6	114.9, 115.0	104.7, 105.9
$N_{qu,1}\text{-}Cu\text{-}N_{qu,2}$	142.2	149.8	143.1	150.4	111.0	102.8	108.0	169.3	143.8	150.1
	Structure parameter									
τ_4[a]	0.63	0.43	0.65	0.52	0.72	0.65	0.61	0.60	0.63	0.44
$\Delta\tau_4$	0.20		0.13		0.07		0.00		0.20	
$\varnothing\tau_4$	0.53		0.59		0.68		0.61		0.54	
$\measuredangle$ (CuN_2, CuN'_2)	70.3	46.5	74.4	57.3	81.5	68.2	66.8	74.3	71.9	47.4
$\Delta\measuredangle$	23.8		17.1		13.3		-7.5		24.5	
ρ[b]	0.98, 0.98	1.00, 1.00	0.97, 0.97	1.00, 1.00	0.97, 0.97	1.00, 1.00	0.98, 0.98	0.99, 0.99	0.97, 0.97	1.00, 1.00

[a] $\tau_4 = \frac{360^\circ - (\alpha - \beta)}{141^\circ}$.[24] [b] $\rho = \frac{2a}{b+c}$ with $a = d(C_{Gua}\text{-}N_{Gua})$, $b = d(C_{Gua}\text{-}N_{Amine,1})$ and $c = d(C_{Gua}\text{-}N_{Amine,2})$.[25]

9.3 Results of the NBO calculations

Table S17: Calculated NBO charges (in e units) for selected atoms of the ligands **L1** – **L6** (NBO6.0. TPSSh/def2-TZVP and PCM solvent model for acetonitrile and the empirical dispersion correction with Becke-Johnson damping).

	N_{gua}	N_{qu}	O_{acyl}	O_{alc}
TMGqu (**L1**)	-0.59	-0.43		
TMG2Mequ (**L2**)	-0.59	-0.44		
TMG2^{t}Buqu (**L3**)	-0.59	-0.44		
TMG2^{c}Hexqu (**L4**)	-0.60	-0.44		
TMG2Meequ (**L5**)	-0.59	-0.37	-0.60	-0.47
$TMG4NMe_2qu$ (**L6**)	-0.59	-0.46		

Table S18: Calculated NBO charges, charge-transfer energies and bond lengths of selected atoms and bonds for the Cu(I) and Cu(II) complex cations **C1** – **C10** (NBO6.0; TPSSh/def2-TZVP and PCM solvent model for acetonitrile and the empirical dispersion correction with Becke-Johnson damping).

	$[Cu(TMGqu)_2]^{+/2+}$		$[Cu(TMG2Mequ)_2]^{+/2+}$		$[Cu(TMG2^cHexqu)_2]^{+/2+}$		$[Cu(TMG2Meequ)_2]^{+/2+}$		$[Cu(TMG4NMe_2qu)_2]^{+/2+}$	
	C1 (Cu(I))	**C2** (Cu(II))	**C3** (Cu(I))	**C4** (Cu(II))	**C5** (Cu(I))	**C6** (Cu(II))	**C7** (Cu(I))	**C8** (Cu(II))	**C9** (Cu(I))	**C10** (Cu(II))
	NBO charges [e units]									
Cu	0.95	1.30	0.94	1.30	0.96	1.30	1.00	1.37	0.93	1.29
$N_{gua,1/2}$	−0.69, −0.69	−0.71, −0.71	−0.69, −0.69	−0.71, −0.71	−0.70, −0.70	−0.72, −0.72	−0.69, −0.69	−0.69, −0.69	−0.68, −0.68	−0.71, −0.71
$N_{qu,1/2}$	−0.53, −0.53	−0.52, −0.52	−0.54, −0.54	−0.53, −0.53	−0.54, −0.54	−0.54, −0.54	−0.49, −0.48	−0.47, −0.47	−0.56, −0.56	−0.57, −0.57
$O_{acyl,1/2}$							−0.58, −0.60	−0.61, −0.61		
$O_{alc,1/2}$							−0.46, −0.45	−0.43, −0.43		
	Charge-transfer energies [kcal mol^{-1}]									
$N_{gua,1/2}$→Cu	20.3, 20.3	48.7, 48.7	18.4, 18.4	41.0, 41.0	21.0, 21.0	38.3, 38.3	21.5, 22.3	26.9, 26.9	18.4, 18.4	45.8, 43.8
$N_{qu,1/2}$→Cu	29.6, 29.6	52.8, 52.8	26.7, 26.7	51.1, 51.1	17.7, 17.8	44.3, 44.3	20.3, 19.4	64.2, 64.2	31.4, 31.4	57.6, 57.8
$O_{acyl,11/12}$→Cu							2.6, –	14.1, 14.1		
$O_{alc,1/2}$→Cu							0.1, 2.5	–		
	Bond length [Å]									
Cu-$N_{gua,1/2}$	2.066, 2.066	1.975, 1.975	2.083, 2.084	1.987, 1.987	2.052, 2.053	1.993, 1.993	2.064, 2.045	2.120, 2.120	2.079, 2.079	1.977, 1.982
Cu-$N_{qu,1/2}$	1.997, 1.997	1.979, 1.979	2.001, 2.001	1.987, 1.987	2.035, 2.035	1.991, 1.991	2.024, 2.044	1.951, 1.951	1.991, 1.991	1.960, 1.957
Cu-$O_{acyl,1/2}$							3.001, 4.524	2.407, 2.407		
Cu-$O_{alc,1/2}$							4.448, 2.935	4.306, 4.306		

9.4 Reorganization energy

9.4.1 Theoretical background

The total reorganization energy $\lambda_{11,T}$ of the whole electron self-exchange is divided in the internal reorganization energy $\lambda_{11,I}$ and the solvent reorganization energy $\lambda_{11,S}$ of the whole electron self-exchange (Equation 6).

$$\lambda_{11,T} = \lambda_{11,S} + \lambda_{11,I} \tag{6}$$

The total reorganization energy $\lambda_{11,T}$ and the internal reorganization energy $\lambda_{11,I}$ were calculated using DFT calculations and the Nelsen's four-point method.[33] The solvent reorganization energy $\lambda_{11,S}$ is the difference between the total and the internal reorganization energy.

The total reorganization energy $\lambda_{11,T}$ for the whole electron self-exchange is the sum of the total reorganization energies $\lambda_{Cu(I),T}$ and $\lambda_{Cu(II),T}$ of the Cu(I) and Cu(II) complex of the same redox couple. The total reorganization energy ($\lambda_{Cu(I),T}$ for Cu(I) and $\lambda_{Cu(II),T}$ for Cu(II)) of each complex is calculated with its optimized ground state energy ($E_{Cu(I)L(I)S(I)}$ for Cu(I) and $E_{Cu(II)L(II)S(II)}$ for Cu(II)) and the energy of the complex with the same oxidation state but with the structure and the solvent sphere of the complex with the other oxidation state of the same redox couple ($E_{Cu(I)L(II)S(II)}$ for Cu(I) and $E_{Cu(II)L(I)S(I)}$ for Cu(II)) (Equation 7; Fig. S48, left). The indices Cu(I) or Cu(II) represent the oxidation state, L(I) or L(II) represent the ground state complex structure of the appropriate oxidation state and S(I) or S(II) represent the ground state solvent sphere of the appropriate oxidation state. In Fig. S48 (left) the energies $E_{Cu(I)}(x)$ and $E_{Cu(II)}(x)$ of the Cu(I) and Cu(II) complex are functions of the complex structure and the solvent sphere which are represented by the variable x_{LS}. The ground state complex structures and ground state solvent spheres of the Cu(I) and Cu(II) complex are represented by $x_{L(I)S(I)}$ and $x_{L(II)S(II)}$.

$$\lambda_{11,T} = \lambda_{Cu(II),T} + \lambda_{Cu(I),T} = \left(E_{Cu(II)L(I)S(I)} - E_{Cu(II)L(II)S(II)}\right) + \left(E_{Cu(I)L(II)S(II)} - E_{Cu(I)L(I)S(I)}\right) \tag{7}$$

The internal reorganization energy $\lambda_{11,I}$ for the whole electron self-exchange is the sum of the internal reorganization energies $\lambda_{Cu(I),I}$ and $\lambda_{Cu(II),I}$ of the Cu(I) and Cu(II) complex of the same redox couple. The internal reorganization energy ($\lambda_{Cu(I),I}$ for Cu(I) and $\lambda_{Cu(II),I}$ for Cu(II)) of each complex is calculated with its optimized ground state energy ($E_{Cu(I)L(I)S(I)}$ for Cu(I) and $E_{Cu(II)L(II)S(II)}$ for Cu(II)) and the energy of the complex with the same oxidation state but with the structure of the complex with the other oxidation state of the same redox couple ($E_{Cu(I)L(II)S(I)}$ for Cu(I) and $E_{Cu(II)L(I)S(II)}$ for Cu(II)). In contrast to the total reorganization energy the solvent sphere is allowed to relax for the calculated oxidation state (Equation 8; Fig. S48, right).

$$\lambda_{11,I} = \lambda_{Cu(II),I} + \lambda_{Cu(I),I} = \left(E_{Cu(II)L(I)S(II)} - E_{Cu(II)L(II)S(II)}\right) + \left(E_{Cu(I)L(II)S(I)} - E_{Cu(I)L(I)S(I)}\right) \tag{8}$$

In Fig. S48 (right) the energies $E_{Cu(I)S(I)}(x)$ and $E_{Cu(II)S(II)}(x)$ of the Cu(I) and Cu(II) complex are functions of the complex structure which is represented by the variable x_L. The ground state complex structures of the Cu(I) and Cu(II) complex are represented by $x_{L(I)}$ and $x_{L(II)}$.

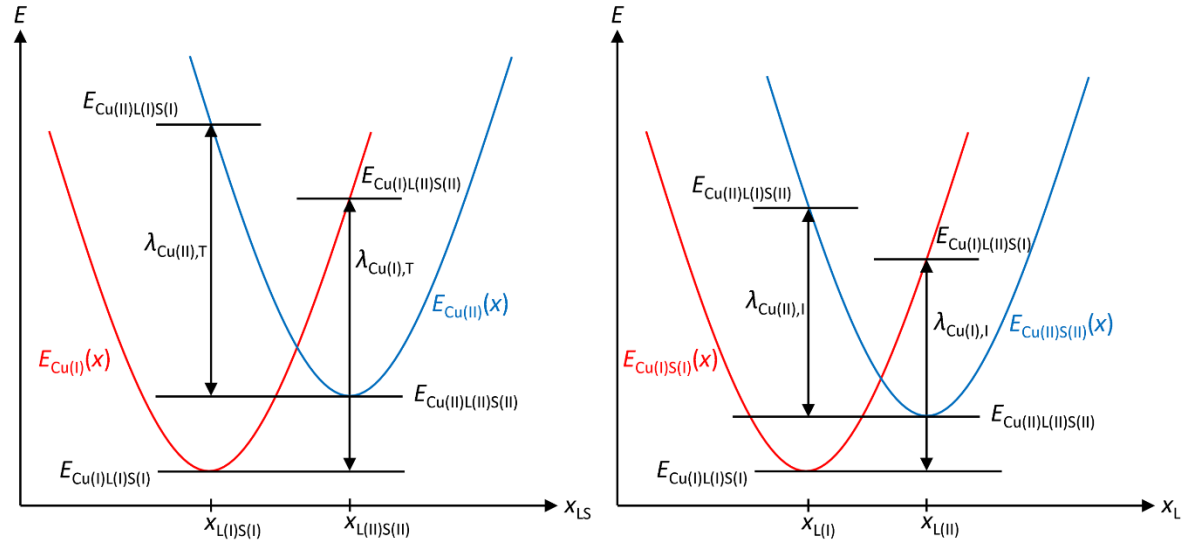

Fig. S48: Schematic illustration of the Nelsen's four-point method for the calculation of the total reorganization energy $\lambda_{11,T}$ (left) and the internal reorganization energy $\lambda_{11,I}$ (right).

The exact DFT calculation procedure is explained in chapter 9.4.3.

9.4.2 Results

Table S19: Calculated energies of the Cu complexes for different configurations and resulting reorganization energies.

	[Cu(TMGqu)$_2$]$^{1+/2+}$		[Cu(TMG2Mequ)$_2$]$^{1+/2+}$		[Cu(TMG^{2}Hexqu)$_2$]$^{1+/2+}$		[Cu(TMG2Meequ)$_2$]$^{1+/2+}$		[Cu(TMG4NMe$_2$qu)$_2$]$^{1+/2+}$	
	C1 (Cu(I))	**C2** (Cu(II))	**C3** (Cu(I))	**C4** (Cu(II))	**C5** (Cu(I))	**C6** (Cu(II))	**C7** (Cu(I))	**C8** (Cu(II))	**C9** (Cu(I))	**C10** (Cu(II))
Total reorganization energy $\lambda_{11,T}$										
$E_{Cu(X)L(I)S(I)}$ [Hartree]	-3167.95097	-3167.75713	-3246.63875	-3246.44300	-3637.58340	-3637.38745	-3623.92456	-3623.72818	-3436.02755	-3435.84373
$E_{Cu(X)L(II)S(II)}$ [Hartree]	-3167.91200	-3167.79503	-3246.60374	-3246.47799	-3637.55231	-3637.41858	-3623.88734	-3623.76909	-3435.98798	-3435.88246
$\lambda_{Cu(X),T}$ [Hartree]	0.0390	0.0379	0.0350	0.0350	0.0311	0.0311	0.0372	0.0409	0.0396	0.0387
$\lambda_{11,T}$ [kJ/mol]	201.8		183.8		163.3		205.1		205.6	
Internal reorganization energy $\lambda_{11,I}$										
$E_{Cu(X)L(I)S(X)}$ [Hartree]	-3167.95097	-3167.78269	-3246.63875	-3246.46719	-3637.58340	-3637.40702	-3623.92456	-3623.75152	-3436.02755	-3435.86789
$E_{Cu(X)L(II)S(X)}$ [Hartree]	-3167.93792	-3167.79503	-3246.62853	-3246.47799	-3637.57489	-3637.41858	-3623.91106	-3623.76909	-3436.01266	-3435.88246
$\lambda_{Cu(X),I}$ [Hartree]	0.013043	0.012339	0.01022	0.01080	0.00851	0.01156	0.01350	0.01757	0.01490	0.01457
$\lambda_{11,I}$ [kJ/mol]	66.6		55.2		52.7		81.6		77.4	
Solvent reorganization energy $\lambda_{11,S}$										
$\lambda_{Cu(X),S}$ [Hartree]	0.0259	0.0256	0.0248	0.0242	0.0226	0.0196	0.0237	0.0233	0.0247	0.0242
$\lambda_{11,S}$ [kJ/mol]	135.2		128.6		110.7		123.5		128.2	

9.4.3 Procedure of the calculation

For the calculation of the total reorganization energy, the energy of the Cu(I) complex with the structure and the solvent sphere of the Cu(II) complex and vice versa is necessary. To calculate these energies, single point energy calculations of the previous optimized Cu(I) and Cu(II) structures were performed to save the information of the solvent sphere. Following input file for $[Cu(TMGqu)_2]^+$ (**C1**) was used:

```
%chk=CuI_TMGqu_SP_tR.chk
# scrf=(solvent=acetonitrile,Read) geom=connectivity def2tzvp
# iop(3/124=40,3/175=2238200,3/177=0452900,3/178=4655000) rtpssh

SP calculation of optimized Cu(I) structure

1 1
 Cu                 0.00000000    0.00000000    0.41865200
 N                 -0.66468500    1.74498200   -0.46630200
 .
 .
 .

NonEq=write
```

The commands `scrf=(solvent=acetonitrile,Read)` in the beginning and `NonEq=write` in the end of the input file are of importance. The command `scrf=(solvent=acetonitrile,Read)` expresses that there is a further command to consider in the end of the input file. The command `NonEq=write` causes that the information about the non-equilibrium solvent sphere is written in the chk file.

This calculation was analogously performed for $[Cu(TMGqu)_2]^{2+}$ (**C2**):

```
%chk=CuII_TMGqu_SP_tR.chk
# scrf=(solvent=acetonitrile,Read) geom=connectivity def2tzvp
# iop(3/124=40,3/175=2238200,3/177=0452900,3/178=4655000) utpssh

SP calculation of optimized Cu(II) structure

2 2
 Cu                 0.00000000    0.00000000    0.23225000
 N                  1.56922900    1.08983000    0.74864400
 .
 .
 .

NonEq=write
```

Then, energy calculations starting from the chk-files generated in the previous calculations were performed but with the oxidation state and multiplicity of the other complex. For $[Cu(TMGqu)_2]^+$ (**C1**) following input file was used:

```
%oldchk=CuII_TMGqu_SP_tR.chk
%chk=CuI_TMGqu_CuII_N4P_tR.chk
# scrf=(solvent=acetonitrile,Read) geom=check def2tzvp
# iop(3/124=40,3/175=2238200,3/177=0452900,3/178=4655000) rtpssh

CuII structure and solvent sphere calculated as CuI

1 1

NonEq=read
```

The commands `scrf=(solvent=acetonitrile,Read)` in the beginning and `NonEq=read` in the end of the input file are of importance. The command `scrf=(solvent=acetonitrile,Read)` expresses that there is a further command to consider in the end of the input file. The command `NonEq=read` causes that the information of the solvent sphere is read out from the chk file.

This calculation was analogously performed for $[Cu(TMGqu)_2]^{2+}$ (**C2**):

```
%oldchk=CuI_TMGqu_SP_tR.chk
%chk=CuII_TMGqu_CuI_N4P_tR.chk
# scrf=(solvent=acetonitrile,Read) geom=check def2tzvp
# iop(3/124=40,3/175=2238200,3/177=0452900,3/178=4655000) utpssh

CuII structure and solvent sphere calculated as CuI

2 2

NonEq=read
```

The necessary energy values are located after the entry `After PCM corrections, the energy is …` in the log-files generated by these calculations.

For the calculation of the internal reorganization energy, the energy of the Cu(I) complex with the structure of the Cu(II) complex but with a relaxed solvent sphere and vice versa is necessary. Therefore, energy calculations starting from the previous optimized structures were performed but with the oxidation state and multiplicity of the other complex. But now with the command `scrf=(solvent=acetonitrile)` in the beginning and without `NonEq=read` in the end of the input file.

10. Comparison of structural XRD, XAS and DFT results

Table S20: Comparison of selected bond lengths, bond angles, and structure parameters of $[Cu(TMGqu)_2]^+$ (**C3**) and $[Cu(TMGqu)_2]^{2+}$ (**C4**) determined by XRD and DFT (TPSSh/def2-TZVP and PCM solvent model for MeCN and empirical dispersion correction with Becke-Johnson damping).[34]

	$[Cu(TMGqu)_2]^+$ (**C1**)		$[Cu(TMGqu)_2]^{2+}$ (**C2**)	
	XRD	DFT	XRD	DFT
	Bond lengths [Å]			
$Cu\text{-}N_{gua,1/2}$	2.068(3), 2.095(3)	2.066, 2.066	1.959(2), 1.964(2)	1.975, 1.975
$Cu\text{-}N_{qu,1/2}$	1.966(4), 1.999(3)	1.997, 1.997	1.976(2), 1.975(2)	1.979, 1.979
	Bond angles [°]			
$N_{gua,1/2}–Cu–N_{qu,1/2}$	82.6(2), 82.1(2)	82.3, 82.3	83.5(1), 83.7(1)	83.4, 83.4
$N_{gua,1}–Cu–N_{gua,2}$	129.1(2)	129.3	149.4(1)	149.4
$N_{gua,1/2}–Cu–N_{qu,2/1}$	108.2(2), 114.1(2)	114.3, 114.3	102.6(1), 103.5(1)	104.6, 104.6
$N_{qu,1}–Cu–N_{qu,2}$	149.0(2)	142.2	154.9(1)	149.8
	Structure parameter			
τ_4	0.58	0.63	0.40	0.43
∢ (CuN_2, CuN'_2)	65.1	70.3	42.5	46.5
ρ[b]	0.97, 0.96	0.98, 0.98	1.00, 0.99	1.00, 1.00

Table S21: Comparison of selected bond lengths, bond angles, and structure parameters of $[Cu(TMG2Mequ)_2]^+$ (**C3**) and $[Cu(TMG2Mequ)_2]^{2+}$ (**C4**) determined by XRD, XAS and DFT (TPSSh/def2-TZVP and PCM solvent model for MeCN and empirical dispersion correction with Becke-Johnson damping).

	$[Cu(TMG2Mequ)_2]^+$ (**C3**)			$[Cu(TMG2Mequ)_2]^{2+}$ (**C4**)		
	XRD	XAS	DFT	XRD	XAS	DFT
	Bond lengths [Å]					
$Cu\text{-}N_{gua,1/2}$	2.091(3), 2.097(3)	2.080 ± 0.010, 2.080 ± 0.010	2.083, 2.084	1.979(4), 1.978(4)	1.979 ± 0.006, 1.979 ± 0.006	1.987, 1.987
$Cu\text{-}N_{qu,1/2}$	1.994(3), 1.994(3)	1.998 ± 0.009, 1.998 ± 0.009	2.001, 2.001	1.987(4), 1.972(4)	1.979 ± 0.006, 1.979 ± 0.006	1.987, 1.987
	Bond angles [°]					
$N_{gua,1/2}–Cu–N_{qu,1/2}$	81.7(2), 81.6(2)		81.9, 81.9	83.2(2), 83.6(2)		83.3, 83.3
$N_{gua,1}–Cu–N_{gua,2}$	126.0(2)		124.6	135.9(2)		136.2
$N_{gua,1/2}–Cu–N_{qu,2/1}$	111.7(2), 113.2(2)		115.9, 115.8	105.4(2), 107.2(2)		107.9, 107.9
$N_{qu,1}–Cu–N_{qu,2}$	149.9(2)		143.1	154.6(2)		150.4
	Structure parameter					
τ_4	0.60		0.65	0.49		0.52
∢ (CuN_2, CuN'_2)	68.2		74.4	54.7		57.3
ρ[b]	0.97, 0.98		0.97, 0.97	1.00, 1.00		1.00, 1.00

Table S22: Comparison of selected bond lengths, bond angles, and structure parameters of $[Cu(TMG2^cHexqu)_2]^+$ (**C5**) and $[Cu(TMG2^cHexqu)_2]^{2+}$ (**C6**) determined by XRD, XAS and DFT (TPSSh/def2-TZVP and PCM solvent model for MeCN and empirical dispersion correction with Becke-Johnson damping).

	$[Cu(TMG2^cHexqu)_2]^+$ (**C5**)			$[Cu(TMG2^cHexqu)_2]^{2+}$ (**C6**)		
	XRD	XAS	DFT	XRD	XAS	DFT
	Bond lengths [Å]					
$Cu\text{-}N_{gua,1/2}$	2.018(3), 2.024(3)	2.048 ± 0.006, 2.048 ± 0.006	2.052, 2.053	1.973(2), 1.973(2)	1.977 ± 0.005, 1.977 ± 0.005	1.993, 1.993
$Cu\text{-}N_{qu,1/2}$	2.084(3), 2.081(3)	2.048 ± 0.006, 2.048 ± 0.006	2.035, 2.035	1.988(2), 1.988(2)	1.977 ± 0.005, 1.977 ± 0.005	1.991, 1.991
	Bond angles [°]					
$N_{gua,1/2}–Cu–N_{qu,1/2}$	81.2(2), 81.3(2)		81.6, 81.5	82.9(1), 82.9(1)		83.0, 83.0
$N_{gua,1}–Cu–N_{gua,2}$	135.0(2)		131.1	124.7(2)		124.7
$N_{gua,1/2}–Cu–N_{qu,2/1}$	128.7(2), 127.9(2)		128.1, 128.0	135.8(1), 135.8(1)		134.5, 134.5
$N_{qu,1}–Cu–N_{qu,2}$	104.9(2)		111.0	100.7(2)		102.8
	Structure parameter					
τ_4	0.68		0.72	0.63		0.65
∢ (CuN_2, CuN'_2)	78.1		81.5	65.5		68.2
ρ[b]	0.99, 0.99		0.97, 0.97	1.01, 1.01		1.00, 1.00

Table S23: Comparison of selected bond lengths, bond angles, and structure parameters of $[Cu(TMG2Meequ)_2]^+$ (**C7**) and $[Cu(TMG2Meequ)_2]^{2+}$ (**C8**) determined by XRD, XAS and DFT (TPSSh/def2-TZVP and PCM solvent model for MeCN and empirical dispersion correction with Becke-Johnson damping).

	$[Cu(TMG2Meequ)_2]^+$ (**C7**)			$[Cu(TMG2Meequ)_2]^{2+}$ (**C8**)		
	XRD	XAS	DFT	XRD	XAS	DFT
	Bond lengths [Å]					
$Cu\text{-}N_{gua,1/2}$	2.047(4), 2.029(4)	2.038 ± 0.010, 2.038 ± 0.010	2.064, 2.045	2.039(2), 2.043(2)	2.029 ± 0.013, 2.029 ± 0.013	2.120, 2.120
$Cu\text{-}N_{qu,1/2}$	2.053(3), 2.083(4)	2.038 ± 0.010, 2.065 ± 0.001	2.024, 2.044	1.960(2), 1.959(2)	1.935 ± 0.013, 1.935 ± 0.013	1.951, 1.951
$Cu\text{-}O_{acyl,1/2}$	2.962(4), 4.312(4)	3.028 ± 0.018 -	3.001, 4.524	2.616(2), 2.595(2)	2.496 ± 0.055, 2.496 ± 0.055	2.407, 2.407
$Cu\text{-}O_{alc,1/2}$	4.511(4), 3.235(4)	- 2.961 ± 0.018	4.448, 2.935	4.428(2), 4.441(2)	-	4.306, 4.306
	Bond angles [°]					
$N_{gua,1/2}–Cu–N_{qu,1/2}$	81.3(2), 81.3(2)		81.7, 81.9	82.2(1), 82.2(1)		80.7, 80.7
$N_{gua,1}–Cu–N_{gua,2}$	124.4(2)		119.6	120.2(1)		110.0
$N_{gua,1/2}–Cu–N_{qu,2/1}$	133.0(2), 137.8(2)		137.7, 136.8	105.3(1), 106.9(1)		105.6, 105.6
$N_{qu,1}–Cu–N_{qu,2}$	105.9(2)		108.0	163.7(1)		169.3
	Structure parameter					
τ_4	0.63		0.61	0.54[c]		0.60
∢ (CuN_2, CuN'_2)	69.0		66.8	65.6		74.3
ρ[b]	0.99, 1.00		0.98, 0.98	1.01, 1.00		0.99, 0.99

Table S24: Selected bond lengths [Å] of $[Cu(TMG4NMe_2qu)_2]^+$ (**C9**) and $[Cu(TMG4NMe_2qu)_2]^{2+}$ (**C10**) determined by XRD, XAS and DFT (TPSSh/def2-TZVP and PCM solvent model for MeCN and empirical dispersion correction with Becke-Johnson damping).

	$[Cu(TMG4NMe_2qu)_2]^+$ (**C9**)			$[Cu(TMG4NMe_2qu)_2]^{2+}$ (**C10**)		
	XRD	XAS	DFT	XRD	XAS	DFT
	Bond lengths [Å]					
$Cu\text{-}N_{gua,1/2}$	2.065(4), 2.146(4)	2.044 ± 0.017, 2.044 ± 0.017	2.079, 2.079	1.964(2), 1.968(2)	1.959 ± 0.008, 1.959 ± 0.008	1.977, 1.982
$Cu\text{-}N_{qu,1/2}$	1.983(4), 1.947(4)	1.958 ± 0.016, 1.958 ± 0.016	1.991, 1.991	1.957(2), 1.952(2)	1.959 ± 0.008, 1.959 ± 0.008	1.960, 1.957
	Bond angles [°]					
$N_{gua,1/2}–Cu–N_{qu,1/2}$	82.2(2), 82.4(2)		81.7, 81.7	82.9(1), 82.9(1)		83.1, 82.9
$N_{gua,1}–Cu–N_{gua,2}$	119.6(2)		126.7	150.7(1)		148.1
$N_{gua,1/2}–Cu–N_{qu,2/1}$	123.0(2), 107.1(2)		114.9, 115.0	102.9(1), 104.2(1)		104.7, 105.9
$N_{qu,1}–Cu–N_{qu,2}$	145.1(2)		143.8	154.9(1)		150.1
	Structure parameter					
τ_4	0.65		0.63	0.39		0.44
∢ (CuN_2, CuN'_2)	75.6		71.9	41.8		47.4
ρ[b]	0.97, 0.95		0.97, 0.97	1.01, 1.01		1.00, 1.00

11. NMR spectra

11.1 TMG2Mequ (L2) and corresponding precursor and Cu(I) complexes

11.1.1 2-Methyl-8-aminoquinoline (2-Me-8-NH2-qu)

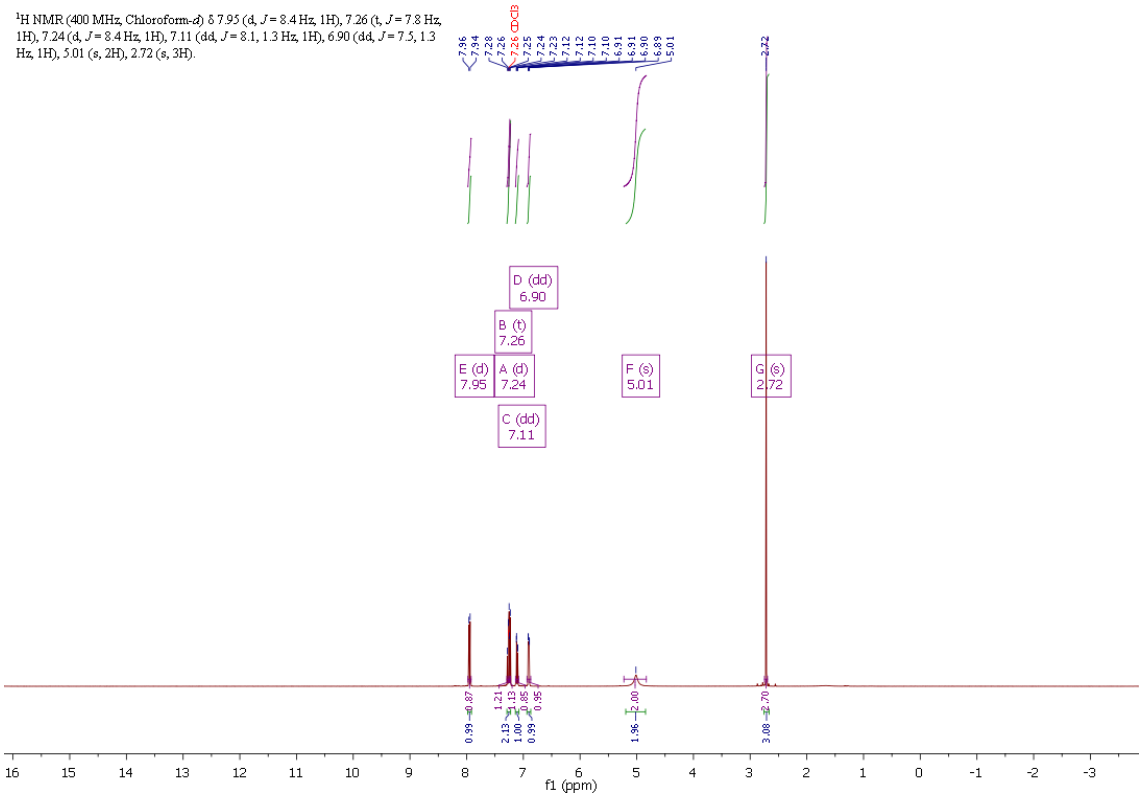

Fig. S49: ^{1}H NMR spectra of 2-Me-8-NH_2-qu in $CDCl_3$.

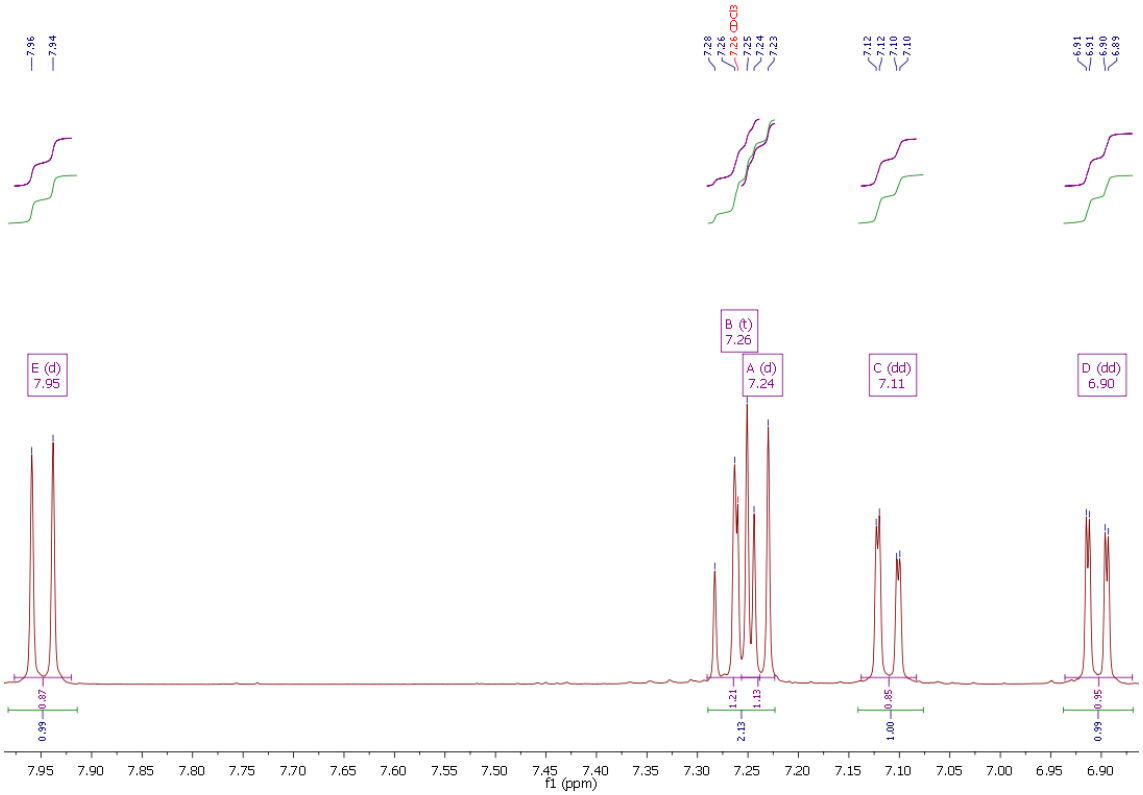

Fig. S50: Magnification of the ^{1}H NMR spectra of 2-Me-8-NH_2-qu in $CDCl_3$.

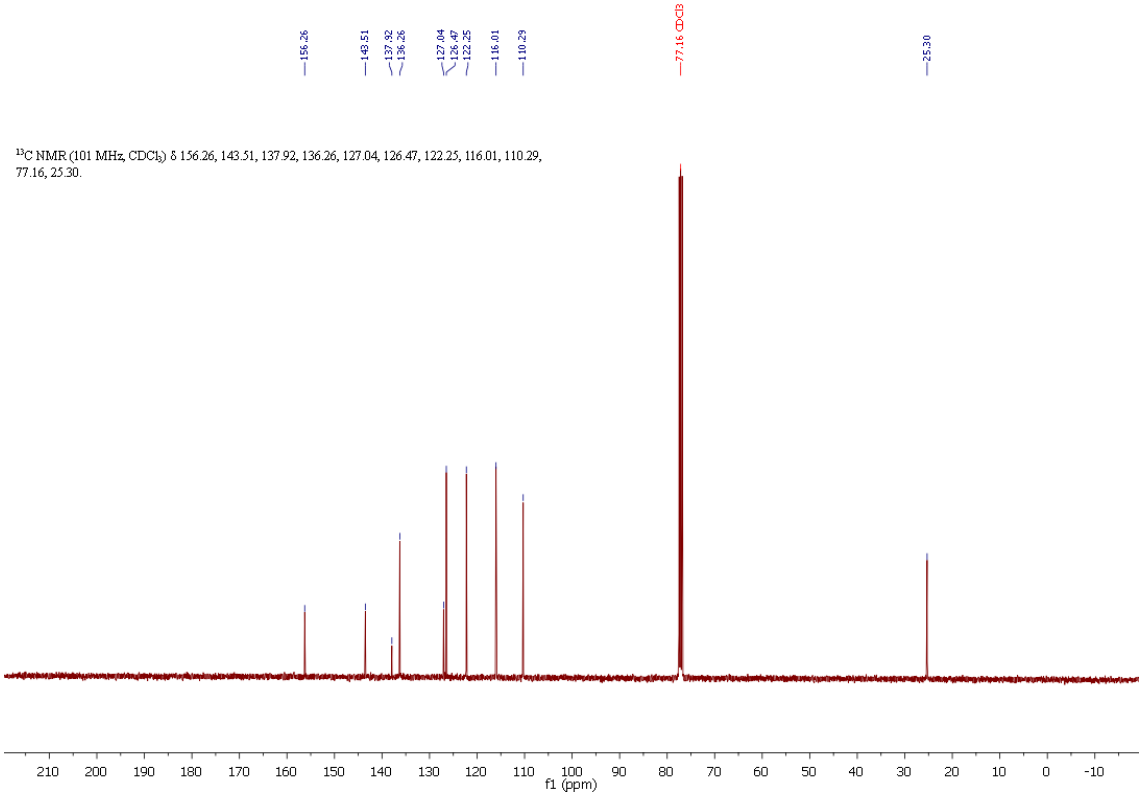

Fig. S51: ^{13}C NMR spectra of 2-Me-8-NH_2-qu in $CDCl_3$.

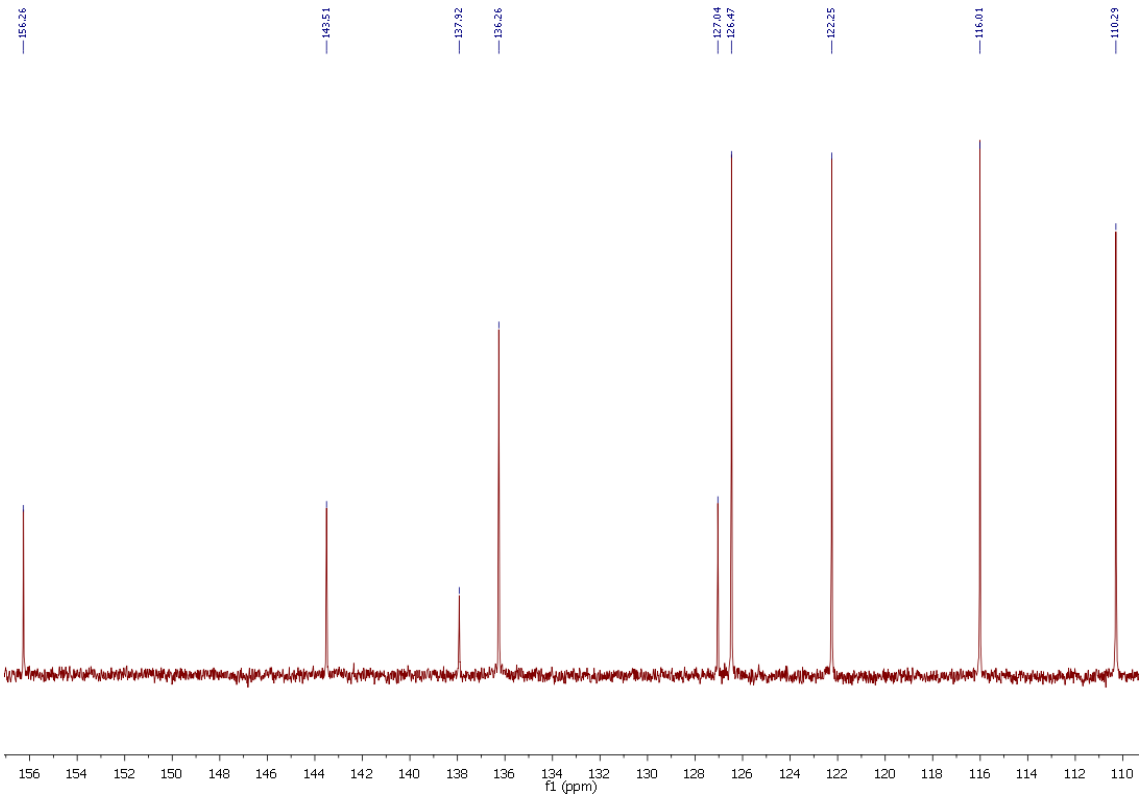

Fig. S52: Magnification of the ^{13}C NMR spectra of 2-Me-8-NH_2-qu in $CDCl_3$.

11.1.2 TMG2Mequ (L2)

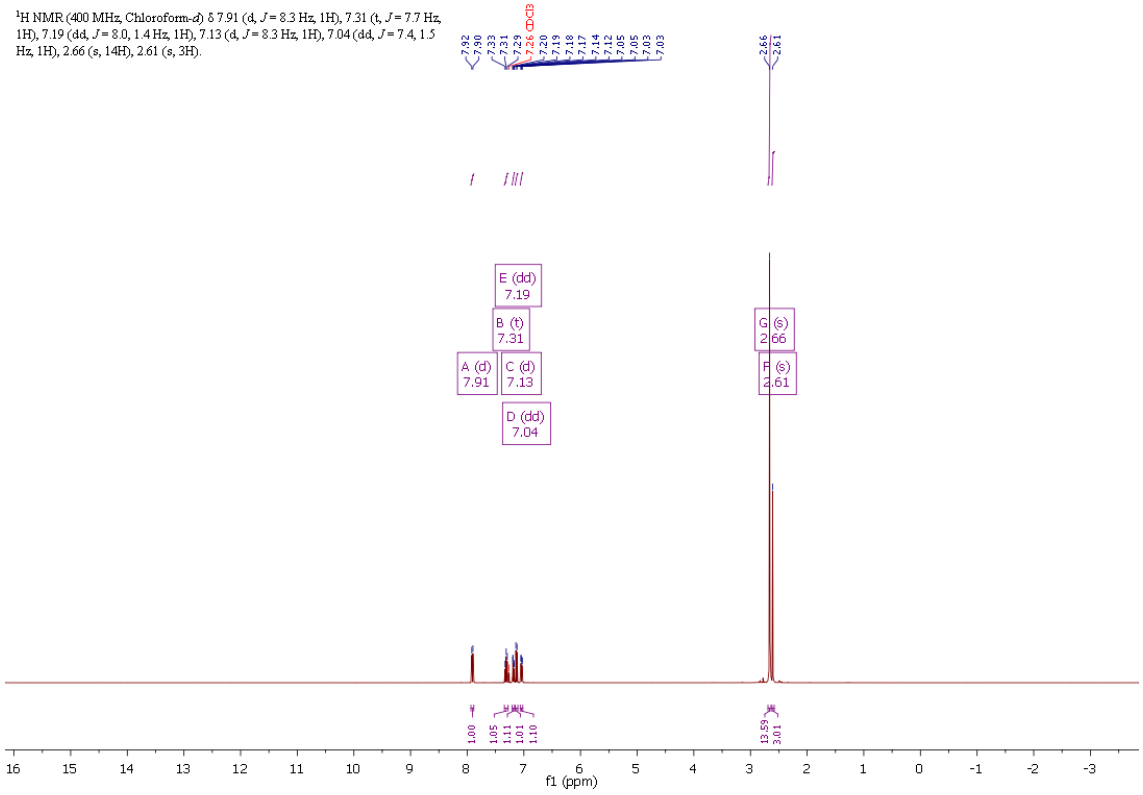

Fig. S53: ^{1}H NMR spectra of TMG2Mequ in $CDCl_3$.

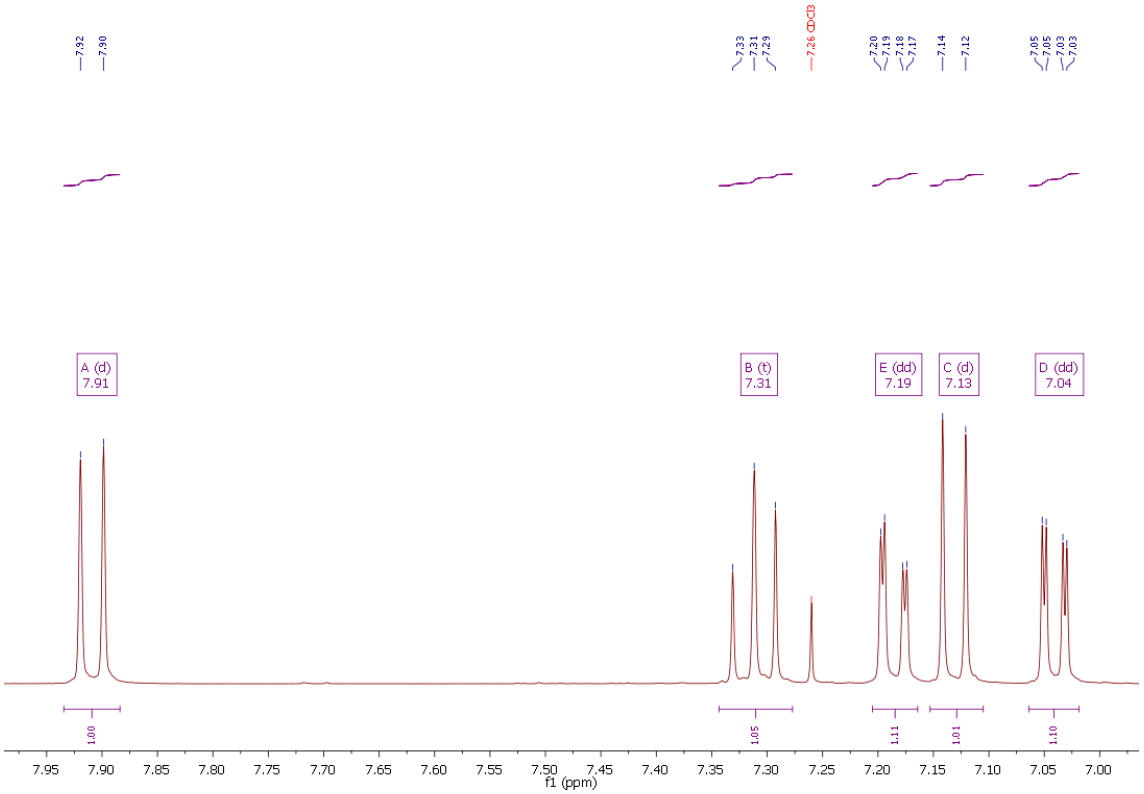

Fig. S54: Magnification of the ^{1}H NMR spectra of TMG2Mequ in $CDCl_3$.

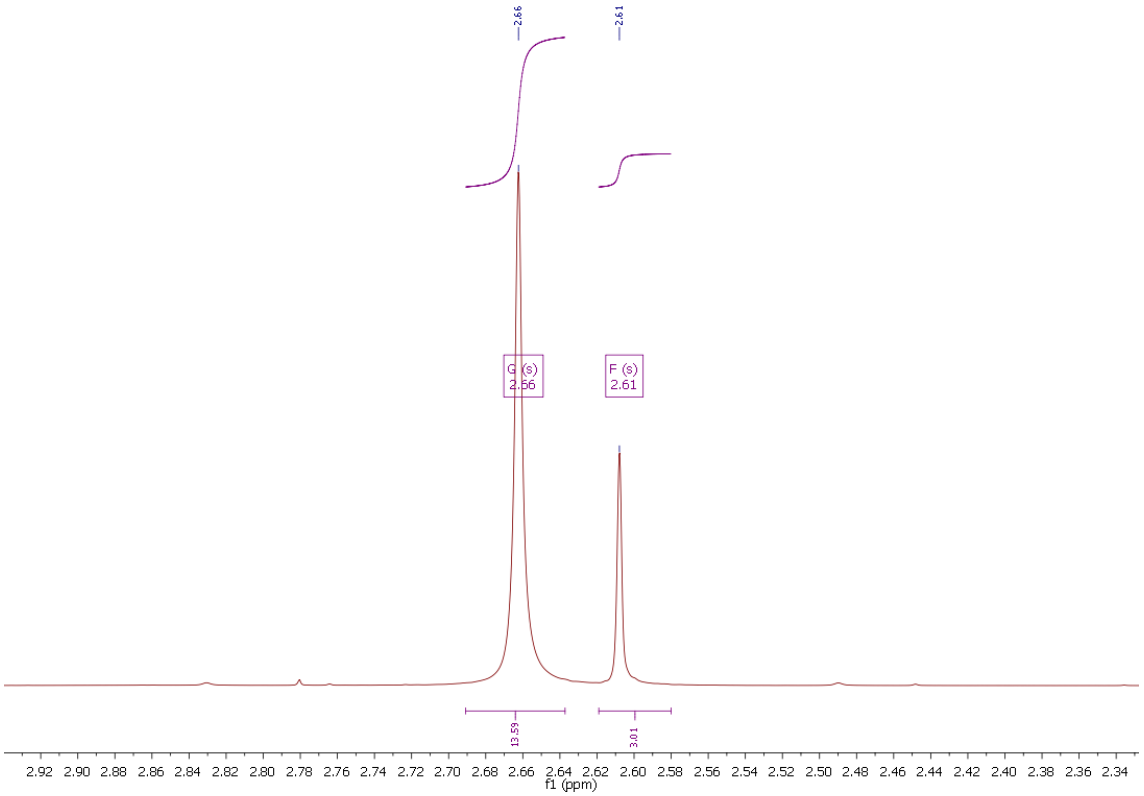

Fig. S55: Magnification of the ^{1}H NMR spectra of TMG2Mequ in $CDCl_3$.

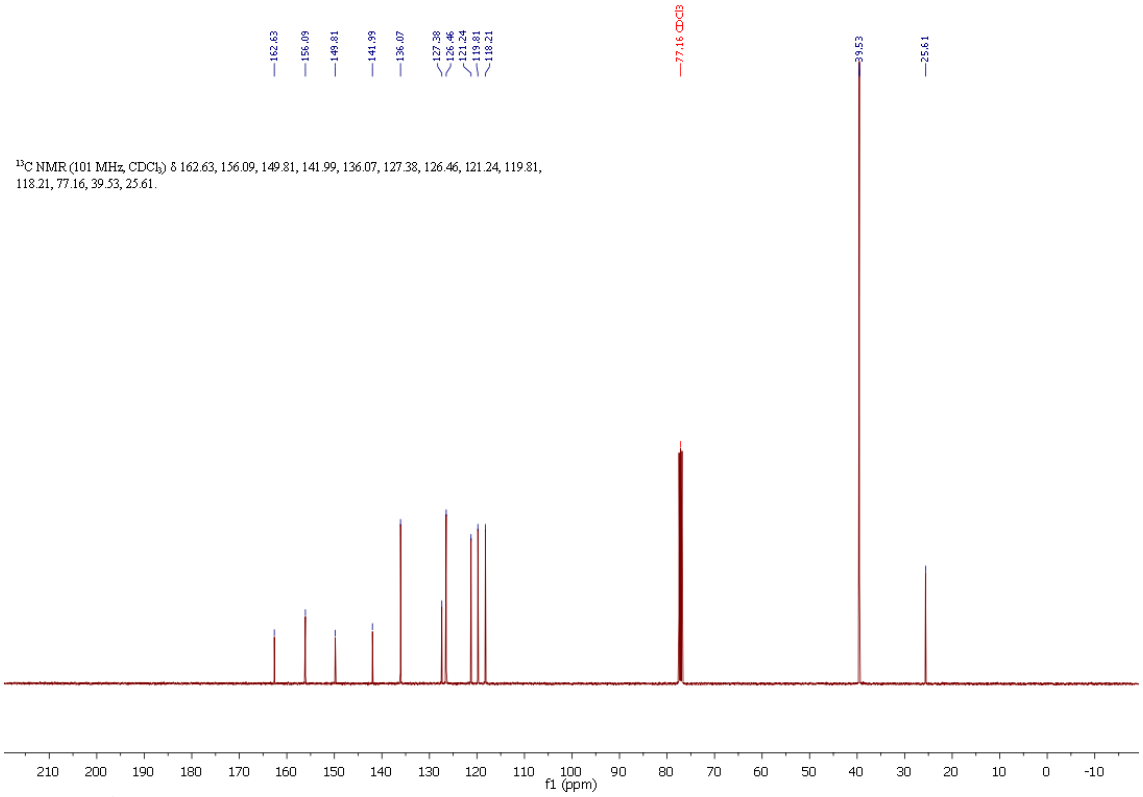

Fig. S56: ^{13}C NMR spectra of TMG2Mequ in $CDCl_3$.

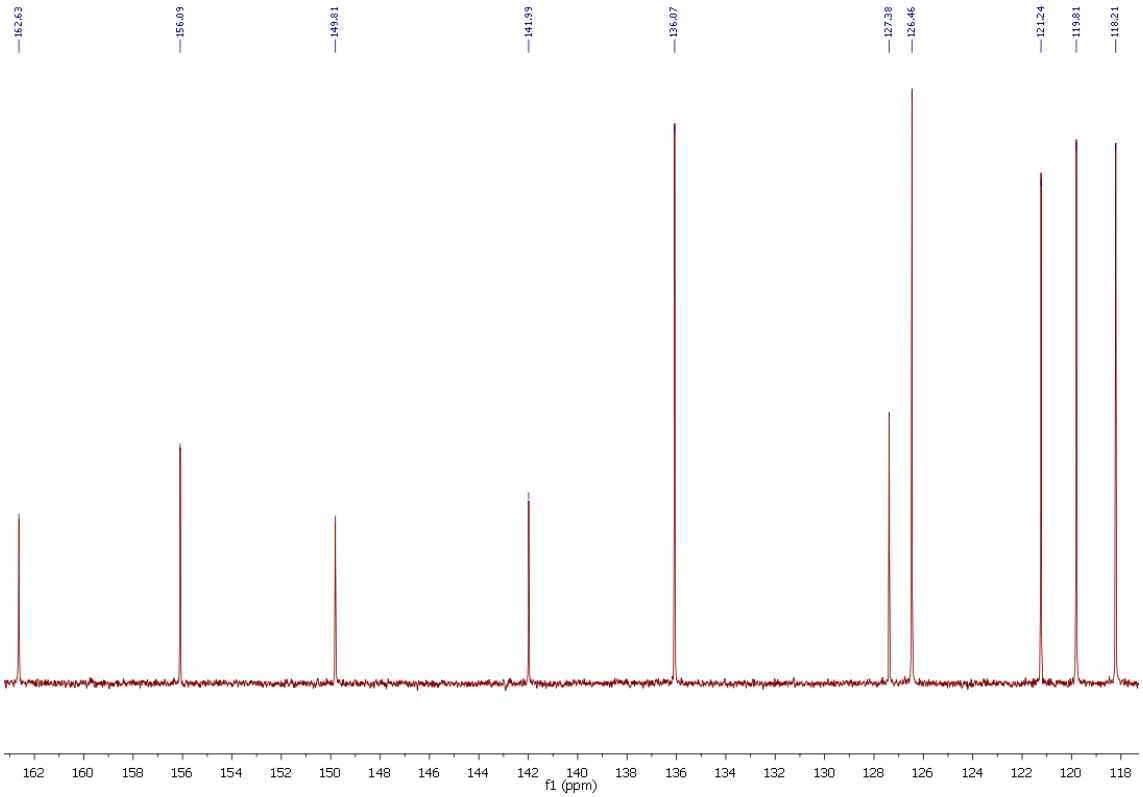

Fig. S57: Magnification of the ^{13}C NMR spectra of TMG2Mequ in $CDCl_3$.

11.1.3 [Cu(TMG2Mequ)$_2$]PF$_6$ (C3–PF$_6$)

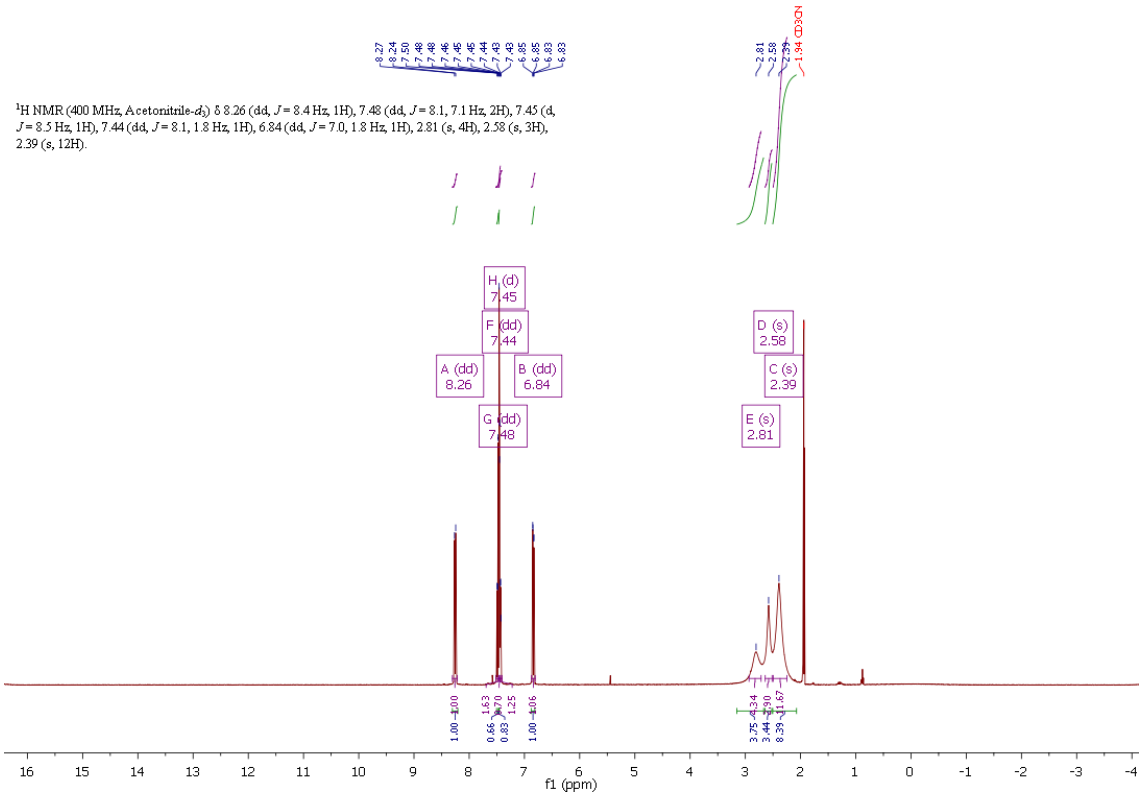

Fig. S58: ^{1}H NMR spectra of [Cu(TMG2Mequ)$_2$]PF$_6$ (**C3–PF$_6$**) in MeCN-d3.

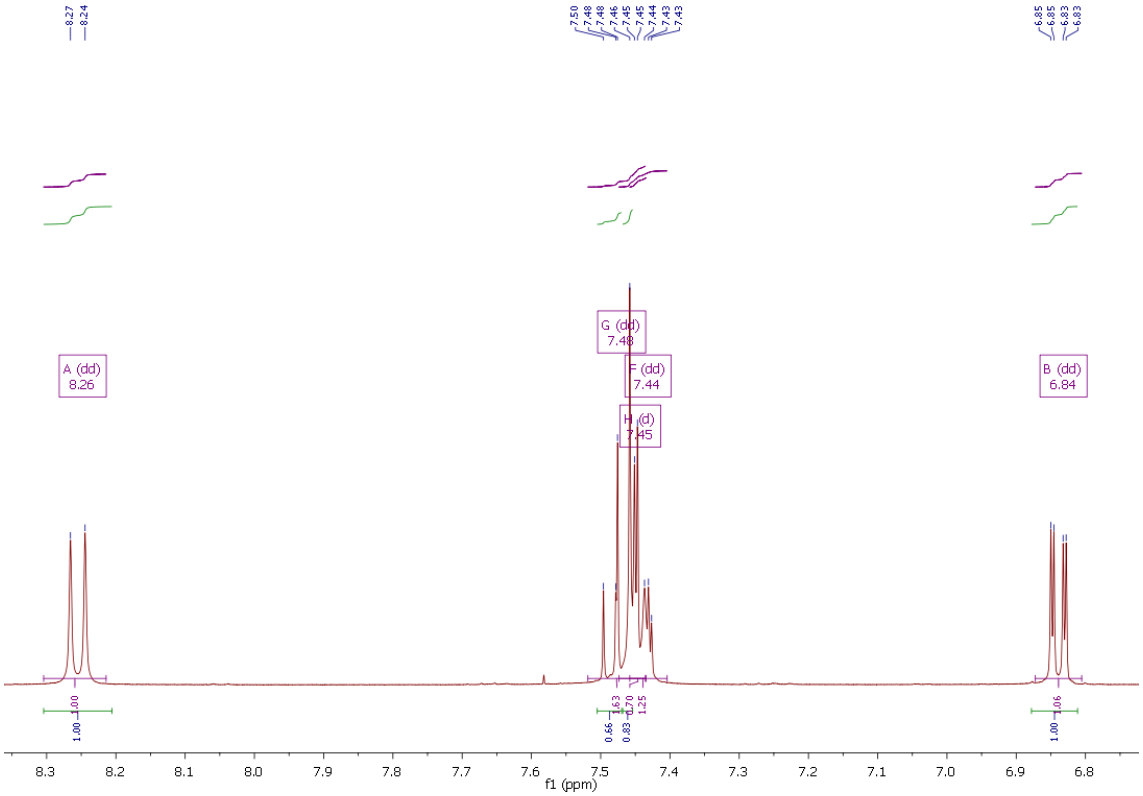

Fig. S59: Magnification of the ^{1}H NMR spectra of [Cu(TMG2Mequ)$_2$]PF$_6$ (**C3–PF$_6$**) in MeCN-d3.

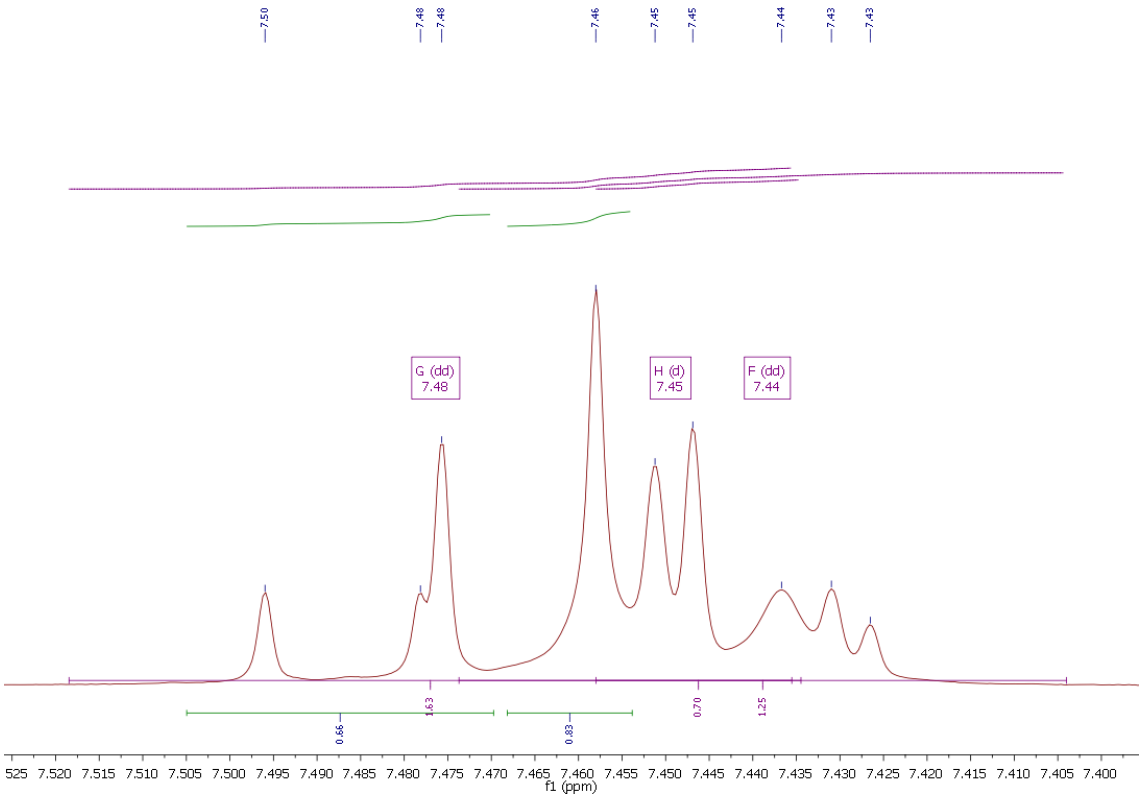

Fig. S60: Magnification of the ^{1}H NMR spectra of [Cu(TMG2Mequ)$_2$]PF$_6$ (**C3–PF$_6$**) in MeCN-d3.

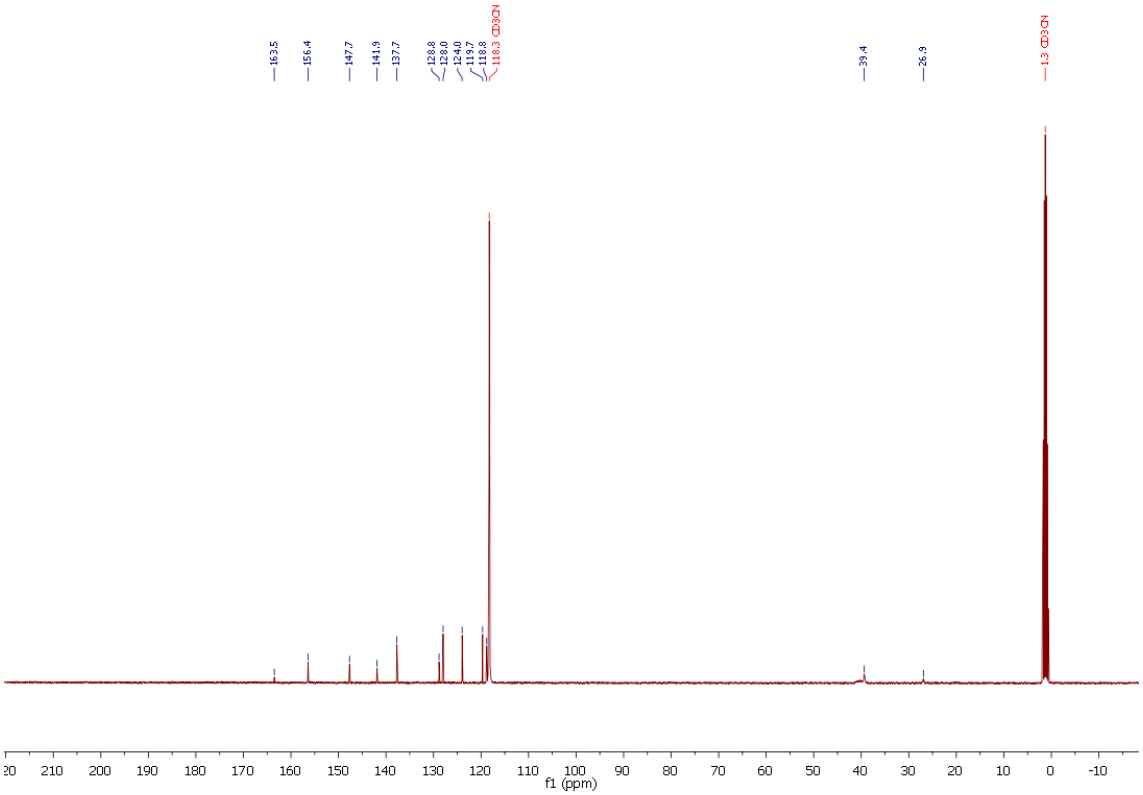

Fig. S61: ^{13}C NMR spectra of [Cu(TMG2Mequ)$_2$]PF$_6$ (**C3–PF$_6$**) in MeCN-d3.

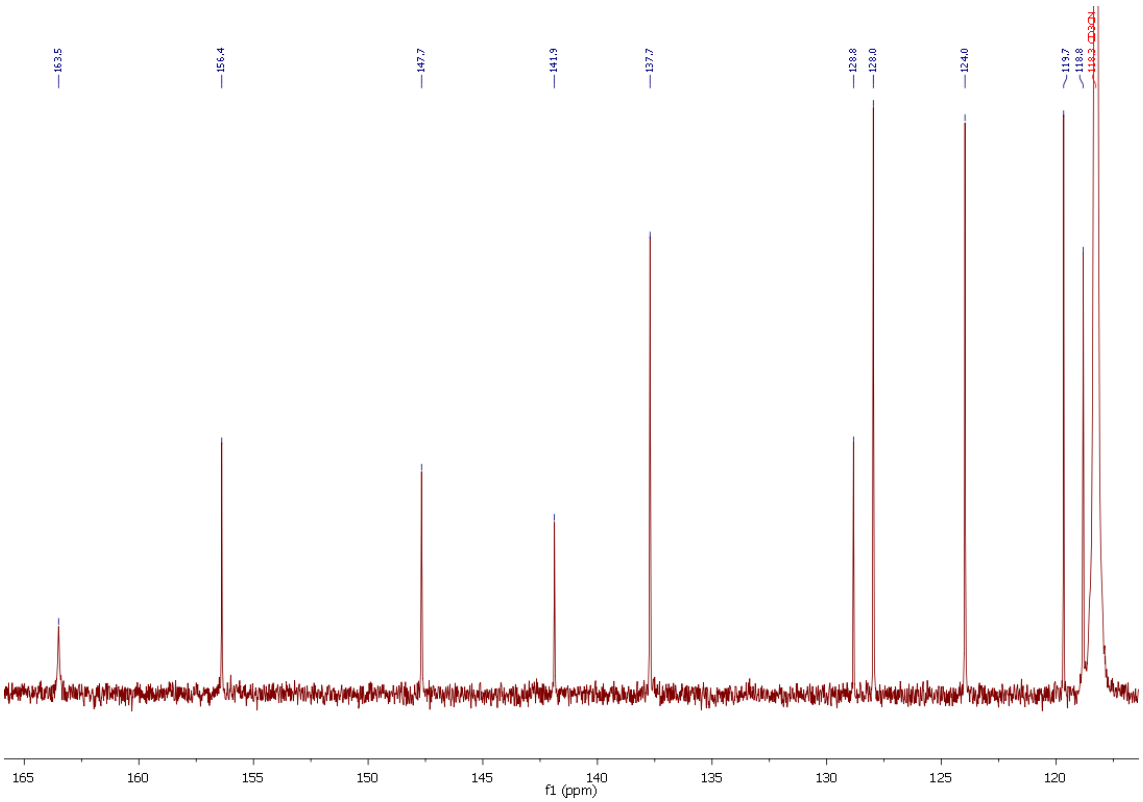

Fig. S62: Magnification of the ^{13}C NMR spectra of $[Cu(TMG2Mequ)_2]PF_6$ (**C3–PF$_6$**) in MeCN-d3.

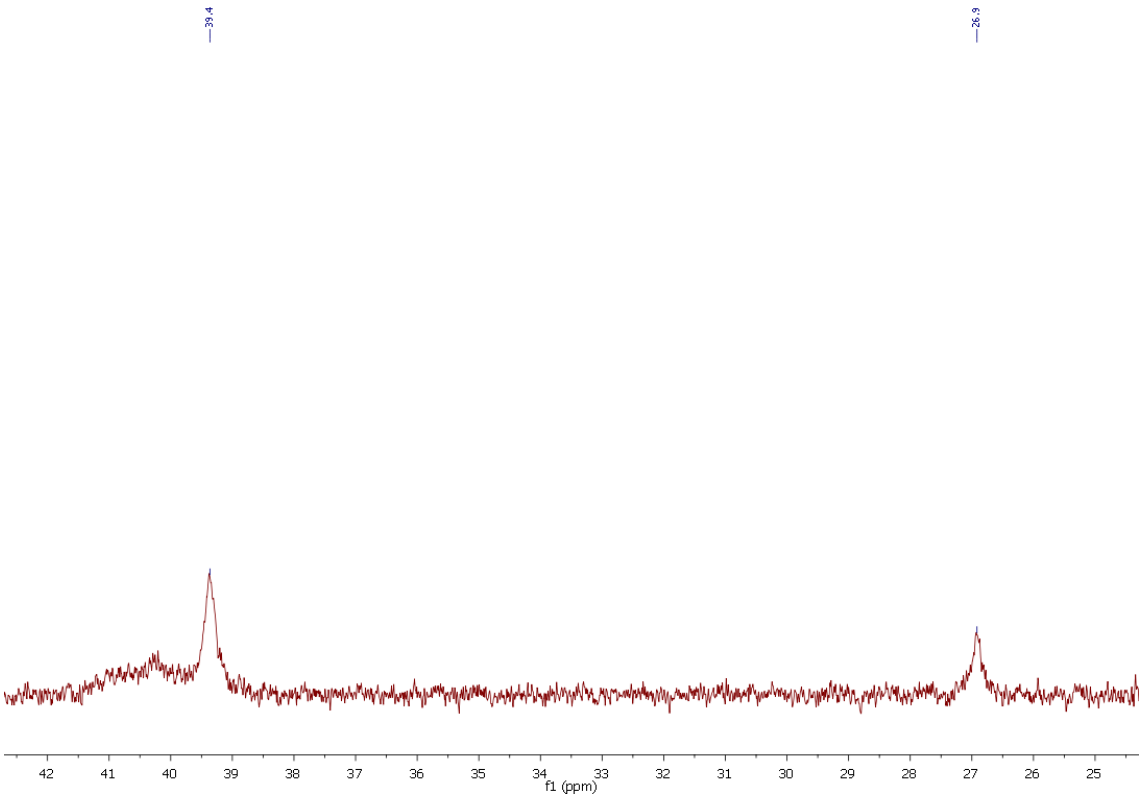

Fig. S63: Magnification of the ^{13}C NMR spectra of $[Cu(TMG2Mequ)_2]PF_6$ (**C3–PF$_6$**) in MeCN-d3.

11.1.4 [Cu(TMG2Mequ)$_2$]OTf (C3−OTf)

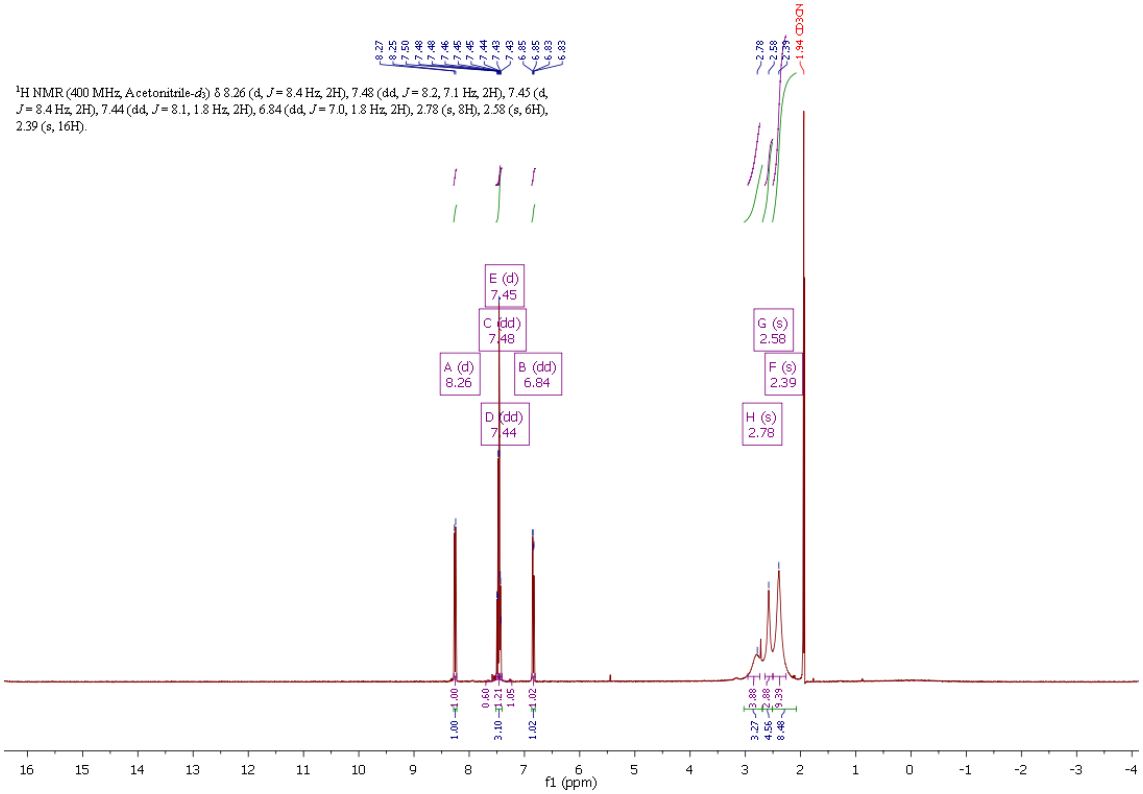

Fig. S64: ^{1}H NMR spectra of [Cu(TMG2Mequ)$_2$]OTf (**C3−OTf**) in MeCN-d3.

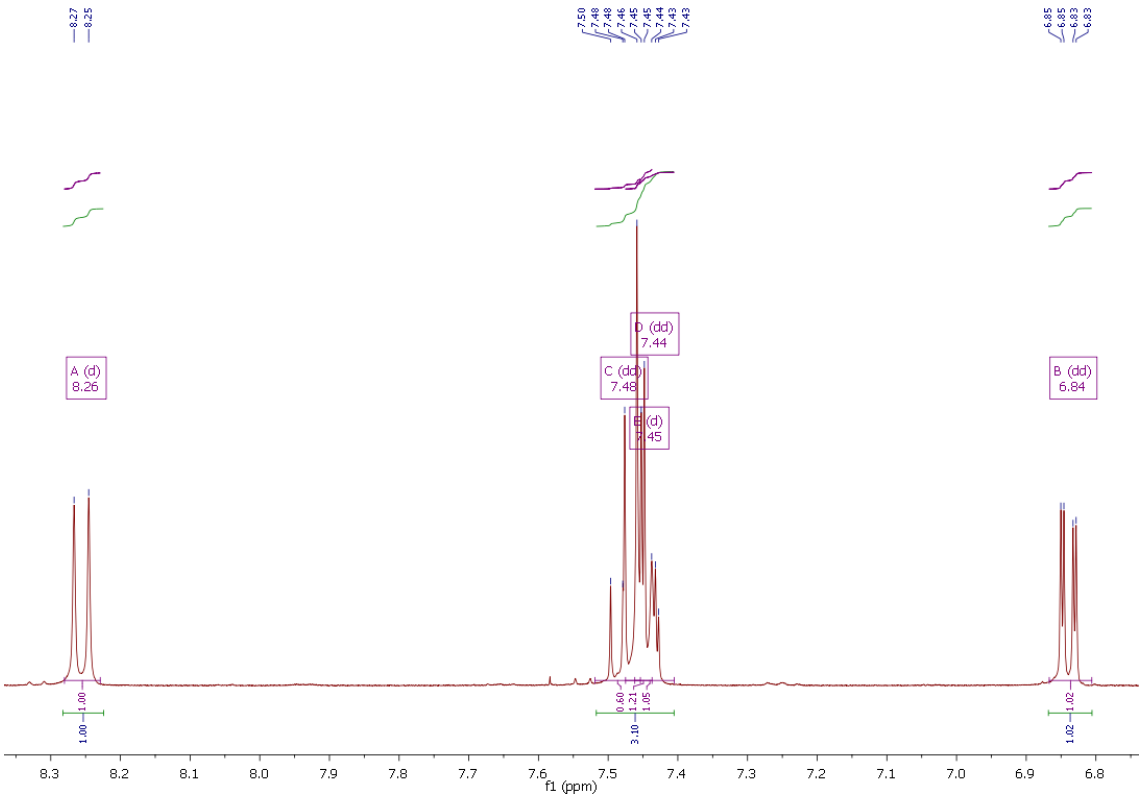

Fig. S65:Magnification of the ^{1}H NMR spectra of [Cu(TMG2Mequ)$_2$]OTf (**C3−OTf**) in MeCN-d3.

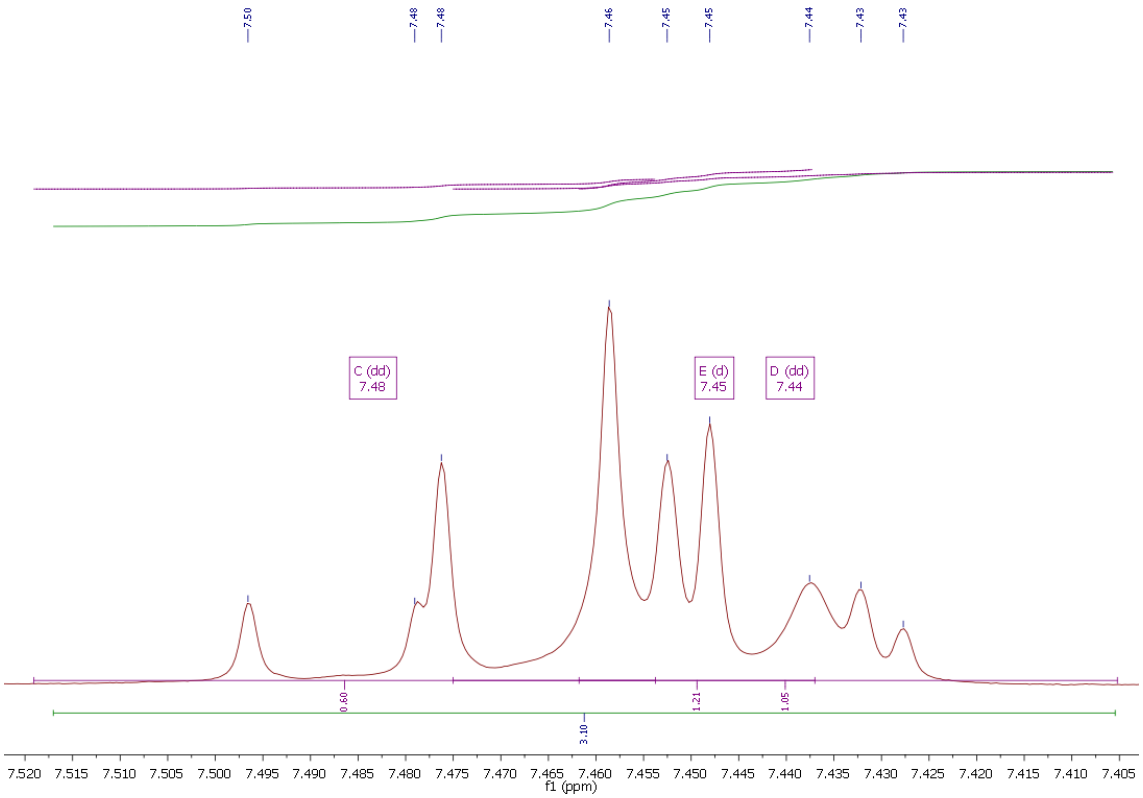

Fig. S66: Magnification of the ^{1}H NMR spectra of [Cu(TMG2Mequ)$_2$]OTf (**C3–OTf**) in MeCN-d3.

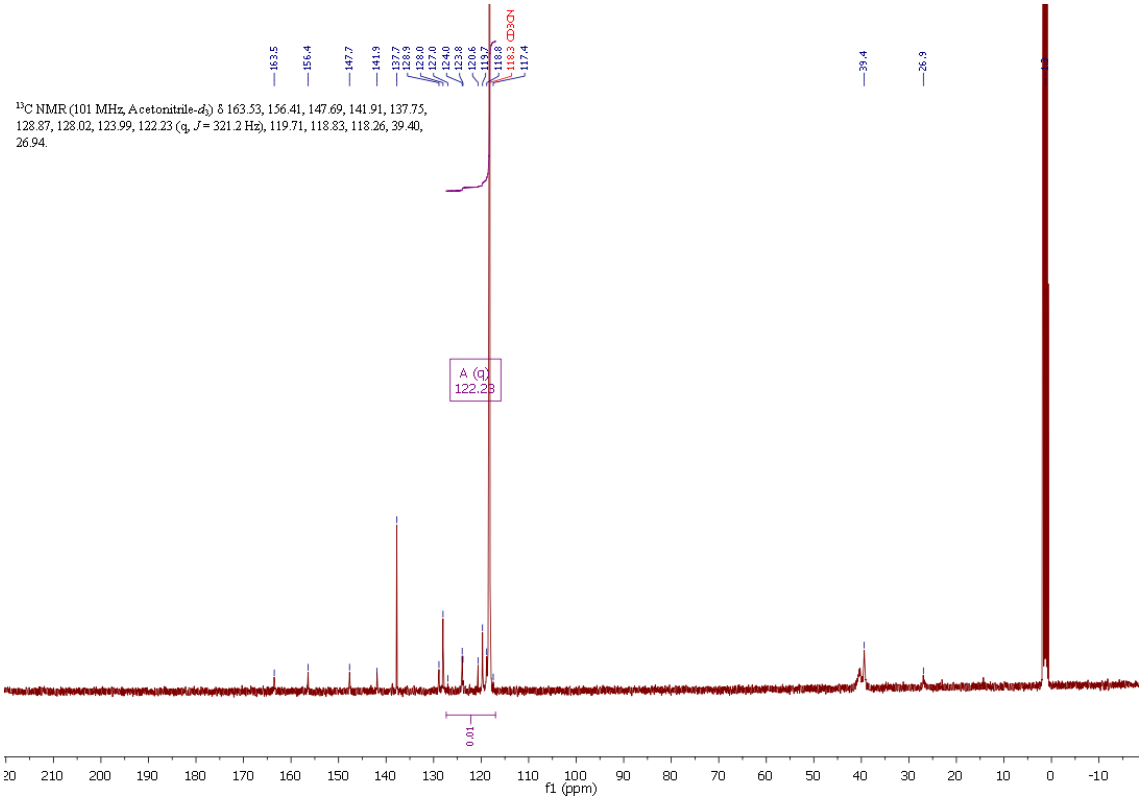

Fig. S67: ^{13}C NMR spectra of [Cu(TMG2Mequ)$_2$]OTf (**C3–OTf**) in MeCN-d3.

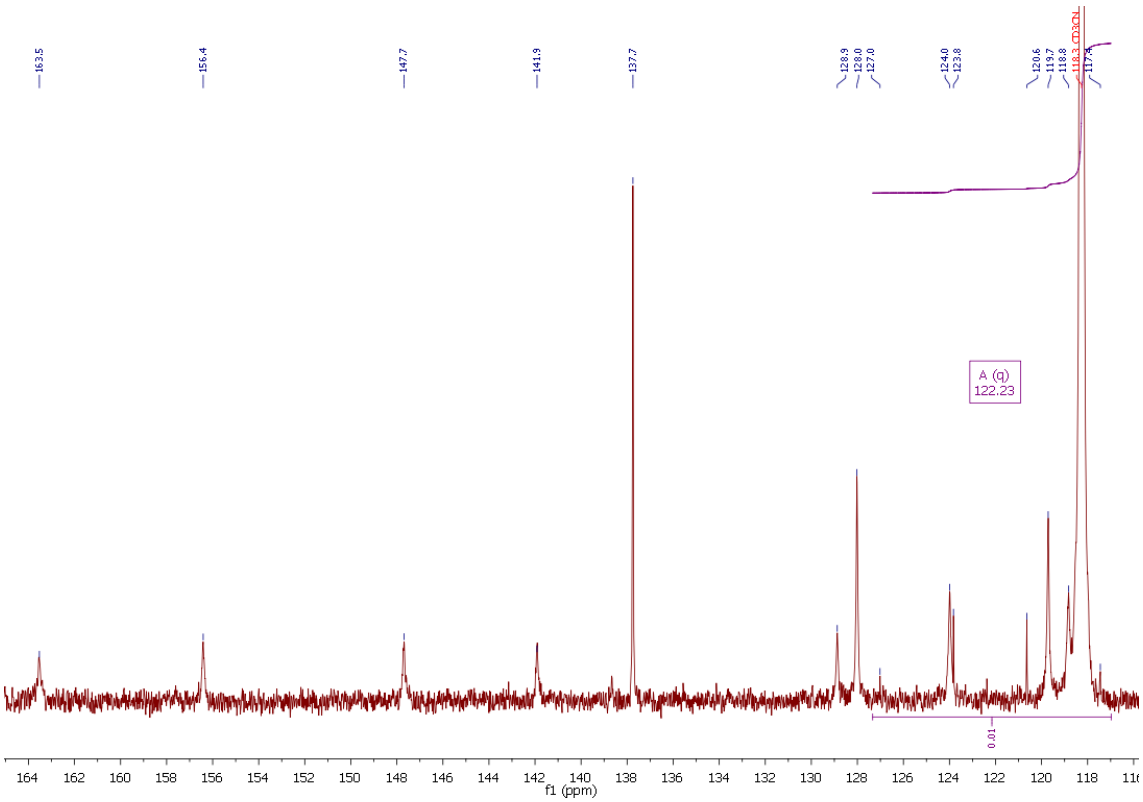

Fig. S68: Magnification of the ^{13}C NMR spectra of [Cu(TMG2Mequ)$_2$]OTf (**C3–OTf**) in MeCN-d3.

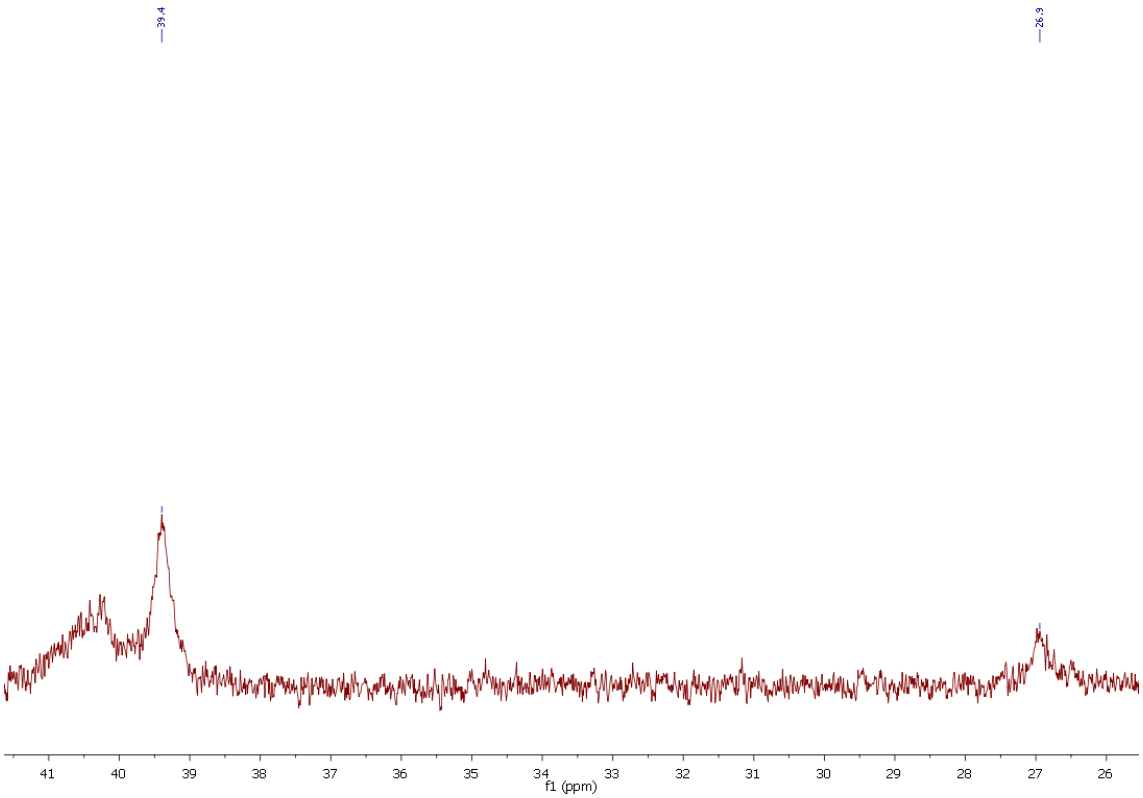

Fig. S69: Magnification of the ^{13}C NMR spectra of [Cu(TMG2Mequ)$_2$]OTf (**C3–OTf**) in MeCN-d3.

11.2 TMG2^{t}Buqu (L3) and corresponding precursors and Cu(I) complex

11.2.1 2-*tert*-Butyl-8-nitroquinoline (2-^{t}Bu-8-NO_2-qu)

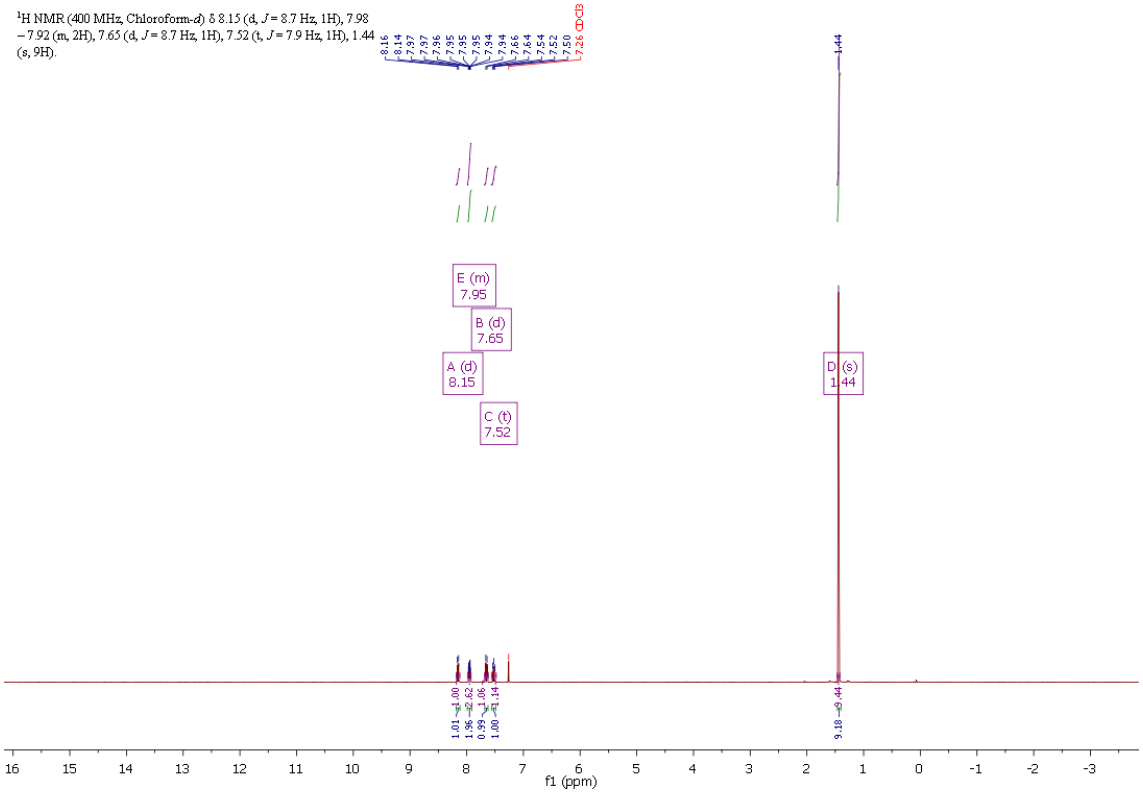

Fig. S70: ^{1}H NMR spectra of 2-^{t}Bu-8-NO_2-qu in $CDCl_3$.

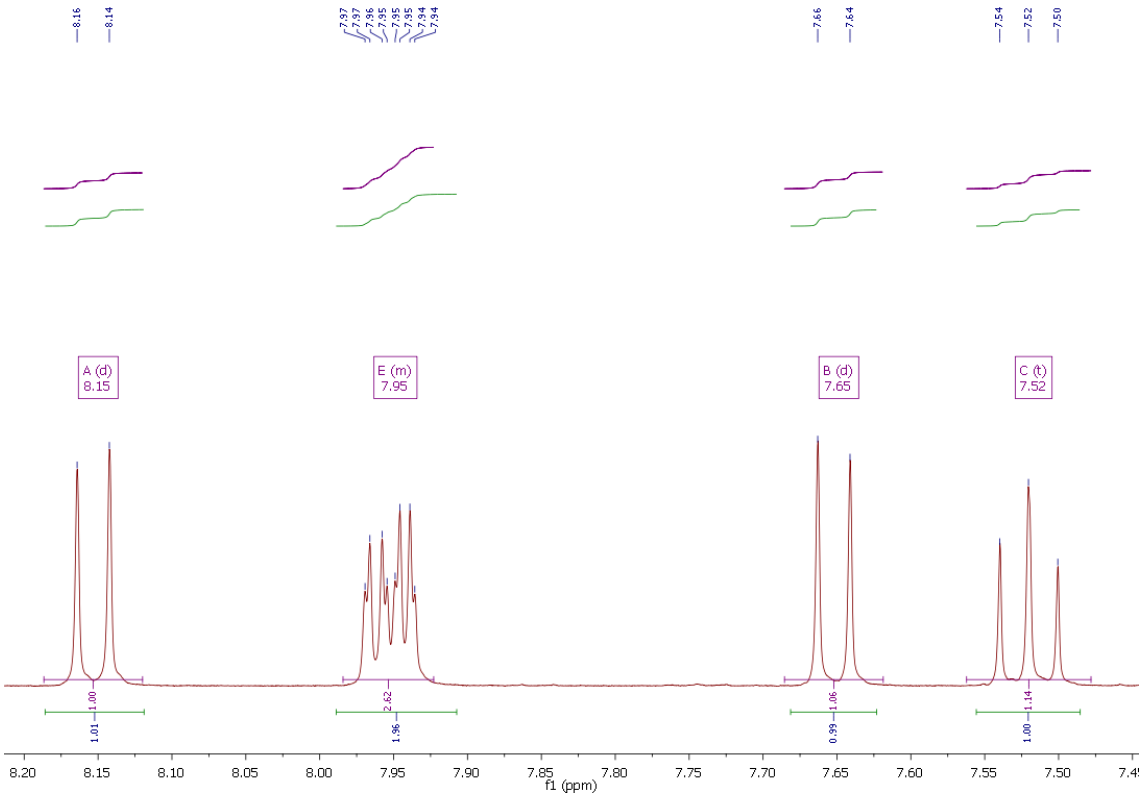

Fig. S71: Magnification of the ^{1}H NMR spectra of 2-^{t}Bu-8-NO$_2$-qu in CDCl$_3$.

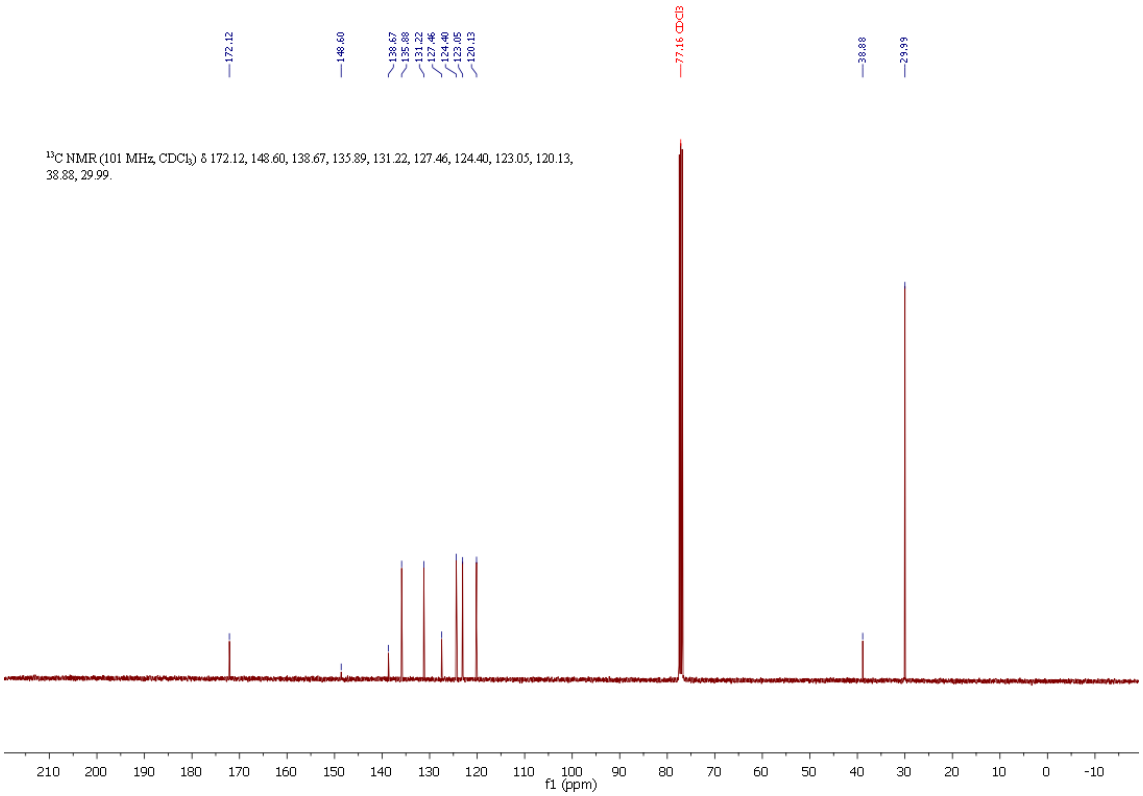

Fig. S72: ^{13}C NMR spectra of 2-^{t}Bu-8-NO$_2$-qu in CDCl$_3$.

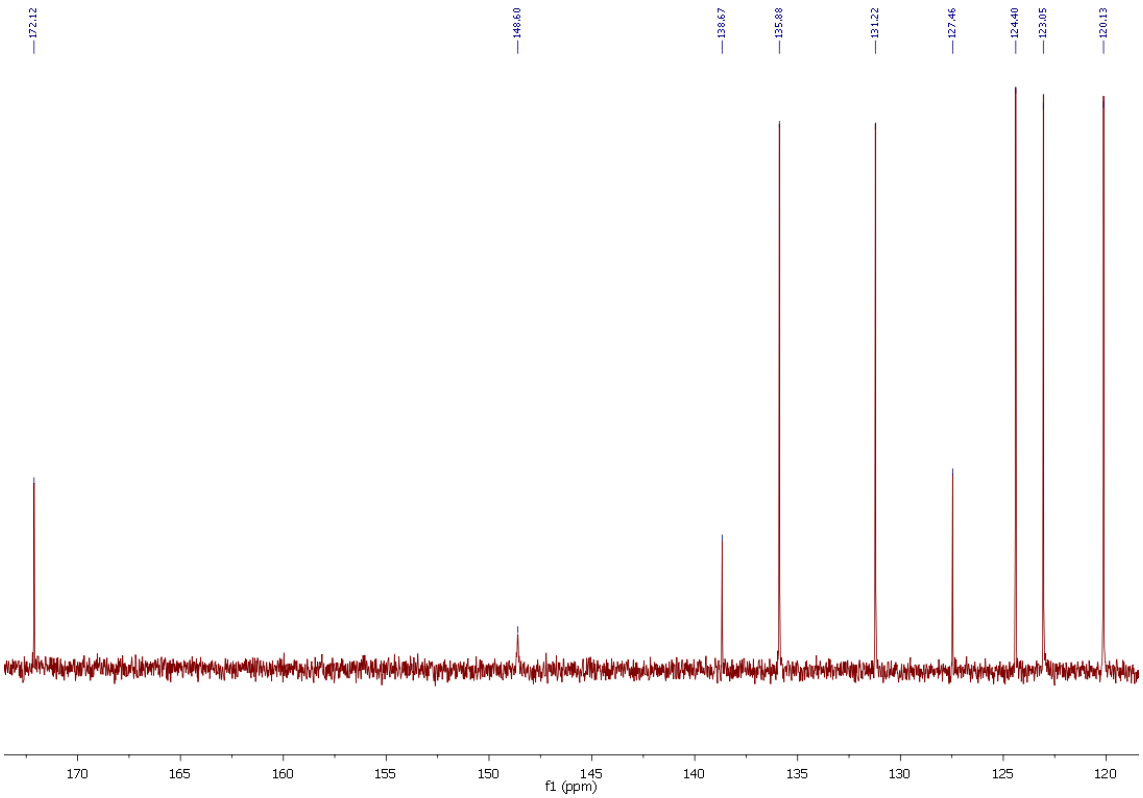

Fig. S73: Magnification of the ^{13}C NMR spectra of 2-^{t}Bu-8-NO_2-qu in $CDCl_3$.

11.2.2 2-*tert*-Butyl-8-aminoquinoline (2-^{t}Bu-8-NH_2-qu)

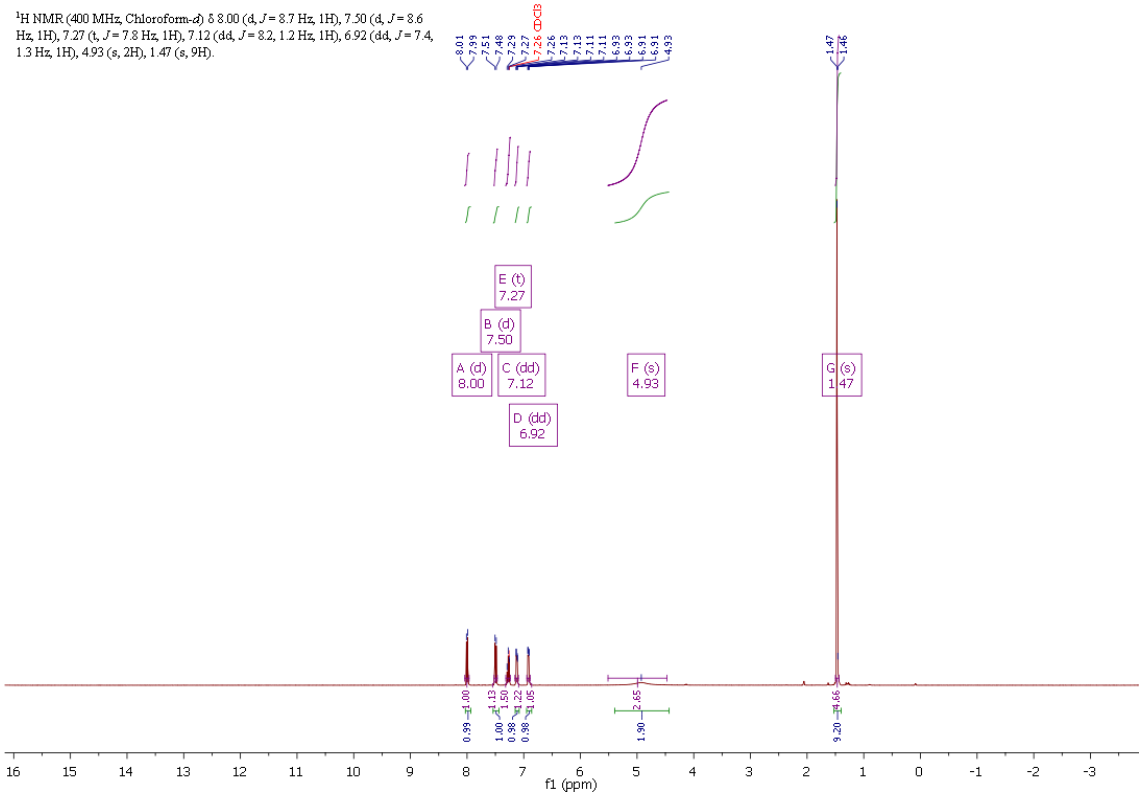

Fig. S74: ^{1}H NMR spectra of 2-^{t}Bu-8-NH_2-qu in $CDCl_3$.

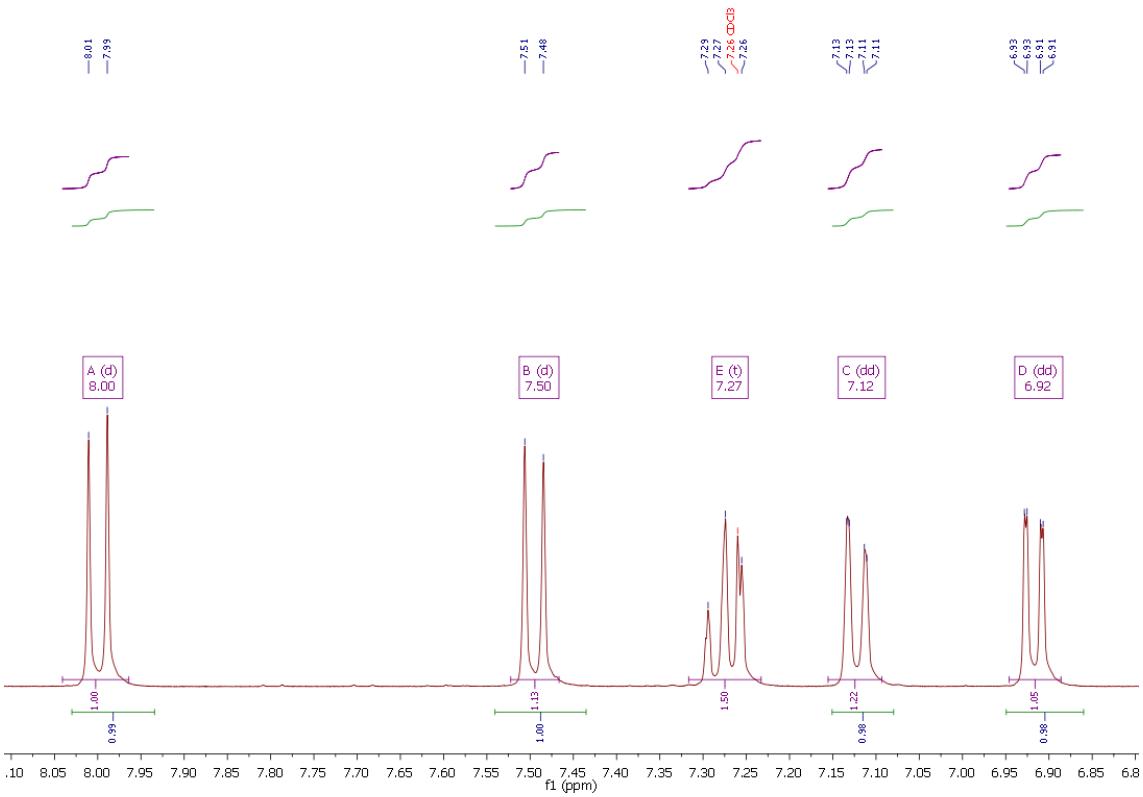

Fig. S75: Magnification of the ^{1}H NMR spectra of 2-^{t}Bu-8-NH$_2$-qu in CDCl$_3$.

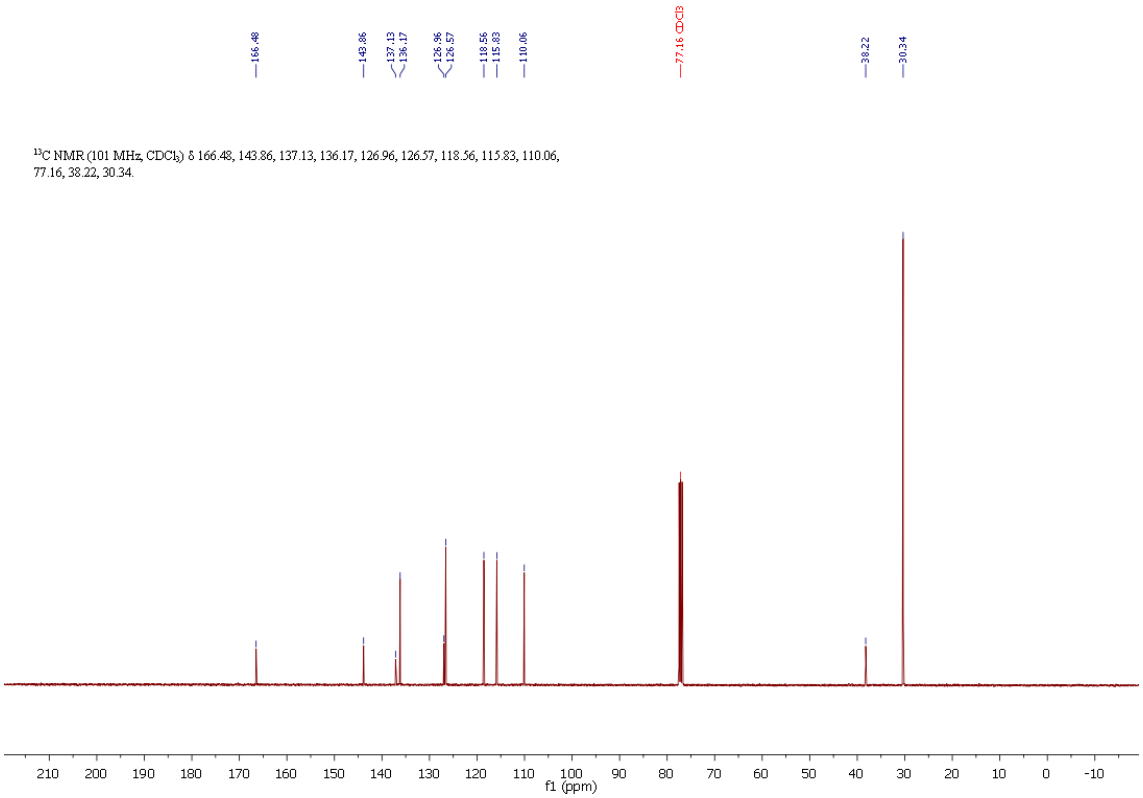

^{13}C NMR (101 MHz, CDCl$_3$) δ 166.48, 143.86, 137.13, 136.17, 126.96, 126.57, 118.56, 115.83, 110.06, 77.16, 38.22, 30.34.

Fig. S76: ^{13}C NMR spectra of 2-^{t}Bu-8-NH$_2$-qu in CDCl$_3$.

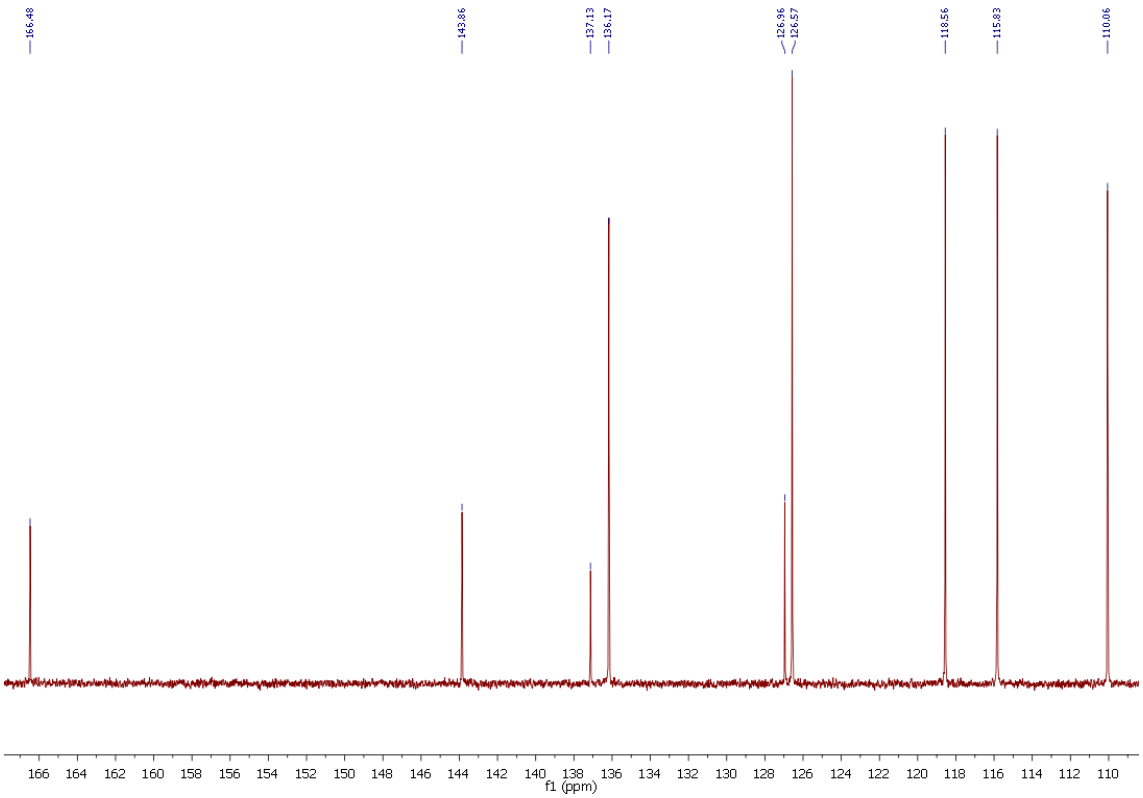

Fig. S77: Magnification of the ^{13}C NMR spectra of 2-^{t}Bu-8-NH$_2$-qu in CDCl$_3$.

11.2.3 TMG2^{t}Buqu (L3)

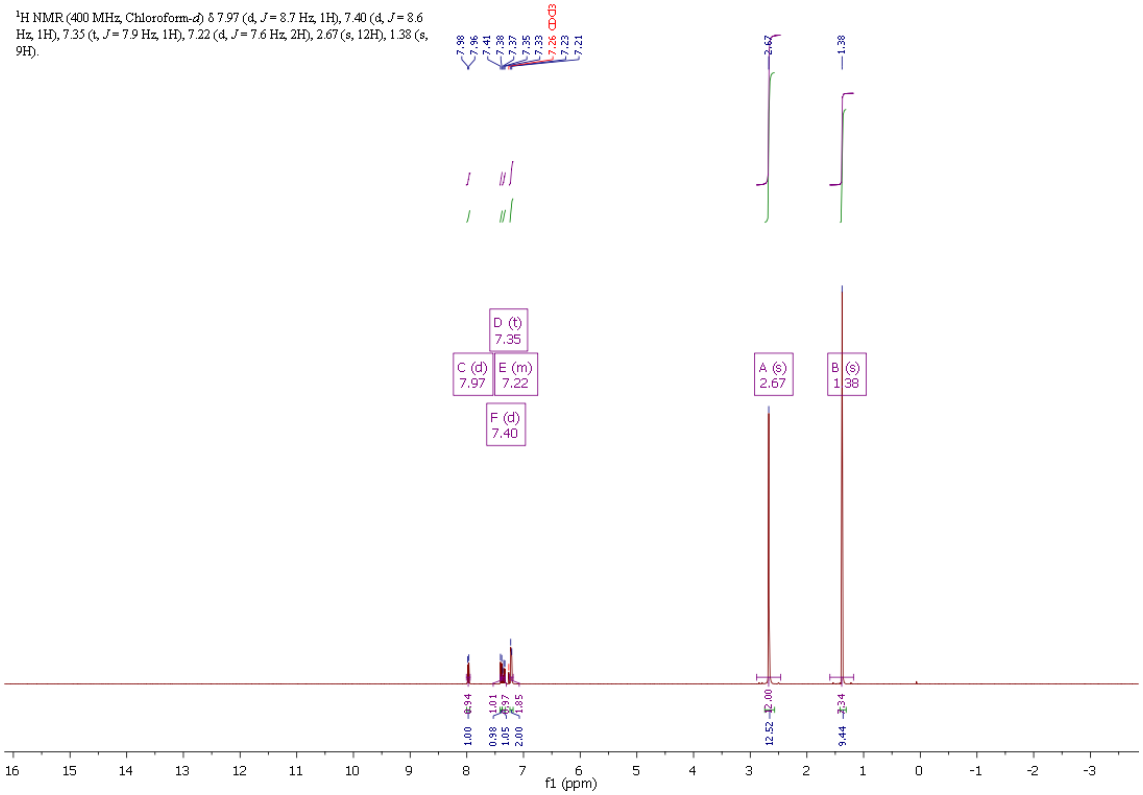

Fig. S78: ^{1}H NMR spectra of TMG2^{t}Buqu in CDCl$_3$.

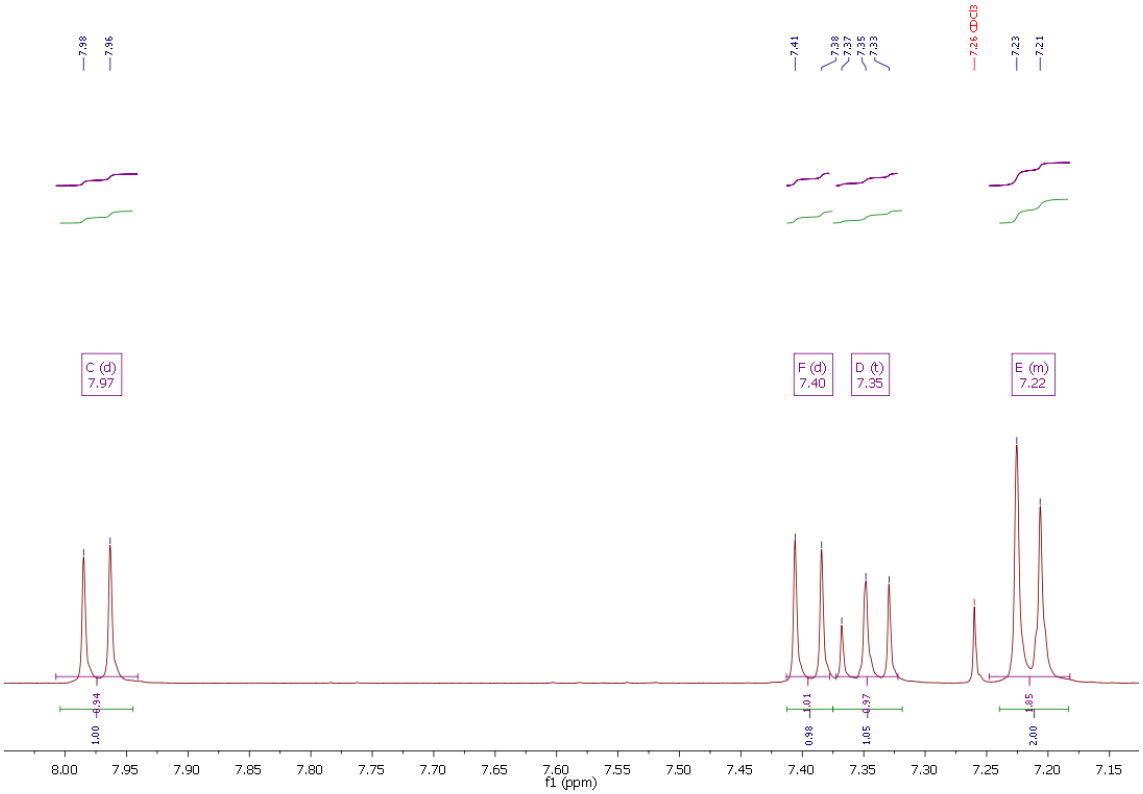

Fig. S79: Magnification of the ^{1}H NMR spectra of TMG2^{t}Buqu in $CDCl_3$.

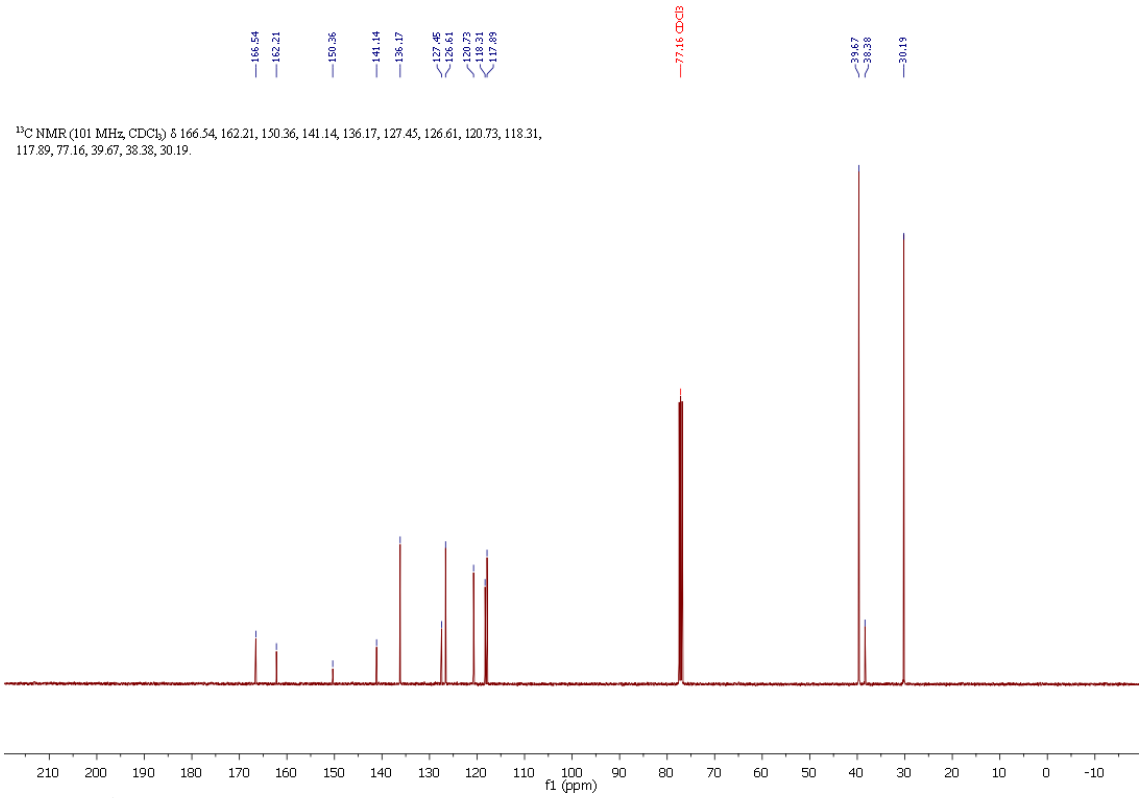

Fig. S80: ^{13}C NMR spectra of TMG2^{t}Buqu in $CDCl_3$.

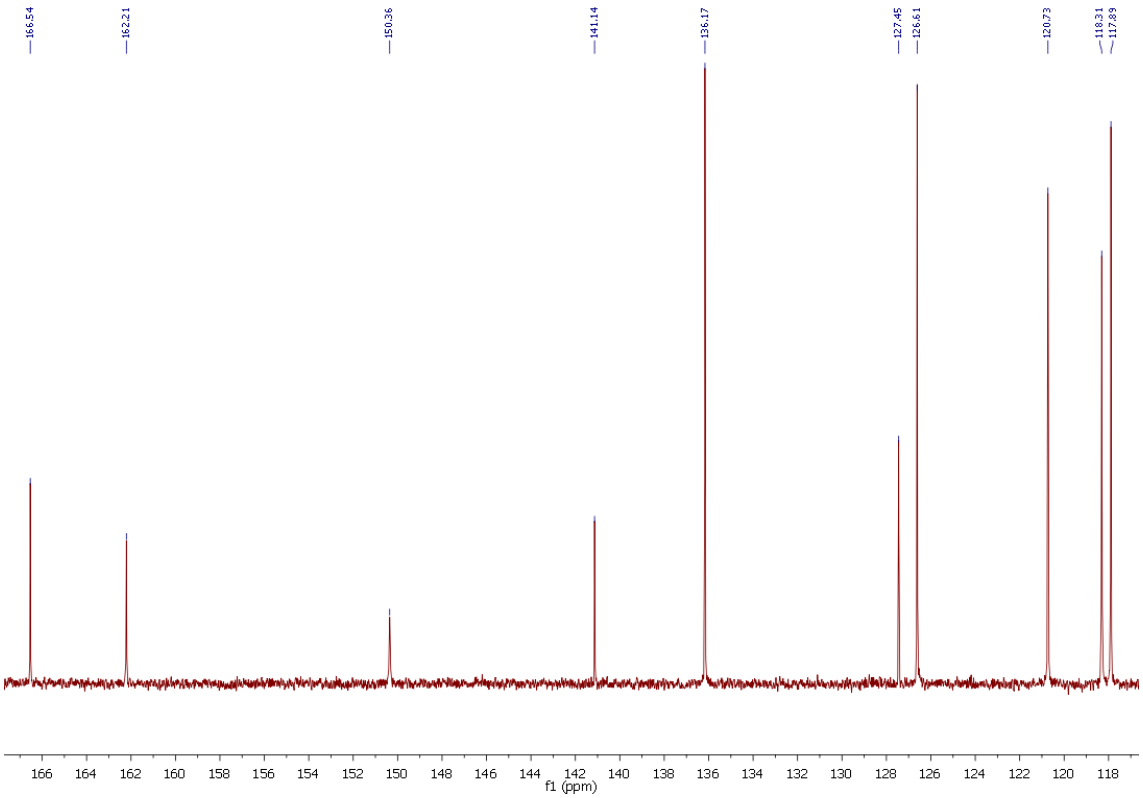

Fig. S81: Magnification of the ^{13}C NMR spectra of TMG2^{t}Buqu in $CDCl_3$.

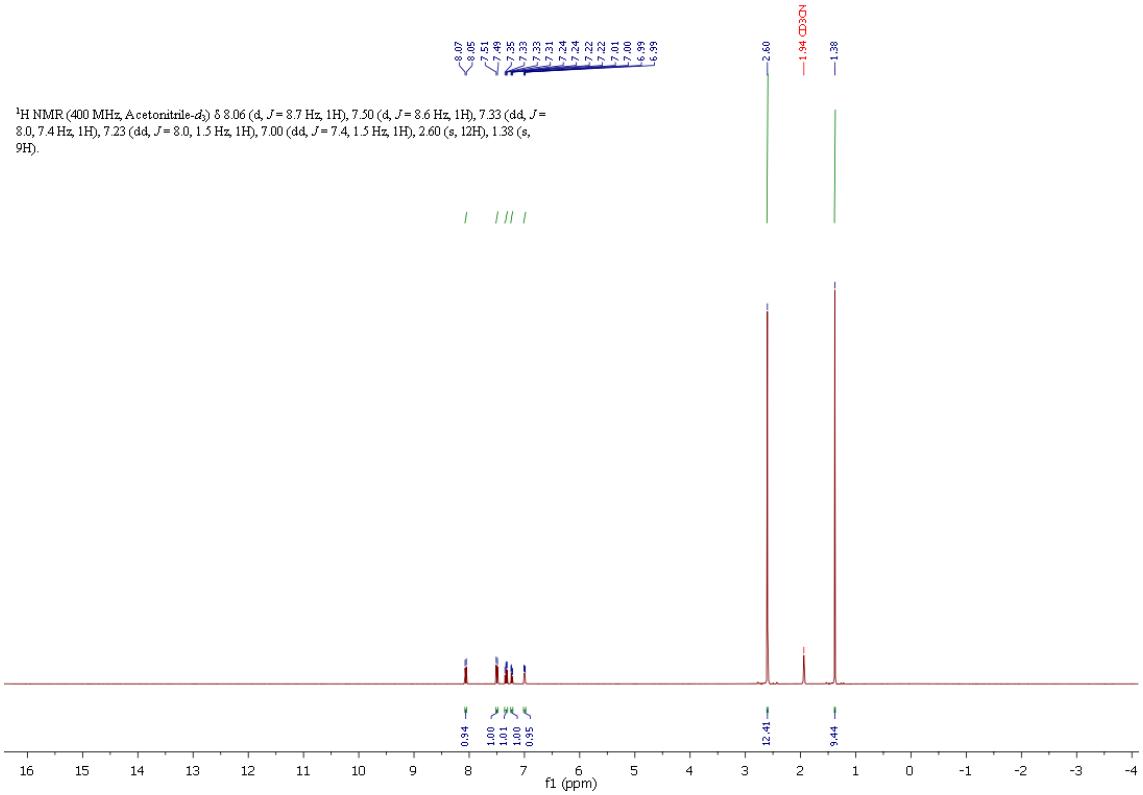

^1H NMR (400 MHz, Acetonitrile-d_3) δ 8.06 (d, J = 8.7 Hz, 1H), 7.50 (d, J = 8.6 Hz, 1H), 7.33 (dd, J = 8.0, 7.4 Hz, 1H), 7.23 (dd, J = 8.0, 1.5 Hz, 1H), 7.00 (dd, J = 7.4, 1.5 Hz, 1H), 2.60 (s, 12H), 1.38 (s, 9H).

Fig. S82: ^1H NMR spectra of TMG2^{t}Buqu in CD_3CN.

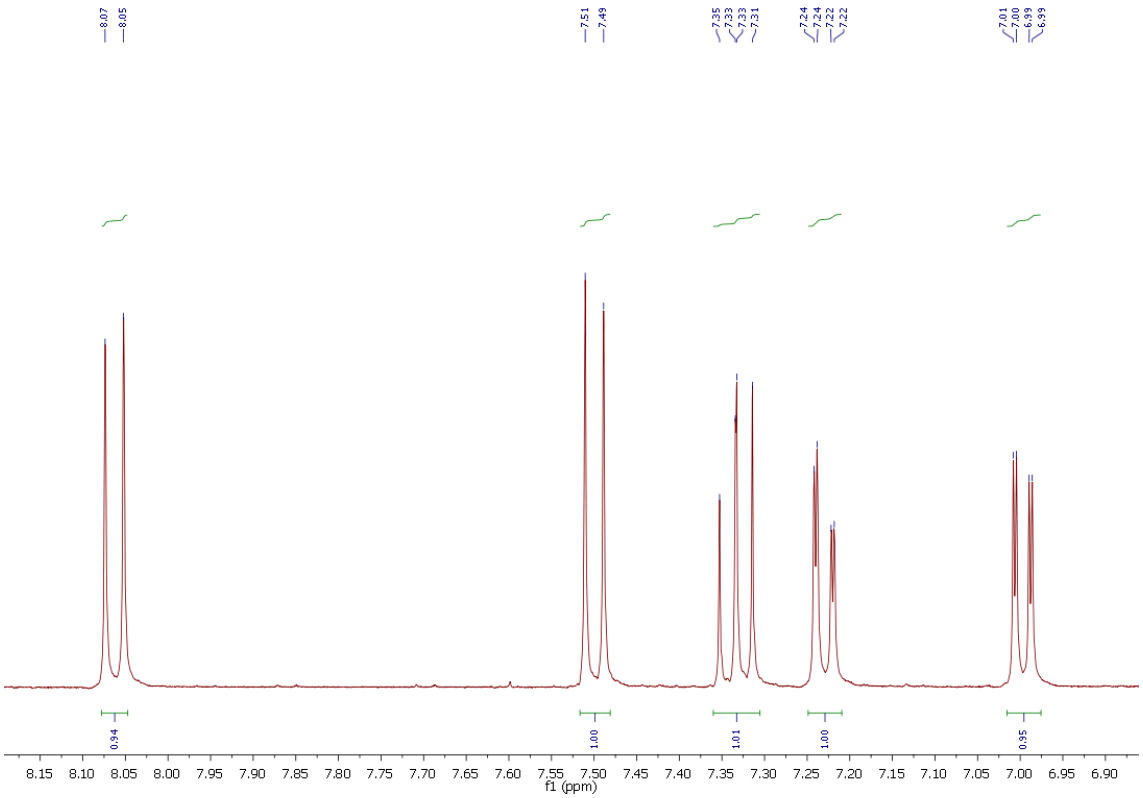

Fig. S83: Magnification of the ^{1}H NMR spectra of TMG2^{t}Buqu in CD_3CN.

11.2.4 [Cu(TMG2^{t}Buqu)]PF_6

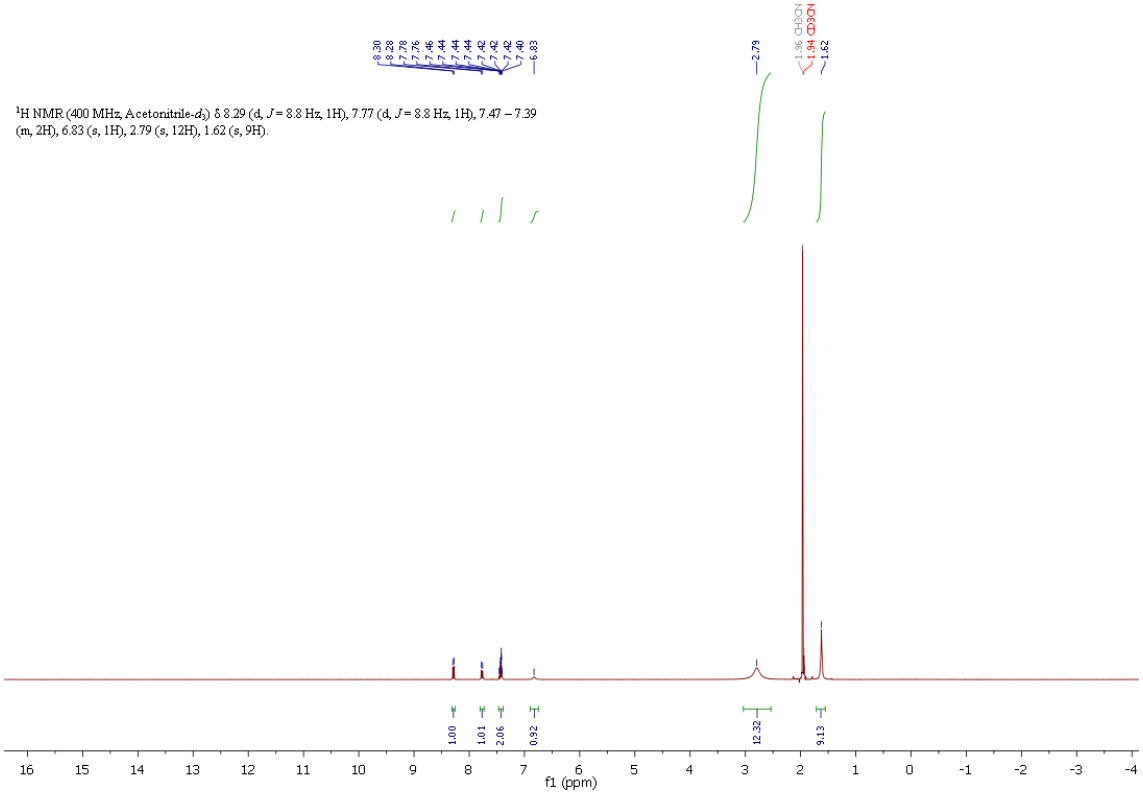

Fig. S84: ^{1}H NMR spectra of the *in situ* prepared complex [Cu(TMG2^{t}Buqu)]PF_6 in CD_3CN.

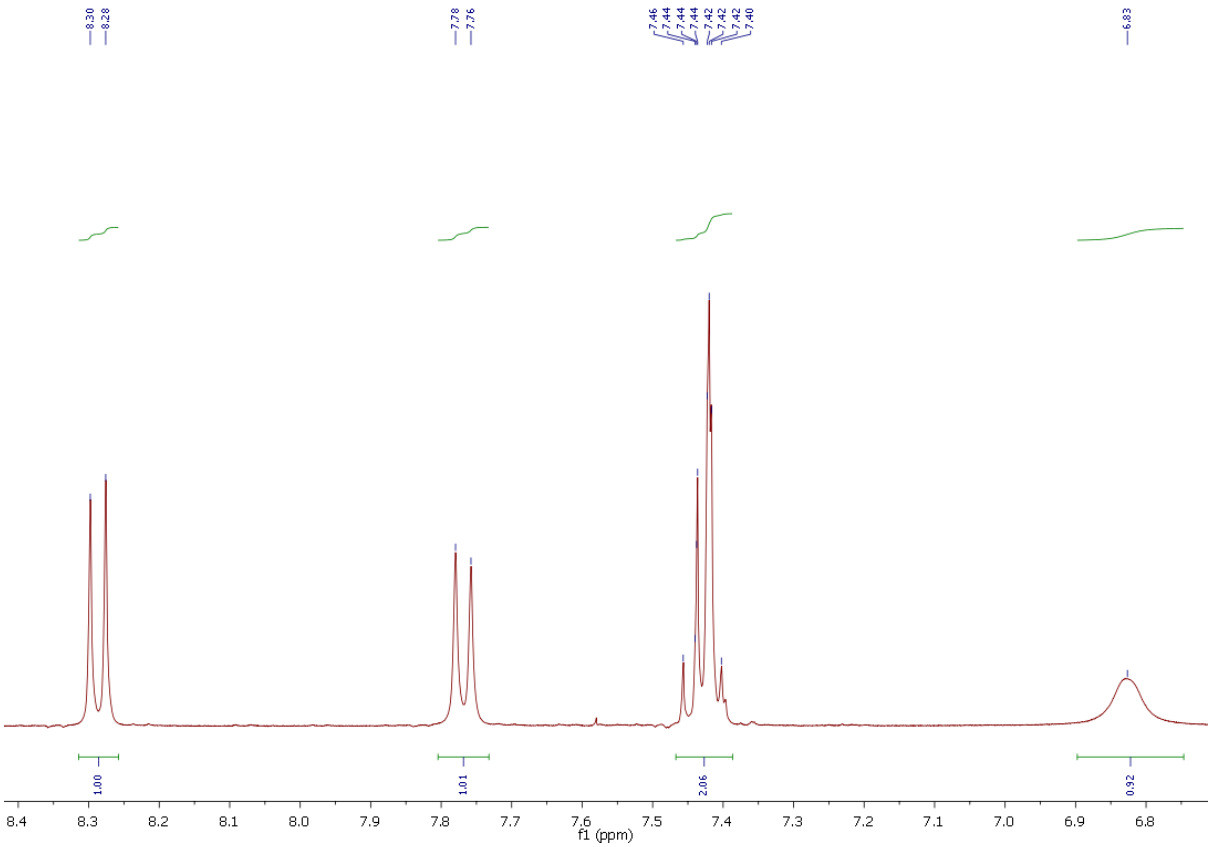

Fig. S85: Magnification of the ^{1}H NMR spectra of the *in situ* prepared complex [Cu(TMG2^{t}Buqu)]PF_6 in CD_3CN.

11.3 TMG2^{c}Hexqu (L4) and corresponding precursors and Cu(I) complex

11.3.1 2-Cyclohexyl-8-nitroquinoline (2-^{c}Hex-8-NO_2-qu)

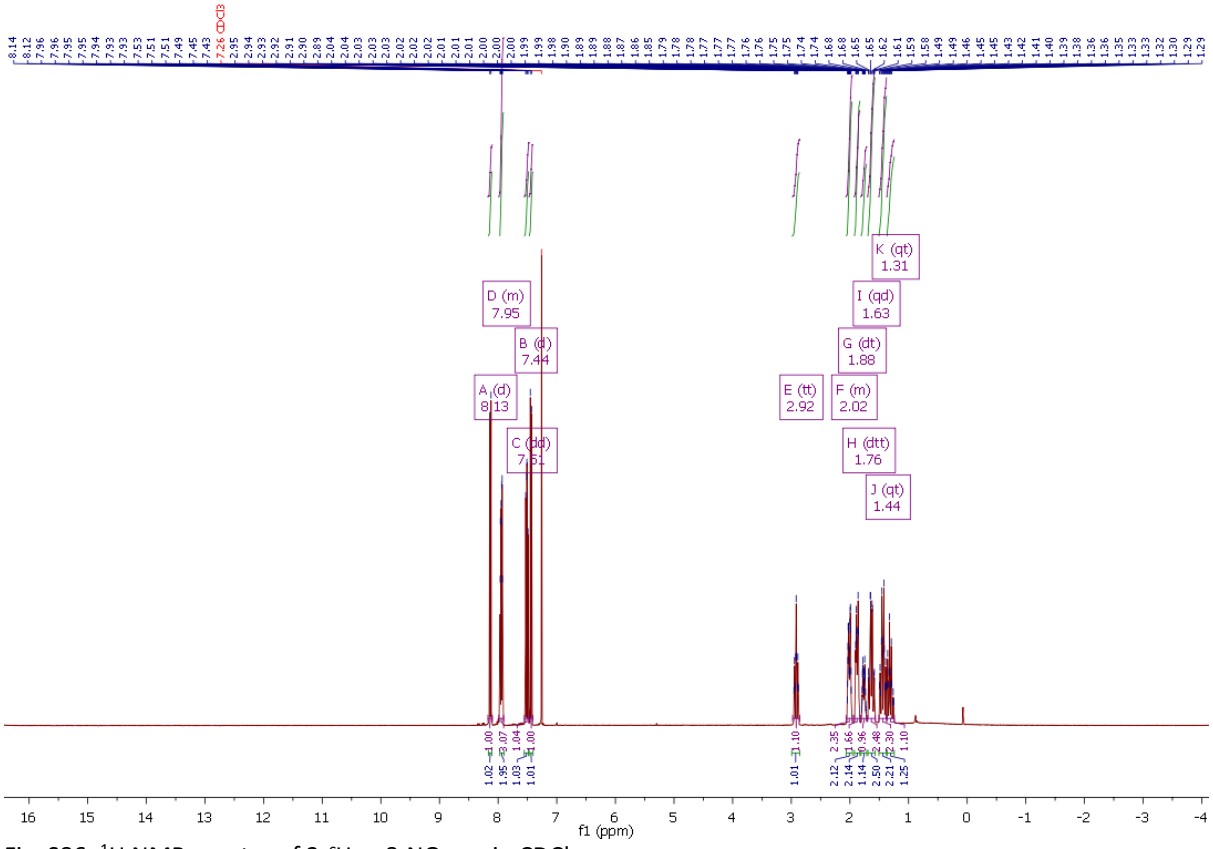

Fig. S86: ^{1}H NMR spectra of 2-^{c}Hex-8-NO_2-qu in $CDCl_3$.

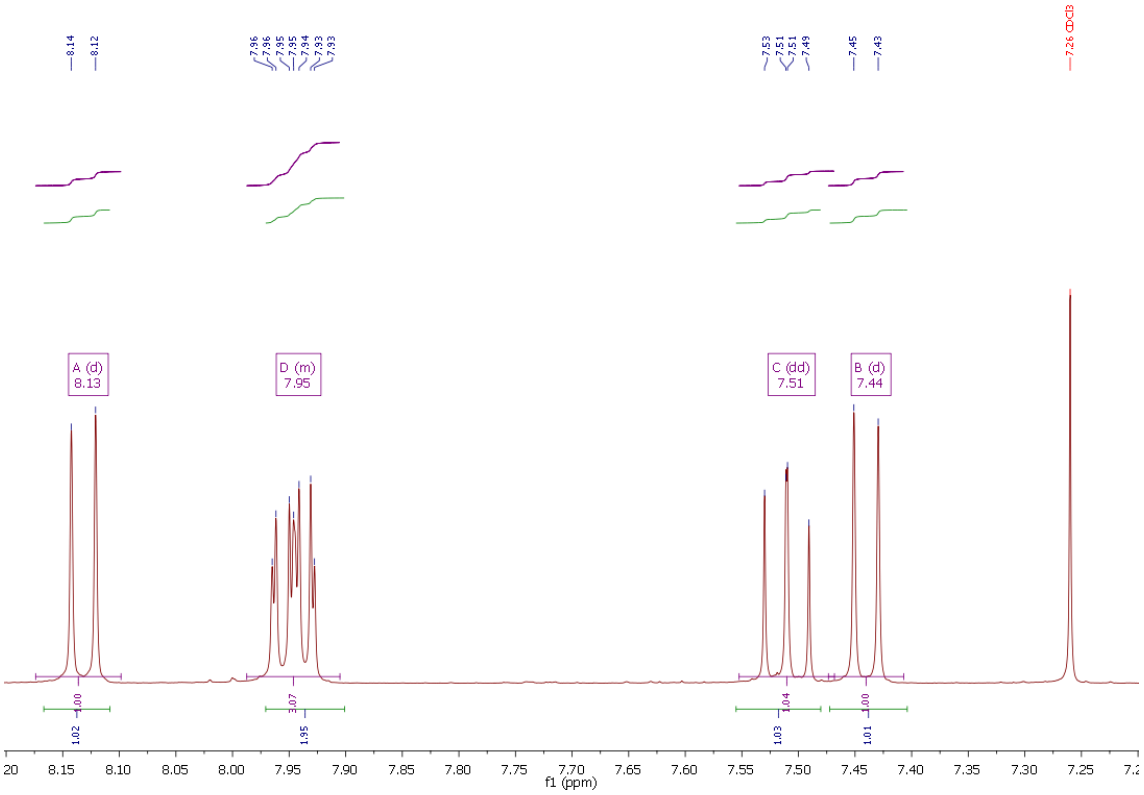

Fig. S87: ^{1}H NMR spectra of 2-^{c}Hex-8-NO_2-qu in $CDCl_3$.

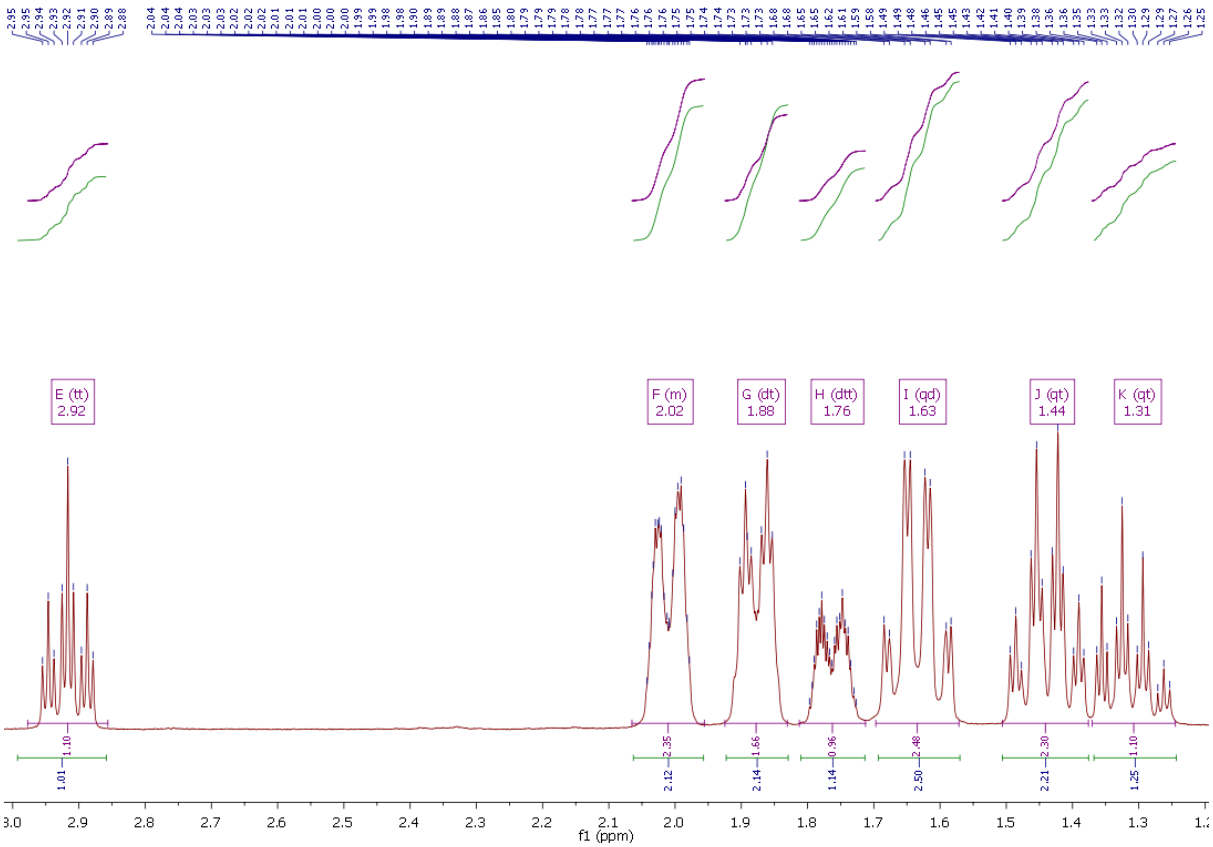

Fig. S88: Magnification of the ^{1}H NMR spectra of 2-^{c}Hex-8-NO_2-qu in $CDCl_3$.

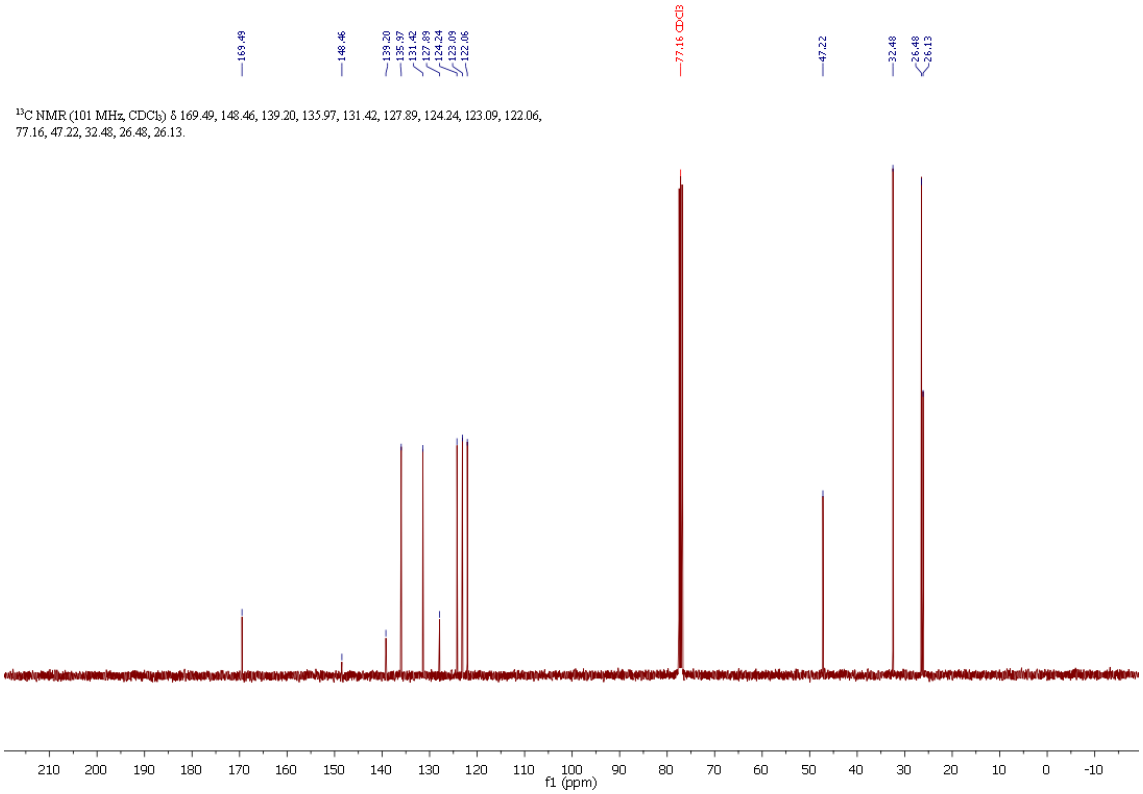

Fig. S89: ^{13}C NMR spectra of 2-^{c}Hex-8-NO_2-qu in $CDCl_3$.

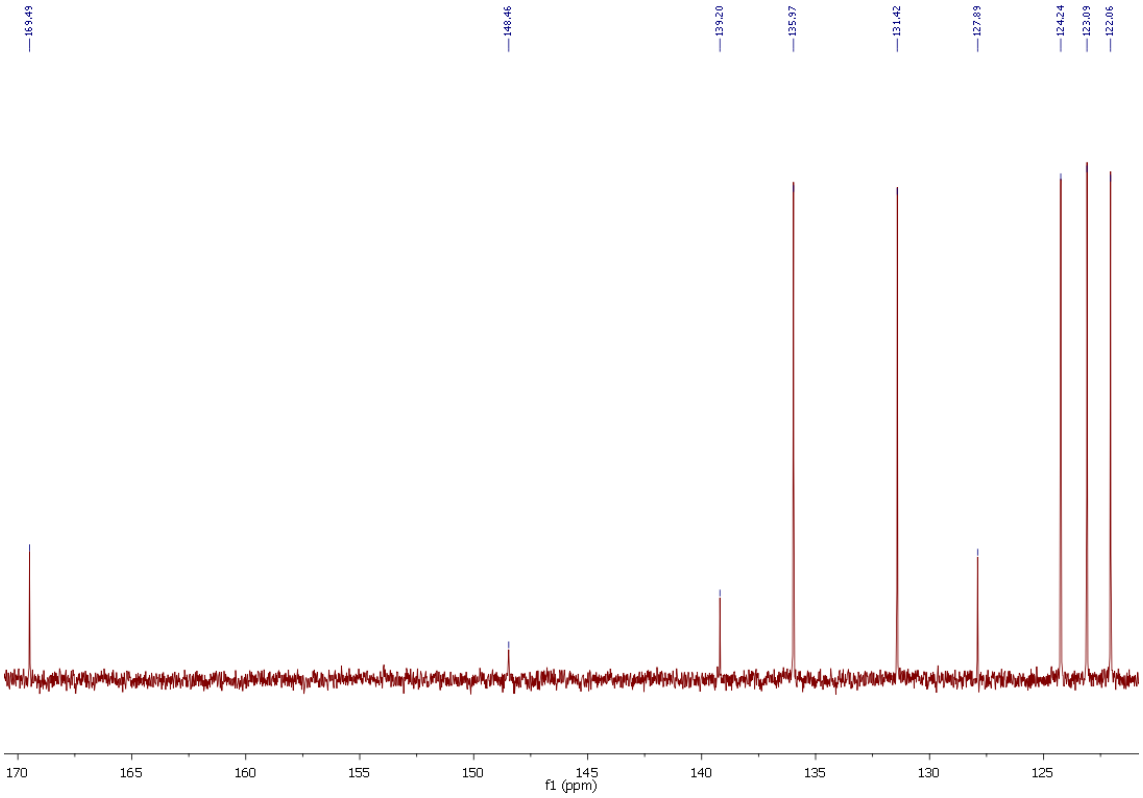

Fig. S90: Magnification of the ^{13}C NMR spectra of 2-^{c}Hex-8-NO_2-qu in $CDCl_3$.

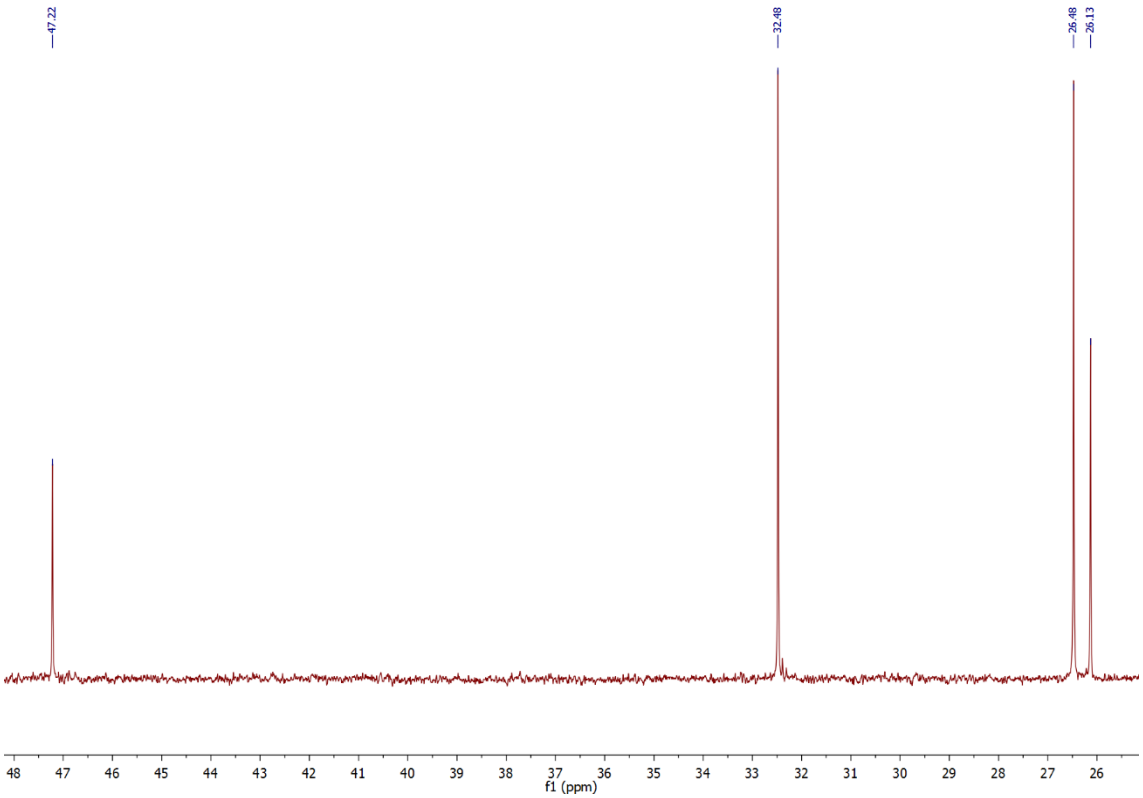

Fig. S91: Magnification of the ^{13}C NMR spectra of 2-^{c}Hex-8-NO_2-qu in $CDCl_3$.

11.3.2 2-Cyclohexyl-8-aminoquinoline (2-^{c}Hex-8-NH_2-qu)

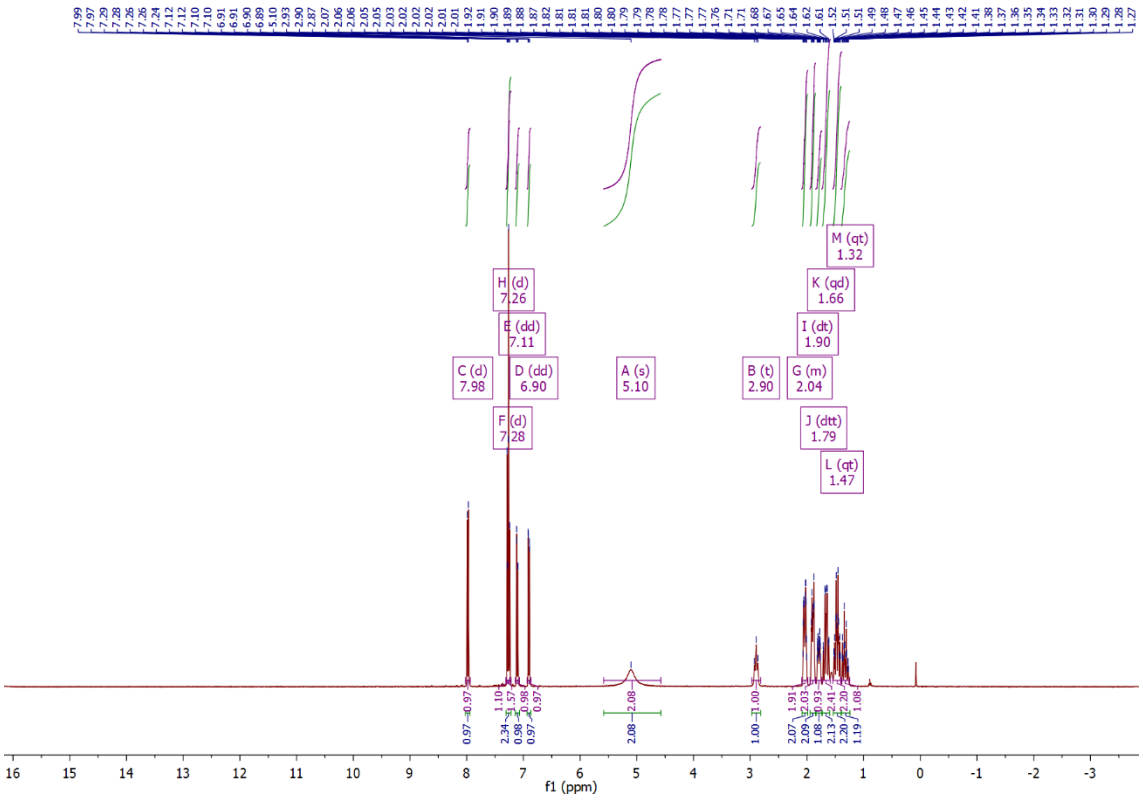

Fig. S92: ^{1}H NMR spectra of 2-^{c}Hex-8-NH_2-qu in $CDCl_3$.

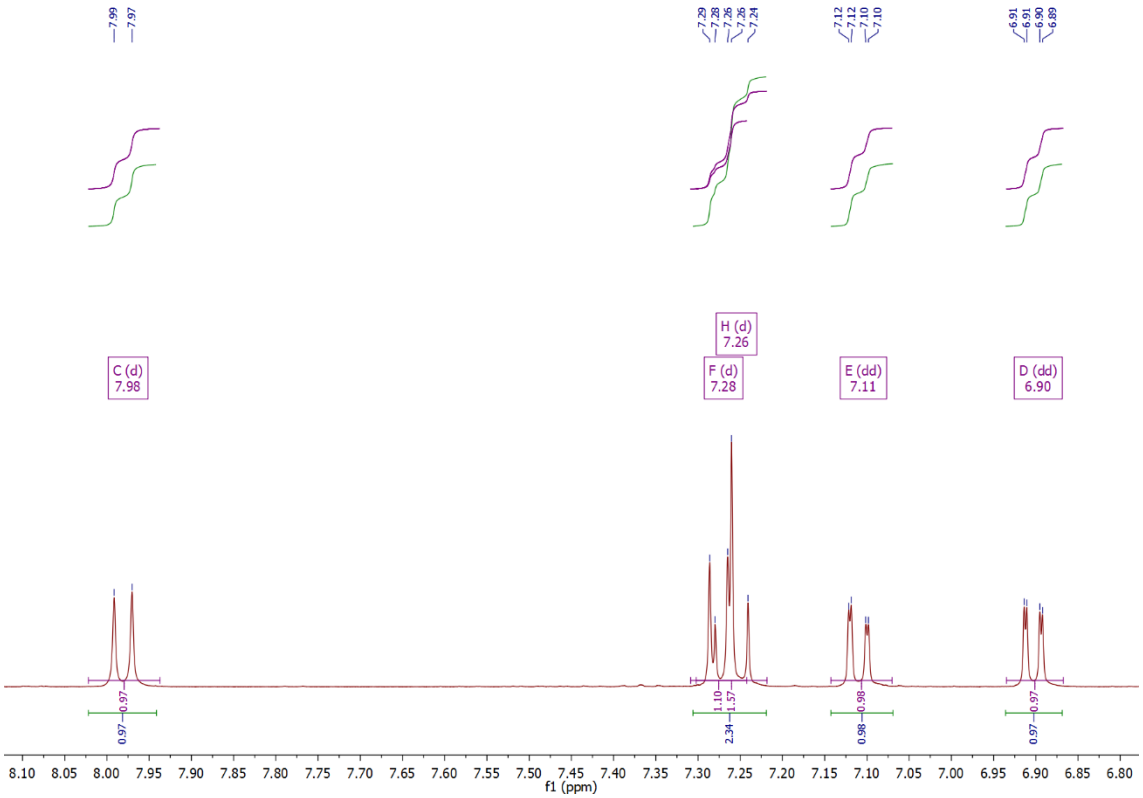

Fig. S93: Magnification of the ^{1}H NMR spectra of 2-^{c}Hex-8-NH$_2$-qu in CDCl$_3$.

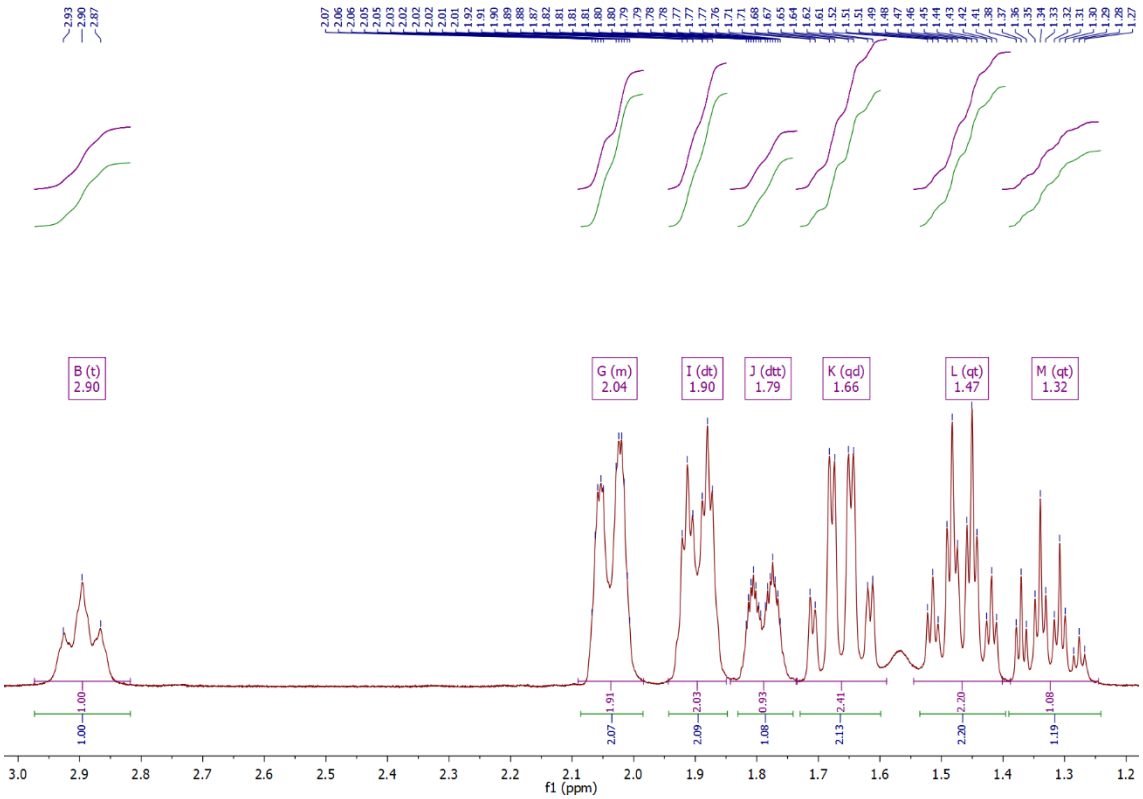

Fig. S94: Magnification of the ^{1}H NMR spectra of 2-^{c}Hex-8-NH$_2$-qu in CDCl$_3$.

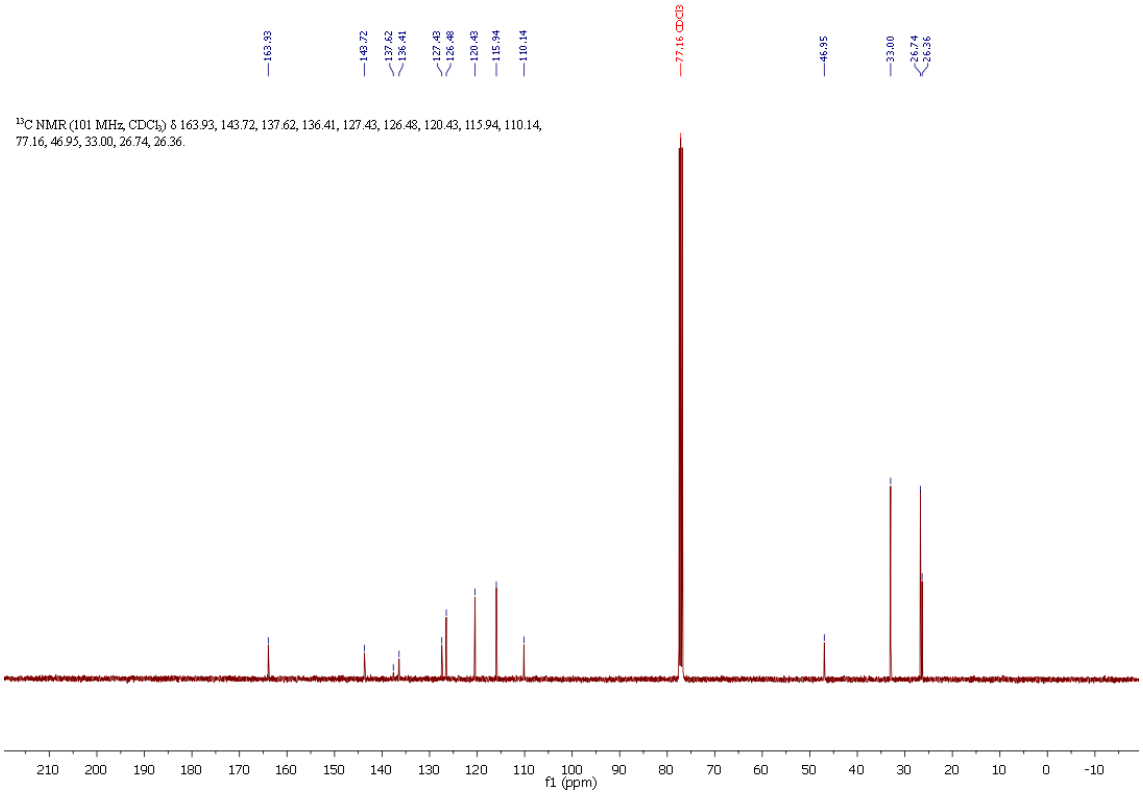

Fig. S95: ^{13}C NMR spectra of 2-^{c}Hex-8-NH$_2$-qu in CDCl$_3$.

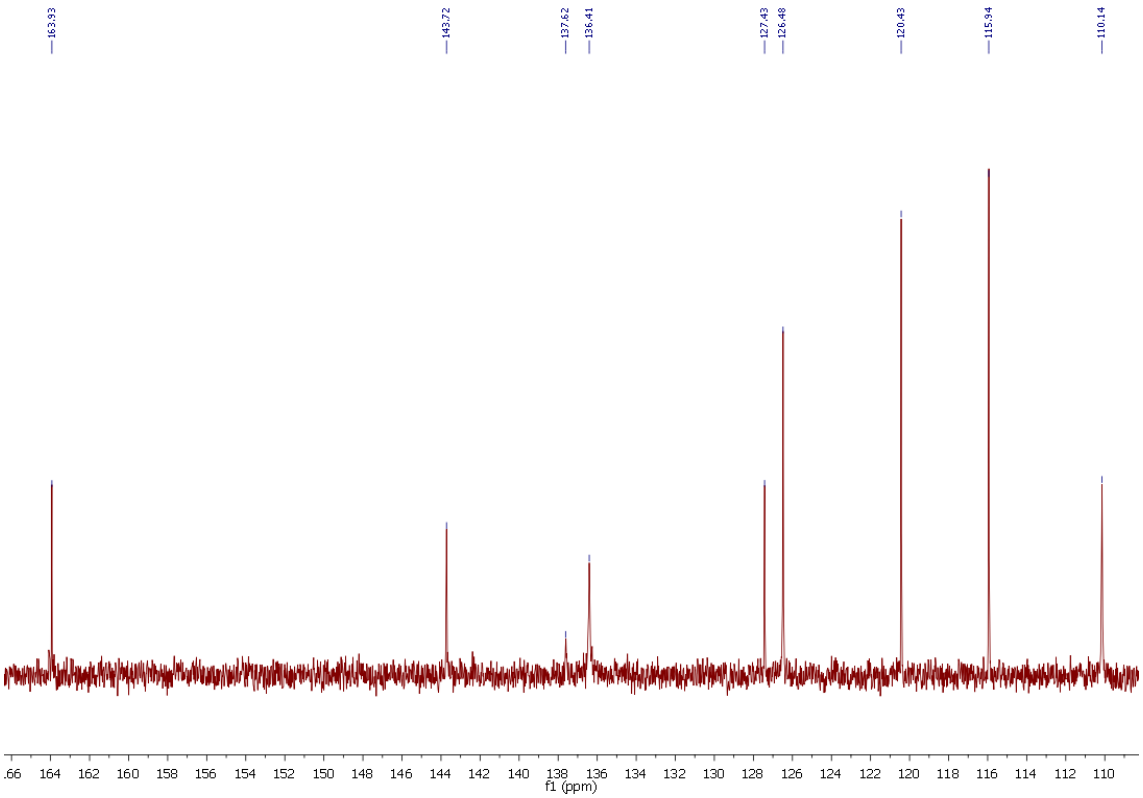

Fig. S96: Magnification of the ^{13}C NMR spectra of 2-^{c}Hex-8-NH$_2$-qu in CDCl$_3$.

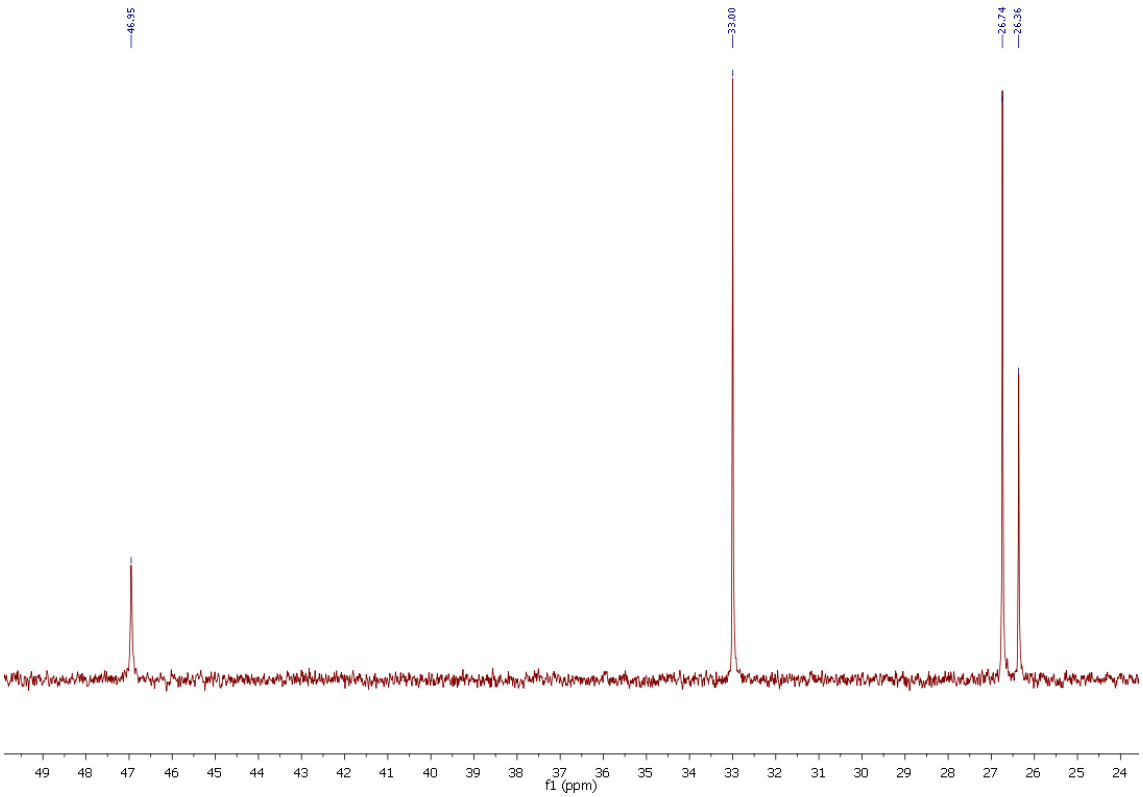

Fig. S97: Magnification of the ^{13}C NMR spectra of 2-^{c}Hex-8-NH_2-qu in $CDCl_3$.

11.3.3 TMG2^{c}Hexqu (L4)

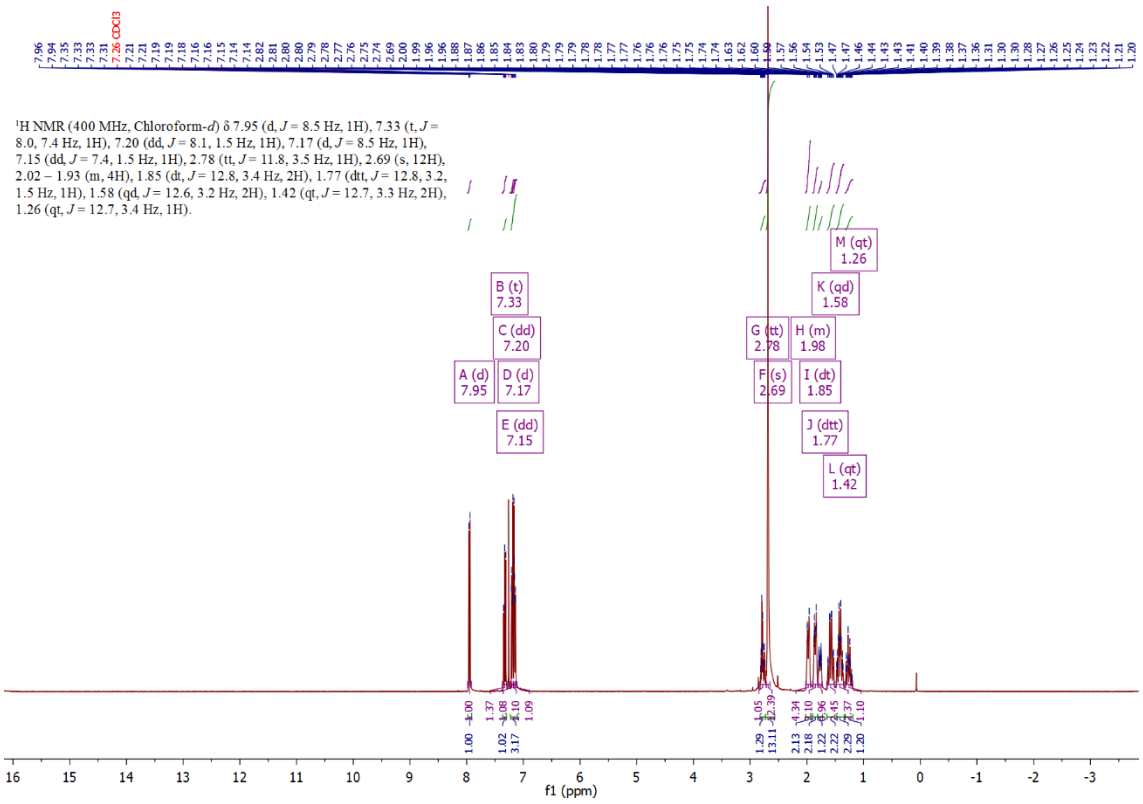

Fig. S98: ^1H NMR spectra of TMG2^{c}Hexqu in $CDCl_3$.

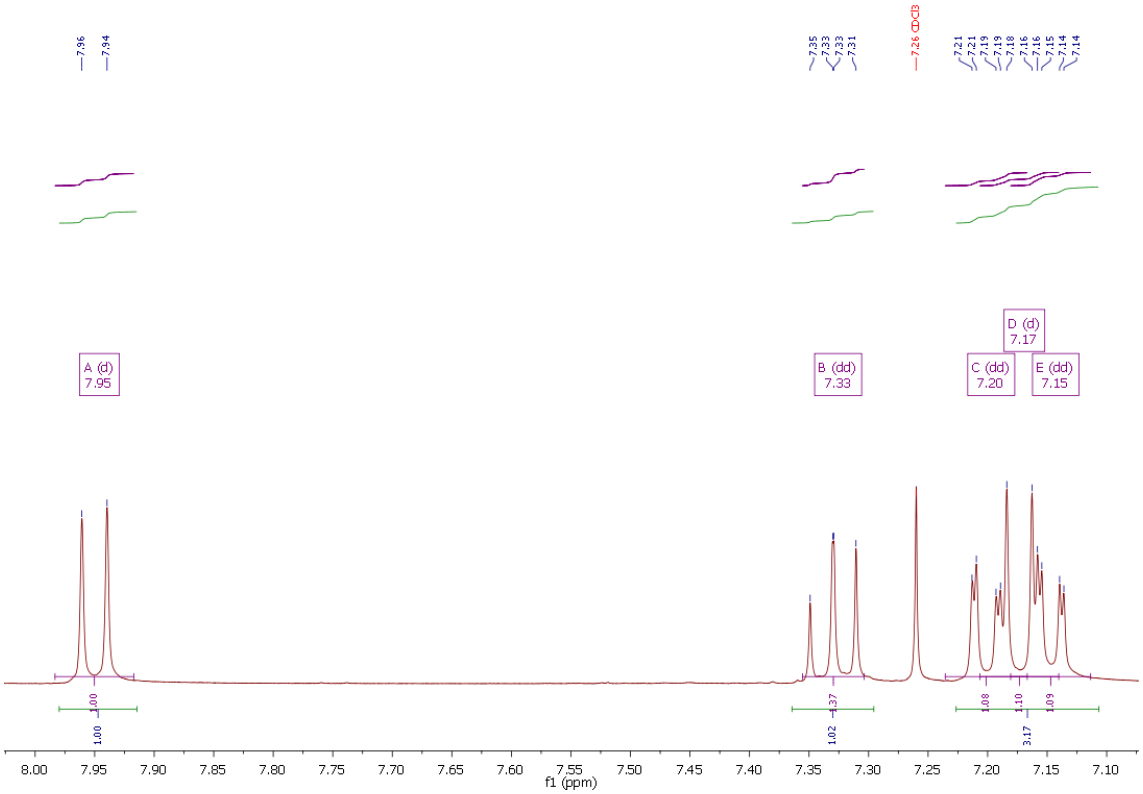

Fig. S99: Magnification of the ^{1}H NMR spectra of TMG2^{c}Hexqu in $CDCl_3$.

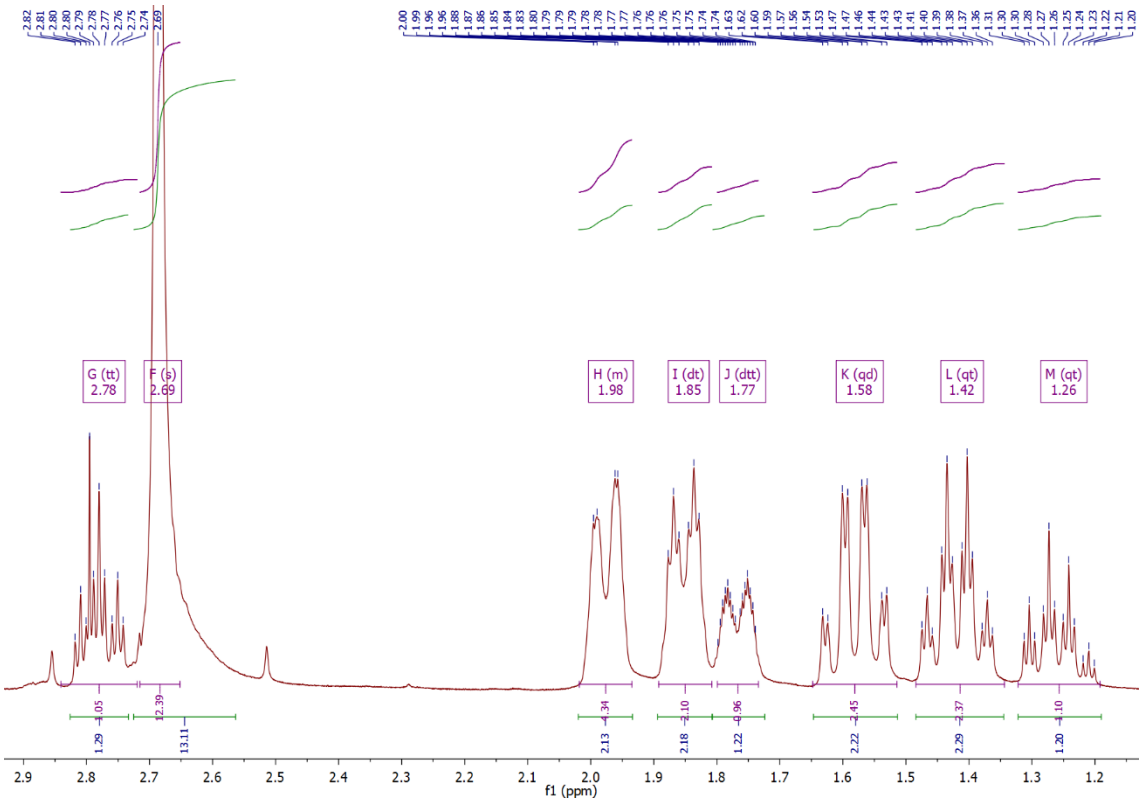

Fig. S100: Magnification of the ^{1}H NMR spectra of TMG2^{c}Hexqu in $CDCl_3$.

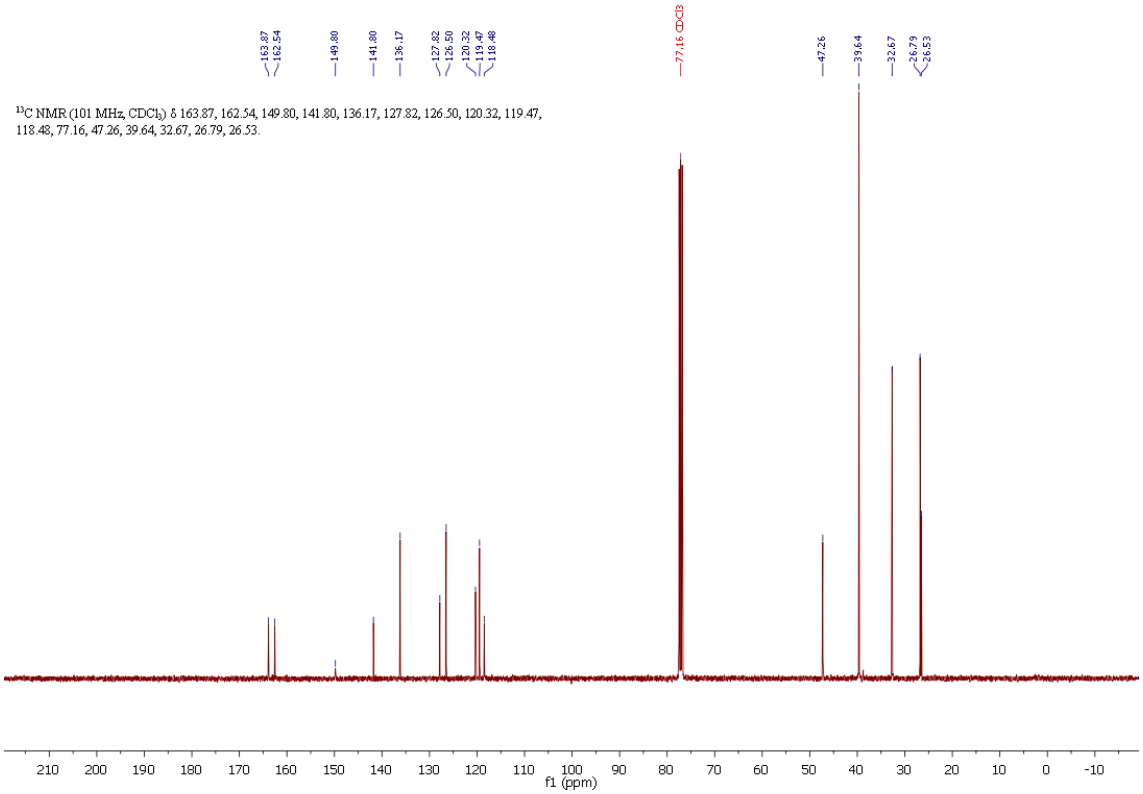

Fig. S101: ^{13}C NMR spectra of TMG2^{c}Hexqu in $CDCl_3$.

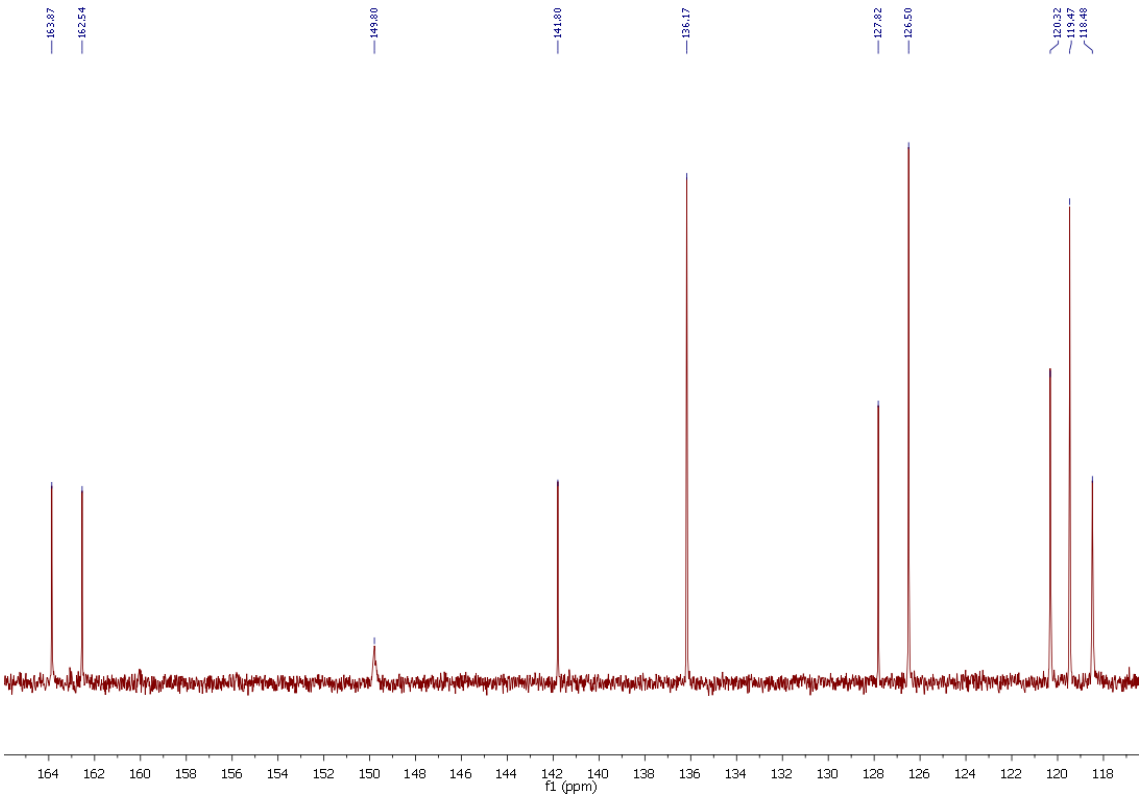

Fig. S102: Magnification of the ^{13}C NMR spectra of TMG2^{c}Hexqu in $CDCl_3$.

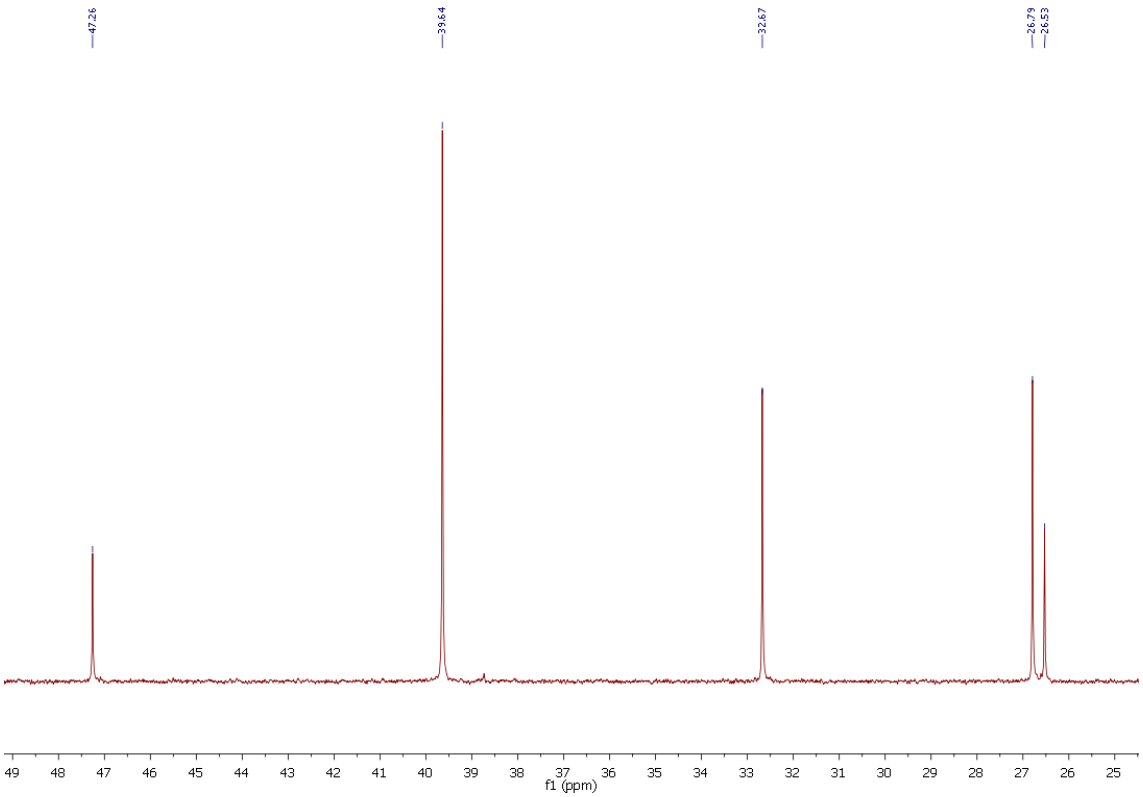

Fig. S103: Magnification of the ^{13}C NMR spectra of TMG2^{c}Hexqu in $CDCl_3$.

11.3.4 [Cu(TMG2^{c}Hexqu)$_2$]PF_6 (C5–PF_6)

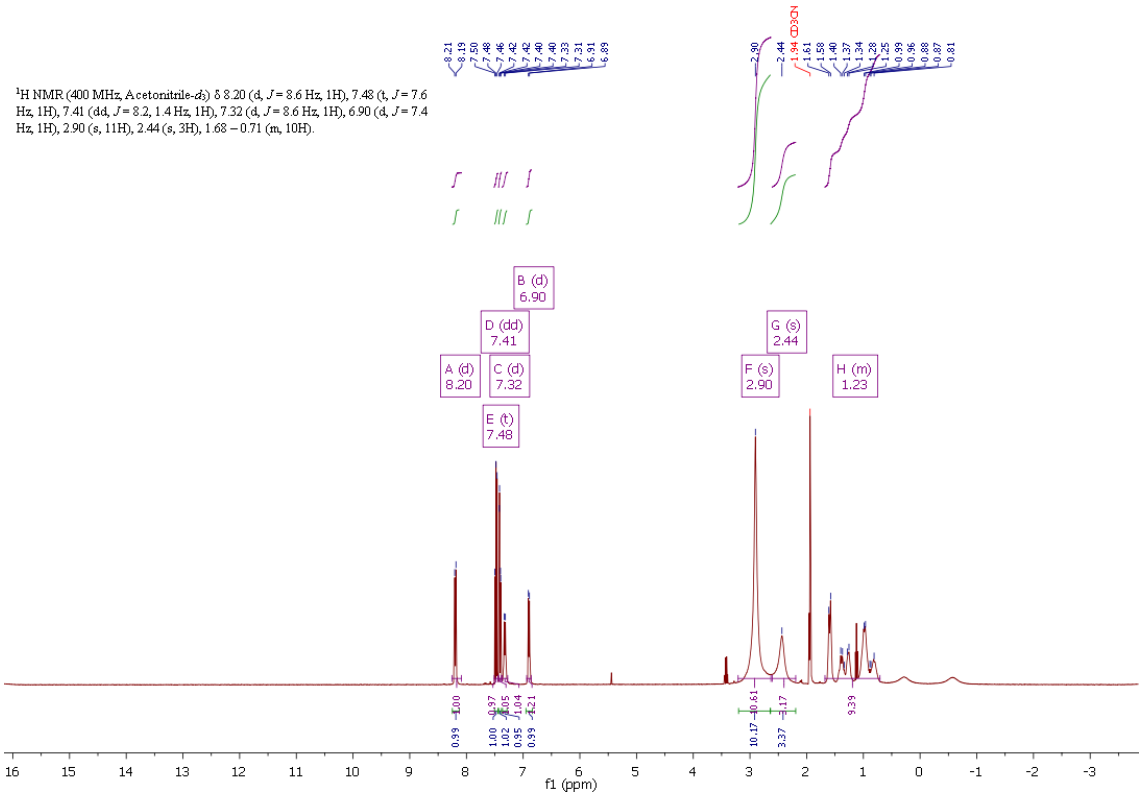

Fig. S104: ^{1}H NMR spectra of [Cu(TMG2^{c}Hexqu)$_2$]PF_6 (**C5–PF_6**) in MeCN-d3.

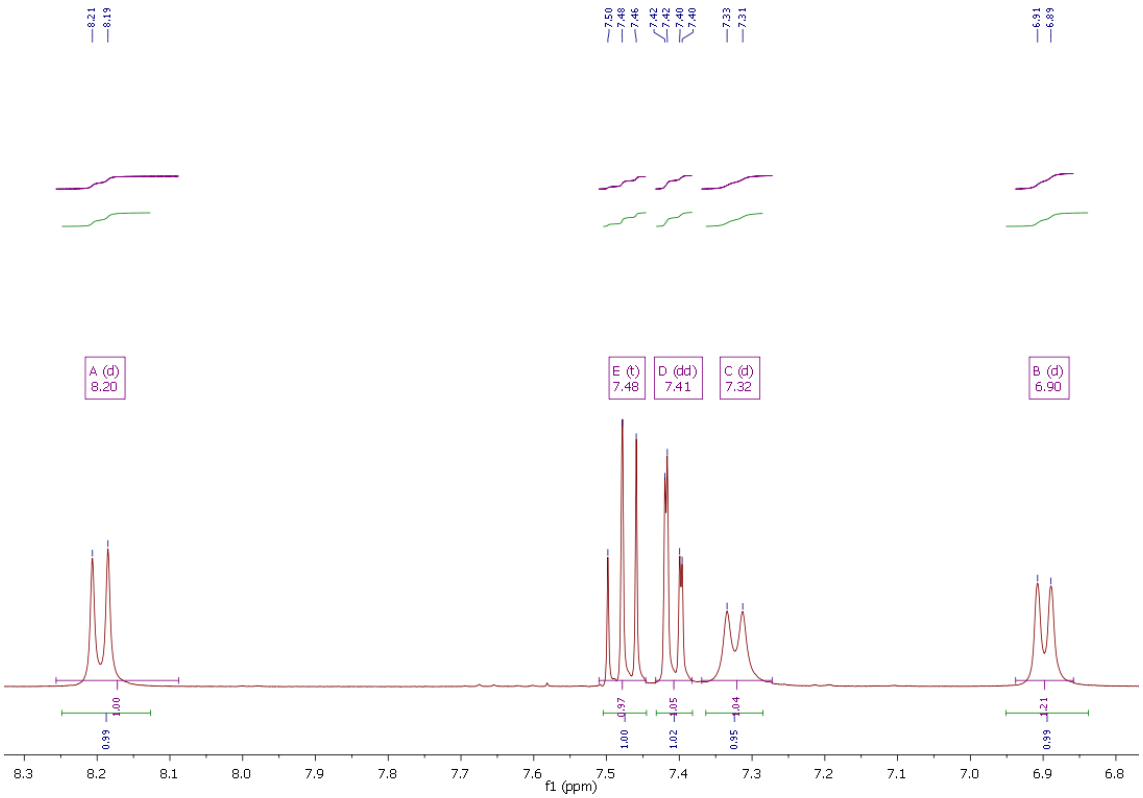

Fig. S105: Magnification of the ^{1}H NMR spectra of [Cu(TMG2^{c}Hexqu)$_2$]PF$_6$ (**C5–PF$_6$**) in MeCN-d3.

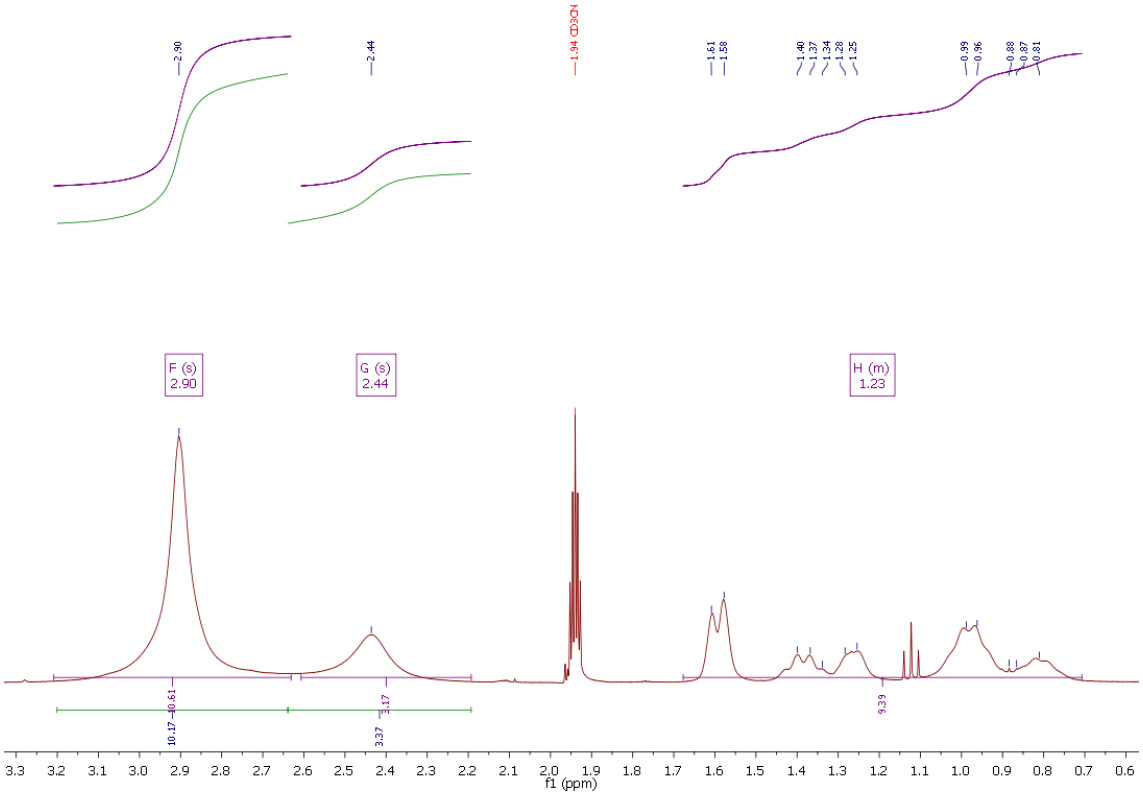

Fig. S106: Magnification of the ^{1}H NMR spectra of [Cu(TMG2^{c}Hexqu)$_2$]PF$_6$ (**C5–PF$_6$**) in MeCN-d3.

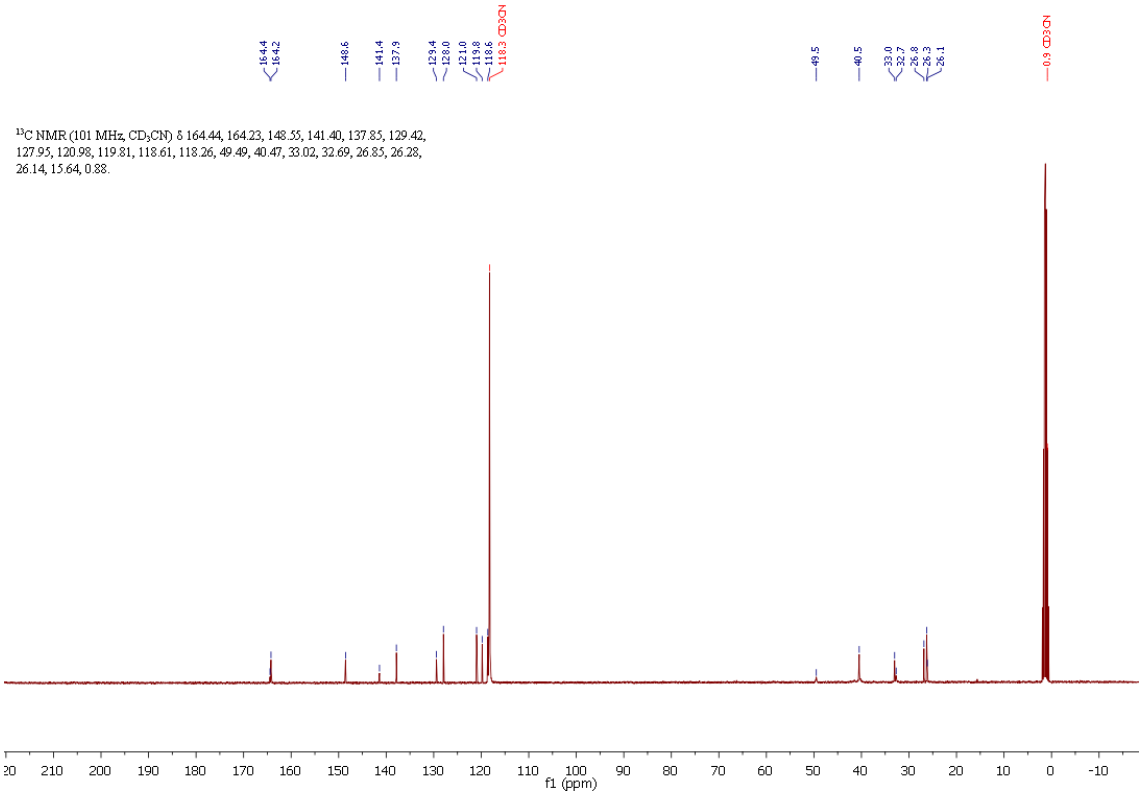

Fig. S107: ^{13}C NMR spectra of [Cu(TMG2^{c}Hexqu)$_2$]PF_6 (**C5–PF_6**) in MeCN-d3.

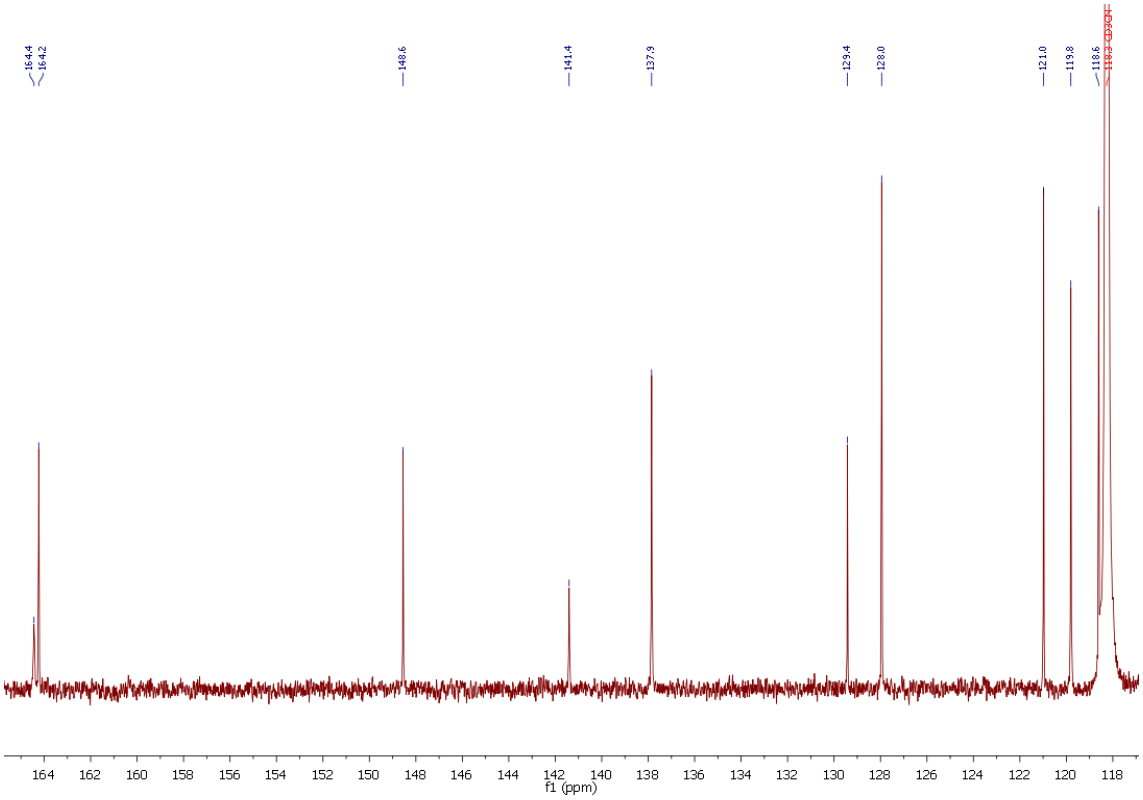

Fig. S108: Magnification of the ^{13}C NMR spectra of [Cu(TMG2^{c}Hexqu)$_2$]PF_6 (**C5–PF_6**) in MeCN-d3.

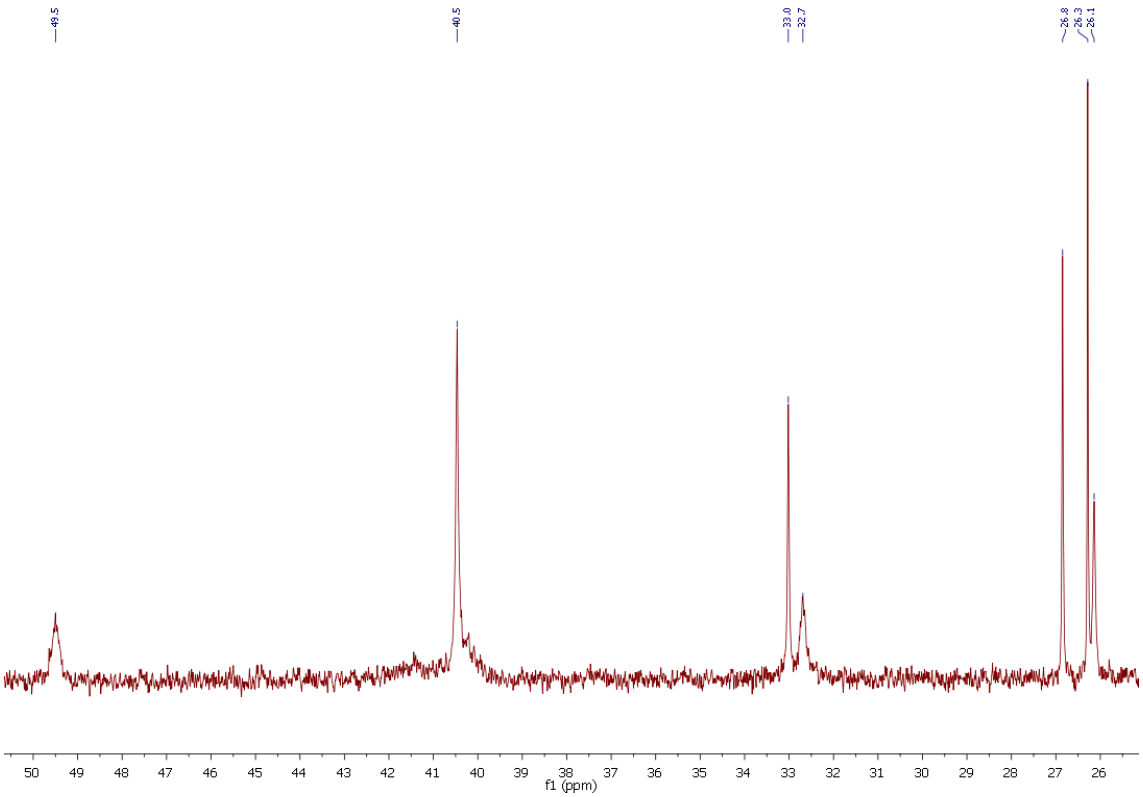

Fig. S109: Magnification of the ^{13}C NMR spectra of $[Cu(TMG2^{c}Hexqu)_2]PF_6$ (**C5–PF_6**) in MeCN-d3.

11.4 TMG2Meequ (L5) and corresponding precursors and Cu(I) complex

11.4.1 2-Tribromomethyl-8-nitroquinoline (2-CBr_3-8-NO_2-qu)

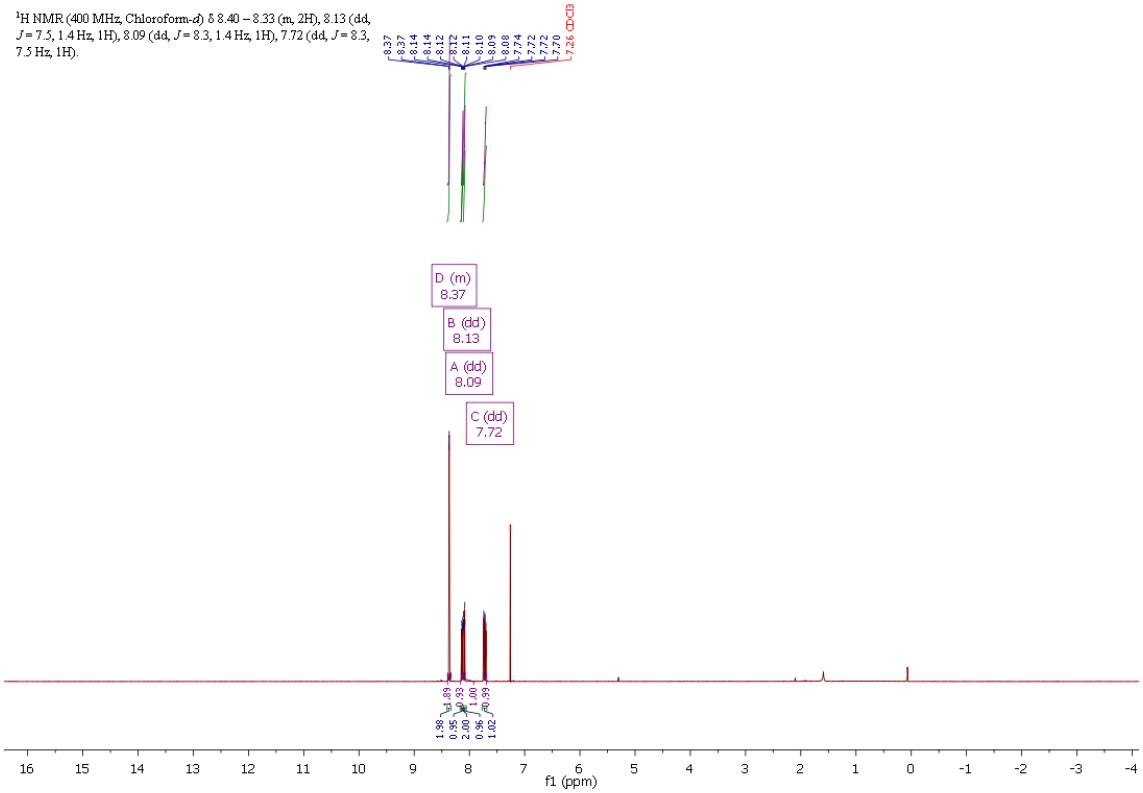

Fig. S110: ^{1}H NMR spectra of 2-CBr_3-8-NO_2-qu in $CDCl_3$.

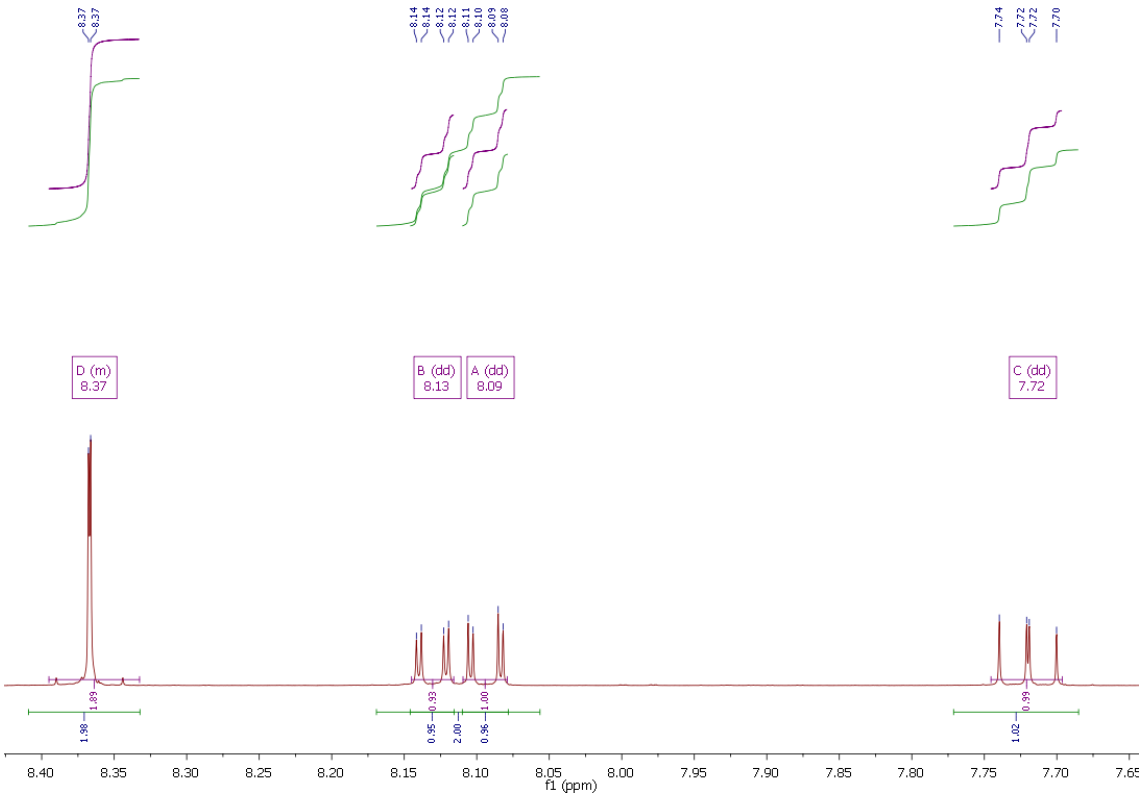

Fig. S111: Magnification of the ^{1}H NMR spectra of 2-CBr_3-8-NO_2-qu in $CDCl_3$.

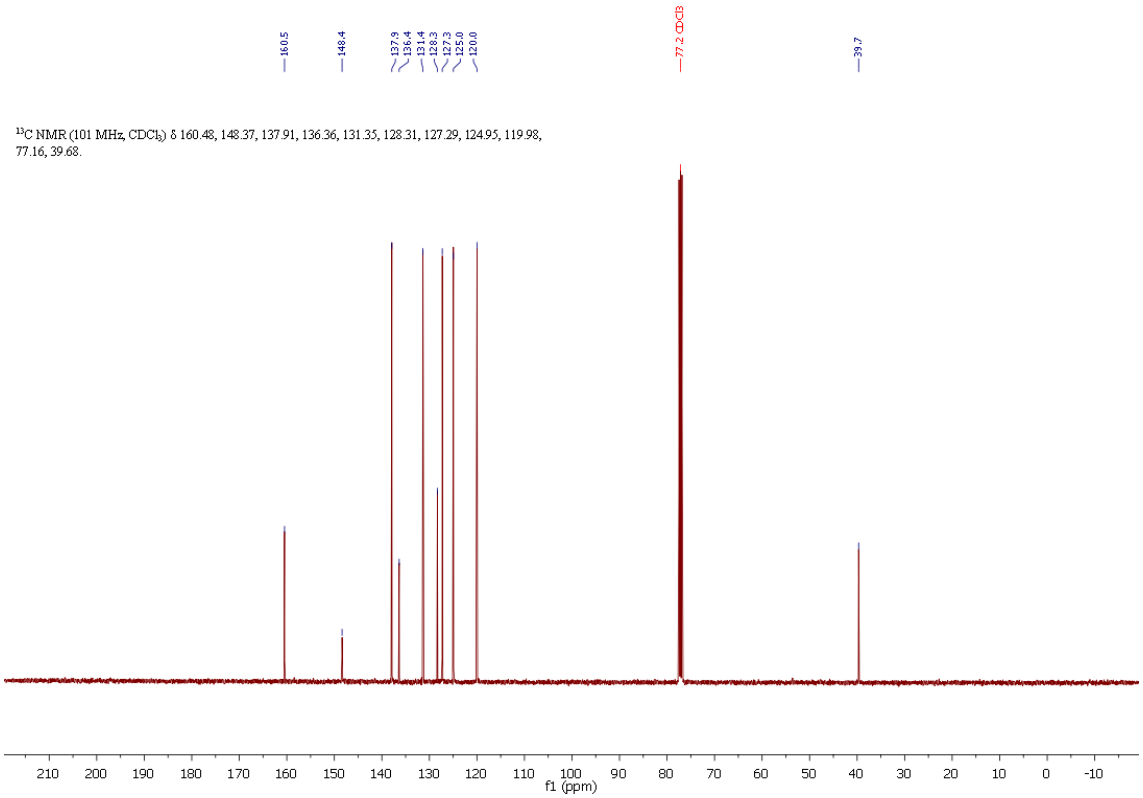

Fig. S112: ^{13}C NMR spectra of 2-CBr_3-8-NO_2-qu in $CDCl_3$.

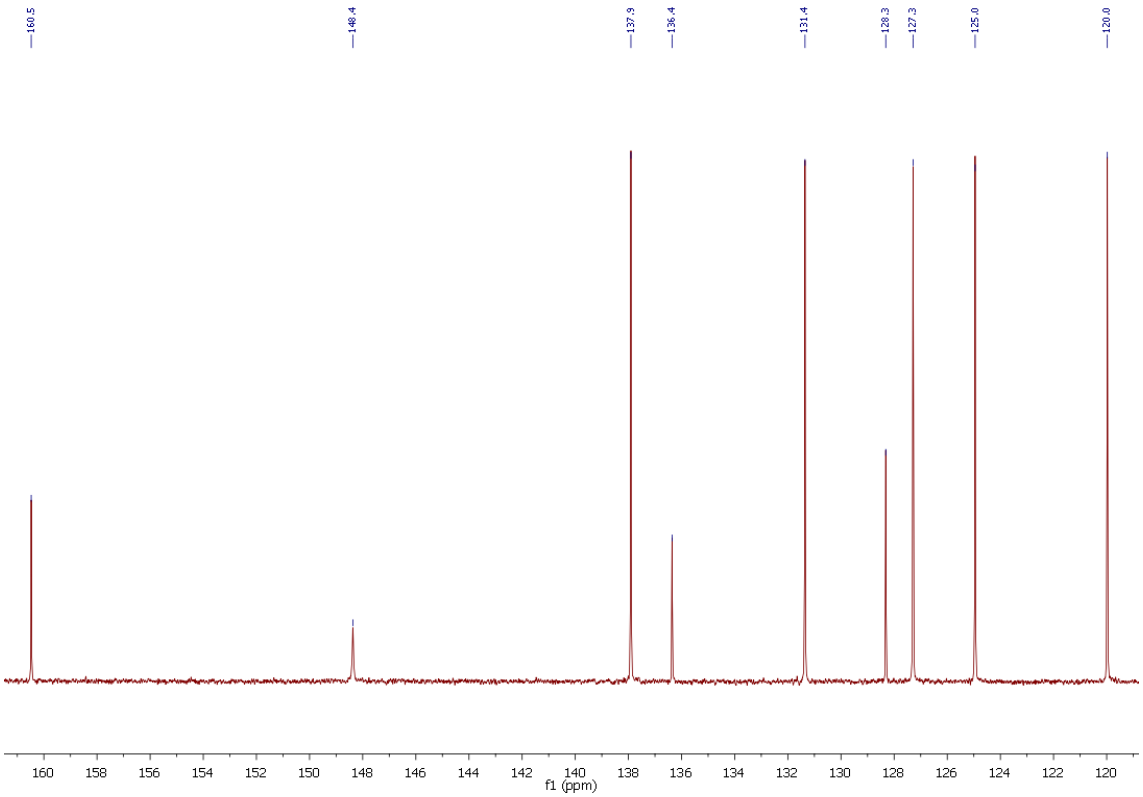

Fig. S113: Magnification of the ^{13}C NMR spectra of 2-CBr_3-8-NO_2-qu in $CDCl_3$.

11.4.2 8-Nitroquinoline-2-carboxylic acid (2-COOH-8-NO_2-qu)

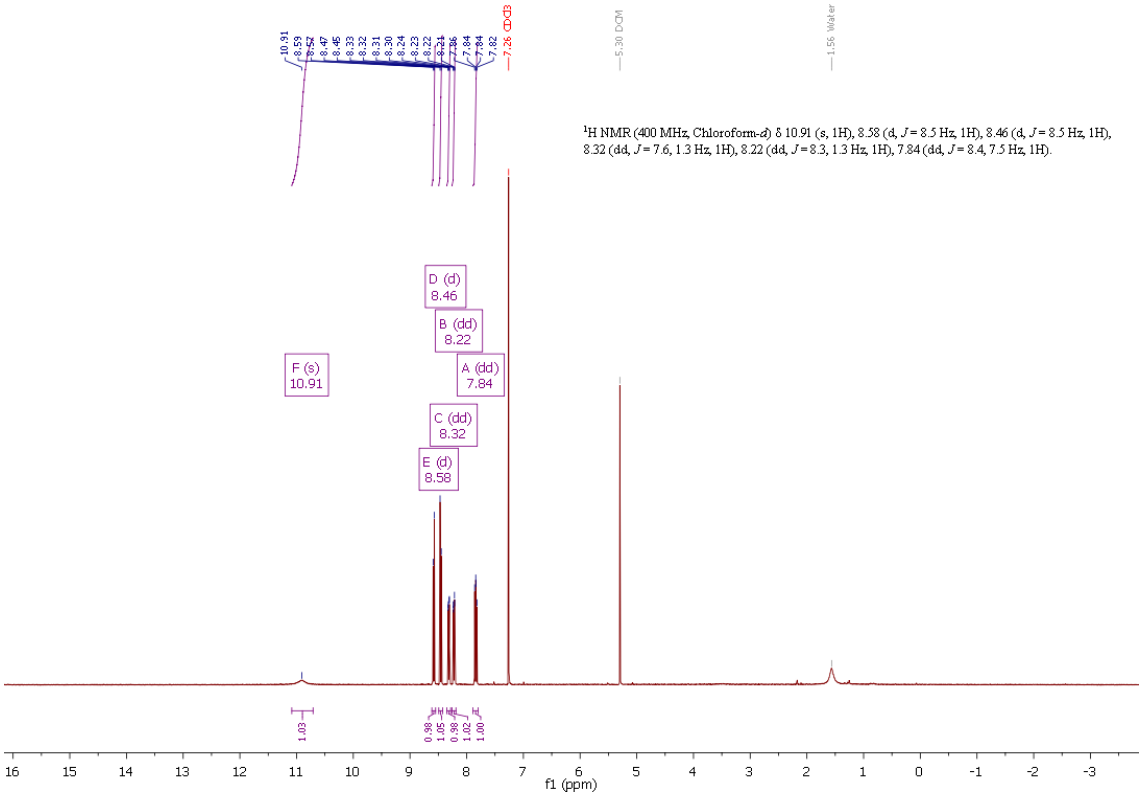

Fig. S114: ^1H NMR spectra of 2-COOH-8-NO_2-qu in $CDCl_3$.

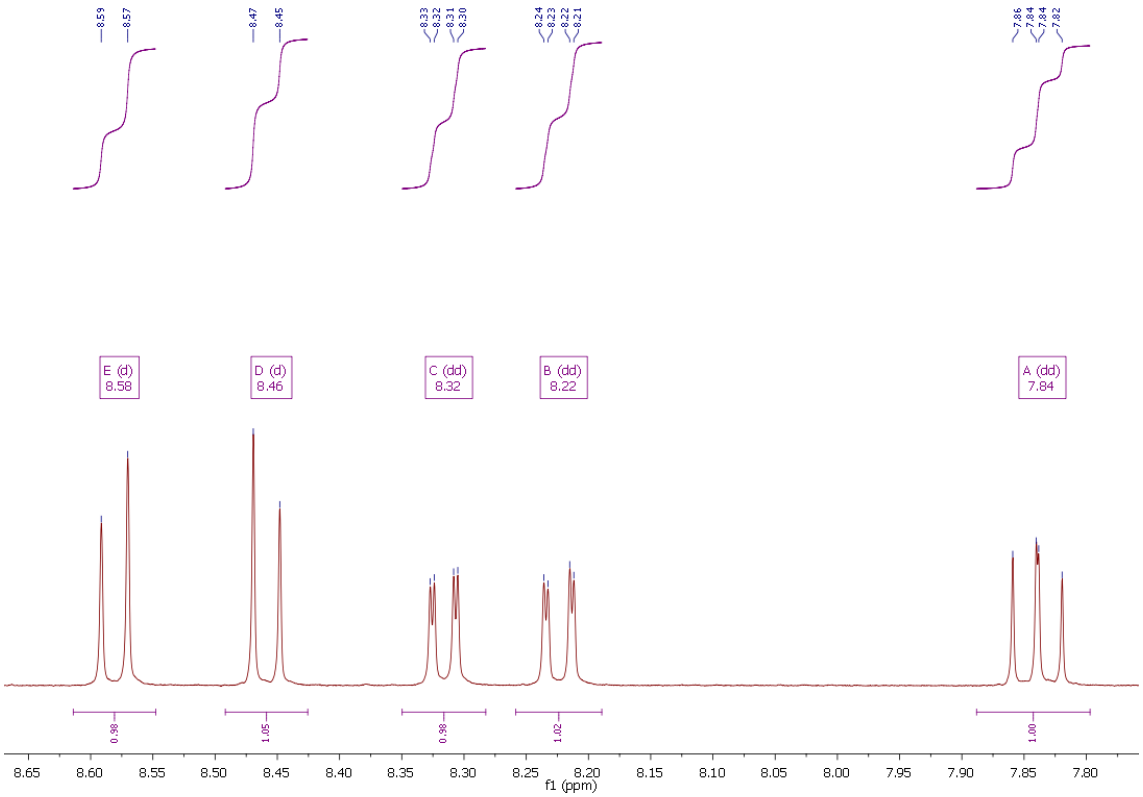

Fig. S115: Magnification of the ^{1}H NMR spectra of 2-COOH-8-NO_2-qu in $CDCl_3$.

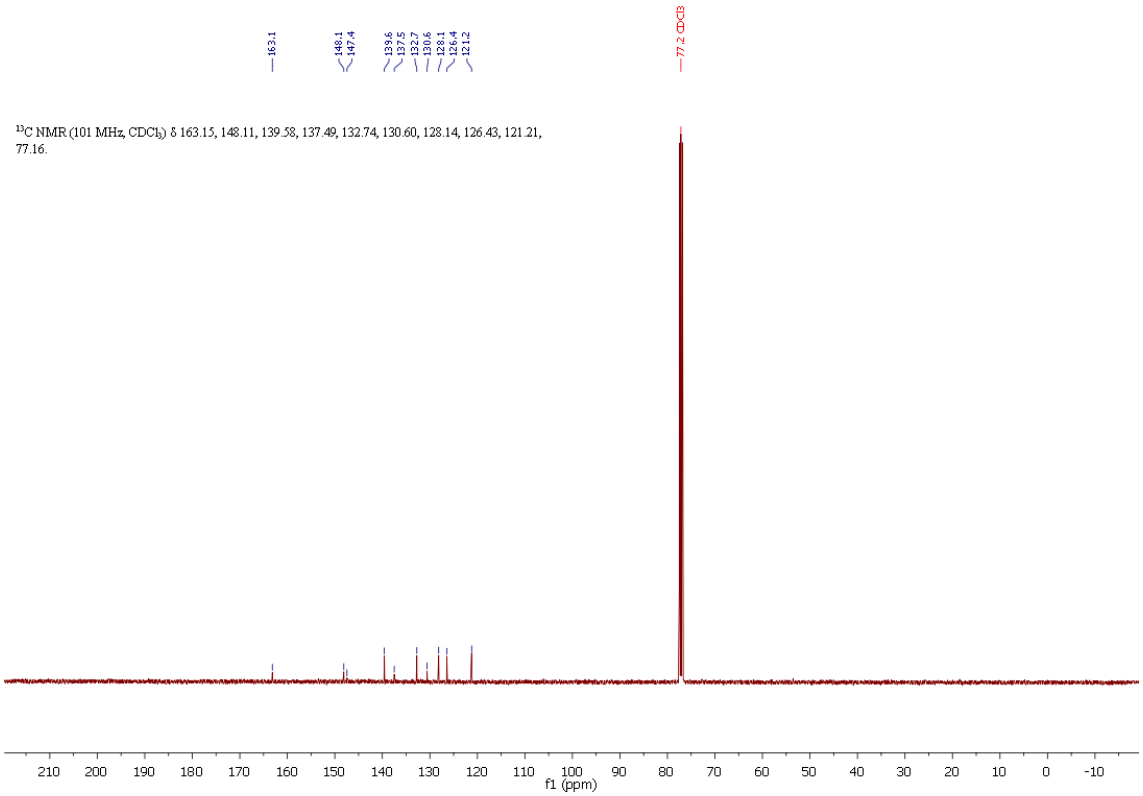

Fig. S116: ^{13}C NMR spectra of 2-COOH-8-NO_2-qu in $CDCl_3$.

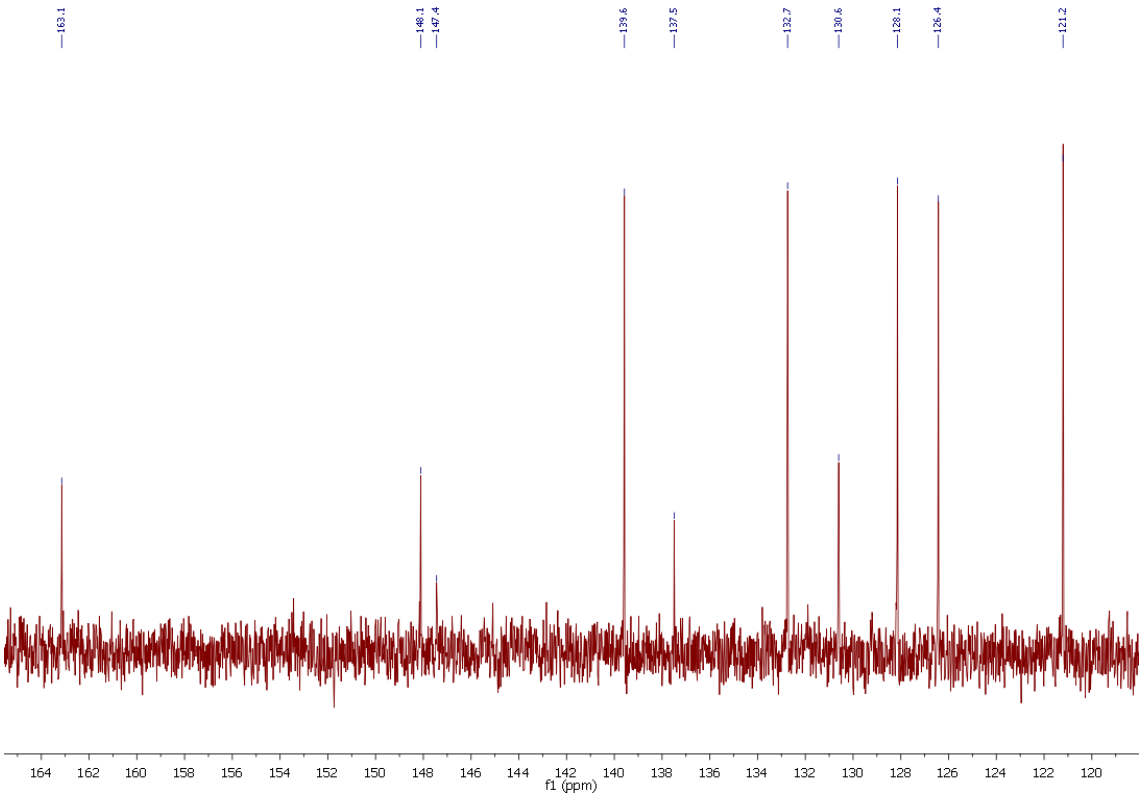

Fig. S117: Magnification of the ^{13}C NMR spectra of 2-COOH-8-NO_2-qu in $CDCl_3$.

11.4.3 Methyl 8-nitroquinoline-2-carboxylate (2-Mee-8-NO_2-qu)

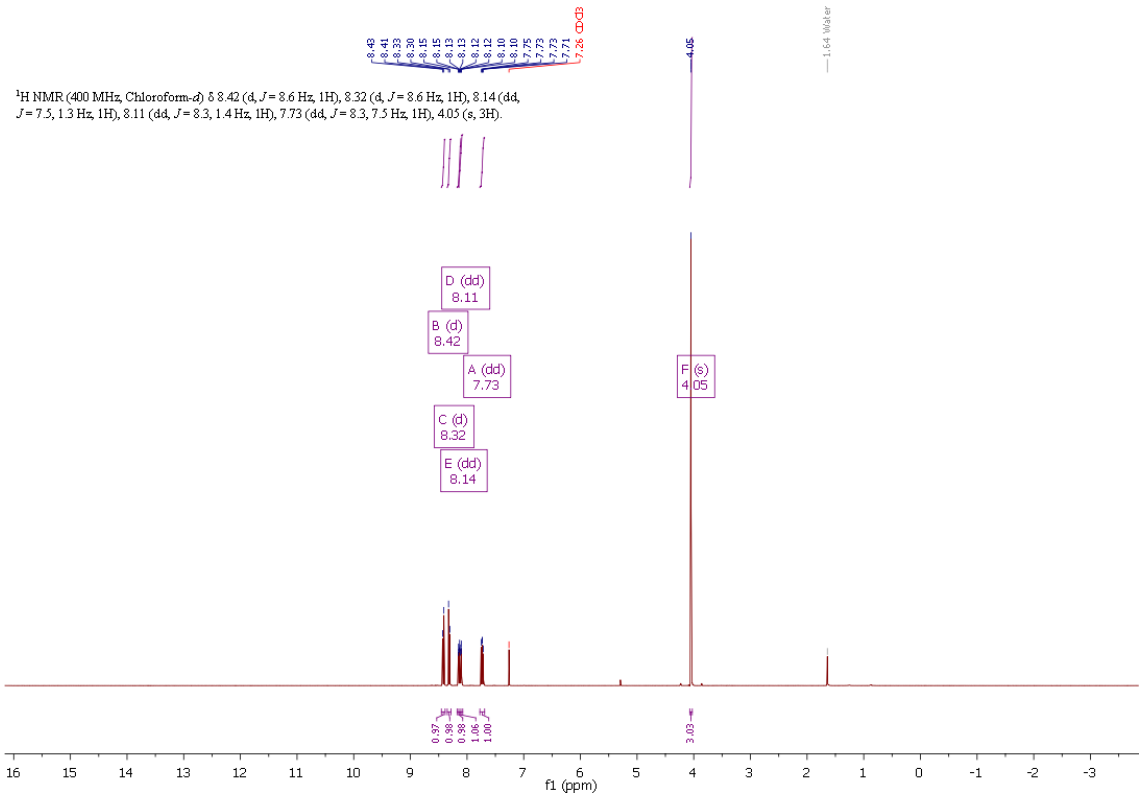

Fig. S118: ^{1}H NMR spectra of 2-Mee-8-NO_2-qu in $CDCl_3$.

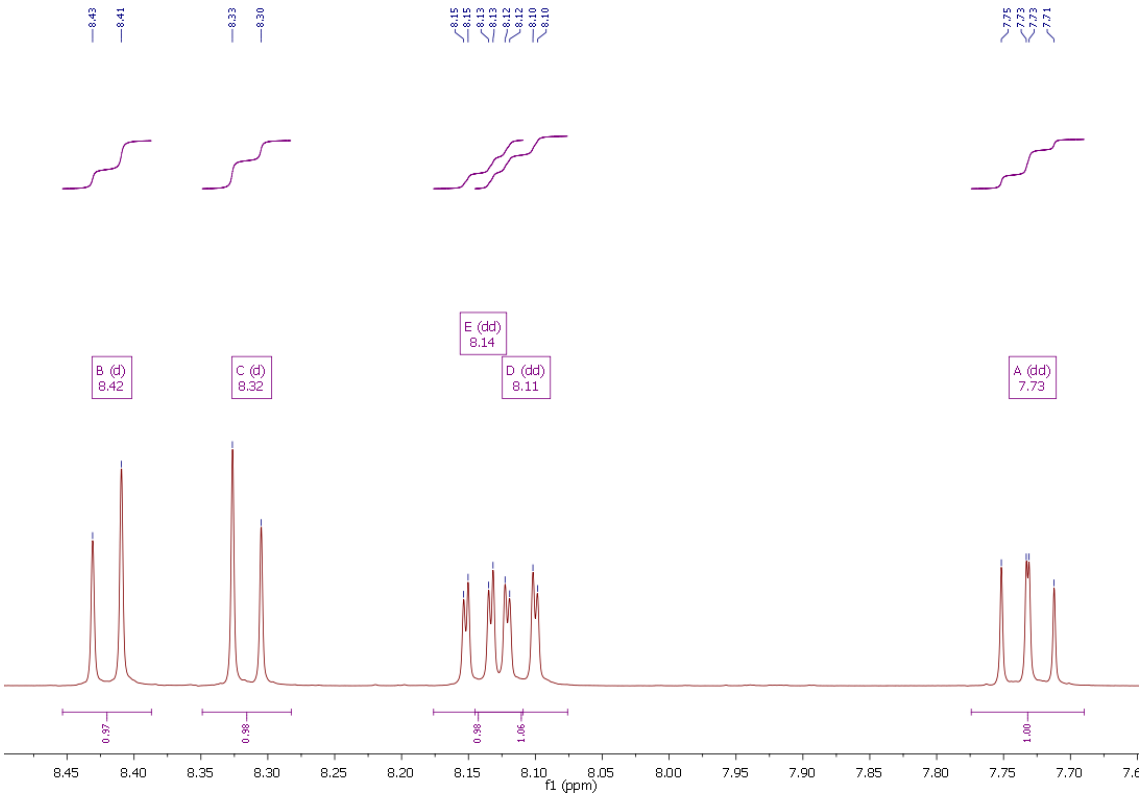

Fig. S119: Magnification of the ^{1}H NMR spectra of 2-Mee-8-NO_2-qu in $CDCl_3$.

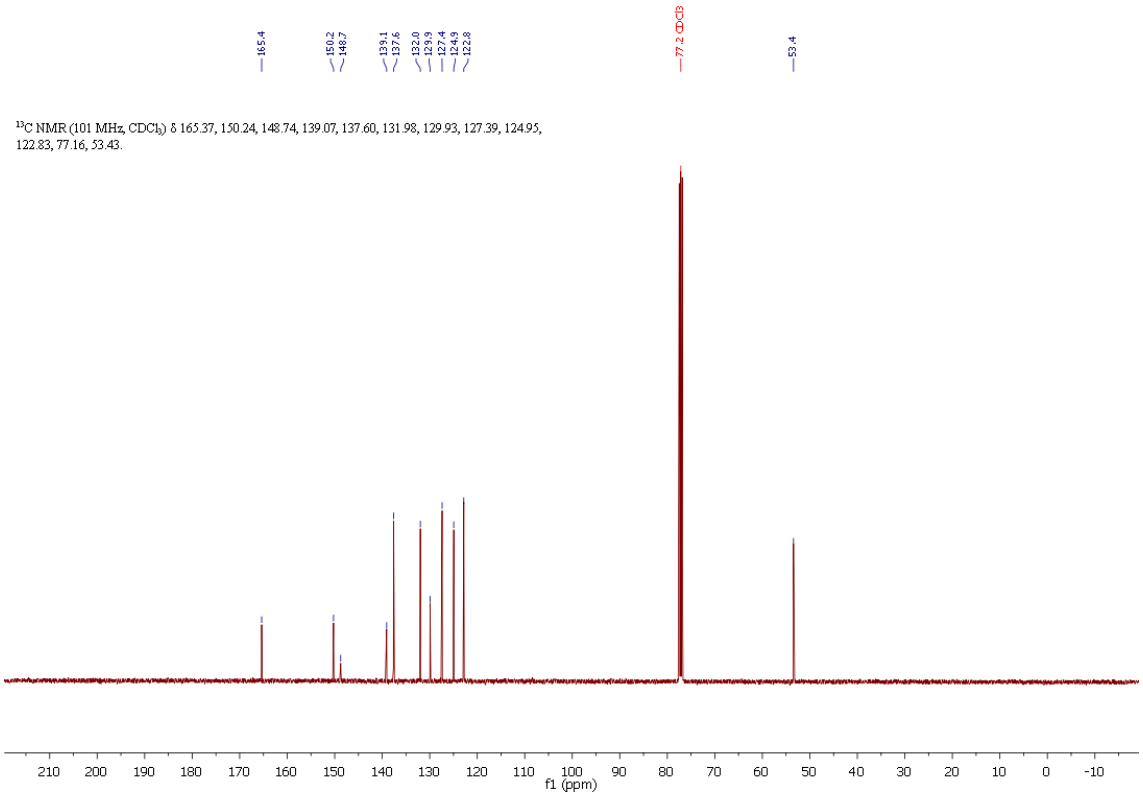

Fig. S120: ^{13}C NMR spectra of 2-Mee-8-NO_2-qu in $CDCl_3$.

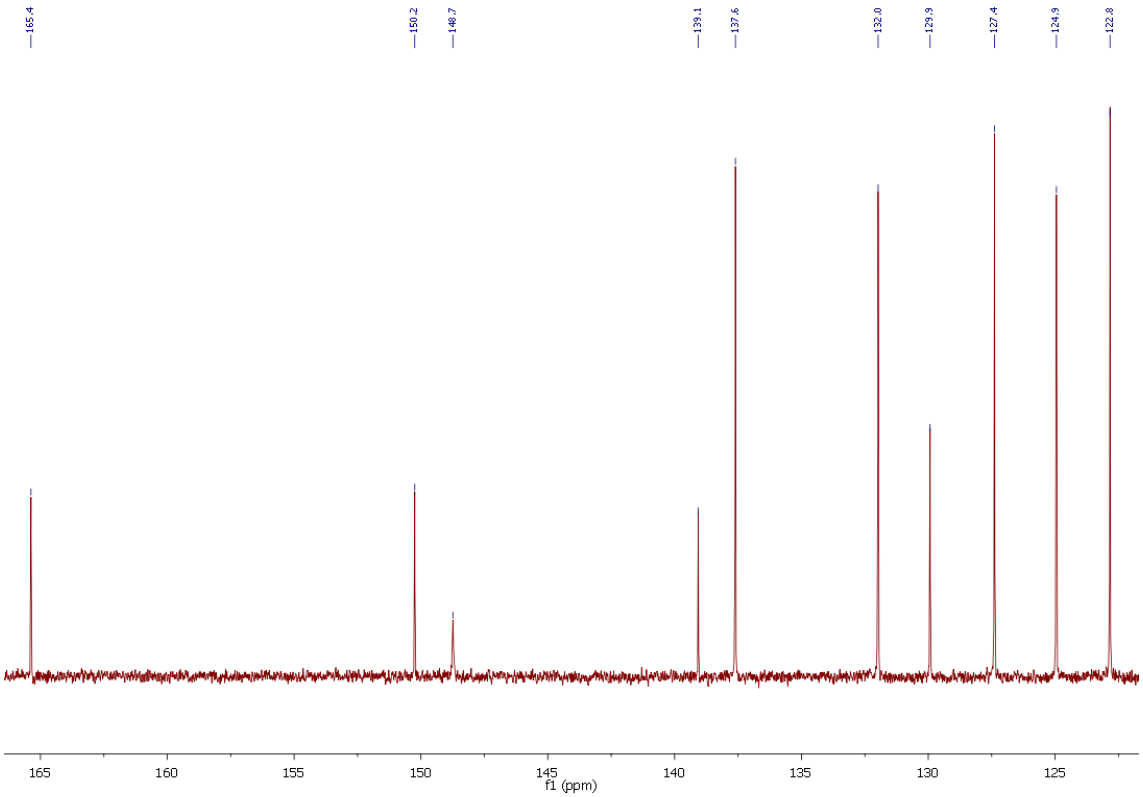

Fig. S121: Magnification of the ^{13}C NMR spectra of 2-Mee-8-NO_2-qu in $CDCl_3$.

11.4.4 Methyl 8-aminoquinoline-2-carboxylate (2-Mee-8-NH_2-qu)

^1H NMR (400 MHz, Chloroform-*d*) δ 8.18 (d, *J* = 8.6 Hz, 1H), 8.11 (d, *J* = 8.5 Hz, 1H), 7.42 (dd, *J* = 8.2, 7.6 Hz, 1H), 7.16 (dd, *J* = 8.2, 1.2 Hz, 1H), 6.95 (dd, *J* = 7.6, 1.2 Hz, 1H), 5.17 (s, 2H), 4.04 (s, 3H).

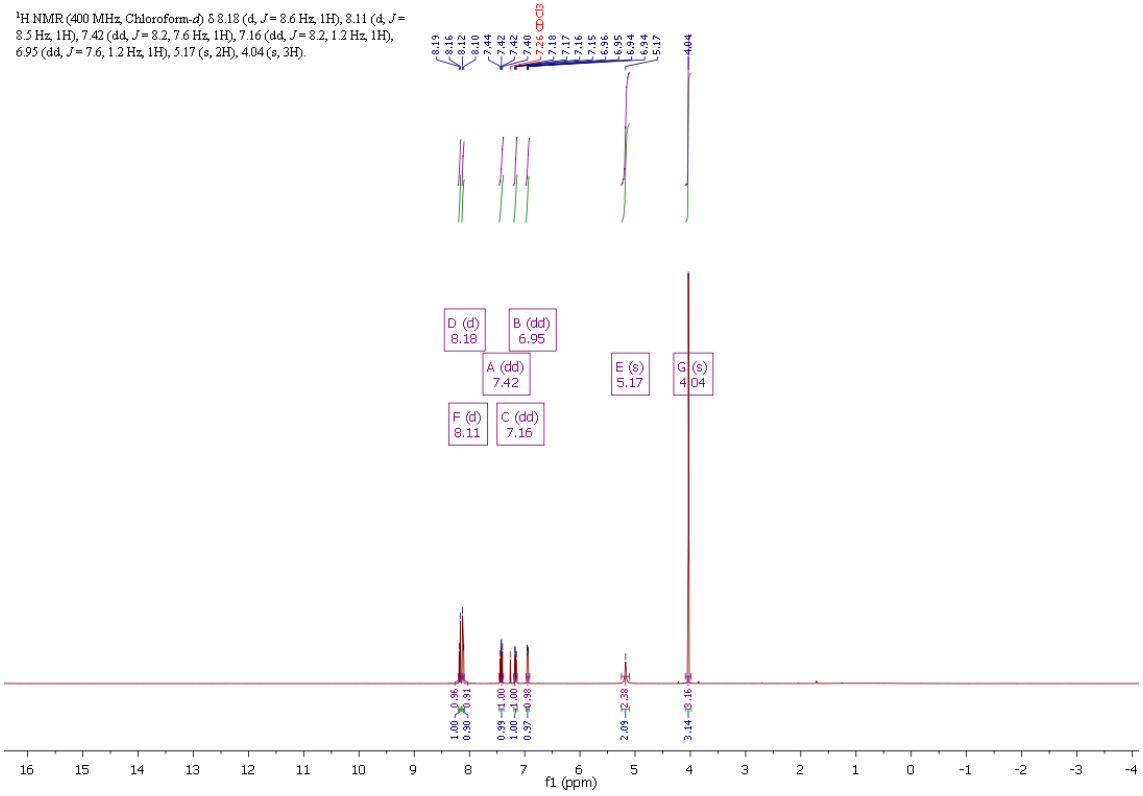

Fig. S122: ^1H NMR spectra of 2-Mee-8-NH_2-qu in $CDCl_3$.

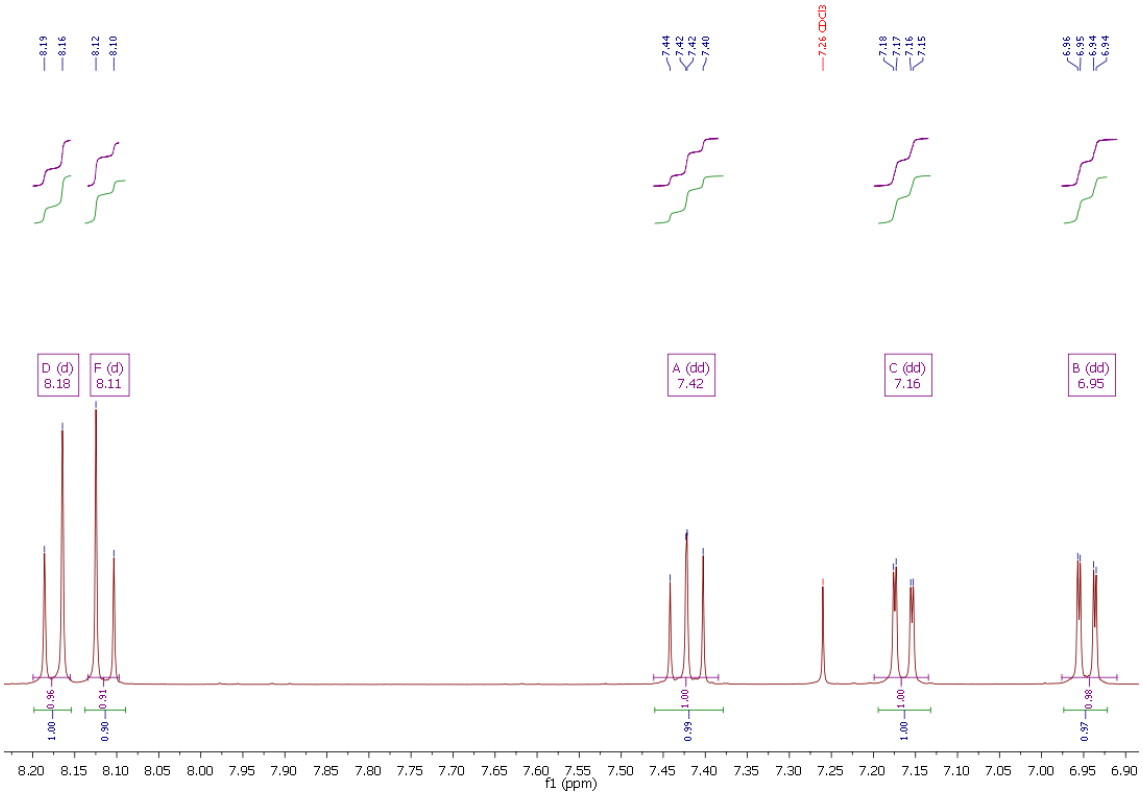

Fig. S123: Magnification of the ^{1}H NMR spectra of 2-Mee-8-NH_2-qu in $CDCl_3$.

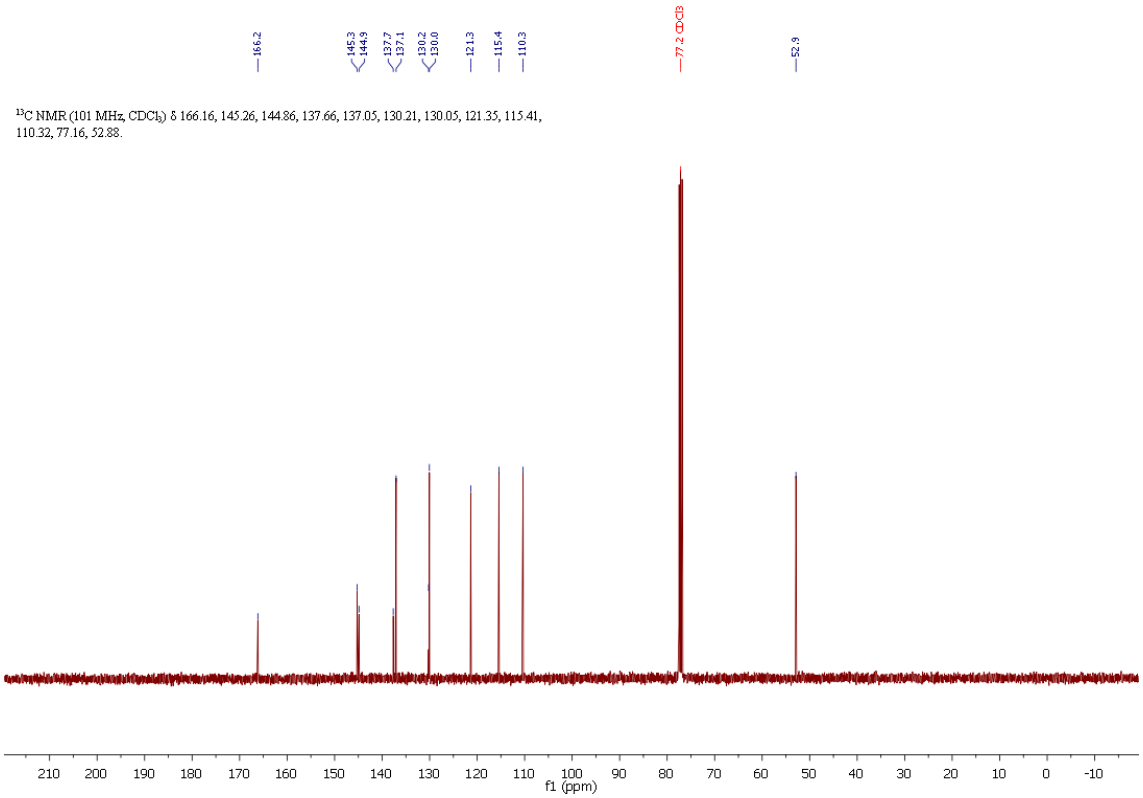

^{13}C NMR (101 MHz, $CDCl_3$) δ 166.16, 145.26, 144.86, 137.66, 137.05, 130.21, 130.05, 121.35, 115.41, 110.32, 77.16, 52.88.

Fig. S124: ^{13}C NMR spectra of 2-Mee-8-NH_2-qu in $CDCl_3$.

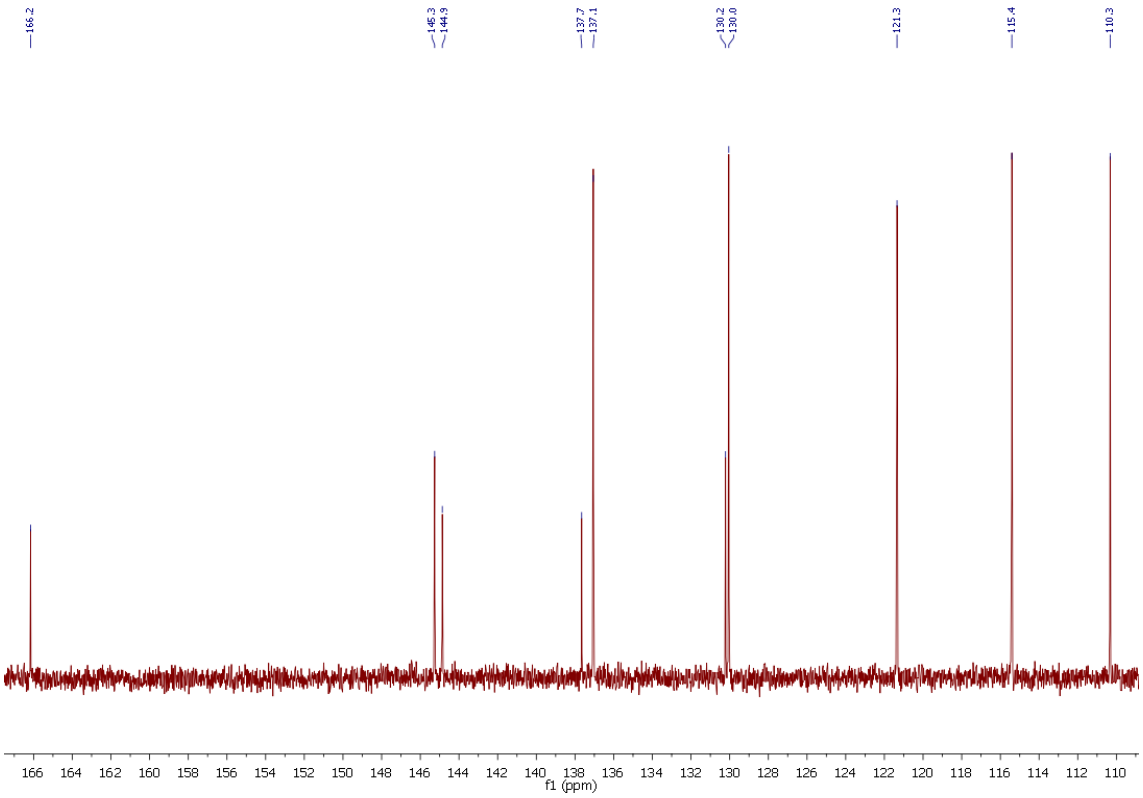

Fig. S125: Magnification of the ^{13}C NMR spectra of 2-Mee-8-NH_2-qu in $CDCl_3$.

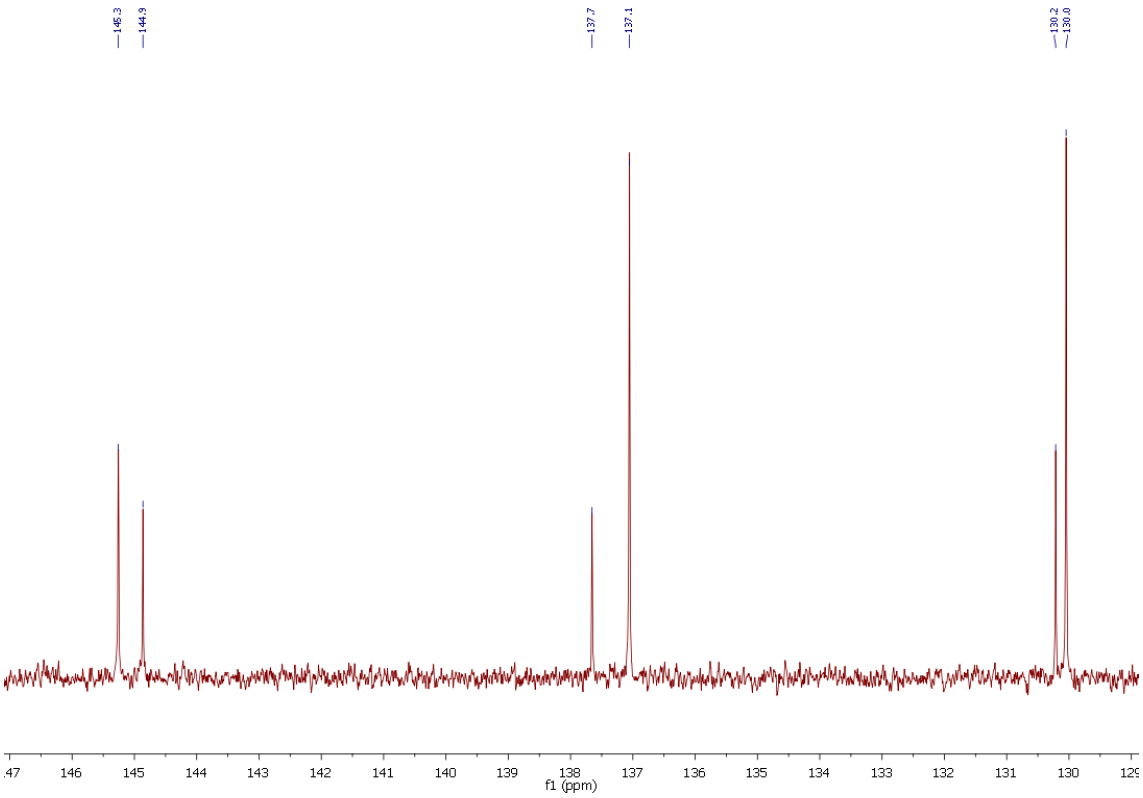

Fig. S126: Magnification of the ^{13}C NMR spectra of 2-Mee-8-NH_2-qu in $CDCl_3$.

11.4.5 TMG2Meequ (L5)

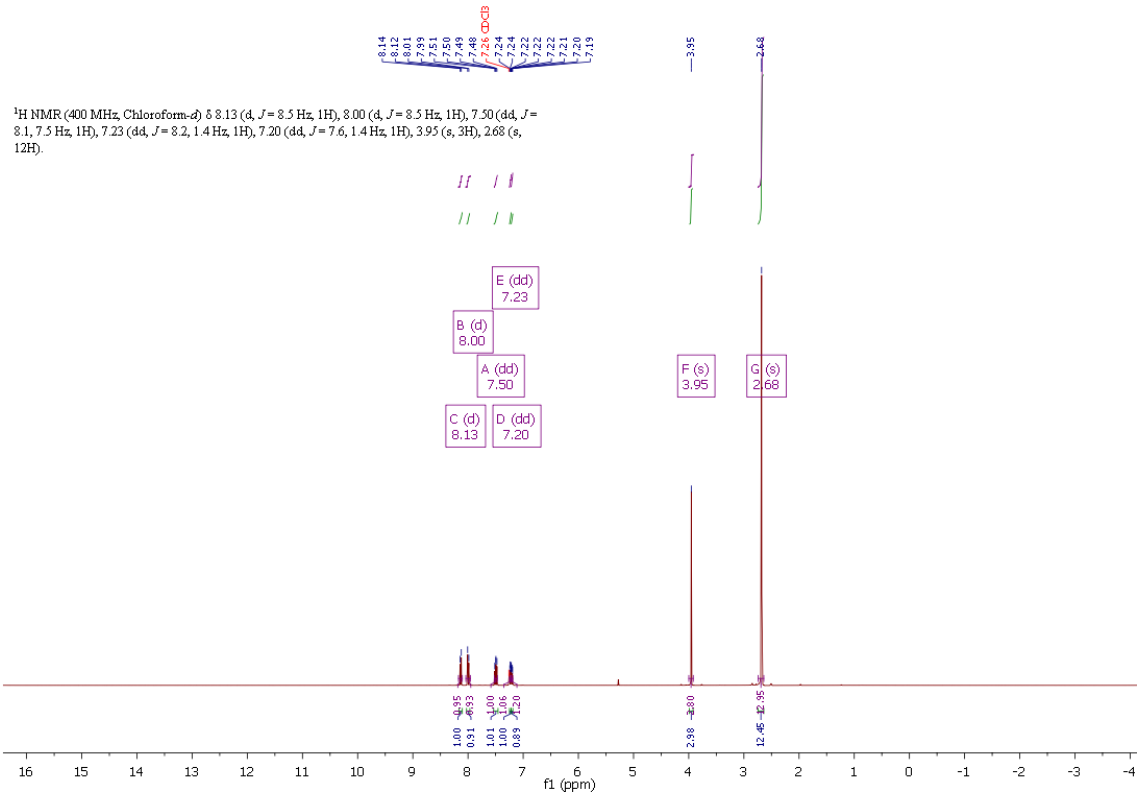

Fig. S127: ^{1}H NMR spectra of TMG2Meequ in $CDCl_3$.

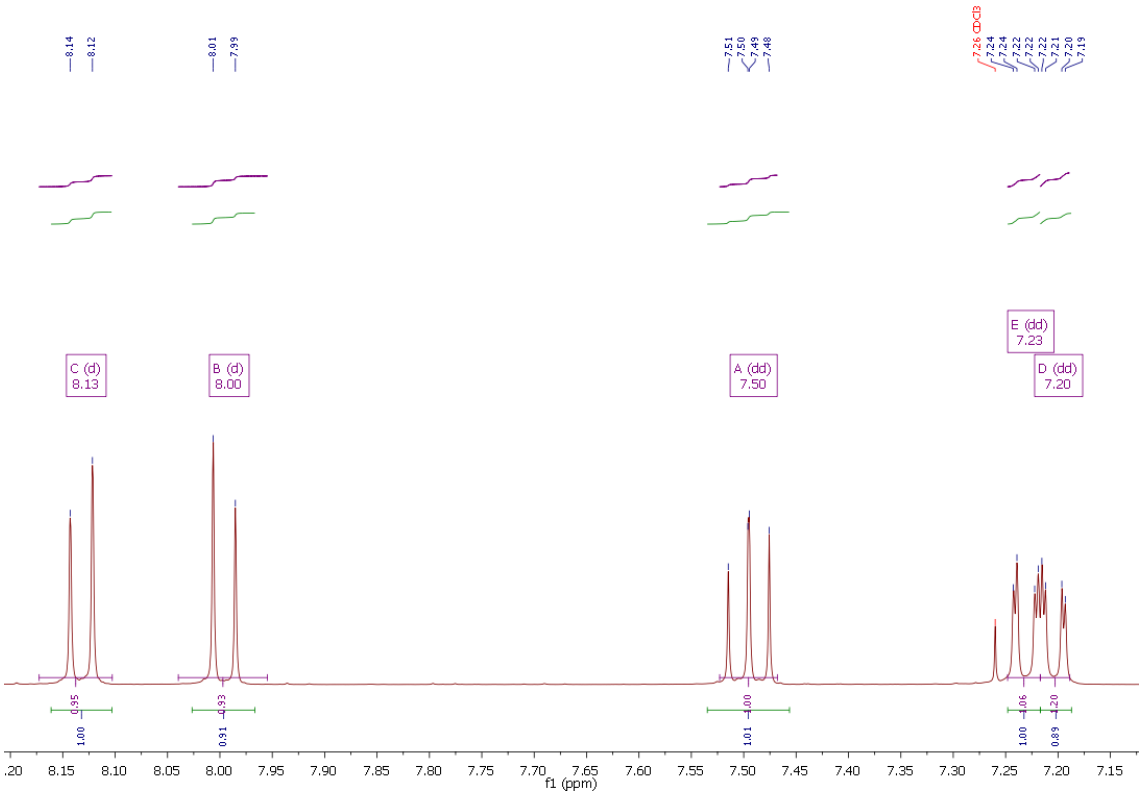

Fig. S128: Magnification of the ^{1}H NMR spectra of TMG2Meequ in $CDCl_3$.

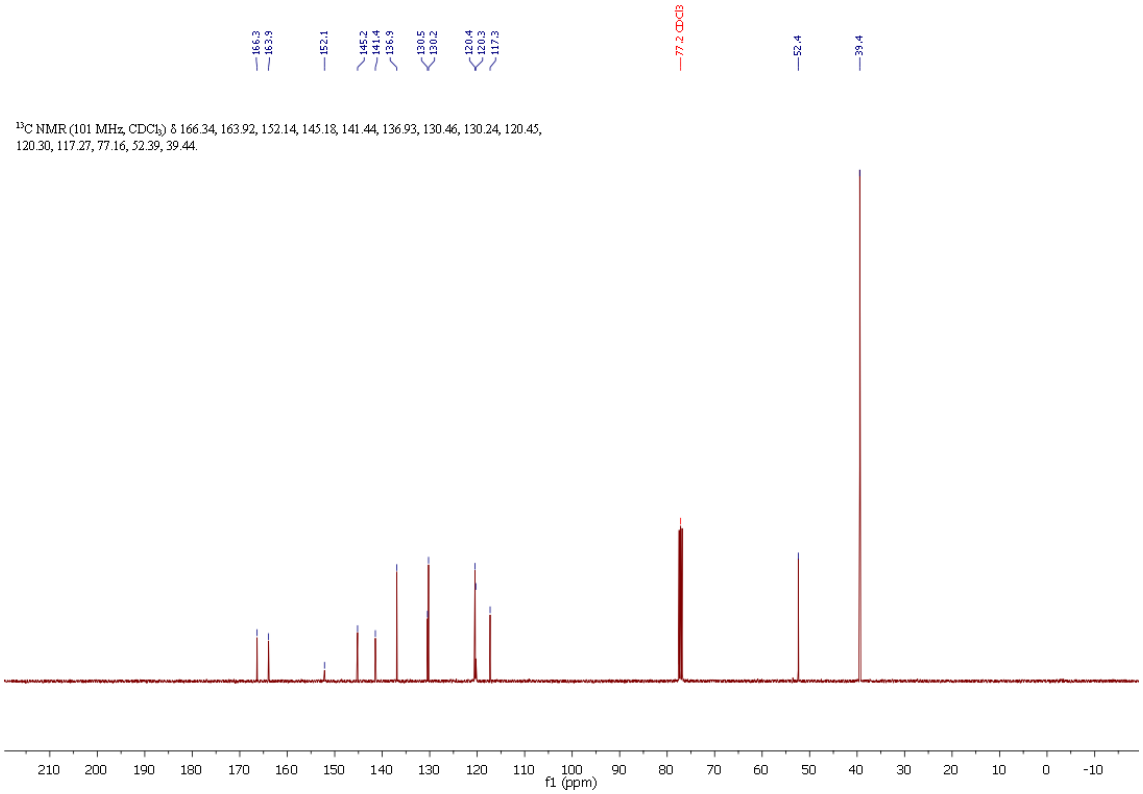

Fig. S129: ^{13}C NMR spectra of TMG2Meequ in $CDCl_3$.

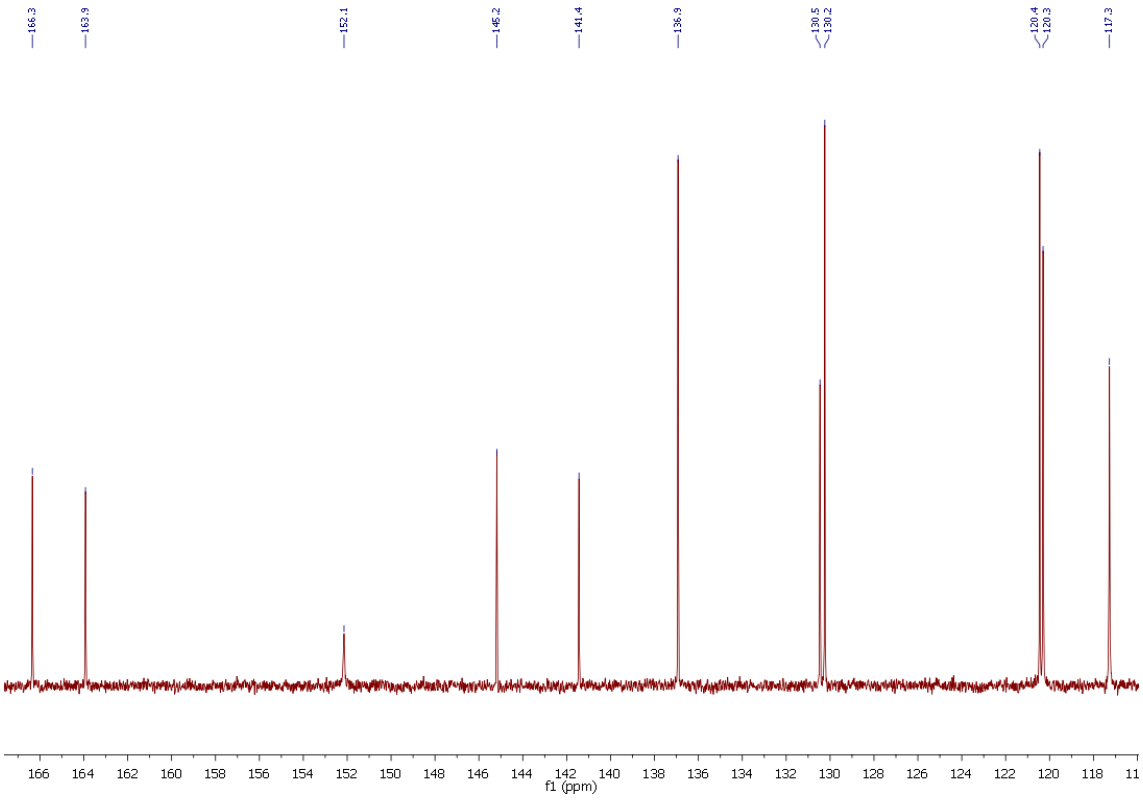

Fig. S130: Magnification of the ^{13}C NMR spectra of TMG2Meequ in $CDCl_3$.

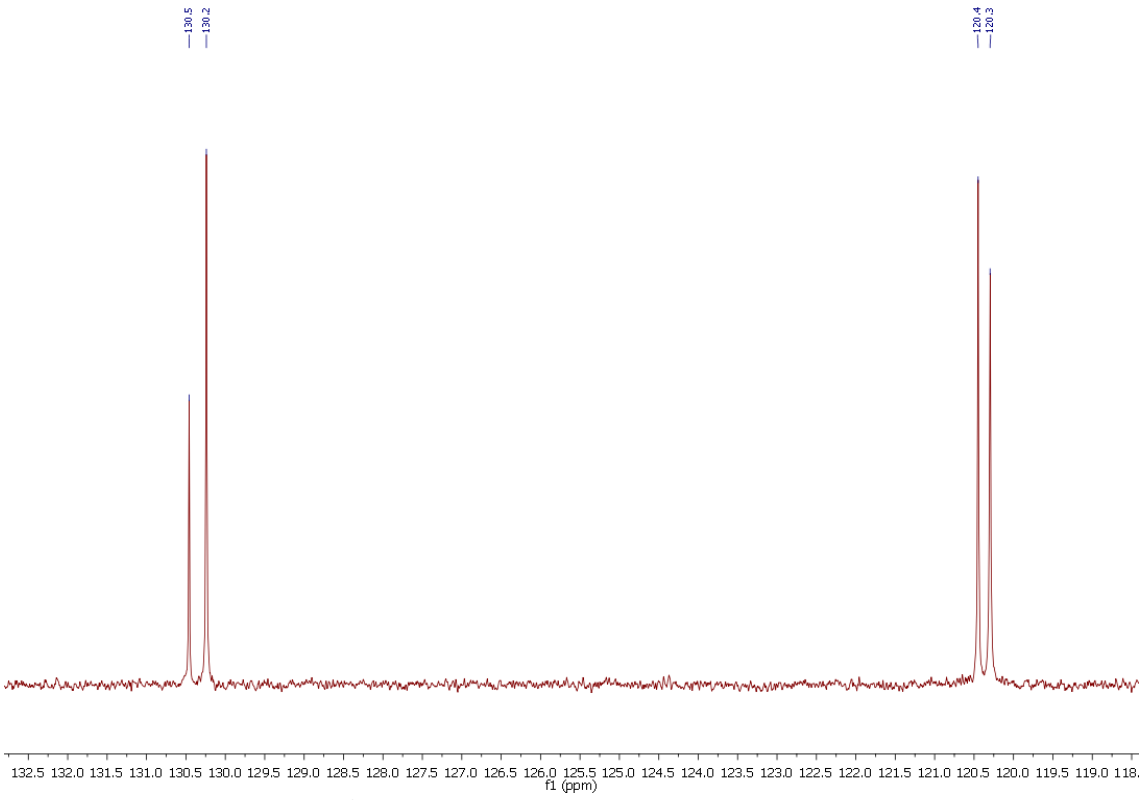

Fig. S131: Magnification of the ^{13}C NMR spectra of TMG2Meequ in $CDCl_3$.

11.4.6 [Cu(TMG2Meequ)$_2$]PF$_6$ (C7–PF$_6$)

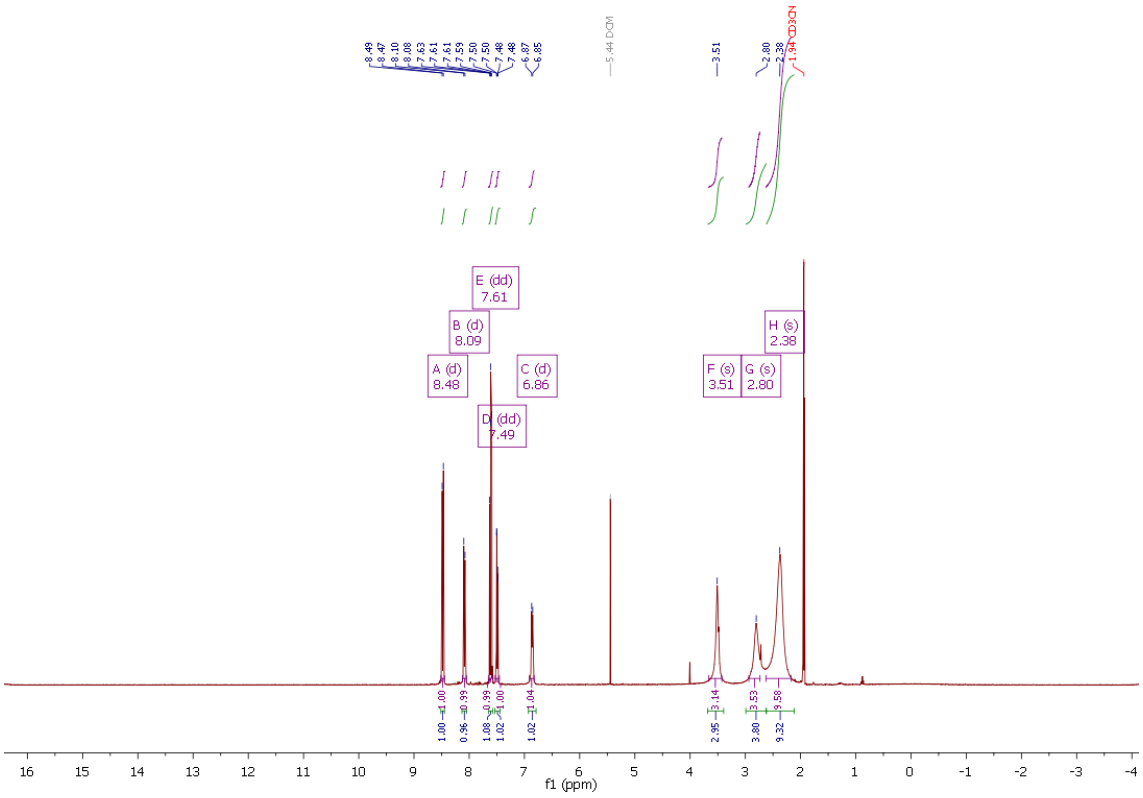

Fig. S132: ^{1}H NMR spectra of [Cu(TMG2Meequ)$_2$]PF$_6$ (**C7–PF$_6$**) in MeCN-d3.

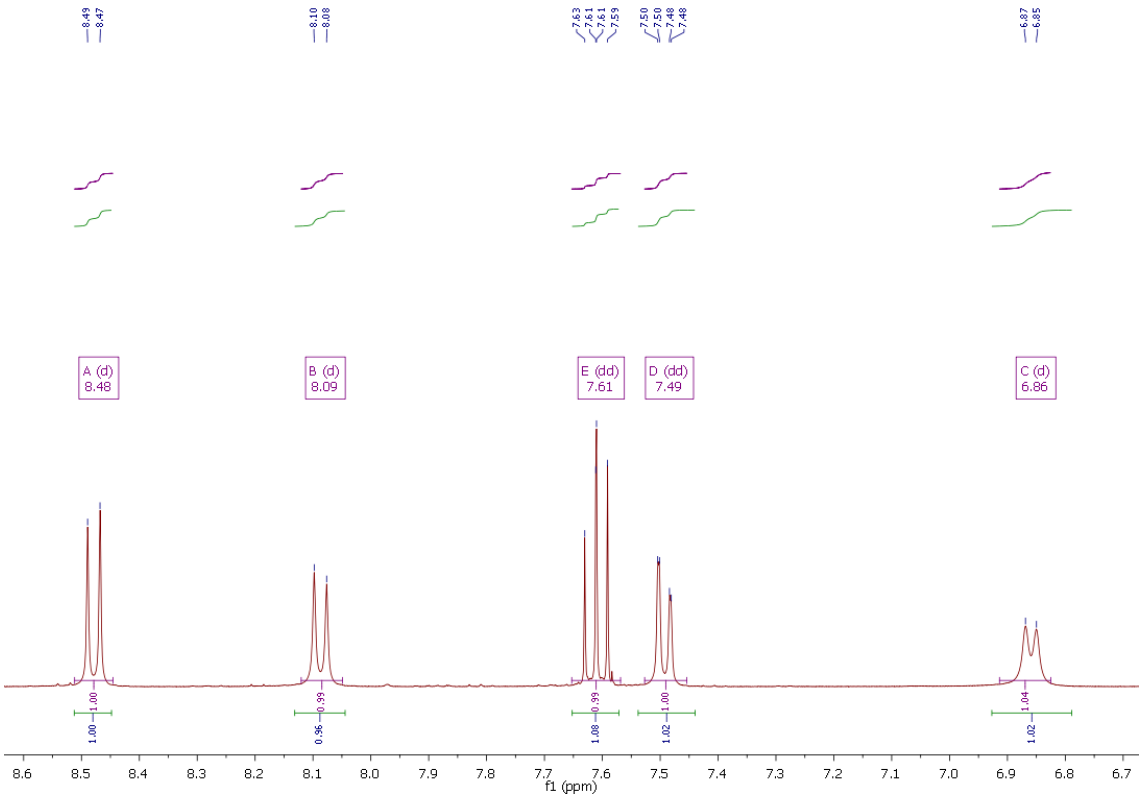

Fig. S133: Magnification of the ^{1}H NMR spectra of [Cu(TMG2Meequ)$_2$]PF$_6$ (**C7–PF$_6$**) in MeCN-d3.

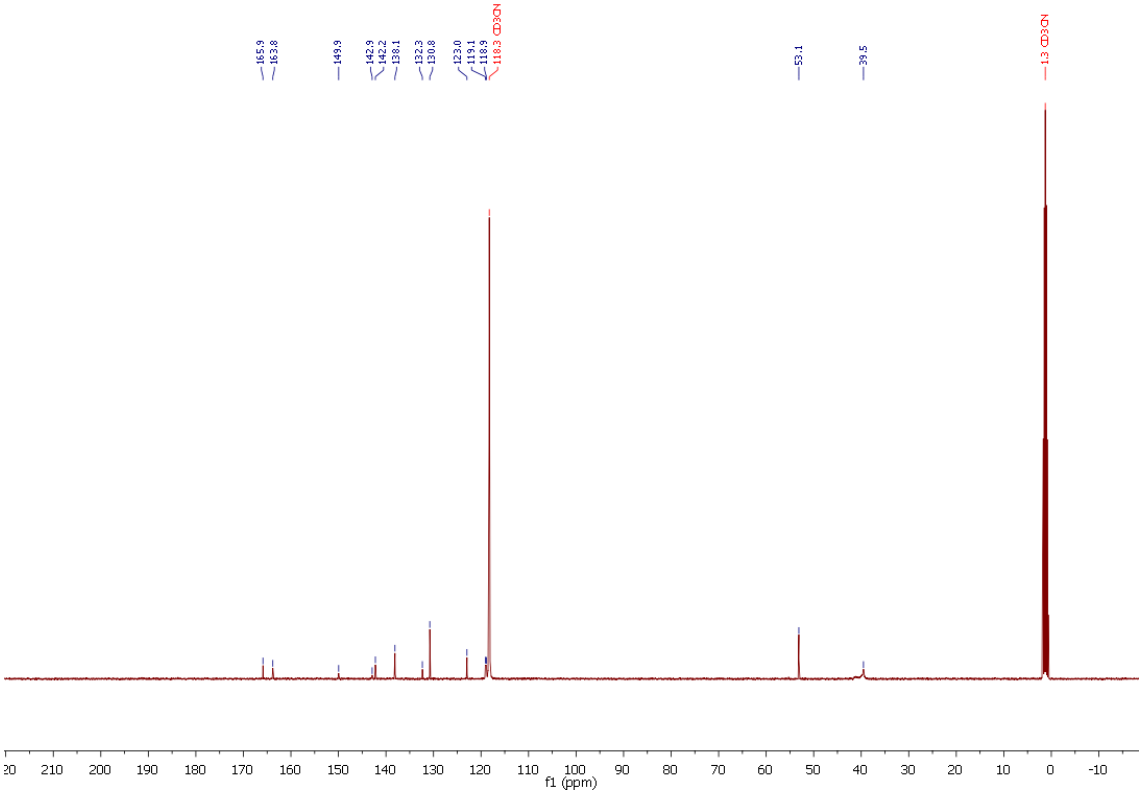

Fig. S134: : ^{13}C NMR spectra of [Cu(TMG2Meequ)$_2$]PF$_6$ (**C7–PF$_6$**) in MeCN-d3.

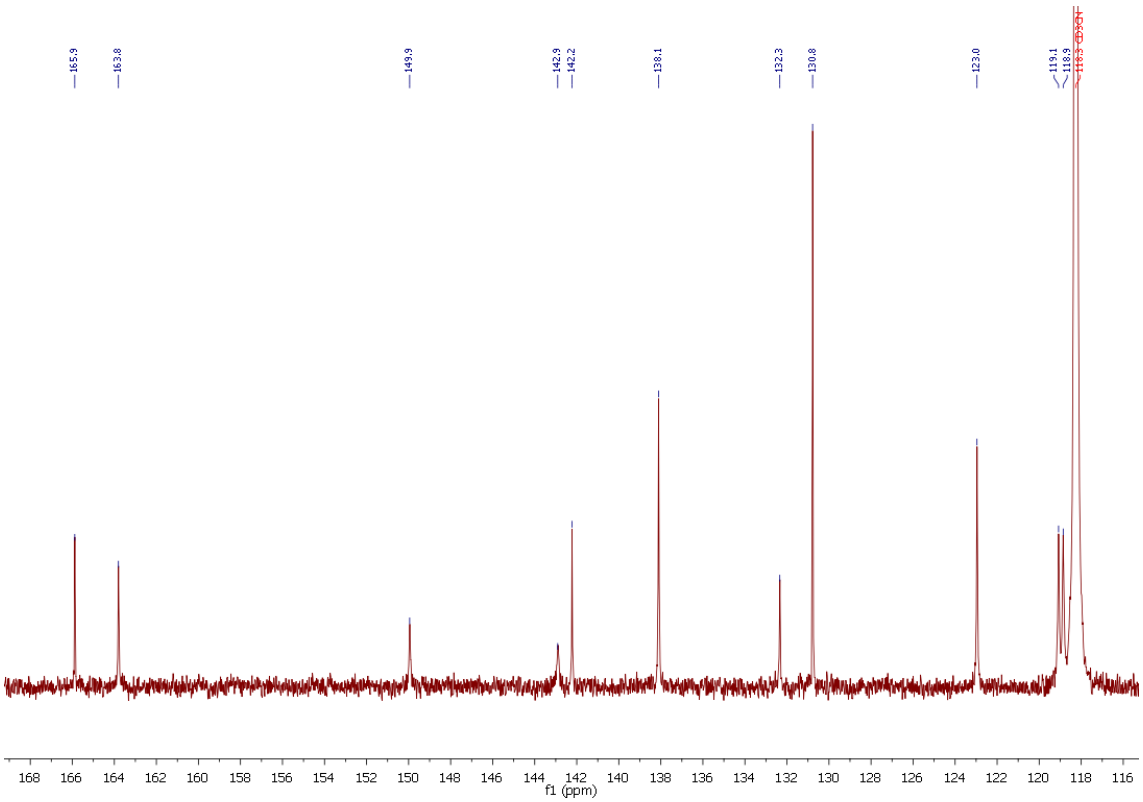

Fig. S135: Magnification of the ^{13}C NMR spectra of $[Cu(TMG2Meequ)_2]PF_6$ (**C7–PF$_6$**) in MeCN-d3.

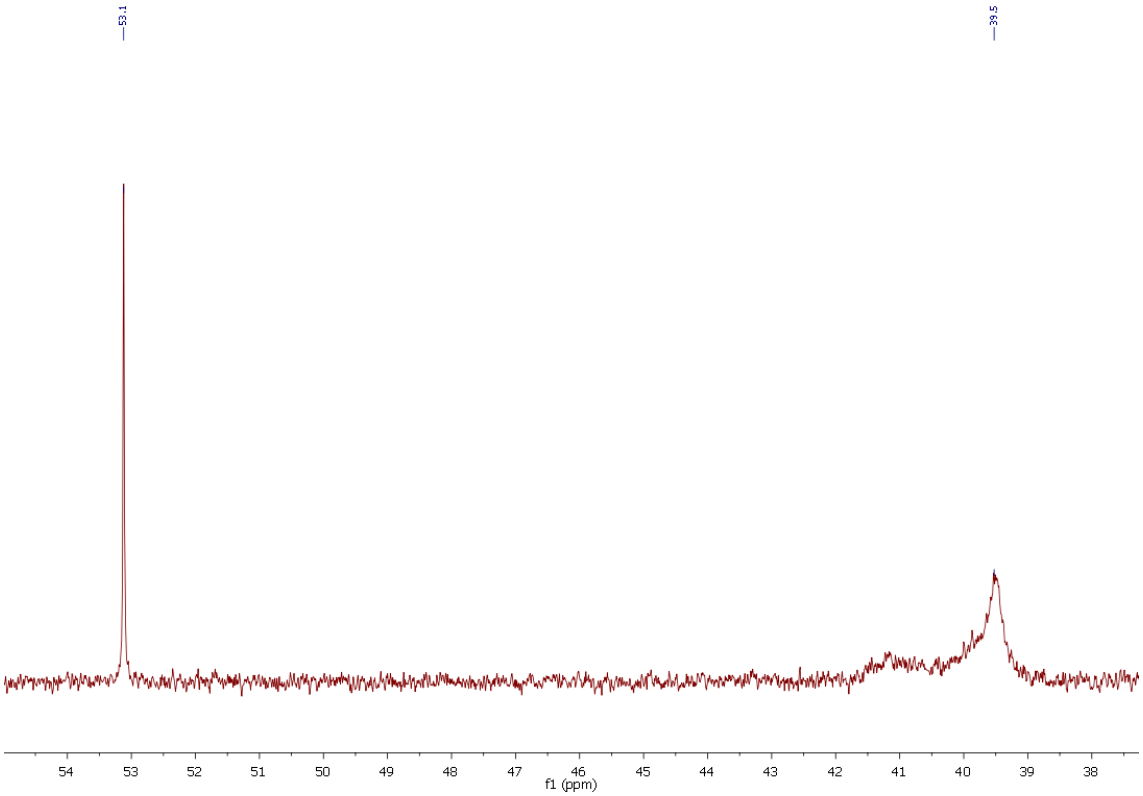

Fig. S136: Magnification of the ^{13}C NMR spectra of $[Cu(TMG2Meequ)_2]PF_6$ (**C7–PF$_6$**) in MeCN-d3.

11.5 TMG4NMe$_2$qu (L6) and corresponding precursors and Cu(I) complex

11.5.1 4-Chloro-8-nitroquinoline (4-Cl-8-NO$_2$-qu)

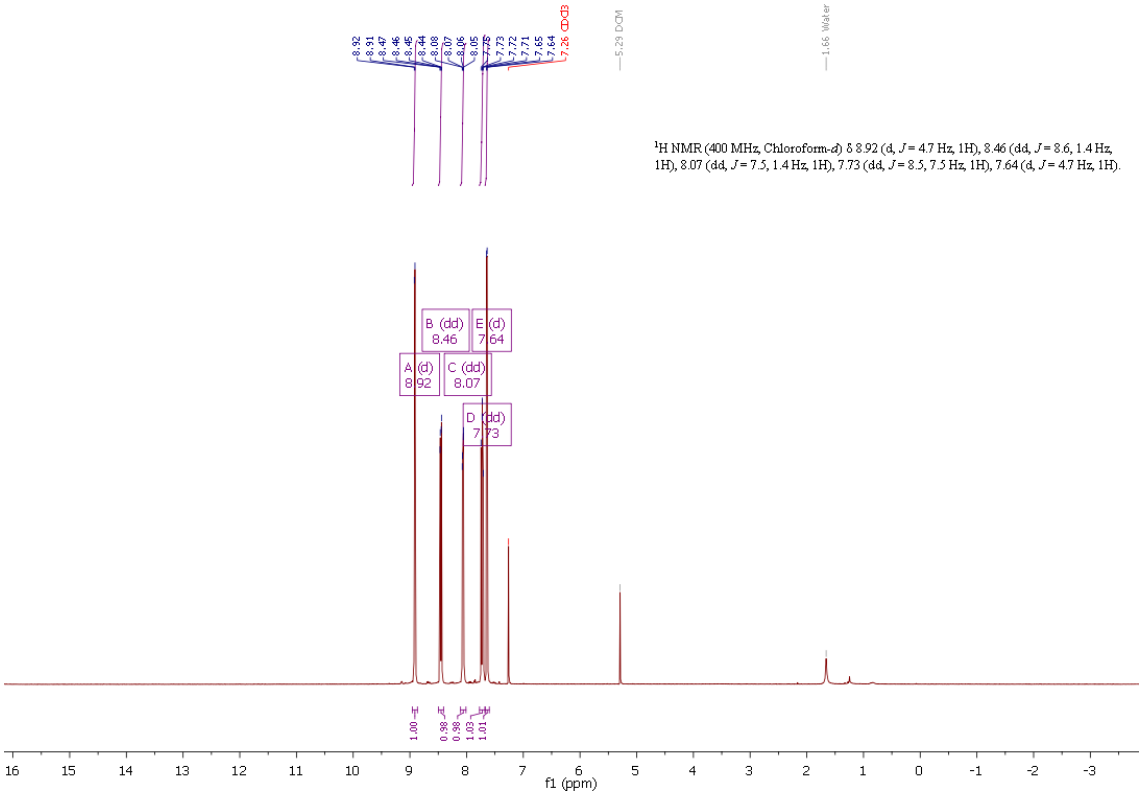

Fig. S137: ^{1}H NMR spectra of 4-Cl-8-NO$_2$-qu in CDCl$_3$.

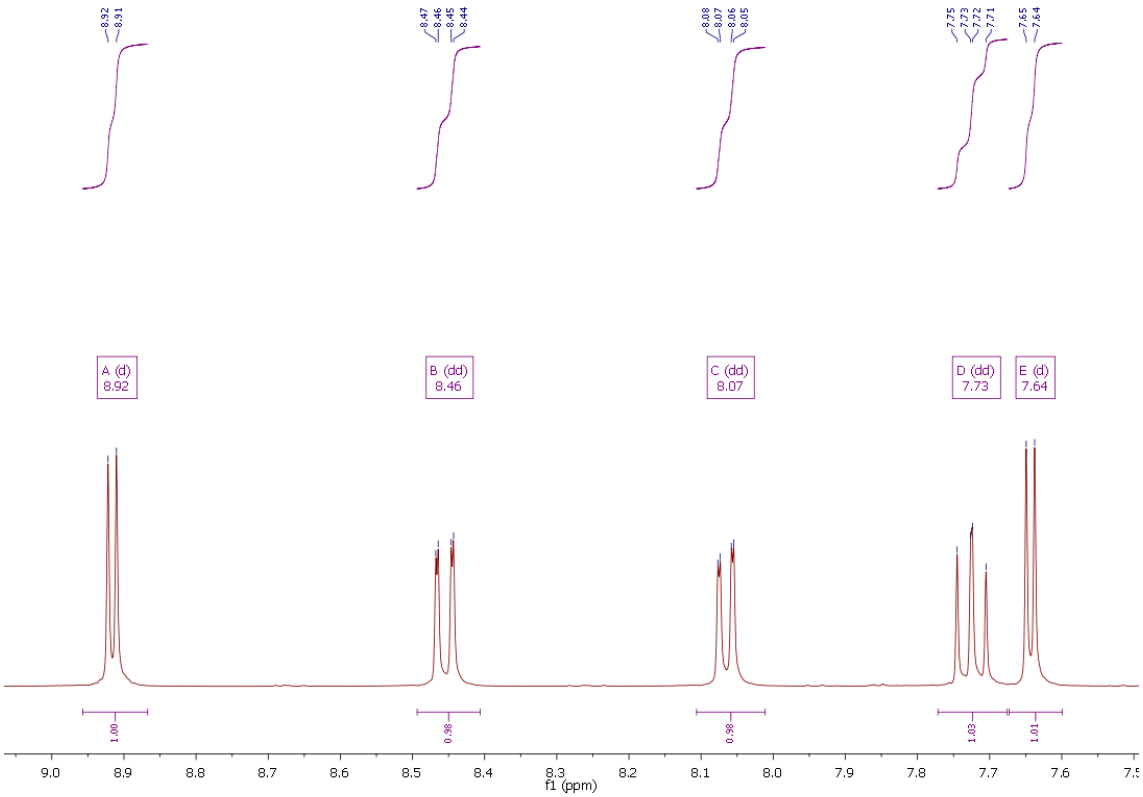

Fig. S138: Magnification of the ^{1}H NMR spectra of 4-Cl-8-NO_2-qu in $CDCl_3$.

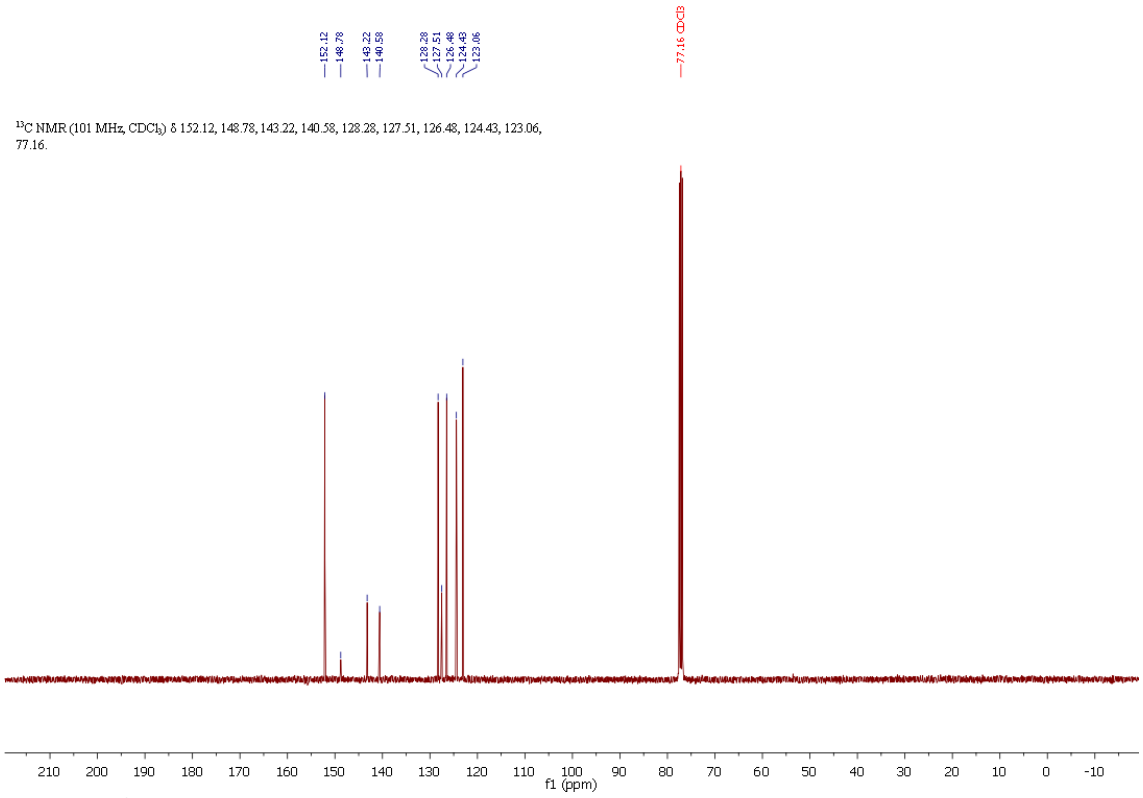

Fig. S139: ^{13}C NMR spectra of 4-Cl-8-NO_2-qu in $CDCl_3$.

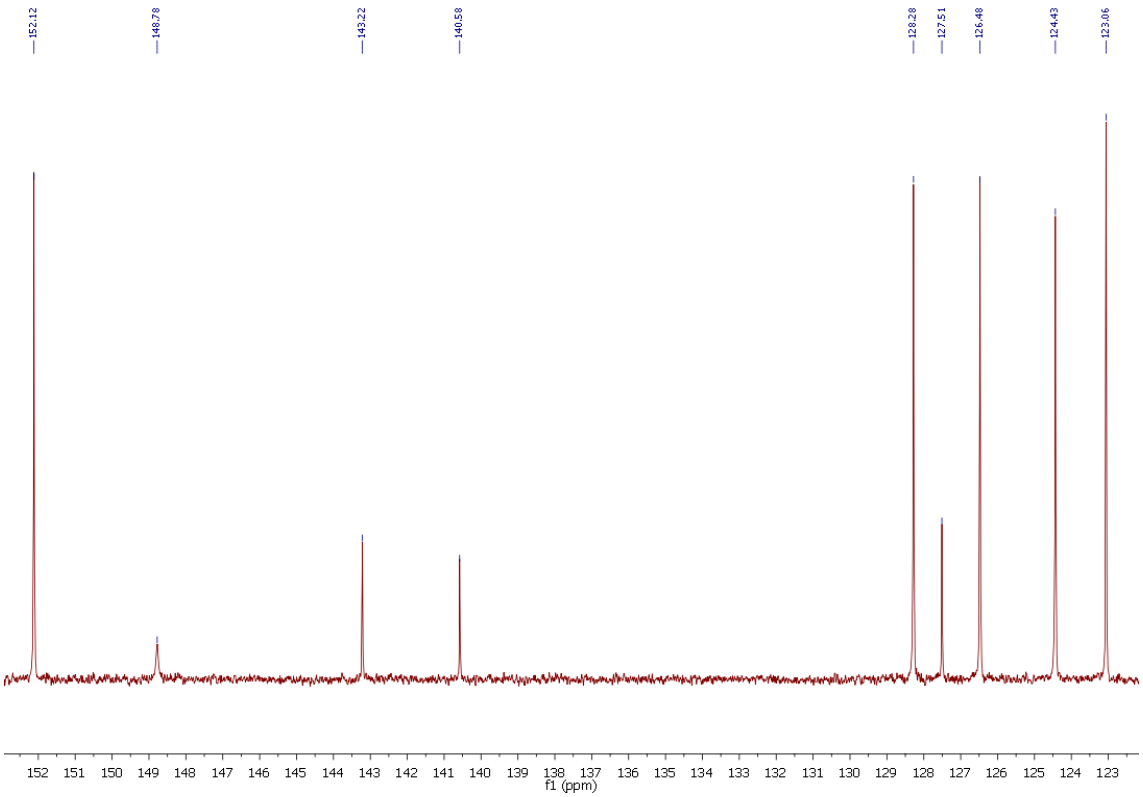

Fig. S140: Magnification of the ^{13}C NMR spectra of 4-Cl-8-NO_2-qu in $CDCl_3$.

11.5.2 4-Dimethylamine-8-nitroquinoline (4-NMe_2-8-NO_2-qu)

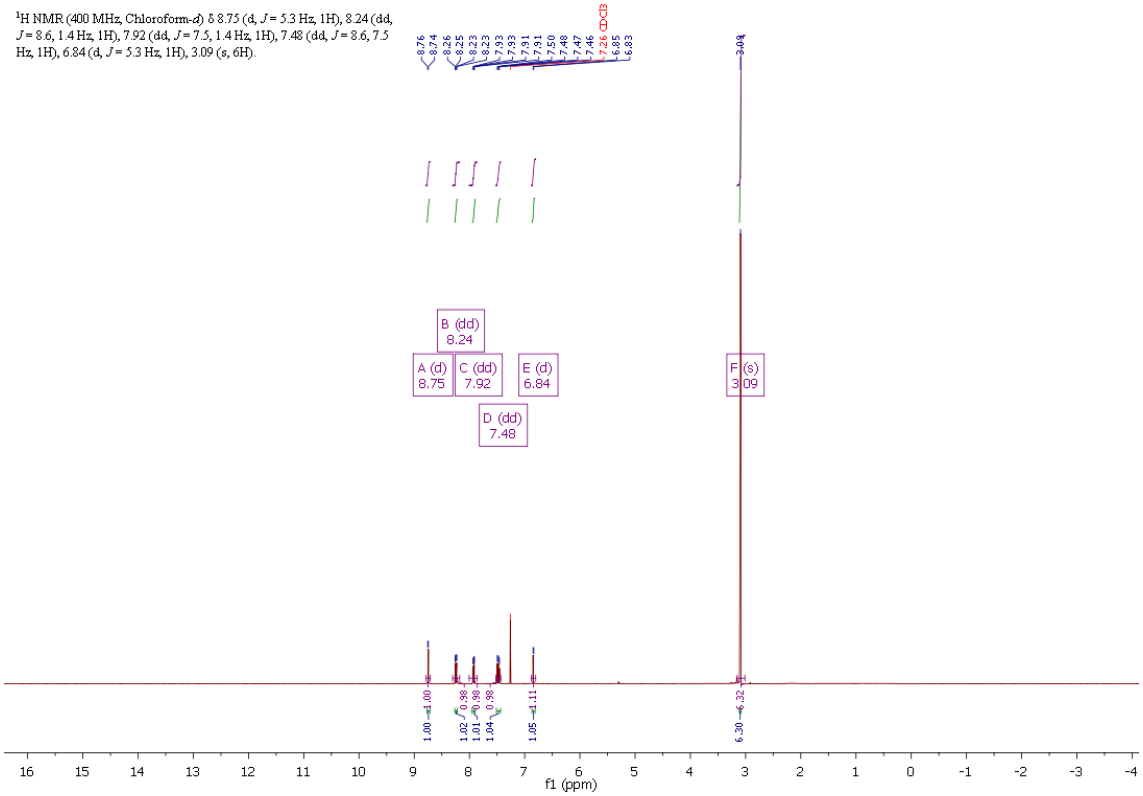

Fig. S141: ^{1}H NMR spectra of 4-NMe_2-8-NO_2-qu in $CDCl_3$.

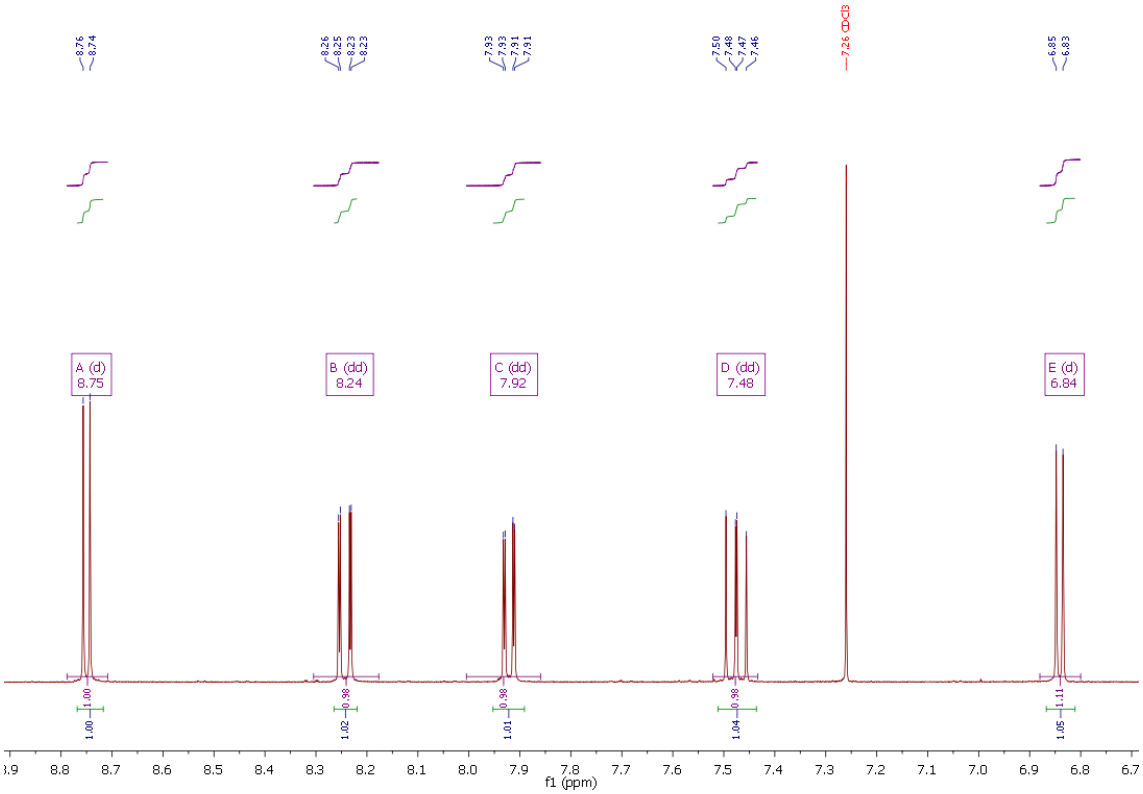

Fig. S142: Magnification of the ^{1}H NMR spectra of 4-NMe$_2$-8-NO$_2$-qu in CDCl$_3$.

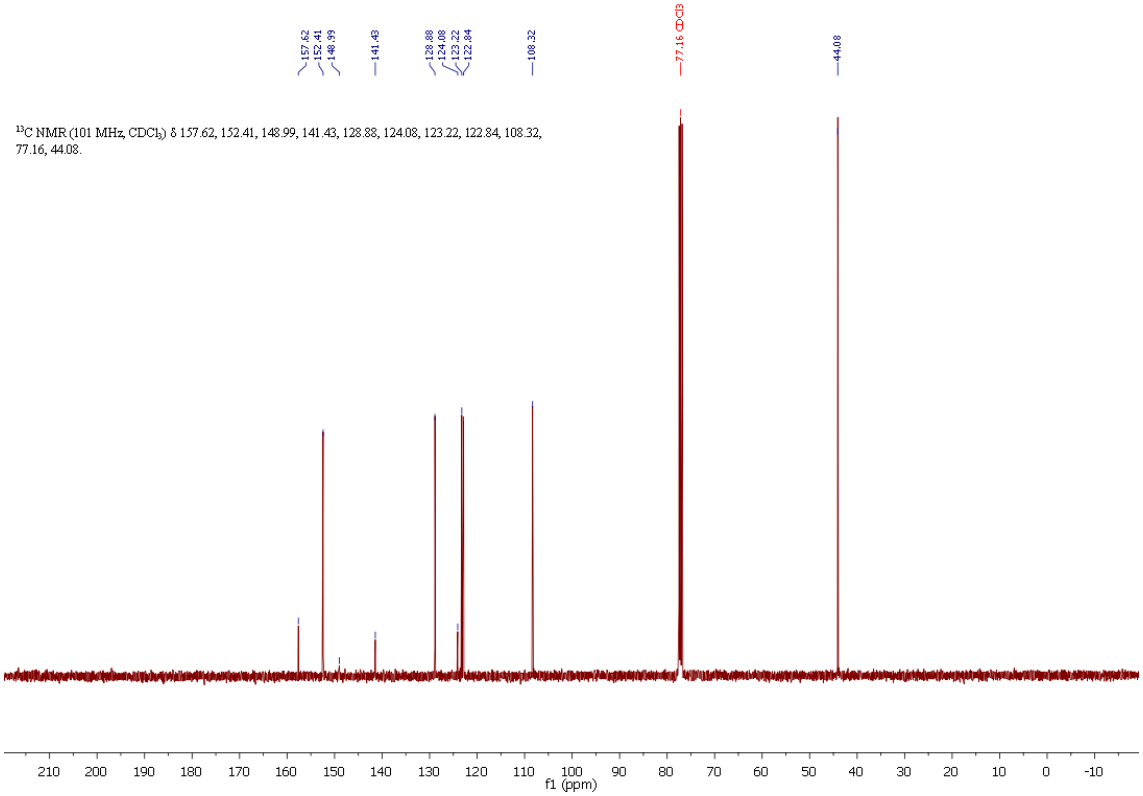

Fig. S143: ^{13}C NMR spectra of 4-NMe$_2$-8-NO$_2$-qu in CDCl$_3$.

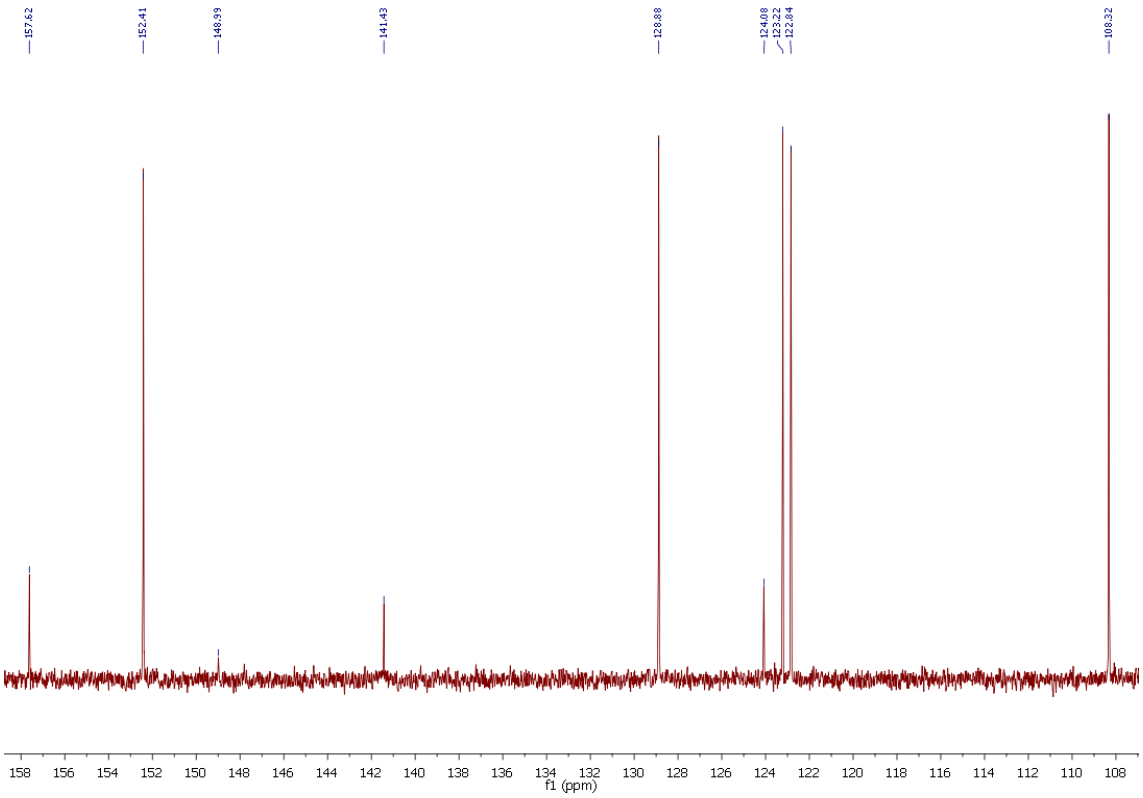

Fig. S144: Magnification of the ^{13}C NMR spectra of 4-NMe_2-8-NO_2-qu in $CDCl_3$.

11.5.3 4-Dimethylamine-8-aminoquinoline (4-NMe_2-8-NH_2-qu)

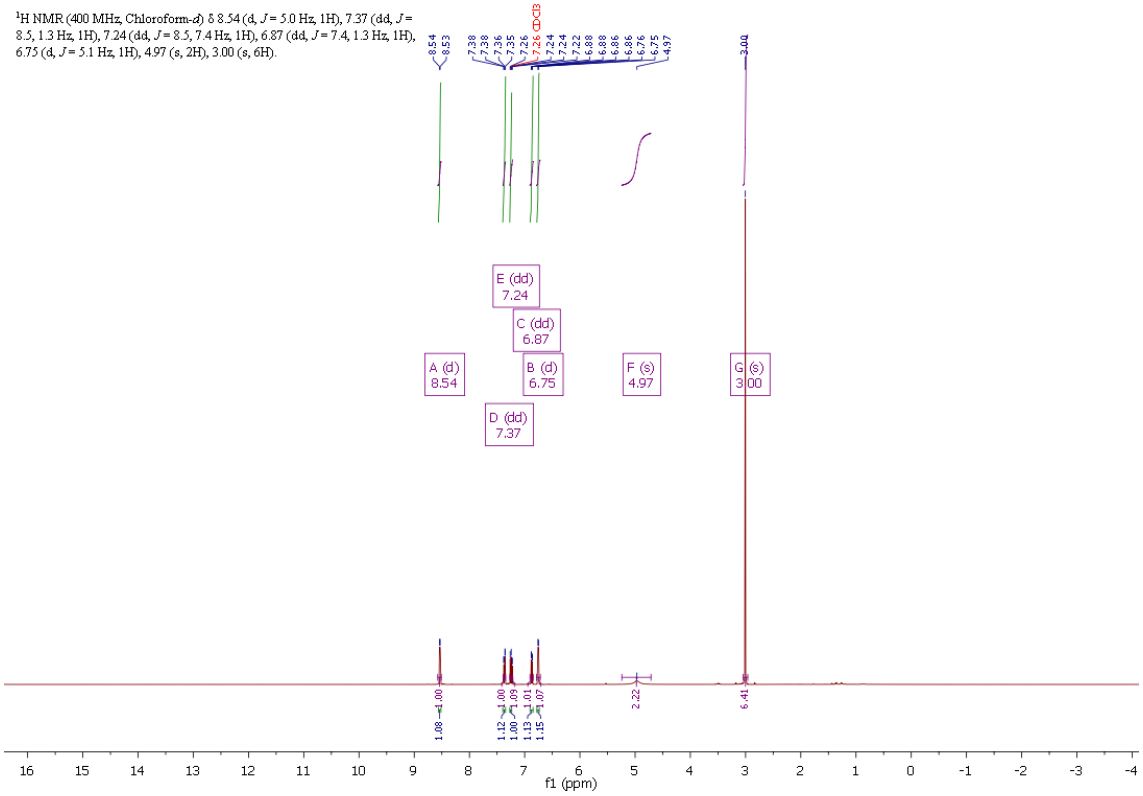

Fig. S145: ^1H NMR spectra of 4-NMe_2-8-NH_2-qu in $CDCl_3$.

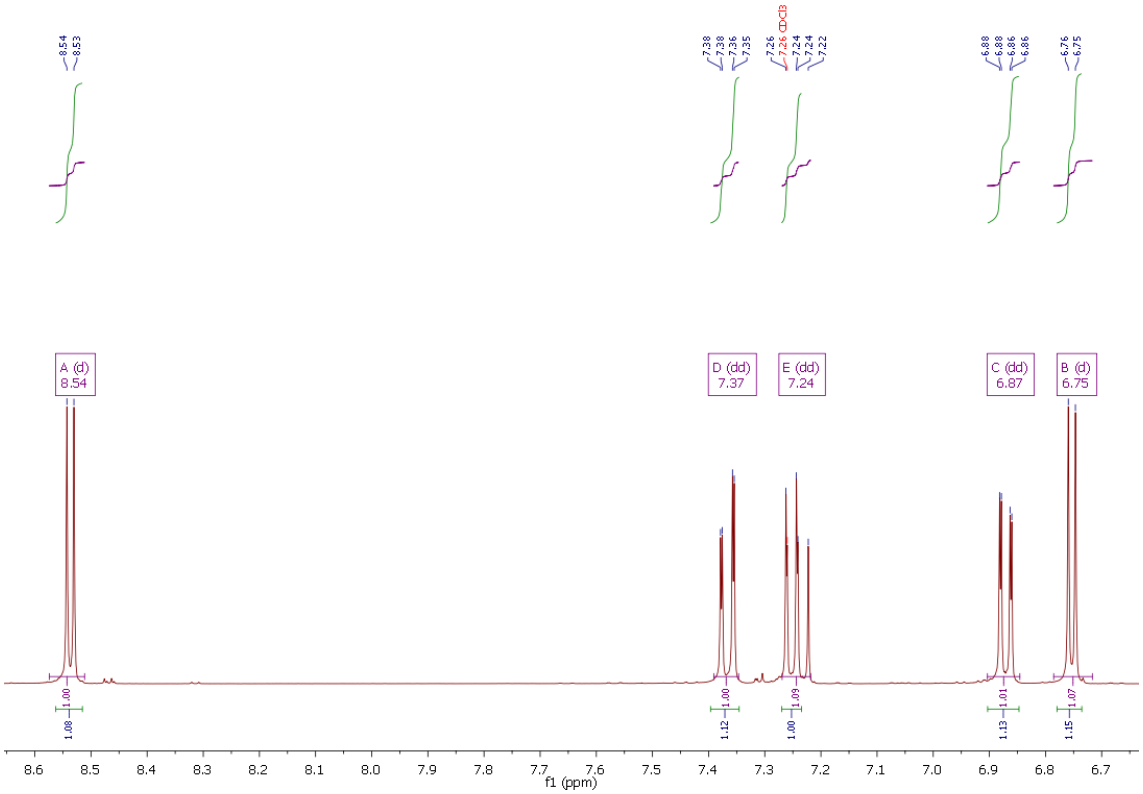

Fig. S146: Magnification of the ^{1}H NMR spectra of 4-NMe$_2$-8-NH$_2$-qu in CDCl$_3$.

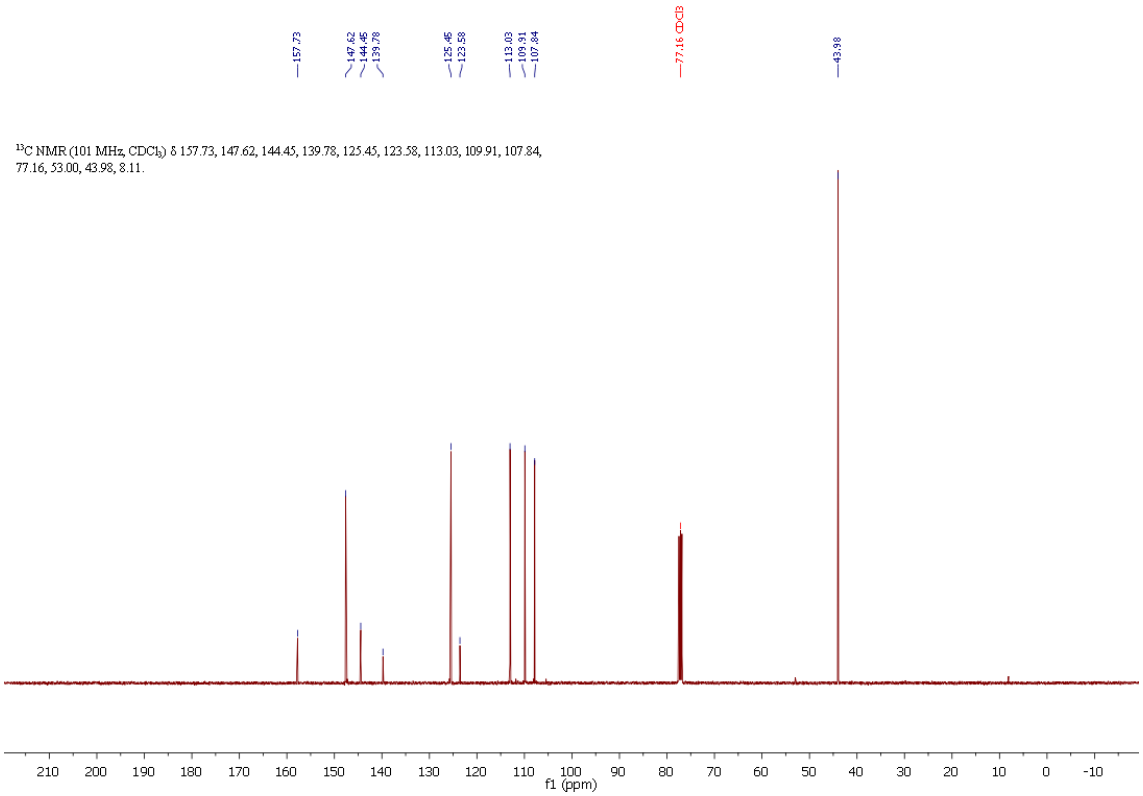

Fig. S147: ^{13}C NMR spectra of 4-NMe$_2$-8-NH$_2$-qu in CDCl$_3$.

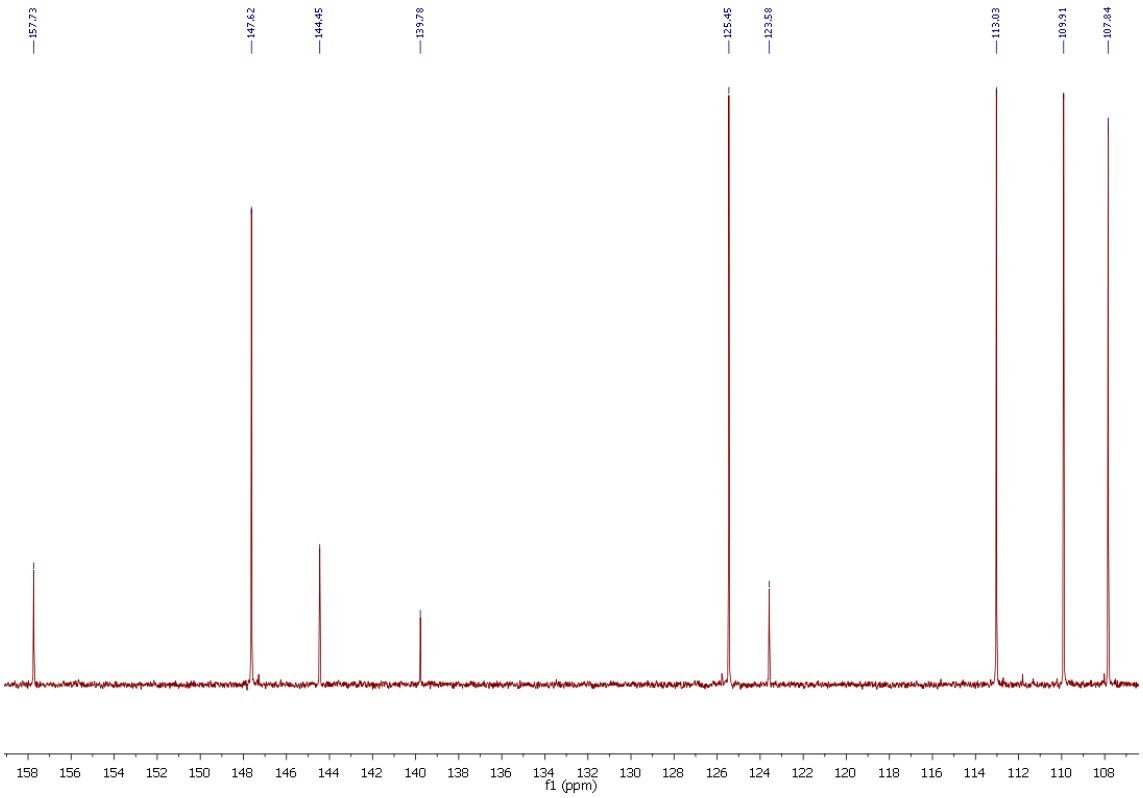

Fig. S148: Magnification of the ^{13}C NMR spectra of 4-NMe_2-8-NH_2-qu in $CDCl_3$.

11.5.4 TMG4NMe$_2$qu (L6)

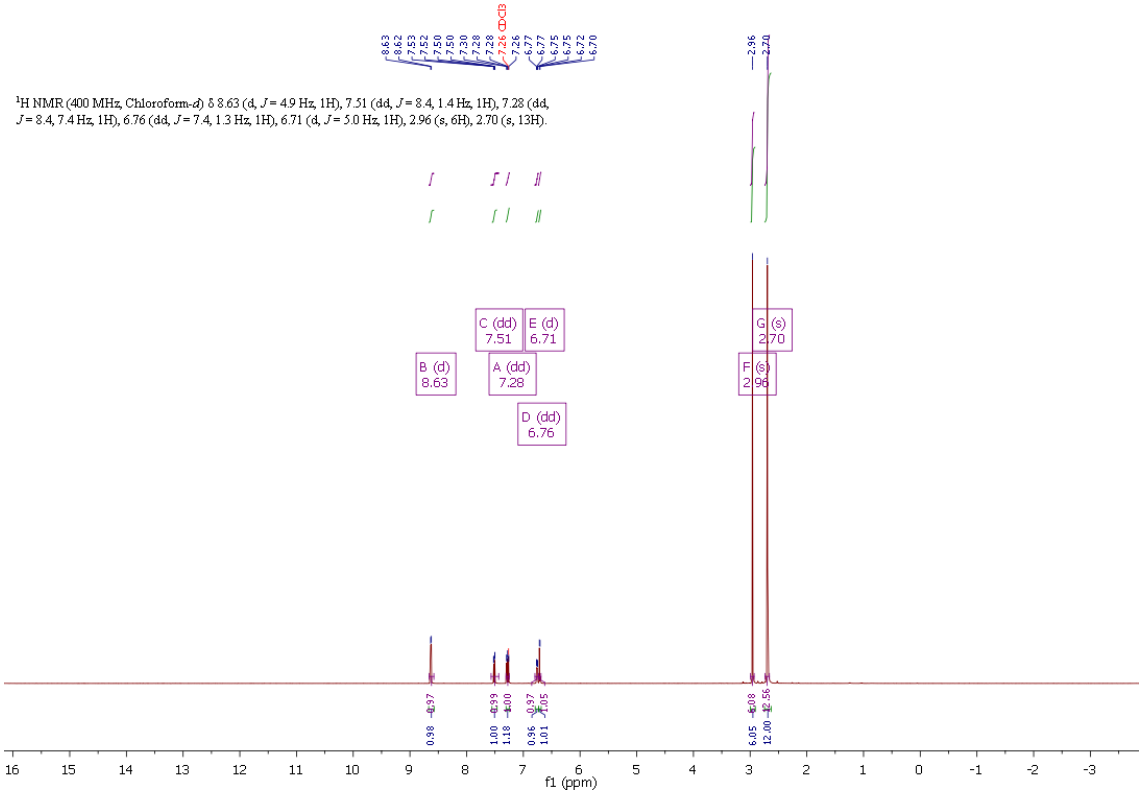

Fig. S149: ^1H NMR spectra of TMG4NMe$_2$qu in $CDCl_3$.

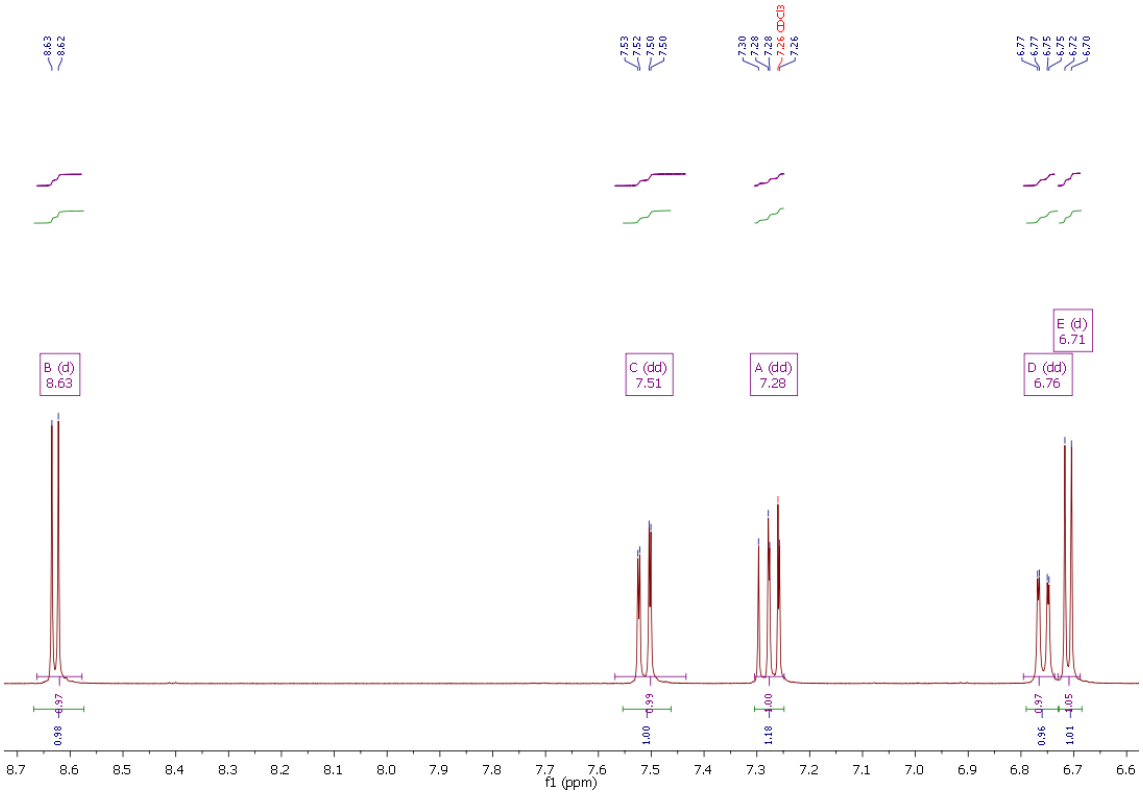

Fig. S150: Magnification of the ^{1}H NMR spectra of TMG4NMe$_2$qu in CDCl$_3$.

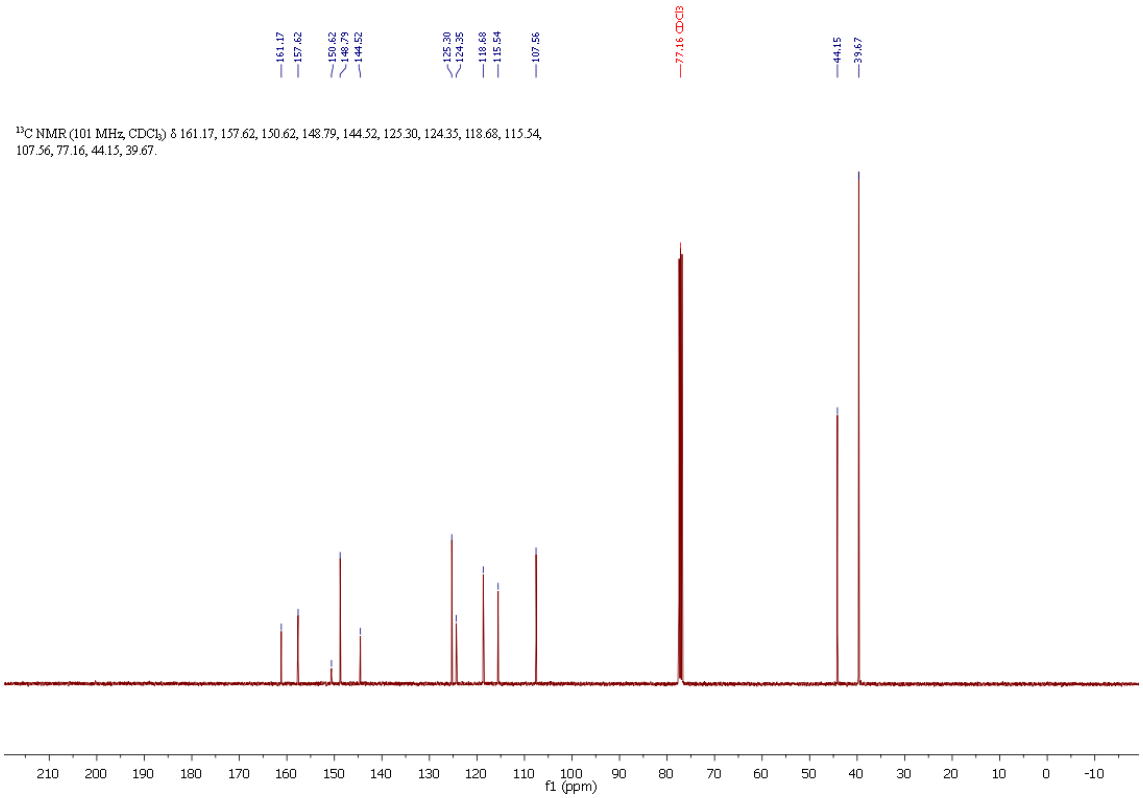

^{13}C NMR (101 MHz, CDCl$_3$) δ 161.17, 157.62, 150.62, 148.79, 144.52, 125.30, 124.35, 118.68, 115.54, 107.56, 77.16, 44.15, 39.67.

Fig. S151: ^{13}C NMR spectra of TMG4NMe$_2$qu in CDCl$_3$.

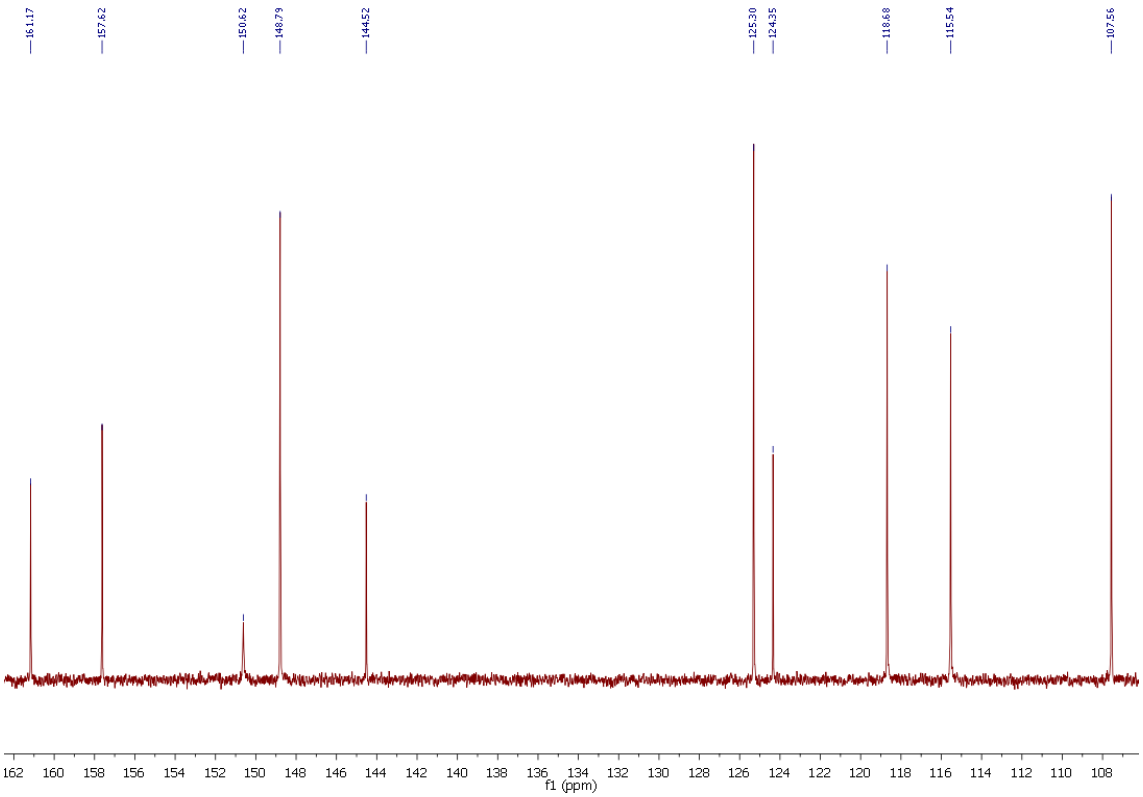

Fig. S152: Magnification of the ^{13}C NMR spectra of TMG4NMe$_2$qu in $CDCl_3$.

11.6 $[Co(bpy)_3](PF_6)_3$

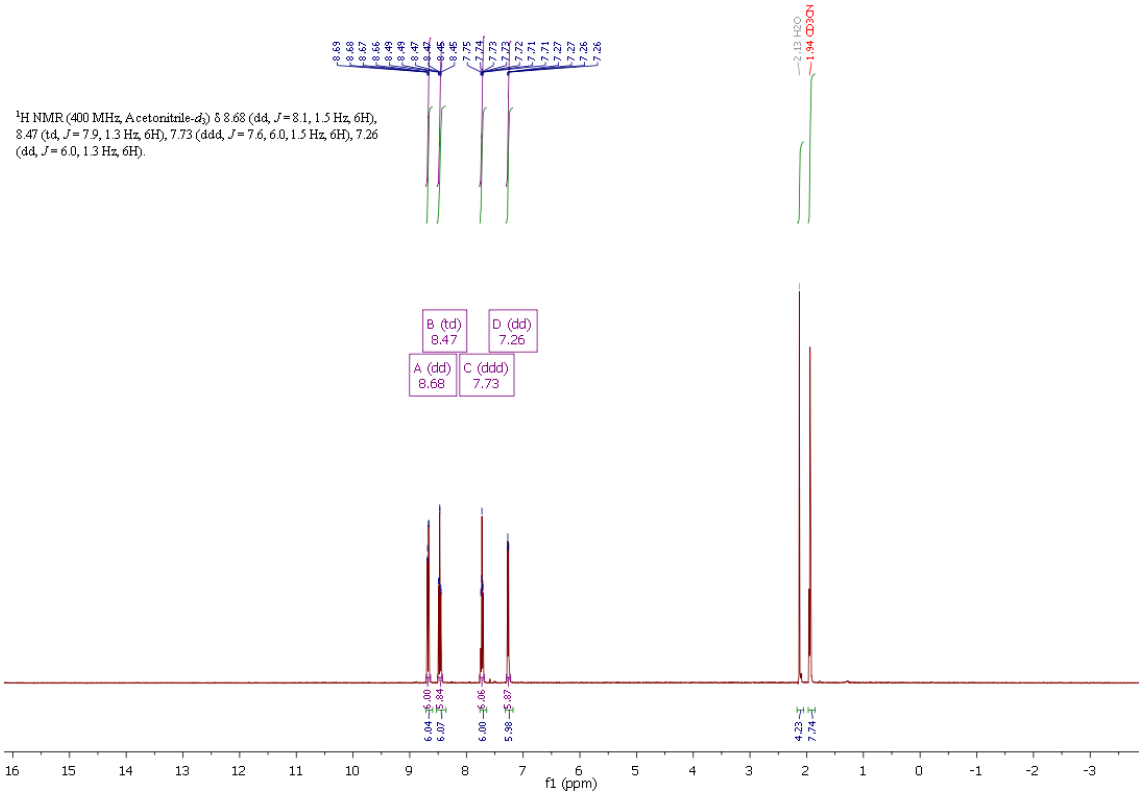

Fig. S153: ^{1}H NMR spectra of $[Co(bpy)_3](PF_6)_3$ in MeCN-d3.

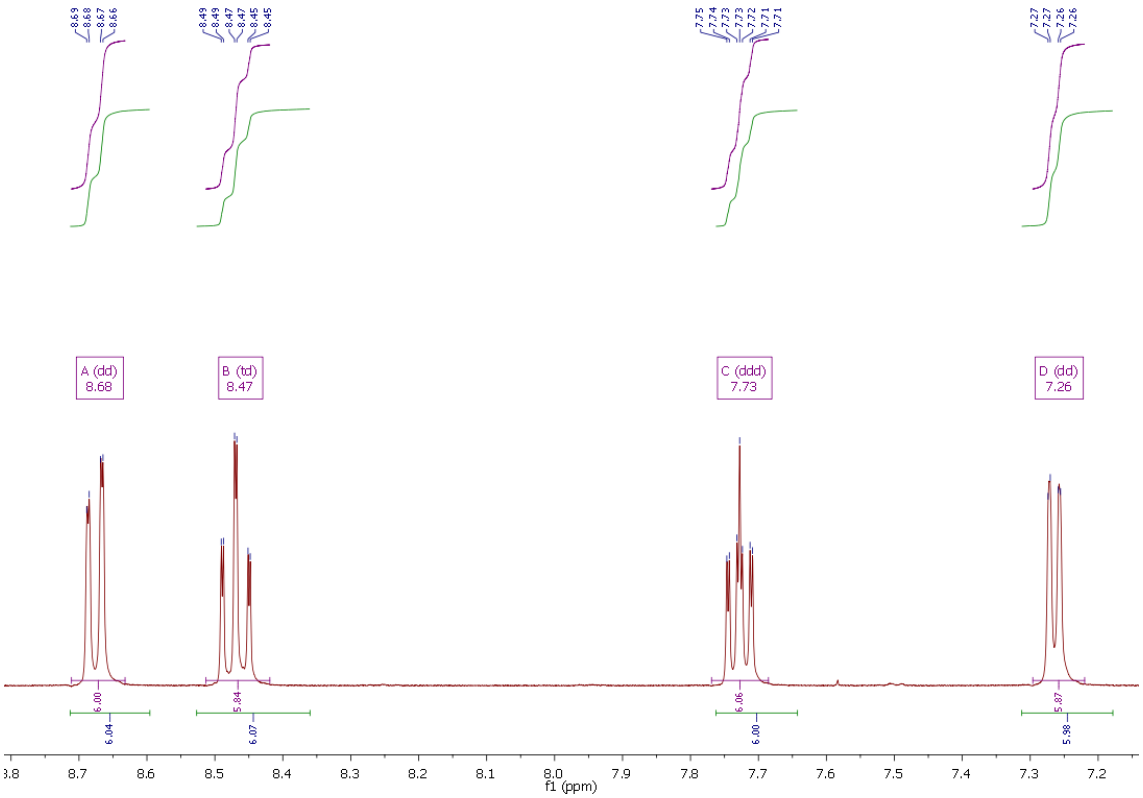

Fig. S154: Magnification of the ^{1}H NMR spectra of $[Co(bpy)_3](PF_6)_3$ in MeCN-d3.

12. PXRD spectra

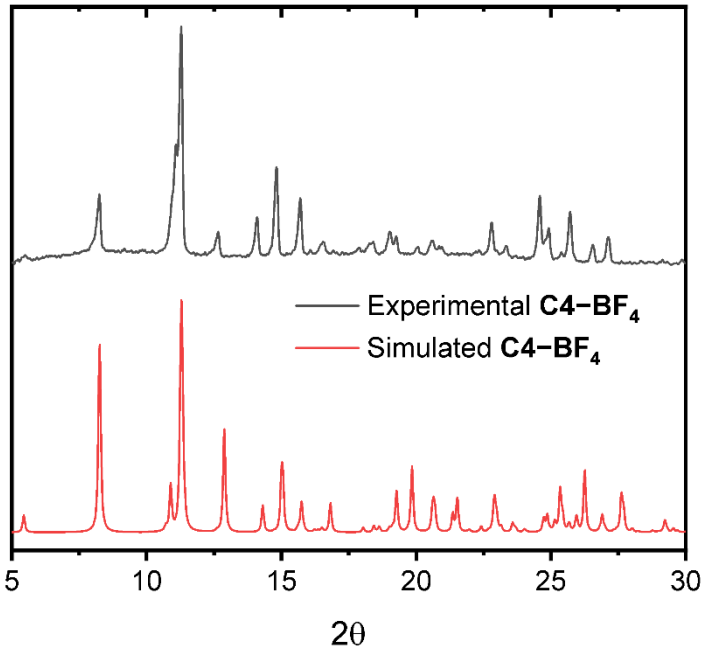

Fig. S155: Experimental und simulated PXRD spectra of **C4−BF$_4$**.

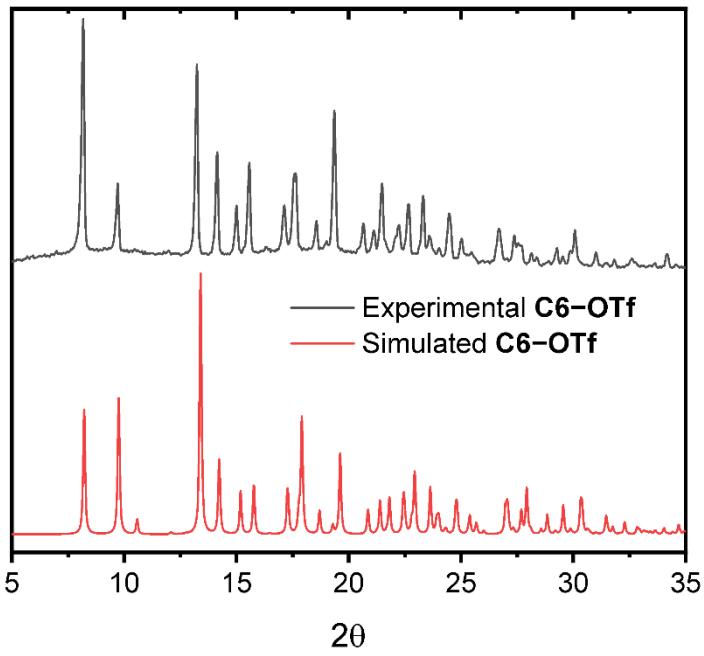

Fig. S156: Experimental and simulated PXRD spectra of **C6−OTf**.

13. Literature

[1] A. J. Niestroj, M. E. Maier, *Angew. Chem.* **1997**, *109*, 1854.

[2] a) G. J. Kubas, B. Monzyk, A. L. Crumbliss, *Inorg. Synth.* **1979**, 90; b) B. J. Hathaway, D. G. Holah, A. E. Underhill, *J. Chem. Soc.* **1962**, *0*, 2444; c) B. J. Hathaway, D. G. Holah, J. D. Postlethwaite, *J. Chem. Soc.* **1961**, 3215.

[3] a) W. Kantlehner, E. Haug, W. W. Mergen, P. Speh, T. Maier, J. J. Kapassakalidis, H.-J. Bräuner, H. Hagen, *Liebigs Ann. Chem.* **1984**, *1984*, 108; b) H. Wittmann, V. Raab, A. Schorm, J. Plackmeyer, J. Sundermeyer, *Eur. J. Inorg. Chem.* **2001**, *2001*, 1937.

[4] S. Herres-Pawlis, A. Neuba, O. Seewald, T. Seshadri, H. Egold, U. Flörke, G. Henkel, *Eur. J. Org. Chem.* **2005**, *2005*, 4879.

[5] I. d. Santos Vieira, S. Herres-Pawlis, *Z. Naturforsch. B* **2012**, *67*, 320.

[6] T. Rösener, A. Hoffmann, S. Herres-Pawlis, *Eur. J. Inorg. Chem.* **2018**, *2018*, 3164.

[7] S. Vangapandu, M. Jain, R. Jain, S. Kaur, P. P. Singh, *Bioorg. Med. Chem.* **2004**, *12*, 2501.

[8] F. Fontana, F. Minisci, M. C. Nogueira Barbosa, E. Vismara, *Tetrahedron* **1990**, *46*, 2525.

[9] S. Y. Gadomsky, I. K. Yakuschenko, *Russ. Chem. Bull., Int. Ed.* **2016**, *65*, 816.

[10] T. G. Ribelli, M. Fantin, J.-C. Daran, K. F. Augustine, R. Poli, K. Matyjaszewski, *J. Am. Chem. Soc.* **2018**, *140*, 1525.

[11] a) B. M. Klahr, T. W. Hamann, *J. Phys. Chem. C* **2009**, *113*, 14040; b) S. M. Feldt, E. A. Gibson, E. Gabrielsson, L. Sun, G. Boschloo, A. Hagfeldt, *J. Am. Chem. Soc.* **2010**, *132*, 16714.

[12] a) *SADABS (Version 2014/4)*, Bruker AXS Inc., Madison, Wisconsin, USA, **2014**; b) *SAINT (Version 8.37A)*, Bruker AXS Inc., Madison, Wisconsin, USA; c) *SMART (Version 5.631)*, Bruker AXS Inc., Madison, Wisconsin, USA.

[13] *X-Area Pilatus3_SV 1.31.131.0*, STOE, **2017**.

[14] *X-Area Integrate 1.71.0.0*, STOE, **2016**.

[15] *X-Area Pecipe 1.33.0.0*, STOE, **2015**.

[16] *X-Area LANA 1.74.4.0*, STOE, **2017**.

[17] Bruker, *Xprep V5.1*, Bruker AXS Inc., Madison, Wisconsin, USA, **1997**.

[18] G. M. Sheldrick, *Acta Crystallogr. Sect. A* **2008**, *64*, 112.

[19] G. M. Sheldrick, *Acta Crystallogr. Sect. A* **2015**, *71*, 3.

[20] G. M. Sheldrick, *Acta Crystallogr. Sect. C* **2015**, *71*, 3.

[21] C. B. Hübschle, G. M. Sheldrick, B. Dittrich, *J. Appl. Crystallogr.* **2011**, *44*, 1281.

[22] A. L. Spek, *PLATON, A Multipurpose Crystallographic Tool*, Utrecht University, Utrecht, The Netherlands, **2008**.

[23] A. L. Spek, *Acta Crystallogr. Sect. D* **2009**, *65*, 148.

[24] E. Welter, R. Chernikov, M. Herrmann, R. Nemausat, *A beamline for bulk sample x-ray absorption spectroscopy at the high brilliance storage ring PETRA III*, AIP Conference Proceedings 2054, 040002, **2019**.

[25] B. Ravel, M. Newville, *J. Synchrotron Rad.* **2005**, *12*, 537.

[26] a) R. A. Marcus, N. Sutin, *Biochim. Biophys. Acta Rev. Bioenerg.* **1985**, *811*, 265; b) R. A. Marcus, *Angew. Chem. Int. Ed.* **1993**, *32*, 1111; *Angew. Chem.* **1993**, *105*, 1161; c) R. A. Marcus, *Pure Appl. Chem.* **1997**, *69*, 13.

[27] a) M. J. Martin, J. F. Endicott, L. A. Ochrymowycz, D. B. Rorabacher, *Inorg. Chem.* **1987**, *26*, 3012; b) P. Comba, M. Kerscher, A. Roodt, *Eur. J. Inorg. Chem.* **2004**, *2004*, 4640.

[28] Gaussian 16, Revision B.01, M. J. Frisch, G. W. Trucks, H. B. Schlegel, G. E. Scuseria, M. A. Robb, J. R. Cheeseman, G. Scalmani, V. Barone, G. A. Petersson, H. Nakatsuji, X. Li, M. Caricato, A. V. Marenich, J. Bloino, B. G. Janesko, R. Gomperts, B. Mennucci, H. P. Hratchian, J. V. Ortiz, A. F. Izmaylov, J. L. Sonnenberg, D. Williams-Young, F. Ding, F. Lipparini, F. Egidi, J. Goings, B. Peng, A. Petrone, T. Henderson, D. Ranasinghe, V. G. Zakrzewski, J. Gao, N. Rega, G. Zheng, W. Liang, M. Hada, M. Ehara, K. Toyota, R. Fukuda, J. Hasegawa, M. Ishida, T. Nakajima, Y. Honda, O. Kitao, H. Nakai, T. Vreven, K. Throssell, J. A. Montgomery, Jr., J. E. Peralta, F. Ogliaro, M. J. Bearpark, J. J. Heyd, E. N. Brothers, K. N. Kudin, V. N. Staroverov, T. A. Keith, R. Kobayashi, J. Normand, K. Raghavachari, A. P. Rendell, J. C. Burant, S. S. Iyengar, J. Tomasi, M. Cossi, J. M. Millam, M. Klene, C. Adamo, R. Cammi, J. W. Ochterski, R. L. Martin, K. Morokuma, O. Farkas, J. B. Foresman, and D. J. Fox, Gaussian, Inc., Wallingford CT, 2016.

[29] a) J. Tao, J. P. Perdew, V. N. Staroverov, G. E. Scuseria, *Phys. Rev. Lett.* **2003**, *91*, 146401; b) V. N. Staroverov, G. E. Scuseria, J. Tao, J. P. Perdew, *J. Chem. Phys.* **2003**, *119*, 12129.

[30] a) F. Weigend, R. Ahlrichs, *Phys. Chem. Chem. Phys.* **2005**, *7*, 3297; b) A. Schäfer, C. Huber, R. Ahlrichs, *J. Chem. Phys.* **1994**, *100*, 5829; c) K. Eichkorn, F. Weigend, O. Treutler, R. Ahlrichs, *Theor. Chem. Acc.* **1997**, *97*, 119.

[31] a) S. Grimme, S. Ehrlich, L. Goerigk, *J. Comput. Chem.* **2011**, *32*, 1456; b) L. Goerigk, S. Grimme, *Phys. Chem. Chem. Phys.* **2011**, *13*, 6670; c) A. Hoffmann, R. Grunzke, S. Herres-Pawlis, *J. Comput. Chem.* **2014**, *35*, 1943.

[32] a) F. Weinhold, C. R. Landis, *Valency and Bonding − A Natural Bond and Orbital Donor−Acceptor Perspective*, Cambridge University Press, New York, **2005**; b) E. D. Glendening, J. K. Badenhoop, A. E. Reed, J. E. Carpenter, J. A. Bohmann, C. M. Morales, C. R. Landis, F. Weinhold, *NBO 6.0*, Theoretical Chemistry Institute, University of Wisconsin: Madison, **2013**; c) E. D. Glendening, C. R. Landis, F. Weinhold, *J. Comput. Chem.* **2013**, *34*, 1429.

[33] a) S. F. Nelsen, S. C. Blackstock, Y. Kim, *J. Am. Chem. Soc.* **1987**, *109*, 677; b) S. F. Nelsen, M. J. R. Yunta, *J. Phys. Org. Chem.* **1994**, *7*, 55.

[34] A. Hoffmann, S. Binder, A. Jesser, R. Haase, U. Flörke, M. Gnida, M. Salomone Stagni, W. Meyer-Klaucke, B. Lebsanft, L. E. Grünig, S. Schneider, M. Hashemi, A. Goos, A. Wetzel, M. Rübhausen, S. Herres-Pawlis, *Angew. Chem. Int. Ed.* **2014**, *53*, 299; *Angew. Chem.* **2014**, *126*, 305.